NANOSTRUCTURED PERVAPORATION MEMBRANES FOR BIOETHANOL DEHYDRATION

Inauguraldissertation
zur
Erlangung der Würde eines Doktors der Philosophie
vorgelegt der
Philosophisch-Naturwissenschaftlichen Fakultät
der Universität Basel

von

Alessandro Angelini

2024

Genehmigt von der Philosophisch-Naturwissenschaftlichen Fakultät

auf Antrag von

Erstbetreuer: Prof. Dr. Wolfgang P. Meier (Universität Basel, Departement Chemie)

Erstbetreuer: Prof. Dr. Cornelia G. Palivan (Universität Basel, Departement Chemie)

Zusätzlicher Erstbetreuer: Dr. Wilfredo Yave (DeltaMem AG)

Zweitbetreuer: Prof. Dr. Edwin C. Constable (Universität Basel, Departement Chemie)

Externer Experte: Prof. Dr. Mathias Ulbricht (Universität Duisburg-Essen)

Basel, 21.06.2022

Prof. Dr. Marcel Mayor

Dekan

Dedicated to my parents,

for their endless love, support and encouragement

Abstract

Current commercial membranes are applied for drying first generation of bioethanol, but the purification and drying of second and third generation of bioethanol are big challenges due to the impurities (fusel alcohols, organic acids, aldehydes, etc.) that are present in the industrial streams. Those impurities harm the membrane materials, either polymeric or ceramic. Even molecular sieves suffer damages due to these harmful components. Therefore, the development of next generation pervaporation membranes is crucial to make pervaporation more attractive and more competitive.

In the first part of the thesis, we investigate the ability of commercial membranes to trigger a specific behavior under different media. Dehydration of binary methyl acetate–water mixtures under neutral, acidic, and basic conditions was carried out by using PERVAP™ composite membranes based on poly(vinyl alcohol) (PVA) and poly(*N*-vinylpyrrolidone-*co*-(2-(dimethylamino)ethyl methacrylate)) P(NVP-*co*-DMAEMA). The effects of an acid (HCl) and a base (NaOH) on the separation performance of the membrane during the pervaporation process were investigated. The pH-responsive nature of membranes has been confirmed by swelling tests and analysis of the chemical structure of polymeric membranes. In addition, a mechanism of ring-opening of NVP units is proposed and correlated to the changes of membrane separation performance. Such membranes are known to be stable in the presence of impurities such as acetaldehyde. However, the membranes typically exhibit poor performance in ethanol/water separation due to low selectivity which is linked to the use of a commercial copolymer designed for other applications, thus discouraging their use for bioethanol dehydration processes. This motivated the need for customizing the copolymer properties to enhance membrane formulations for specific applications like ethanol dehydration.

In the second part of the thesis, we deepen the investigation of the copolymer. Rather than commercial copolymers, tailor-made poly(*N*-vinylpyrrolidone-*co*-(2-(dimethylamino)ethyl methacrylate)) P(NVP-*co*-DMAEMA) and poly(*N*-vinylpyrrolidone-*co*-*N*-vinylimidazole) P(NVP-*co*-PNVIm) with defined monomer molar ratio are synthesized via free radical polymerization. The random copolymers are fully characterized and then blended with PVA to investigate their chemical and thermal properties as membrane materials. Composite membranes are further prepared from the PVA/copolymer blends on a porous support, which are evaluated in terms of separation performance for the dehydration of ethanol by

pervaporation. The membranes prepared from the blends exhibit up to four times higher water permeances than pristine PVA membrane, albeit the selectivity is slightly lower. Nevertheless, the membranes from blends with a ratio of 95:5 (PVA/copolymer) show improved selectivity and higher permeance values compared to the commercial PERVAP™ 4155–80, especially the blends composed by the copolymers of coPDMAEMA60 and coPDMAEMA20. The membrane prepared from the blend containing the homopolymer coPDMAEMA100 exhibits the highest water/ethanol selectivity and shows stable separation performance throughout the whole long-term stability test, while exposed to acetaldehyde. Thus, this study demonstrates that by synthesizing tailored copolymers (rather using the commercial ones) and blending with PVA, the separation performance of membranes can be significantly improved and tuned for specific dehydration processes. These prototypes have proven their efficiency and stability for second and third generation bioethanol dehydration processes. Thus, a considerable step towards the deployment of these membranes has been made.

In the last part, tailor-made poly(vinyl alcohol)-*b*-poly(styrene) copolymers (PVA-*b*-PS) for separation membranes are synthesized by the combination of reversible-deactivation radical polymerization techniques. The special features of these di-block copolymers are the high molecular weight (> 70 kDa), the high PVA content (> 80 wt.%), and the good film-forming property. They are soluble only in hot dimethyl sulfoxide, but through the “solvent-switch” technique, they self-assemble in aqueous media to form micelles. When the self-assembled micelles are cast on a porous substrate, thin-film membranes with higher water permeance than that of PVA homopolymer are obtained. Thus, by using these tailor-made PVA-*b*-PS copolymers, it is demonstrated that chemical cross-linkers and acid catalysts can no longer be needed to produce PVA membranes, since the PS nanodomains within the PVA matrix act as cross-linking points. Lastly, subsequent thermal annealing of the thin film enhances the membrane selectivity due to the improved microphase separation.

Acknowledgments

I would like to express my deep gratitude to Prof. Dr. Wolfgang Meier. I would have liked so much to be able to finish this doctorate with the possibility to thank you in person. Unfortunately, fate decided otherwise. I have always admired the way you supervised us. You always gave me the opportunity to express our opinions and to decide on the research directions I wanted to take in my project. It is this freedom of choice that allowed me to thrive in the group. I thank you for that and for the inspiration you were to me. Also, I would like to thank Prof. Dr. Cornelia Palivan for her unquestionable support throughout this journey. I thank you for the discussions, your availability but also for your kindness in providing optimal working conditions. I thank Prof. Dr. Mathias Ulbricht for agreeing to be the external expert and to take part in the examination of this thesis. Thanks also to Prof. Dr. Edwin Constable for accepting to be my second supervisor and to Prof. Dr. Michael Nash for chairing my defense.

This work would never have been possible without the support of all the staff of the University of Basel, and especially those of the Chemistry Department. My special thanks go to Maya Greuter, Mariella Schneiter, Dr. Mike Devereux, Dr. Bernhard Jung, Markus Hauri, Susanne Foley, Philipp Knöpfel, Hisni Meha, Martin Grischa, Markus Ast, Pascal Andrek, Susanne Erpel.

I would like to thank all the students whom I had the pleasure of teaching the vapor pressure experiment. It was always a fantastic moment with you, I really enjoyed this teaching experience.

These four years have allowed me to meet great people. I would like to thank all my current and former colleagues for allowing me to travel through your different origins and cultures. I feel extremely lucky to have had the opportunity to work with such talented people. I have been inspired by all of you. Thank you Agata, Andrea, Christoph, Claire, Cora, Davy, Dalila, Dalin, Daniel, Danut, Dimitri, Elena, Evan, Flavien, Gaby, Ioana, John, Katrin, Luisa, Lukas, Maria, Martina, Maryame, Michal, Moritz, Myrto, Olivia, Phally, Rémy, Ricco, Sagana, Serena, Stefano, Sven Vichi, Vittoria, Viviana, Xinan, I wish you all the best.

I am deeply grateful to my supervisors: Dr. Anja Car, Dr. Csaba Fodor and Dr. Ionel Adrian Dinu. I thank you for your trust and also for all the advice and discussions. Thanks to you, I have learned a lot. I really appreciated your commitment and motivation for this achievement.

I would also like to thank all the staff at DeltaMem AG. Since my internship with you, you have always welcomed me warmly and put me in optimal working conditions. To Luigi Leva and Dr. Wilfredo Yave, I cannot thank you enough for everything you have given me. Both humanly and professionally, you have greatly contributed to my personal development these last years. If today I write these few lines, it is thanks to our first meeting for the interview of my internship in 2017. From then on, I discovered the wonderful world of membranes. I am sincerely grateful to you for all this, I hope to be able to return it to you.

J'aimerais remercier la famille Di Lorenzo et le personnel du restaurant O Sole Mio. En commençant cette aventure, j'ai arrêté mon job étudiant. Chez vous, je me sentais comme à la maison. Bien plus qu'un travail, c'était un véritable plaisir et bonheur de venir travailler avec vous au restaurant.

Un grand merci à mes amis. Merci pour tout le soutien et l'équilibre que vous m'avez apporté. Mais aussi pour tous ces moments de joies et bonne humeur.

Merci à ma chère Mathilde, tu as toujours été patiente, compréhensive, attentionnée. Merci pour tous ces moments partagés ensemble, tu me combles de bonheur. Ta présence a grandement contribué à mon apaisement tout au long de ces quatre années. Le meilleur reste à venir !

Enfin, je tiens à remercier mes parents du plus profond du cœur. Les personnes les plus chères à mes yeux. Je suis fier de notre parcours et de partager chacune de ces réussites avec vous. Grâce à votre amour inconditionnel et à votre soutien sans faille, chaque pas fait en avant était toujours un énorme succès. Je ne vous remercierai jamais assez pour tout cela.

Contents

List of Figures

List of Tables

Abbreviations

A	Effective membrane area
a_0	Contact area of the head group
AIBN	2,2′-azobis(2-methylpropionitrile)
ARGET ATRP	Activator regenerated by electron transfer atom transfer radical polymerization
ATR–FTIR	Attenuated total reflection–Fourier transform infrared
ATRP	Atom transfer radical polymerization
BCP	Block copolymer
BPO	Dibenzoyl peroxide
CA	Contact angle
$CDCl_3$	Deuterated chloroform
CNT	Carbon nanotube
CRP	Controlled radical polymerization
CS	Chitosan
CTA	Chain transfer agent
CuAAC	Copper-catalyzed azide-alkyne cycloaddition
$Đ$	Dispersity
DLS	Dynamic light scattering
DMAc	*N*,*N*-dimethylacetamide
DMAEMA	2-(dimethylamino)ethyl methacrylate
DMF	*N*,*N*-dimethylformamide
DMSO-d_6	Deuterated dimethyl sulfoxide
DPn	Degree of polymerization
DSC	Differential scanning calorimetry
EG	Ethylene glycol
ESR	Equilibrium swelling ratio
EtOH	Ethanol
f	Hydrophilic ratio
FRP	Free radical polymerization
GC	Gas chromatography
GFT	Gesellschaft für Trenntechnik

GO	Graphene oxide
GPC	Gel permeation chromatography
HSP	Hansen solubility parameter
HT	Heat treatment
ICAR ATRP	Initiators for continuous activator regeneration ATRP
IPA	Isopropanol
J	Permeate flux
KPS	Potassium persulfate
l_c	Length of the hydrophobic part
LbL	Layer-by-layer
m	Amount of permeate
MMM	Mixed matrix membrane
MOF	Metal organic framework
MOXA	2-methyl-2-oxazoline
Na-Alg	Sodium alginate
NMP	*N*-Methyl-2-pyrrolidone
NMR	Nuclear magnetic resonance
NRTL	Non-random two-liquid
NVIm	*N*-Vinylimidazole
NVP	*N*-Vinylpyrrolidone
p	Packing parameter
P	Permeability
P/l	Permeance
PA	Polyamide
PAA-*b*-PBD	Poly(acrylic acid)-*block*-polybutadiene
PAN	Poly(acrylonitrile)
PBD	Polybutadiene
PDMAEMA	Poly(2-(dimethylamino)ethyl methacrylate)
PDMS	Poly(dimethyl sulfoxide)
PDMS-*b*-PEO	Poly(dimethyl siloxane)-*block*-poly(ethylene oxide)
PDMS-*b*-PMOXA	Poly(dimethyl sulfoxide)-*block*-poly(2-methyl-2-oxazoline)
PEC	Polyelectrolyte complex
PEO-*b*-PEE	Poly(ethylene oxide)-*block*-poly(ethyl ethylene)
PEO-*b*-PHPMA	Poly(ethylene oxide)-*block*-poly(2-hydroxypropyl methacrylate)

PES	Polyethersufone
PI	Polyimide
PISA	Polymerization induced self-assembly
PNVIm	Poly(*N*-vinylimidazole)
PNVP	Poly(*N*-vinylpyrrolidone)
P(NVP-*co*-DMAEMA)	Poly(*N*-vinylpyrrolidone-*co*-(2-(dimethylamino)ethyl methacrylate))
P(NVP-*co*-PNVIm)	Poly(*N*-vinylpyrrolidone-*co*-*N*-vinylimidazole)
PS	Polystyrene
PS-*b*-P4VP	Polystyrene-*block*-poly(4-vinylpyridine)
PNVIm	Poly(*N*-vinylimidazole)
PNVP	Poly(*N*-vinylpyrrolidone)
P*t*BA	Poly(*tert*-butyl acrylate)
PV	Pervaporation
PVA	Poly(vinyl alcohol)
PVAc	Poly(vinyl acetate)
PVDF	Poly(vinylidene fluoride)
RAFT	Reversible addition fragmentation chain transfer
RI	Refractive index
RT	Room temperature
SDG	Sustainable Development Goals
SEM	Scanning electron microscopy
SHF	Separated Hydrolysis and Fermentation
SSF	Simultaneous Saccharification and Fermentation
t	Operating time between sample collection
TEM	Transmission electron microscopy
T_g	Glass transition temperature
TMS	Tetramethylsilane
UNIQUAC	Universal Quasi Chemical
v	Volume of the hydrophobic part
XPS	X-ray photoelectron spectroscopy

1. Introduction

This chapter contains parts of a published work: Elena C. dos Santos, Alessandro Angelini, Dimitri Hürlimann, Wolfgang Meier and Cornelia G. Palivan. *Chemistry* **2020,** *2* (2), 470-489.

Two centuries ago, the discovery of energy production from fossil fuels led to the Industrial Revolution, a major turning point in history that ushered our modern civilization. According to the Sustainable Development Goals (SDG) from the United Nations, "energy is central to nearly every major challenge and opportunity the world faces today".[1] Therefore, energy access is the key and main driving force of development. While fossil fuels bore many benefits, several major negative consequences came up (greenhouse gas emissions, non-renewable resources, accidents during production, water pollution and oil spill, etc.). Nowadays, more than 80% of global primary energy comes from fossil fuels. Hence, it is fundamental to significantly reduce their use, in particular through the renewable, clean and safe resources.[2-6] One of the greatest challenges remains in the efficient use of these renewable materials, in order to ensure a sufficient supply of energy.[7-11]

1.1. Bioethanol production

Among biofuels, bioethanol is the most widely produced, especially in countries such as Brazil and the United States, which are known to be the largest producers due to the large number of operating plants.[12-14] Conventionally, after fermentation, the ethanol content is between 10 and 20%. The product is concentrated by distillation without difficulty to 80-85%. The ethanol/water mixture is known to form an azeotrope when its composition reaches 96% ethanol. At this stage, the separation is thermodynamically limited and the process becomes very energy intensive. A specific azeotropic distillation is typically involved at this stage to reach low moisture content bringing more complexity to the overall setup. Alternatively, separation methods such as molecular sieves or pervaporation[15-18] can easily meet the specifications and contribute to reduce the energy costs.[19-21] The molecular sieves are adsorbents with high regeneration cost and in addition, it exists the potential contamination of the feed during the process. This aspect is not concerned by pervaporation.[22]

This section describes the different generations of bioethanol production processes and the techniques used to purify ethanol to achieve the required specifications for use as a biofuel (> 99.7%).[23]

1.1.1. Generations of bioethanol

1.1.1.1. First generation bioethanol

First generation bioethanol is obtained through alcoholic fermentation of fermentable sugars (glucose, sucrose, etc.).[24] Sugar cane, corn and sugar beet are the main crops for bioethanol production. Sugarcane is mainly grown in tropical regions, especially in Brazil, and is an important bioethanol resource due to its high content of easily fermentable sugar.[25] In the United States, corn is commonly used as a source of bioethanol; The starch is converted into fermentable sugars through enzymatic hydrolysis.[26] In Europe, sugar beet is also a significant source of bioethanol and benefits from high fermentable sugar content, similar to that of sugar cane.[27]

The production process begins with the preparation of the raw materials, which are delivered, cleaned, and milled to facilitate the extraction of soluble sugars and starches. For sugar-rich raw materials, such as sugar cane and sugar beet, soluble sugars are obtained directly milling. These sugars are then dissolved in water to form a juice extract. For starch-rich raw materials such as corn and wheat, liquefaction and saccharification stages are added after milling. The starch is mixed with water and heated to form a slurry. This mixture is then treated with enzymes, such as α-amylases, which break down the starch into the simpler sugar maltose. Subsequently, other enzymes, such as glucoamylases, are added to convert maltose into glucose. The latter is then fermented, where microorganisms, typically yeast, convert the sugar into ethanol and carbon dioxide. After fermentation, the mixture is distilled to separate the ethanol from water and other residues. At this stage, an ethanol product with a purity of 95% can be obtained. In order to obtain high-purity bioethanol, a final dehydration step is necessary. The concentrated ethanol is dehydrated, typically by adsorption using molecular sieves, by azeotropic distillation or by pervaporation/vapor permeation to remove residual water, producing an anhydrous ethanol (> 99.7% ethanol). Despite its technical and industrial maturity, the main limitation associated with first generation bioethanol concerns its potential impact on global food security, as the raw materials used for its production come from food resources. This poses a risk of competition between food and energy needs, which could further exacerbate tensions over food supplies. In addition, the use of food resources for bioethanol

production can lead to an increase in food prices, which has a negative impact on the overall economy and social stability, especially in regions where access to food is already scarce. This situation requires a reassessment of bioethanol production strategies to mitigate the negative impacts on the availability and cost of food resources.[24-25, 28]

1.1.1.2. Second generation bioethanol

The second generation bioethanol production process uses advanced technologies to convert agricultural and forestry residues that are not competitive for food use into bioethanol. In contrast to first generation bioethanol, which mainly uses food crops, this process uses all components of the biomass, especially the lignocellulosic components.

Lignocellulosic biomass is a complex substrate composed of three main fractions: cellulose, hemicellulose and lignin. The ethanol production process involves optimizing the production of monosaccharides from the cellulose and hemicellulose fractions and their subsequent conversion into ethanol. The pretreatment stage represents the first process step in which the biomass is prepared for subsequent chemical and enzymatic reactions. This is achieved through a combination of physical and chemical modifications to its structure. The specific pretreatment methods used may include mechanical (grinding), thermal (heating), chemical (acids, alkalis, solvents), or a combination of these techniques. The overall goal is to reduce the crystallinity of cellulose and separate lignin from polysaccharides, thereby facilitating the hydrolysis of cellulose and hemicellulose fibers. After pretreatment, the biomass undergoes hydrolysis to break down the long chains of cellulose and hemicellulose into simpler sugars, mainly hexoses (such as glucose) and pentoses (such as xylose). While hemicellulose is easily hydrolyzed, the hydrolysis of cellulose to glucose is a rather complicated step due to its structure, crystallinity, and association with lignin and hemicelluloses, which are still present despite pretreatment. The hydrolysis must therefore be catalyzed either by an acid (diluted or concentrated) or by specific enzymes called cellulases. The sugars produced during hydrolysis are fermented by micro-organisms (yeast or bacteria) to produce ethanol. In some cases, genetically modified organisms are used to efficiently ferment both pentoses and hexoses. The ethanol is then concentrated (96%) by distillation. As with the first generation process, ethanol is further dehydrated (> 99.7%) by molecular sieve adsorption, azeotropic distillation or pervaporation/vapor permeation. Although the technology for producing second generation bioethanol has now reached industrial maturity, global production is still largely dominated by first generation bioethanol. The latter is economically more attractive due to its conversion efficiency and often lower costs. The production of second generation bioethanol is technically more complex,

requiring costly pre-treatments to make fermentable sugars accessible, which raises production costs. Besides the issue raised by this work, *i.e.*, the unstable poly(vinyl alcohol) (PVA)-based pervaporation membranes towards bioethanol impurities, one of the primary issues concerning the production of bioethanol from second generation is the need for advanced technologies and facilities to facilitate the biomass conversion process.[23, 29-31]

1.1.1.3. Third generation bioethanol

The third generation of bioethanol, produced from micro- and macro-algae, represents a promising advance over previous generations that utilize food crops and lignocellulosic residues. This generation focuses on the use of algae due to its rapid growth ability, high lipid (for biodiesel) and carbohydrate (for bioethanol) content, and lower dependence on agricultural land use, thereby minimizing its impact on food security. The production process is similar to that of previous generations, with several steps involved. First, the algae are harvested and pretreated, which usually includes drying and grinding. The biomass is then subjected to hydrolysis, in which the algae polysaccharides are broken down into simple sugars either by acid hydrolysis or enzymatic hydrolysis. This step is crucial because it prepares the biomass for fermentation. During fermentation, sugars are converted into ethanol and carbon dioxide by microorganisms such as Saccharomyces cerevisiae. Two approaches are commonly employed: fermentation separated from hydrolysis (Separated Hydrolysis and Fermentation, SHF) and simultaneous fermentation with saccharification (Simultaneous Saccharification and Fermentation, SSF). The latter is often the preferred option due to its capacity to reduce production time and associated costs. As in the other two previous generations of bioethanol, the ethanol is then concentrated by distillation and further dehydrated by molecular sieve adsorption, azeotropic distillation or pervaporation/vapor permeation (> 99.7%). This method, though promising, still faces significant challenges, particularly in terms of production costs, economic viability and industrial scale. Technological advances and continuous improvement in algae cultivation and ethanol extraction techniques are therefore crucial to the future of third generation bioethanol.[32-35]

1.1.2. Separation processes for (bio)ethanol purification

To be suitable for use as a biofuel, bioethanol must be purified to over 99.7%. This final purification step is common to all generations of bioethanol presented in the previous sections. The main difficulty lies in the separation of the azeotropic ethanol-water mixture, which limits the efficiency of conventional distillation. Conventional distillation can produce up to about

90% pure ethanol, but beyond this concentration the separation becomes more complex and energy-intensive, making the process less economically attractive.[36] To solve this problem and obtain anhydrous ethanol, several advanced techniques are used.

Extractive distillation is a separation technique used when conventional distillation is inefficient, primarily due to the formation of azeotropes or minimal differences in volatility between components. This method involves adding a miscible, non-volatile solvent that influences the volatile properties of the components in the mixture, thus facilitating their separation.[37] Industrial purification of ethanol above the azeotropic point has proven to be effective when using ethylene glycol (EG). EG is added from the top of the distillation column, where it increases the activity of water, thereby reducing its relative volatility compared to ethanol. The heavier mixture of water and EG is recovered at the bottom of the column while ethanol, now the more volatile component, is collected from the top of the column. The recovered mixture of EG and water is subsequently separated by a further distillation step or other separation techniques and then reused in the process.[22]

An alternative method of breaking the azeotrope is to introduce a third component, resulting in the formation of a new heterogeneous low boiling point azeotrope. This process is called azeotropic distillation.[38] Substances such as benzene, cyclohexane or heptane form azeotropes that are more volatile with water than the ethanol-water azeotrope. Typically, ethanol is first concentrated near the azeotrope by simple distillation. In a subsequent distillation column, the entrainer is then added from the top tray to form a more volatile azeotrope with water, which is then removed at the top and pure ethanol is recovered from the bottom of the column. The overhead effluent is then condensed to separate the water from the entrainer, which can be reused. Although azeotropic distillation is an effective and widely used process in industry, it is very energy-intensive and environmentally harmful due to the use of toxic entrainers. Therefore, safer alternatives for dehydration, such as molecular sieves or membrane processes, are preferred to minimize potential toxicity problems.[39]

In the bioethanol dehydration process, molecular sieves work by selectively adsorbing water molecules using the steric exclusion principle. These materials, often composed of zeolites (3A), have uniform pore sizes (3 Å) that are slightly larger than water molecules (2.8 Å) but smaller than ethanol molecules (4.4 Å). When the mixture of ethanol and water from distillation is passed through the molecular sieve, the smaller water molecules are captured by the sieve pores through physical and chemical interactions. Ethanol molecules that are too large to penetrate the pores continue to pass through the sieve without being adsorbed. Once the sieve

pores are saturated with water, the adsorption process is temporarily interrupted to allow the sieve to regenerate. This process typically involves heating the molecular sieve or reducing the pressure (pressure swing adsorption) to release the adsorbed water so that the sieve can be reused for further adsorption cycles. In an industrial plant, several sieve beds can be used alternately to enable continuous production. While one bed regenerates, the others continue to process the ethanol stream, ensuring uninterrupted operation. In bioethanol production (first and second generation), the use of molecular sieves for dehydration is well established. For example, type 3A zeolite-based molecular sieves are commonly used to remove water from bioethanol. Molecular sieves are generally less energy-intensive than azeotropic or extractive distillation processes, as they require less heat and pressure to operate efficiently, a key factor in their industrial success. Sieves can be regenerated and reused several times, which reduces the amount of waste generated and can reduce long-term operating costs. Although reusable, molecular sieves require frequent regeneration, which can involve energy-intensive heating cycles. Molecular sieves are susceptible to contamination by other chemicals present in raw bioethanol, which can decrease their efficiency and lifespan. While molecular sieves offer significant advantages in terms of product purity and energy efficiency, they require higher initial investment and careful management to maximize their efficiency and longevity.[40-42]

Pervaporation is a promising alternative, offering considerable advantages in terms of energy efficiency and operating costs.[43] The process is distinguished by its ability to separate azeotropic mixtures without requiring additional chemicals, unlike extractive or azeotropic distillation. In contrast to molecular sieves, pervaporation does not require a regeneration step, and operating costs are relatively low because pervaporation requires less thermal energy than traditional distillation methods. It can also be integrated directly into existing processes to improve efficiency without involving major structural modifications. This can be particularly useful in configurations where space is limited. Pervaporation is becoming more and more popular as an alternative to molecular sieves for bioethanol separation and purification. The main difference between pervaporation and molecular sieves is their greater energy efficiency. The use of Whitefox's pervaporation technology in bioethanol production plants is a perfect example of the gradual replacement of molecular sieves by more advanced, energy-efficient solutions. Designed to optimize production and reduce operating costs, the Whitefox pervaporation system enables bioethanol plants to minimize energy consumption while maximizing ethanol recovery.[44-48] Whitefox Technologies' ICE systems use pervaporation hollow fiber membranes specially designed for ethanol dehydration. These membranes are typically polyimide membranes, known for their high performance, thermal and chemical

stability, and excellent selectivity for water.[18] Another major actor, Mitsubishi Chemical, has also deployed its ZEBREX systems worldwide in the bioethanol industry. These systems use advanced zeolite-based membrane technology, optimized for efficient ethanol dehydration. Mitsubishi's ZEBREX membranes are capable of significantly reducing energy consumption compared with traditional methods. They are used in first- and second generation bioethanol plants, processing both food feedstocks such as corn and sugarcane, and non-food lignocellulosic substrates.[49-51] PVA-based membranes, previously commercialized by Sulzer and subsequently by DeltaMem, have demonstrated their effectiveness in bioethanol dehydration processes, as for example in a pilot study carried out in 2013.[52] These membranes were used for ethanol dehydration, exploiting their high selectivity and ability to operate under less energy-intensive conditions compared to traditional methods. In some industrial plants, hydrophilic PVA-based membranes are used for the final dehydration stage of bioethanol produced from first generation feedstocks. However, the application of these membranes for the dehydration of second generation bioethanol derived from more complex feedstocks presents significant challenges. In particular, the presence of impurities such as acetaldehyde in second generation bioethanol streams can severely degrade membrane performance. Acetaldehyde affects the cross-linking of PVA, reducing membrane stability and lifetime. Despite their lower cost than competitors' membranes, which makes them particularly attractive, these PVA-based membranes require improvements in terms of chemical stability to extend their lifetime and maintain their efficiency under various industrial conditions. These developments are crucial for industrial scale-up and for fully exploiting the potential for cost reduction associated with these membrane technologies in bioethanol production.[18]

1.2. Pervaporation

Pervaporation is an advanced membrane separation technique that exploits the differences in chemical affinity of components in a liquid mixture with a selective membrane to separate them, particularly from azeotropic mixtures or compounds with close boiling points. The process involves two main steps: preferential sorption of the permeable component at the membrane surface on the feed side, followed by diffusion through the membrane, and finally evaporation as a vapor phase on the permeate side under partial vacuum or inert gas sweep. The advantages of pervaporation lie mainly in its ability to separate complex mixtures without the need for additional chemicals or high temperatures, thus preserving the thermal integrity of sensitive compounds and reducing energy consumption. In addition, this technique offers high selectivity

due to the specificity of the membrane, which can be designed to target specific components by adjusting its composition and structure. The membranes used can be optimized to increase their hydrophilicity or hydrophobicity, depending on the separation requirements. As a result, pervaporation is particularly relevant for industrial applications such as the dehydration of organic solvents or the treatment of aqueous waste streams, offering a low environmental impact and economically viable solution when dealing with challenging separations.[53]

1.2.1. Membranes for pervaporation

1.2.1.1. Membrane structure and fabrication methods

The choice of the membrane to be used in a pervaporation process is an important step in the adopted strategy. Before going into detail on the material choice that constitute the membrane, which directly influence the transport properties, the importance of the morphology and structure of the membrane together with the common method to produce membranes are described and discussed. As the purpose of this work is focused on pervaporation membranes, porous membranes will not be presented as they are related to other membrane separation processes.

Dense (isotropic) nonporous membranes consist of a thick layer, typically between 10-100 µm. As mentioned in the previous section, the thickness is a major factor to consider due to the mass transfer resistance phenomenon. Hence, this type of membranes are not suitable for industrial separation processes.[54] Nevertheless, they are great tools to characterize the membrane material properties on a laboratory scale. Dense films are commonly produced by solution casting using a casting knife (Figure 1-1). The formation of a dense film results of the transformation from a liquid to a solid state, called phase inversion. In order to control the thickness of the prepared film, the gap between the blade and the surface is adjusted to the targeted final thickness. The casted solution is left at room temperature or placed in an oven to enable the solvent to evaporate. The solvent choice is crucial as it influences the speed of formation of the film. In general, high boiling point solvents are not suitable for the evaporation induced phase separation due to the too low evaporation rate. Such solvents, like DMF, NMP or DMAc are rather used for the preparation of porous membrane by immersion precipitation in a coagulation bath containing a nonsolvent.

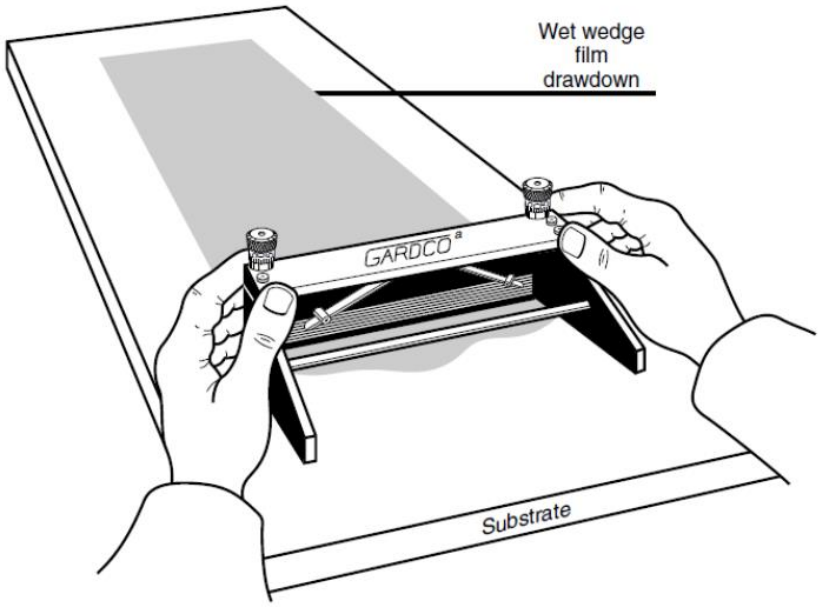

Figure 1-1. Dense film preparation using a casting knife.[55]

Anisotropic membranes, more specifically composite, are of much greater interest for pervaporation applications as they enable higher permeation fluxes. These membranes are usually produced by coating a thin layer on a suitable thicker porous support (e.g., ultrafiltration membranes) in order to provide enough mechanical strength for handling the membrane. The most important technique to coat a thin layer is dip-coating. Usually, the thickness ranges within 0.5-2.0 µm.

The presence of a nonporous top layer directly governs the transport properties of these membranes. Hence, the choice of material according to the physical and chemical properties is fundamental based on the separation that needs to be performed.

1.2.1.2. Membrane materials

In general, hydrophilic pervaporation membranes are used for solvent dehydration, while hydrophobic membranes are used for organic solvent recovery.[56] As the focus is on hydrophilic pervaporation membranes for bioethanol, hydrophobic membranes are beyond the scope of this thesis. Pervaporation processes involving hydrophobic membranes have a different approach than dehydration using hydrophilic membranes. In fact, such membranes typically work with aqueous ethanol solutions and display poor selectivity. As a consequence, the permeate need additional treatments. This is not the case using hydrophilic membranes. The latter can reach low moisture content without including additional steps. Hence high purity grade (bio)ethanol

is obtained at the end of the process. Recent reviews reporting the latest achievements on hydrophobic membranes can be found in the literature.[57-58]

1.2.1.2.1. Polymeric membranes

Since the first pervaporation installation using PVA membranes, four decades have passed and PVA still remains the benchmark material for the dehydration of alcohols.[55, 59-60] Together, with the good film forming ability, PVA is a material of choice for hydrophilic pervaporation membranes and several other applications due to its numerous advantageous features.[61-64] The polymeric structure consists of a simple backbone with hydroxyl pendant side groups. The amount of these moieties depends on the degree of hydrolysis of the poly(vinyl acetate) (PVAc) precursor. PVA has a glass transition temperature around 80°C and it starts to decompose above 200°C. Due to the high amount of available hydrogen bonding sites, PVA tends to swell excessively whenever the water content starts to be considerable. For this reason, crosslinking is commonly applied between the polymer chains to prevent this phenomenon from happening. Commercially available PVA membranes are crosslinked by chemical modification in presence of compounds such as dianhydrides, dialdehydes, etc.[65-66] Besides the excellent dehydration properties, some limitations are evidenced in some cases. The resulting acetal/hemiacetal bonds formed are prone to hydrolysis, especially in the presence of impurities. In particular, complex mixtures from fermentation broths that contain such harmful chemicals, make the membrane performance unstable and not suitable for application.[67]

The research is still ongoing to improve PVA based membrane.[68-70] Recently, major improvements were introduced to the PERVAP™ membrane series from DeltaMem AG (Switzerland), which make the membranes more robust in terms of separation performances and process sustainability.[71]

While the semi-crystalline nature of PVA and low free volume provide excellent selectivity, the water flux is often weak. One strategy to improve this feature is blending PVA with hydrophilic polymers. Common polymers such as chitosan (CS), sodium alginate (Na-Alg) and polyvinylpyrrolidone (PNVP) are employed to prepare blends and were also investigated on their own in some cases. Nonetheless, those studies often failed to implement such membrane materials on larger scales.[72-74]

Besides PVA, other hydrophilic polymeric materials such as polyelectrolyte complex (PEC) and polyamide (PA) are commonly studied. PEC membranes are fabricated using a layer-by-layer (LbL) assembly, which enables to have good control on the thickness deposited.[75] With

thin selective layers, high fluxes can be readily obtained. However the manufacturing of defect-free membranes is challenging, hence stability can be compromised.[56] To contrast this issue, thicker depositions were found to be efficient. On the other side, such strategy led to balanced separation performances by sacrificing the fluxes.[76]

Another class of polymeric membrane materials is polyimides (PI). High hydrophilicity is ensured by the presence of imide functional groups, able to form hydrogen bonds with water molecules.[77] Even though the results were promising and encouraging, some issues were faced in infrastructures for cellulosic ethanol, probably due to hydrolytic scission reactions between the imide groups and water molecules present in the feed.[78]

1.2.1.2.2. Inorganic membranes

Several inorganic membranes for pervaporation have been developed for pervaporation. The greatest advantage of using such materials is due to their high chemical and thermal stability. In addition, compared to polymeric membranes they do not suffer from swelling. These materials are typically zeolite, silica or metal-organic framework (MOF).

Zeolite membranes, commonly produced via hydrothermal synthesis or secondary growth method, are crystal layers with sub-nanometer pores.[79] The most studied zeolite is the NaA membrane (LTA-type) produced and commercialized by Mitsui Engineering and Shipbuilding Co. (Japan).[80] This material displayed outstanding separation performances for ethanol dehydration by pervaporation with water fluxes of 9 $kg.m^{-2}.h^{-1}$ and a separation factor of 10000 for a water concentration in the feed of 10 wt.%.[81] The CHA type not only showed excellent dehydration properties, but also strong stability towards acid (pH 3, 550 h).[82]

While, the results are appealing for ethanol dehydration, the application at larger scale is not easily implemented due to the manufacturing process. Compared to polymeric material, the costs are considerably more expensive (up to 100 times). Furthermore, it has been observed that inter-crystalline defects can occur due to adsorption of water inside the NaA zeolite. As a result, the selectivity drastically decrease at lower water concentrations.[83] Thus, some challenges still remain before the zeolite membranes can affirm their potential on the market.

Silica is another class of inorganic membranes. Major improvements have been achieved over the last decades. The current available membranes or latest developed prototypes show great butanol/isopropanol (IPA) dehydration performances with impressive water fluxes of approximately 10 $kg.m^{-2}.h^{-1}$ and water concentration in the permeate of 98 wt.%. The

membranes can perform at high temperatures (150°C) and are stable over long period of operation.[84-85] However the performance for ethanol dehydration are not convincing yet.[86-87]

1.2.1.2.3. Mixed matrix membranes (MMM)

A more recent and elegant approach to produce membranes with improved separation properties is to incorporate inorganic or hybrid nanofillers into a polymeric continuous phase to form mixed matrix membranes.[88] With the right choice of fillers, specific attributes can be assigned to the newly formed membrane. The idea is similar to polymer blending. The difference arises from the nature of the filler that are generally inorganic high performance particles. They are typically prepared by dispersing the fillers under vigorous stirring and sonication to facilitate their uniform distribution. MMM obtained from PVA and NaA zeolite particles were investigated. The resulting performances did not show great synergetic effect.[89]

1.2.1.3. Membrane characterization methods

Characterization techniques are an essential part of the development and optimization of polymeric pervaporation membranes, as they provide a detailed understanding of the membrane, from its structural and chemical composition to its thermal and mechanical properties. The main objective of membrane characterization is to establish the relationship between the membrane's inherent properties and its pervaporation performance.

1.2.1.3.1. Membrane morphology

The morphology of membranes is a major part of membrane characterization. It provides a large amount of information from different techniques and plays an important role at every stage of a membrane, from development and optimization to performance evaluation.

Scanning electron microscopy (SEM) operates on the principle of scanning a focused electron beam across the surface of a material to create high-resolution images. The electron beam interacts with the atoms of the sample, producing different signals. These signals are collected by detectors to form images. SEM provides fundamental insights about the morphology of both the surface and the cross-section of the composite membrane. Compared to optical microscopes, the resolution offered by SEM is significantly higher, allowing the visualization of structures down to the nanometer scale. Images of the membrane surface can reveal defects such as cracks and pinholes,[90-91] while cross-sectional images can be used to determine important parameters such as the thickness of the thin selective layer, and porous substrate information like pore size, porosity, anisotropy, and more.[92-93] Transmission electron microscopy (TEM) expands the capabilities of electron microscopy by providing nanoscale

resolution, thus allowing visualization of the finest membrane features. The main difference between the SEM and the TEM lies in how they are used to generate images: the SEM scans the surface of the sample with an electron beam to obtain topographical images, while the TEM focuses an electron beam through an ultrathin sample to reveal the internal structure and atomic composition. This technique is useful for evaluating the distribution of inorganic fillers in nanocomposite membranes, detecting microvoids, and measuring the thickness of active layers.[94-95] In combination with electron microscopy, atomic force microscopy (AFM) provides a more detailed view of the membrane surface. AFM is a technique that measures the interaction forces between a sharp probe (cantilever with a nanometric tip) and the surface of a sample. As the probe scans the surface, the cantilever is deflected by the attractive or repulsive forces between the tip and the sample. The deflection is measured by a laser beam that is reflected from the top of the cantilever into a photodetector. The cantilever's movements are used to collect data that is then used to create high-resolution topographical images of the surface. This enables the visualization of surface features and roughness.[92, 96] In addition to topographic analysis, AFM can also probe the mechanical properties of the membrane surface, such as stiffness and elasticity, which can be used to further identify specific materials and provide information about membrane homogeneity.[97-99]

1.2.1.3.2. Thermal properties

The thermal properties of pervaporation membranes, such as their thermal stability and response to temperature changes, are critical factors that directly affect their performance and lifetime in separation processes. Differential Scanning Calorimetry (DSC) and Thermogravimetric Analysis (TGA) are the main methods used for thermal characterization.

DSC measures the heat absorbed or released by a sample as it is heated or cooled over a range of temperatures. It is useful for determining the temperature of phase transitions, including the glass transition temperature, as well as melting and crystallization phenomena. The operating principle of DSC is based on the comparison of heat flows between a sample and an inert reference. The sample and reference are placed in separate crucibles inside the DSC calorimeter and heated or cooled at a controlled and uniform rate. The instrument measures the difference in heat flux required to maintain the sample and reference at the same temperature, which is recorded as a function of temperature or time. Thermal transitions in the sample, such as melting, crystallization, glass transition, and exothermic or endothermic reactions, produce changes in heat flux. These changes are detected by DSC and presented as curves, where the peaks represent the thermal events. The area under the peaks corresponds to the amount of heat

absorbed or released during the transition, allowing for the determination of thermodynamic properties such as transition enthalpy and specific heat capacity.[100] The glass transition temperatures and the degree of crystallinity are very important properties for pervaporation membranes.[101] The former provides information about the applicable temperature range for the process, due to the higher degree of thermal motion of a semi-crystalline polymer, specifically in its amorphous phases but also essential indications about blends and composition of fabricated membranes.[102] The latter provides indications about the robustness of the membrane matrix. Crystalline regions are impermeable, making them an important factor when it comes to producing membranes with high selectivity.[94, 103-104] TGA complements DSC by providing a detailed profile of the thermal stability of the membrane by measuring weight changes as a function of temperature. TGA can identify the onset of thermal degradation and quantify the residual mass at elevated temperatures. This offers insights into the compositional changes that occur during thermal exposure.[105] Such analysis is useful in evaluating the compatibility of membrane materials with manufacturing processes. By evaluating the appropriate temperature range, it is possible to prevent thermal degradation that may lead to performance degradation in high temperature pervaporation applications.[106] A particular useful aspect is the determination of the composition of the membrane, *e.g.*, the content of blends of different polymers or (block) copolymers.[107-108]

1.2.1.3.3. Structural and chemical properties

Pervaporation is a membrane separation process that relies on the chemical affinity between the permeants and the membrane material. Therefore, the physicochemical properties and chemical composition of the membrane determine its separation properties. Several analytical methods can be used to evaluate the different properties, such as Fourier Transform Infrared (FTIR) spectroscopy, Raman spectroscopy, Nuclear Magnetic Resonance (NMR) spectroscopy, etc.

FTIR spectroscopy is a widely used technique for determining qualitatively and quantitatively the functional groups present in the membrane material and their interaction with permeating species. When a sample is exposed to infrared radiation, certain radiations are absorbed, resulting in molecular vibrations including stretching, bending, or twisting modes. The corresponding spectrum represents the molecular absorption and transmission, creating a molecular fingerprint of the sample. Each chemical bond has a characteristic absorption signature in the IR spectrum, allowing the identification of functional groups and the overall chemical composition of the membrane. In attenuated total reflectance mode, this spectroscopy enables the identification of functional groups present over a thickness of around 1 μm.[109] This

technique is useful for verifying the chemical integrity of the membrane, *e.g.* after manufacture or after operation during troubleshooting analysis. It can be used to detect any chemical changes or degradation that may occur. By analyzing the absorption spectra, researchers can identify specific functional groups, such as hydroxyl or carboxylic acid groups, that affect the membrane's affinity for water or organic compounds in pervaporation processes. Another common use is to assess the degree of crosslinking in PVA membranes by monitoring the characteristic peaks of hydroxyl groups and the corresponding carbonyl stretch that appear after the crosslinking reaction has occurred.[110-111] A complementary method to FTIR is Raman spectroscopy. This technique operates on the principle of inelastic scattering of monochromatic light, called the Raman effect. The incident light interacts with molecular vibrations, resulting in scattered photons of different energy. The measurement of the wavelength and intensity of these scattered photons as a function of the incident light forms the basis of Raman spectroscopy. The shift in energy gives information about the vibrational modes of the molecules and thus the chemical structure and molecular interactions.[112] This method proved to play an important role in membrane development studies, such as confirming the functionalization and dispersion of carbon nanotubes (CNTs) in poly(vinyl amine)-poly(vinyl alcohol) composite membranes. It also assessed their structural integrity and interactions, which was crucial for enhancing the performance of these membranes in the pervaporation dehydration of ethylene glycol.[113] Alternatively, Raman spectroscopy was employed to characterize the structural features and defects in graphene oxide (GO), crucial for determining the material's quality and suitability for fabricating composite membranes aimed at improving pervaporation desalination processes.[114] The outermost surface chemistry of a membrane can be analyzed by X-ray photoelectron spectroscopy (XPS). The technique utilizes the photoelectric effect to measure the elemental composition, as well as the respective chemical and electronic states within a material. The irradiation of a sample by X-rays leads to the ejection of core electrons from their atomic orbits within the material being analyzed. This phenomenon occurs only if the X-ray photon energy exceeds the binding energy of the electrons. The ejected electrons travel toward a detector where they are quantified and their kinetic energy is measured. As a result, the binding energy of electrons can be calculated, which is characteristic of the type of atom and its chemical state, allowing the identification of the elements present on the surface material, their quantification and their chemical bonding state.[115-116] Such technique is relevant to determine the atomic composition of the elements in the top layer of the membrane, within a thickness of few nanometers. The surface hydrophobicity modification can be estimated by studying the ratio of the appropriate elements.

For instance, XPS was fundamental in confirming the successful grafting of an organic polymer onto the surface of ceramic membranes. The presence of fluorinated groups on membrane surface was evidenced, thereby confirming the modification intended to enhance the membrane's hydrophobic properties.[117] In another study, XPS was employed to confirm the successful crosslinking of chitosan membranes by monitoring the reaction between the anhydride groups of maleic acid and the amine groups of the chitosan.[118] Analyzing the molecular structure and determining the functional groups can also be accomplished with nuclear magnetic resonance (NMR) spectroscopy. It consists of analyzing the interaction of rotating nuclei in a strong magnetic field. In NMR spectroscopy, a stationary external magnetic field causes certain nuclei in a molecule to absorb selective radio frequencies. The energy absorbed induces a transition in the nuclear spins, which is observed in the NMR spectrum.[119-120] It is essential to accurately characterize the polymers that are used to prepare the membrane during its development. In such study, NMR was utilized to characterize the structure and composition of a polyacrylonitrile-*b*-poly(ethylene glycol)-*b*-polyacrylonitrile block copolymer, essential for the development of membranes for efficient acetone dehydration.[121] In another study, NMR spectroscopy was used to assess the crosslink density of PDMS, crucial for optimizing the structural integrity and performance of nanofiltration membranes.[122] Furthermore, NMR analysis allowed assessing the structural integrity of polysulfone-based anion exchange membranes in water electrolyzers, enabling the detection of chemical changes and degradation in the membrane materials.[123]

1.2.2. Fundamentals of pervaporation

Even though the phenomenon has been observed earlier, the word pervaporation was originally first proposed by P.A. Kober in 1917.[124] Rapidly, several articles were published on this topic, but it is only by the 1980s that came the first economically viable pervaporation systems. In 1982, GFT (Gesellschaft für Trenntechnik) installed the first pilot plant for ethanol dehydration.[55] Over the past decades, the technology has been further developed. Today, pervaporation's efficiency and application on an industrial scale have been widely proven.[43, 56, 125]

1.2.2.1. Membrane performance

The separation performance of a membrane on a liquid mixture is evaluated in terms of quantity of permeate obtained within a timeframe during operation. The quality of the separation is

revealed by the composition of the permeate. The permeation flux J of the component i is defined as,

$$J_i = \frac{m_i}{A \times t} \quad (1)$$

where m_i is the amount of component i collected within the operating timeframe t over the effective membrane area A.

In order to assess the selectivity of the membrane over the components present in the feed, the composition of the collected permeate is analyzed, *e.g.* by gas chromatography (GC). Typically, for binary mixtures, the term of separation factor β_{ij} is employed and defined as,

$$\beta_{ij} = \frac{y_i/y_j}{x_i/x_j} \quad (2)$$

where y and x are the weight fractions of the components i and j in the permeate and in the feed, respectively.

Although the separation factor is explicit, from a practical point of view and especially in industry, the composition of the permeate is very often sufficient. It allows to evaluate the separation in an even more relevant way, because it spontaneously allows to know the quality of the product at the end of the process.

These characteristics make it possible to evaluate the performance of a membrane during a pervaporation process. Nevertheless, these quantities are directly influenced by the intrinsic properties of the membrane material, but also by the experimental conditions.

In a single study, the performance of different membranes can be estimated. In order to compare the different samples, identical experimental conditions must be applied perfectly. This allows the differences in performance due to membrane properties to be highlighted, excluding effects from feed composition, temperature or pressure.[126]

In the research and development of new materials or manufacturing methods, it is important to be able to compare and evaluate the performance of prototypes. Thus, reporting results through normalized characteristic quantities allows for a more accurate comparison, by considering the driving force across the membrane. As in gas separation, a far more relevant way of presenting membrane performance is to use the permeability, which reflects the intrinsic properties of the membrane.[56]

According to the solution-diffusion model, the permeability P of a component i can be determined as,

$$P_i = \frac{J_i \times l}{(x_i \gamma_i p_i^{sat} - y_i p^p)} \quad (3)$$

where J_i is the permeation flux, l is the membrane thickness, x_i and y_i are the mole fraction of i in the feed and the permeate, respectively. p_i^{sat} and p^p are the saturated vapor pressure of i in the feed and the reduced pressure applied in the permeate, respectively. γ_i is the activity coefficient of i in the feed. The saturated vapor pressure can be obtained using Antoine's equation, while the activity coefficient can be calculated using appropriate models, such as Wilson, NRTL or UNIQUAC.[127]

When asymmetric membranes are studied, the thickness of the active layer is unknown and permeability values cannot be reported. In this specific case, the permeance (P/l) is employed to describe the separation performance.

Furthermore, the membrane selectivity α_{ij} is defined by the ratio of the permeabilities of the components i and j,

$$\alpha_{ij} = \frac{P_i}{P_j} \quad (4)$$

where P_i and P_j represent the aforementioned permeabilities of the components i and j.[126, 128]

A trade-off is frequently observed between the permeation through the membrane and the quality of the separation. Through the application of modifications, one is generally improved and leads to the decrease of the other.

1.2.2.2. Transport mechanism in pervaporation

The basic principle of pervaporation relies on the ability to separate components from a liquid mixture. During the separation process, the liquid (commonly specified as feed) is brought into contact with a semi-permeable membrane. The membrane acts as a barrier and the nature of the material employed plays a key role in the preferential sorption of one component from the feed mixture. Heat is usually supplied in order to promote the phase change from liquid to vapor during permeation through the membrane. On the downstream side, the permeating species, called permeate, are collected by cooling the vapors, which are condensed on the walls of a receiver. Either vacuum or sweep gas are employed to generate a gradient of chemical potential across the membrane, which allow to keep a constant driving force for the transport.[56] The

fraction that failed to permeate through the membrane goes back to the feed tank and is defined as the retentate (Figure 1-2). The process is often run in a batch mode and terminates when the required grade or purity is achieved. Besides the ability to overcome azeotropes, pervaporation is favorable for the separation of mixtures containing thermally sensitive components.[129]

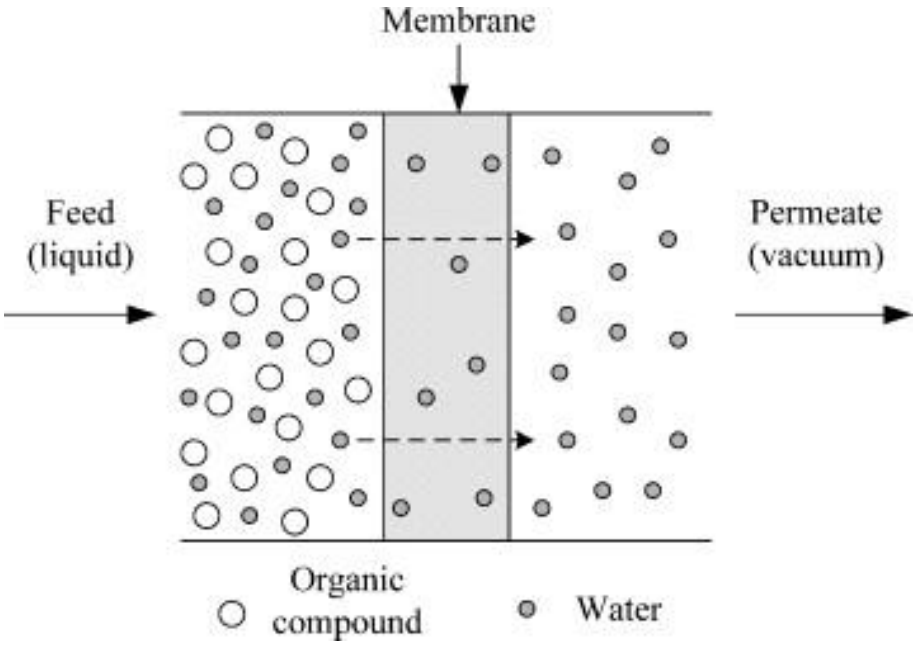

Figure 1-2. Pervaporation process for the dehydration of organic mixtures. Reprinted with permission from[130]

1.2.2.3. Solution–diffusion model

The most widely accepted transport mechanism is the solution-diffusion model, which was first proposed by T. Graham based on gas permeation experiments through homogeneous membranes.[131] The permeation of a component through the membrane is ensured by three consecutive steps. The first step is represented by the preferential sorption of one component into the membrane material at the upstream side. The component diffuses through the membrane to the permeate side, where desorption will conclude the transport phenomenon (Figure 1-3). Desorption is relatively faster than the first two steps. Hence sorption and diffusion are the rate controlling stages, which are thermodynamic and kinetic phenomena, respectively.[132] The permeability P is expressed as a function of the product of the two parameters:

$$P = D \times S \tag{5}$$

where D is the diffusivity and S the solubility.

By adjusting these two parameters, the separation performance of pervaporation membranes can be considerably affected.

The selective behavior depends on the ability of the molecules present in the mixtures to form specific interaction with the membrane material.[133] Using the Hildebrand or Hansen Solubility Parameters (HSP), such interactions can be predicted.[134] As a rule of thumb, similar solubility parameter values between the membrane material and one component from the mixture to separate indicates high probabilities of interactions. In other words, the perm-selectivity of this component is more favorable.[135] For the diffusivity component, the shape and size of the permeating species, as well as the mechanical properties or free volume of the membrane material are key role properties. A typical example is that the permeation flux is inversely proportional to the membrane thickness. A thinner layer generates a lower mass transfer resistance. Therefore, the permeation flux across the membrane is significantly enhanced.[136]

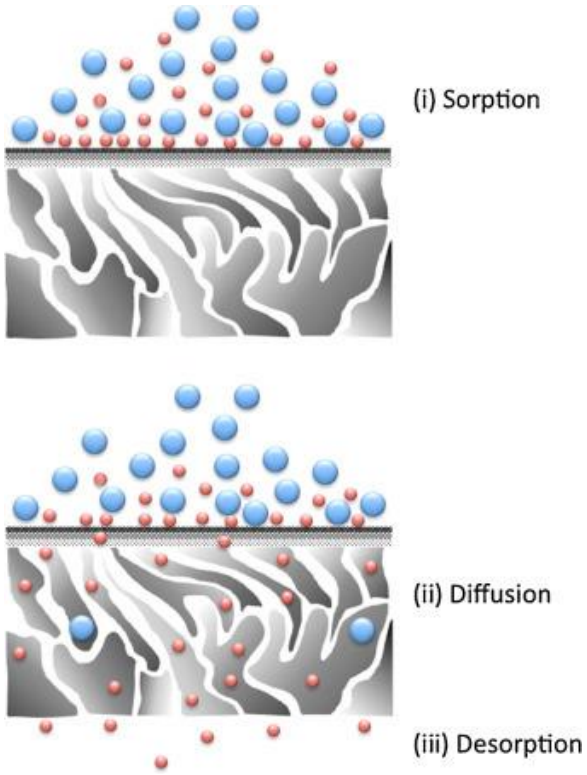

Figure 1-3. Representation of the solution diffusion model. Reprinted with permission from[68]

1.3. Synthesis of polymeric membrane materials

The design and synthesis of new polymeric materials are part of continuous development in many fields. To address the essential properties required for pervaporation and the tailored

fabrication of specific membranes, one must consider the unique demands of separation performance, chemical, thermal and mechanical resistance, and processability.

The primary property of a pervaporation membrane is its selectivity, *i.e.*, the ability to preferentially separate specific components based on differences in solubility and diffusivity within the membrane material. Concurrently, the membrane must exhibit sufficient permeability to ensure a practical flux, reflecting a synergy of properties, each playing crucial roles.[56] Since compound transport initiates at the liquid/membrane interface, the surface chemistry of the membrane, and consequently the choice of polymer, is a fundamental consideration. Regardless of polymer selection, the molecular weight must be sufficient to provide adequate film-forming properties, as polymers with lower molecular weights tend to form brittle films. To effectively separate one compound from another, the target compound must be capable of establishing numerous interactions (*e.g.*, hydrogen bonds, van der Waals forces) with the functional groups of the polymer(s) constituting the membrane. Depending on the separation type required, hydrophilic polymers may be employed to separate water from organic solvents, or hydrophobic polymers to separate organic compounds from water. The hydrophilic or hydrophobic nature of the membrane can be tailored to target the separation of aqueous solutions or organic mixtures, respectively. For example, integrating hydrophilic groups such as –OH, –COOH, or sulfonic groups into the polymer backbone enhances water affinity, beneficial for the dehydration of organic solvents.[137-139] Conversely, increasing hydrophobicity through the incorporation of non-polar moieties such as alkyl or aromatic groups, as well as fluorinated or siloxane segments, can be advantageous for the removal of organic compounds from water.[56, 140] In addition to the presence of functional groups, steric hindrance is another key parameter. Depending on the structure of the side groups, the polymer network can present a more or less packing density. This relates to the free volume, that is, the space not occupied by the polymer chains themselves, providing a path through which molecules of varying sizes can diffuse, related to steric exclusion by sieving.[68] Given the harsh conditions often encountered during pervaporation, such as high temperatures and exposure to aggressive solvents, the thermal and chemical stability of the membrane material is central.[141] Polymers should be solvent resistant, meaning they should swell upon interaction with one of the components to separate, yet not dissolve. Swelling can lead to undesired permeation of molecules due to their co-diffusion with the preferential permeating component.[142] Introducing cross-linking agents during membrane formulation and fabrication can further enhance the membrane's resistance to swelling and degradation. Different types of cross-linking exist, each with their advantages and limitations, often representing the weak points of the membrane due

to degradation because of chemical reactivity with components present in the mixture.[65, 143] Due to high operating temperatures (typically up to 100°C), polymers with high melting temperatures and inherent chemical resistance are required. Semi-crystalline polymers are particularly valuable due to the presence of crystallites which impart additional robustness, thereby considerably improving the resistance of the membrane, and are excellent alternatives to chemical cross-linking.[144] While tailoring membrane properties at the laboratory scale, it is crucial to consider the scalability and economic feasibility of the membrane production process for industrial applications. Composite membranes with the thinnest selective layer possible are necessary to minimize mass transfer resistance.[145] Therefore, the polymer/solution system should permit the preparation of such thin layers on porous supports, ensuring that the solvent used and/or the temperature during the coating process do not dissolve or degrade the substrate. Another fundamental aspect is the type of solvents used and the subsequent waste management. For example, PVA is a prime choice as the polymer is dissolved in water, thereby eliminating the need for hazardous chemicals and avoiding hazardous waste generation, with water readily evaporating at 100°C, which is preferable over solvents with high boiling points that require a higher energy supply for heating.

The design and synthesis of polymers for pervaporation membranes require a strategic approach to polymer chemistry, focusing on achieving a delicate balance between selectivity, permeability, stability, and processability. These properties are intricately linked to the polymer's molecular structure and synthesis approach, underscoring the importance of advanced polymerization techniques and thoughtful monomer selection in developing membranes that meet specific pervaporation needs. In this part, the main concepts about polymer materials synthesis will be presented. The various techniques to achieve specific structures and/or properties, as well as the methods to develop tailored architecture are described.

1.3.1. General concepts about free radical polymerization (FRP)

Since the last century, more than 50% of the manufactured synthetic polymers worldwide are obtained by FRP. Plastic materials settled in human life and contribute to shaping our modern activities.

Among the various polymerization techniques, FRP is relatively easy to implement and highly versatile towards impurities present in the reaction mixture.

The polymerization rely on the generation of free radicals, which further produces propagating radicals. Free radicals are typically produced by thermal or photochemical homolytic cleavage of covalent bonds or by a redox process. The formed radicals are transferred from the initiators to the vinylic monomer. The molecule turned now into another radical which will continue to propagate until all monomers are consumed or termination reaction occurs. The rate of propagation, corresponding to the chain growth, is highly dependent on factors such as radical reactivity, solvent and temperature. At the end of the polymerization, two types of termination can take place: combination between two chain ends or disproportionation which form an unsaturated end-group.

The most common initiators are: 2.2′-azobisisobutyronitrile (AIBN), potassium persulfate (KPS), dibenzoyl peroxide (BPO), and 2-hydroxy-4′-(2-hydroxyethoxy)-2-methylpropiophenone (Irgacure 2959). By adjusting the ratio [Monomer]:[Initiator], it is possible to target a degree of polymerization DPn as follow,

$$DPn = \frac{[M]_0}{[I]} \quad (6)$$

Such polymerization techniques are commonly employed to perform homopolymerization, copolymerization, crosslinking and grafting.

1.3.2. Amphiphilic block copolymer synthesis

The progress in polymer chemistry gave access to a variety of polymers with tailored properties, thus serving to select specific components, where the precise role of each lead to a well-controlled system. Two or more chemically different polymeric domains, covalently bound together are defined as block copolymers. More specifically, amphiphilic block copolymers are composed of both hydrophilic and hydrophobic blocks, often named as diblock (AB), triblock (ABA or ABC) or multiblock (ABCBA, ABCD, etc.). According to the required properties, amphiphilic block copolymers are built/designed by combining specific types of hydrophilic and hydrophobic blocks.

In order to prepare amphiphilic block copolymers, controlled polymerization techniques are commonly used: Atom transfer radical polymerization (ATRP),[146] reversible addition fragmentation chain transfer (RAFT),[147-148] ionic polymerization and combinations thereof.[149-150] Typically, sequential chain extension can be used, in which a first block is polymerized using the aforementioned techniques, forming the so-called macro-initiator. The immediate addition of a second monomer leads to chain-extension, yielding a diblock copolymer. This approach

allows the adjustment of each block length by terminating the corresponding chain extension according to the desired degree of polymerization. Tri- or multiblock copolymers can be obtained analogously either by sequential chain extension (asymmetric ABA, ABC, ABCD, etc.) or by a bifunctional initiator (symmetric ABA, ABCBA, etc.). Monomer conversion as well as the living character of the polymer chain are fundamental parameters to be considered among each chain extension.

1.3.2.1. Ionic polymerizations

1.3.2.1.1. Anionic polymerizations

Living anionic polymerization was demonstrated by Szwarc and coworkers in 1956.[151-152] Anionic polymerization is a chain growth polymerization technique in which polymer chains grow via an anionic propagating intermediate. Initially, a (nucleophilic) initiator reacts with a monomer to form a living anion that remains active throughout the reaction. This reactive anionic species propagates by successive addition of monomers without significant termination or chain transfer until all the monomer is consumed or the reaction is stopped. Anionic polymerization can be employed to polymerize a variety of monomers, including styrenes, dienes, acrylates, methacrylates, among many other vinyl monomers. This technique is also employed in the ring-opening polymerization of cyclic compounds, including epoxides, cyclic trisiloxanes, lactones, lactams, etc. The monomers should be able to stabilize the negative charge through charge delocalization. Temperature, solvent, and the nature of the counterion are critical parameters that affect the reaction kinetics and stability of the living anion. The presence of oxygen, carbon dioxide or moisture should be avoided as these impurities can quench the living anion and stop chain growth. This precise control results in polymers with high molecular weights and a narrow molecular weight distribution, which is critical for applications requiring high material performance.[153]

1.3.2.1.2. Cationic polymerizations

Cationic polymerization[154-155] is a type of chain growth polymerization that involves the growth of polymer chains by the reaction of monomers with a cationic initiator. The initiation step involves the formation of a cation, which is often generated by the action of a Lewis acid or other electrophilic agent (co-initiator), *e.g.*, water. By addition reaction, the proton thus formed cleaves the monomer's double bond, forming a new cation which can then react with another monomer. This type of polymerization is particularly effective when applied to monomers that stabilize positive charges, such as olefins and heterocyclic monomers (lactones, lactams, cyclic

amines) for cationic ring-opening polymerization. These monomers are usable due to their ability to stabilize intermediate carbocations through the presence of electron-donating substituent groups or ring strain of heterocycles. Like for anionic polymerization, cationic polymerization is sensitive to moisture and impurities, as these can quench the active carbocations, thus terminating chain growth.[156]

Ionic polymerization techniques are limited due to their high sensitivity to impurities. Hence, the solvent choice is important and the preparation of each reactant has to be handled very carefully to reach the desired purity grade. On the other hand, with ionic polymerizations, high monomer conversions can easily be reached by maintaining narrow polydispersity.[157] For example, polystyrene-*block*-poly(4-vinylpyridine) (PS-*b*-P4VP) has been successfully synthesized by anionic polymerization in a two steps sequential monomer addition. In some particular cases, modifications are required prior to the addition of the second monomer as for poly(ethylene oxide)-*block*-poly(ethyl ethylene) (PEO-*b*-PEE), in which a polybutadiene (PBD) precursor is first hydrogenated to yield the PEE macroinitiator. Subsequently, ethylene oxide is polymerized to obtain the diblock copolymer.[158] In another study, poly(acrylic acid)-*block*-polybutadiene (PAA-*b*-PBD) was prepared by sequential addition of butadiene and *tert*-butyl acrylate, followed by hydrolysis to its acid form.[159] The combination of different polymerization techniques is another possibility. Namely, the preparation of poly(dimethylsiloxane) (PDMS) by anionic polymerization was followed by activation and cationic ring-opening polymerization of 2-methyl-2-oxazoline (MOXA) monomers to obtain poly(dimethylsiloxane)-*block*-poly(2-methyl-2-oxazoline) (PDMS-*b*-PMOXA) diblock copolymers (Figure 1-4).[160]

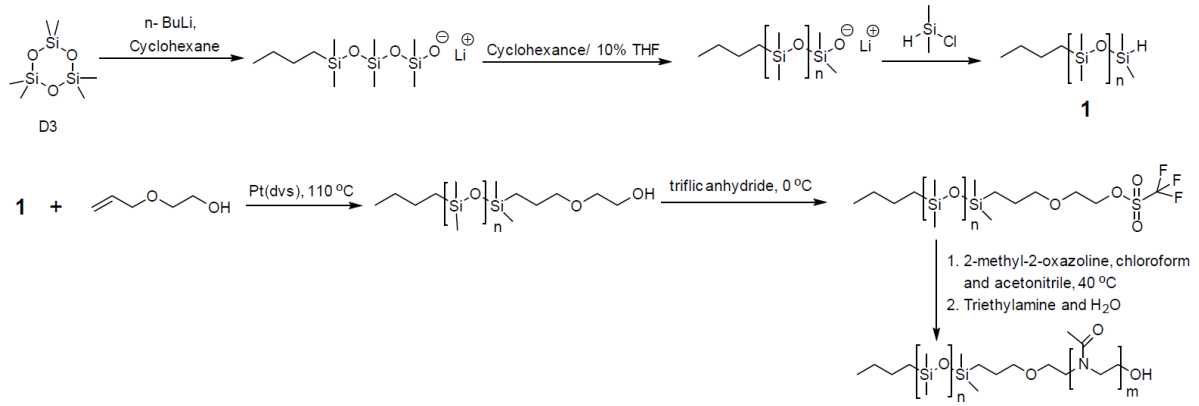

Figure 1-4. Synthesis route of PDMS-*b*-PMOXA combining both types of ionic polymerizations. Reprinted with permission from[160]

1.3.2.2. Controlled radical polymerization

Controlled radical polymerization techniques (CRP), such as ATRP or RAFT, have recently been developed and have provided interesting and more versatile alternatives for the production of block copolymers. Both techniques require an initiator. The polymerization is governed by an equilibrium between active species and dormant ones. The latter is constantly re-initiated in order to form the active species responsible for propagation through the addition of monomers. With these techniques, it is usually recommended not to exceed monomer conversions of 90%, above which the probability of termination is higher, risking to form dead chains unable to continue chain-extension.[147]

1.3.2.2.1. Atom Transfer Radical Polymerization

Atom Transfer Radical Polymerization (ATRP) is a controlled polymerization method that can be applied to synthesize polymers with well-defined molecular architectures and precise monomer composition. This technique is crucial for the manufacture of block copolymers and functionalized polymer materials.[161-163] The ATRP mechanism (Figure 1-5) is based on a redox reaction between a transition metal complex and an alkyl halide. It typically involves an initiator, an alkyl halide, a monomer and a transition metal complex as catalyst, together with its ligand. The metal complex (Mt^m / L_n) initiates the homolytic cleavage of the alkyl-halogen bond of the initiator, resulting in the generation of the metal complex with oxidation state n+1 (X-Mt^{m+1} / L_n) and a radical. The latter reacts with a vinyl monomer, which represents the propagation step. Subsequently, the radical species either terminates with another organic radical or is reversibly deactivated by $Mt^{m+1}X$ / L_n to form a halogenated dormant polymer chain. Then, a reversible equilibrium, involving active and dormant species, can be established. In order to control the polymerization kinetics and molecular weights, it is necessary to shift the equilibrium towards the dormant species that do not react with the monomer. In order to produce narrowly distributed (co)polymers, the transition between active and dormant species must occur rapidly.

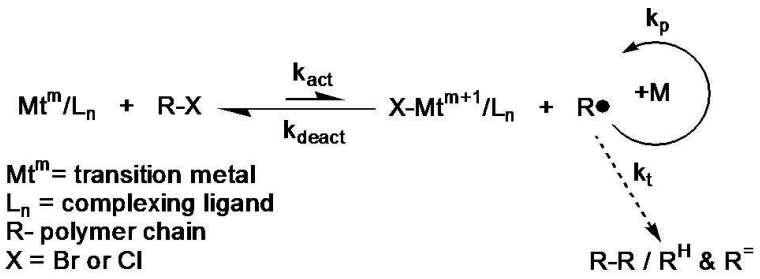

Figure 1-5. Mechanism of transition metal complex-mediated ATRP. Reprinted with permission from[164]

The selection of optimal reaction conditions and components is essential to achieve effective control of the reaction and to ensure the synthesis of high-quality polymers. The choice of ligand for the transition metal complex is crucial, as a suitable ligand stabilizes the redox states of the transition metal and facilitates electron transfer. The concentration of the catalyst directly influences the rate of the reaction and the equilibrium between the active and dormant species. By ensuring proper control, it is possible to minimize chain defects and optimize reaction efficiency. The development of ATRP variants, such as ICAR ATRP (Initiators for Continuous Activator Regeneration ATRP) and ARGET ATRP (Activators Regenerated by Electron Transfer ATRP), has been driven by the need to reduce the amount of copper required and to operate under gentler conditions. In ICAR ATRP, a continuous source of free radicals is employed to regenerate the low level of active copper (I), while in ARGET ATRP, reducing agents are utilized to regenerate copper (I) from copper (II), thus enabling polymerization at lower metal catalyst concentrations.[165]

1.3.2.2.2. Reversible Addition-Fragmentation Chain Transfer

Reversible Addition-Fragmentation Chain Transfer (RAFT) is an advanced technique for synthesizing polymers with precise molecular structures and narrow molecular weight distributions.[166-168] The mechanism of RAFT is based on the use of a specific chain transfer agent (CTA), which is often a thiocarbonylthio compound (R-S-C(=S)-Z), where R and Z are organic groups that modulate the stability and reactivity of the intermediate radicals. The polymerization process is initiated with conventional radical initiators (such as azo compounds and peroxides) that generate primary radicals. These radicals initiate addition to monomers to form growing polymer radicals. The crucial step in RAFT polymerization is the reversible reaction between these growing polymer radicals and the CTA. This reaction leads to fragmentation and the formation of new radicals that can further drive polymerization. This degenerative transfer process crucially mediates control over molecular weight and polydispersity index. The next stage is the propagation step, where more monomers are added

to the polymer chain by the new radicals generated by the RAFT agent. Due to the moderated radical environment afforded by the RAFT agent, termination reactions can still occur, albeit at a slower rate, through combination or disproportionation. This cycle of chain transfer and fragmentation regenerates radicals intermittently, thereby ensuring uniform polymer chain growth while maintaining a narrow molecular weight distribution.

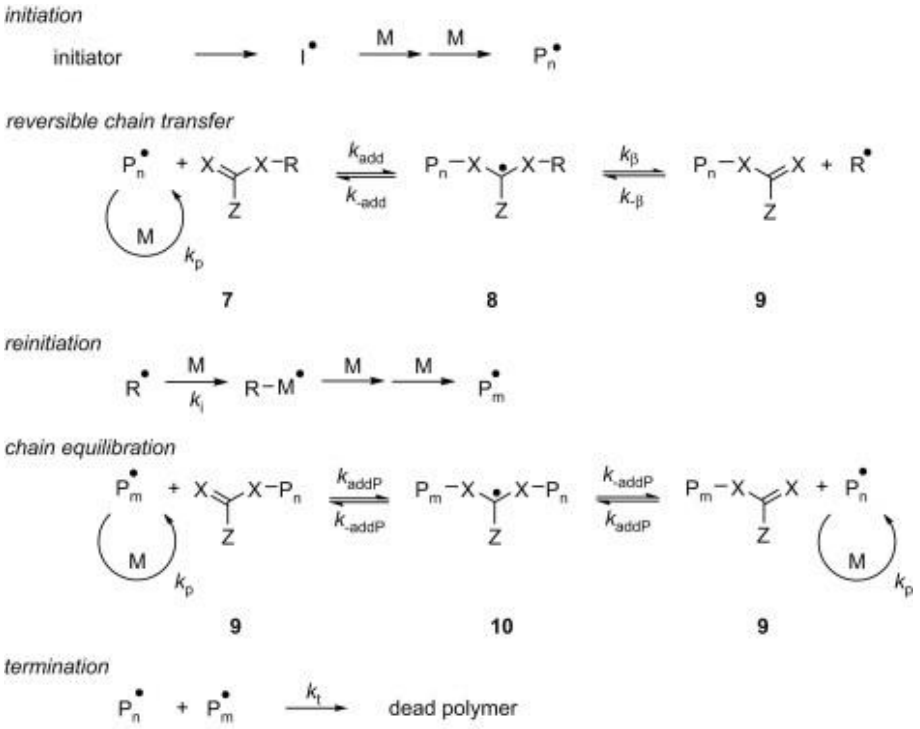

Figure 1-6. Mechanism of RAFT.[168]

The principal advantage of RAFT is its robustness and flexibility, capable of operating efficiently with a wide range of monomers ((meth)acrylates, styrenes, (meth)acrylamides, vinyl esters/amides) and under various polymerization conditions. This versatility makes it a suitable method for the synthesis of block copolymers. Several key parameters influence the efficiency of RAFT polymerization, in particular the nature of the RAFT agent employed. Thioesters, dithioesters, trithiocarbonates and xanthates are commonly used agents, each presenting distinct characteristics in terms of stability and activity depending on the desired polymer structure. The choice of RAFT agent is crucial to achieve good chain growth control and a narrow molecular weight distribution.[168-169]

The combination of techniques is emerging as a powerful strategy for the synthesis of block copolymers with complex architectures and functionalities. The joint use of these controlled polymerization methods not only enables precise manipulation of chain length and block composition, but also the incorporation of a variety of functional monomers that are difficult to

polymerize by a single technique. This hybrid approach offers exceptional flexibility in copolymer design, exploiting the specific advantages of each technique to overcome the limitations inherent in using a single polymerization method. In an innovative approach, a bromoxanthate iniferter was synthesized and used to specifically initiate RAFT polymerization of vinyl acetate (VAc) via a xanthate group. This macroinitiator was then employed to generate block copolymers, including PVAc-*b*-PS, PVAc-*b*-PMA, and PVAc-*b*-PMMA, by ATRP of styrene and methyl (meth)acrylates.[170] In another example, polystyrene-*block*-poly(vinyl alcohol) (PS-*b*-PVA) was obtained from PS prepared by ARGET ATRP and modified to a macroinitiator for RAFT on which PVAc has been polymerized, followed by hydrolysis to yield in the final PVA block.[171]

Although, the possibility of combining synthetic approaches broadens the library of accessible polymers, chemists still need to work hard on the quantitative attachment of the re-initiation site for the next polymerization, which is highly recommended to prevent purification difficulties. To circumvent this problem, two or more homopolymers can be connected together using coupling reactions such as Diels-Alder, copper-catalyzed azide-alkyne cycloaddition (CuAAC) or thiol-ene click chemistry, thus offering an increased number of possibilities. To illustrate, PAA-*b*-PBD has been prepared by combining poly(*tert*-butyl acrylate) (P*t*BA) and PBD homopolymers, both synthesized beforehand. A hydrolysis step leads to the final diblock.[172] Poly(dimethyl siloxane)-*block*-poly(ethylene oxide) (PDMS-*b*-PEO) diblock copolymers were synthesized using ring-opening polymerization of hexamethylcyclotrisiloxane to obtain PDMS-N_3 and further coupling with PEO-Alkyne chains via click chemistry.[173] Complete end-group functionalization and equimolar ratios of both homopolymers are required, preventing the challenging removal of unreacted homopolymers. Increasing the number of blocks introduces more challenges, especially in re-initiation, purification and finding suitable solvent for all the blocks.

1.4. Self-assembly of amphiphilic block copolymers

The self-assembly of amphiphilic block copolymers in solution leads to the formation of many different assemblies including spherical, cylindrical, gyroidal and lamellar structures.[174] These assemblies are directly influenced by intrinsic molecular parameters of the amphiphilic block copolymers and the conditions in which the self-assembly process takes place (concentration of the copolymer, presence of solvents, temperature, etc.). In this respect, the hydrophilic to the total mass ratio (*f*) calculated as the ratio of the molar mass of the hydrophilic block to the total

molar mass of the copolymer is an important parameter, which governs the resulting supramolecular assembly:

$$f = \frac{m_{hydrophilic}}{m_{BCP}} \tag{7}$$

Another molecular parameter influencing the self-assembly into different assemblies is the packing parameter ($p = v/a_0 l_c$; v = volume of the hydrophobic part, a_0 = contact area of the head group, l_c = length of the hydrophobic part) that describes the degree of curvature (Figure 1-7). For low packing parameter values ($0 < p < 0.5$), the curvature gradually decreases from high to medium, resulting in the formation of spherical or cylindrical micelles, respectively. For higher values ($0.5 < p < 1$), the curvature is considerably low, which is more favorable for vesicular structures. The dispersity, $Đ$, of the copolymer is affecting the size distribution of the formed nanostructures: a narrow dispersity typically leads to uniform-sized, whilst on the opposite, a more polydisperse population is obtained.[175-176]

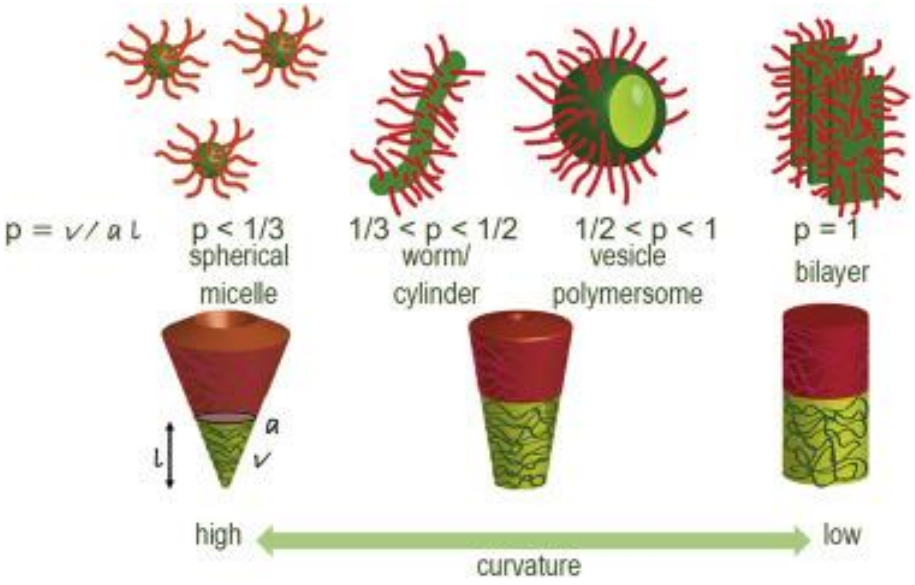

Figure 1-7. Influence of curvature of the amphiphilic block copolymer on the self-assembly formation. Reprinted with permission from[177]

In the film rehydration method, the block copolymers are first dissolved in an appropriate organic solvent, followed by evaporation either with a stream of nitrogen or by applying vacuum in a rotary evaporator. Rehydration takes place by pouring aqueous solution to the dried film, resulting in the detachment of the structures from the substrate surface.

With the solvent switch method, the self-assembly is induced by adding water drop-wise into a dissolved and molecularly dispersed polymer organic solution, thus, gradually exchanging the organic solvent with water. The self-assembly is immediately quenched by being poured slowly

into an excess of water under continuous stirring in order to kinetically trap the structures.[178] Finally, the organic solvent is removed from the solution via dialysis.[179] As it has been demonstrated by Daubian et al.,[180] depending on the chemical nature of the amphiphile, the solvent switch method may perform faster than the film-rehydration, especially when many metastable phases of the block copolymer can be formed, leading mostly to less aggregates.[181]

2. Aim and motivation

As a renewable biofuel, bioethanol plays a major role in the energy landscape worldwide, contributing to the transition to more sustainable energy sources. Used to replace or supplement gasoline, bioethanol reduces dependence on fossil fuels and greenhouse gas emissions, thus aligning with sustainable development goals. Pervaporation is an important option in bioethanol purification, particularly in the final dehydration stage to achieve the purity standards required for its use as a fuel. Polymeric membranes for dehydration of first generation bioethanol by pervaporation were successfully developed in the past. Today, second and third generation bioethanol is produced from non-food crops (*i.e.* wood, organic waste or specific biomass crops) and contains impurities such as organic acids, furfural, aldehydes *etc*.[182] PVA membranes are widely used for their efficiency and relatively low cost, making them attractive for industrial applications. However, the acetaldehyde present in second generation bioethanol can react reversibly with PVA, thus deteriorating the membrane structure. This degradation reduces the stability and lifetime of the membranes, thus requiring improvements to ensure their long-term integrity. Due to these changes, these materials cannot be used as membrane for dehydration processes of second and third generation bioethanol. The main goal is to develop a membrane compatible with those impurities. Therefore, the focus is particularly on the design and development of new polymeric membrane materials. These new membranes will need to offer enhanced chemical resistance, capable of withstanding exposure to aldehydes without undergoing significant degradation. Through copolymers synthesis, molecular manipulation and use of nanotechnology tools, we propose to develop new polymeric pervaporation membranes with a performance beyond what has been reached up to now. Particularly, these membranes shall be more stable to harsh chemicals present in bioethanol.

Although commercial acetaldehyde-resistant membranes (PERVAP™ 4155 series) are already available, their selectivity remains below the required level for demanding applications such as bioethanol purification. An effective approach to improving these systems involves a comprehensive study of existing membranes, with particular emphasis on exploiting the pH-responsive properties of the copolymers used in their composition. Thus, in the first chapter, the pH responsiveness of two commercial PERVAP™ composite membranes containing a PNVP-*co*-DMAEMA copolymer is assessed. To gain a deeper understanding of this phenomenon, experiments conducted under acidic, basic, and neutral conditions can provide valuable insights. The objective of these experiments is to assess variations in membrane

performance and identify optimal conditions for maximizing selectivity. The aim is to gain a better understanding of membrane behavior in different pH environments. In particular, it is of interest to study the structural changes that occur in order to develop strategies to improve membrane selectivity. A significant increase in selectivity could make the membrane efficient enough to justify its use on an industrial scale, offering a viable solution for bioethanol production processes.

The synthesis of tailored copolymers presents an opportunity to overcome the limitations of commercial membranes, in particular by improving their selectivity while preserving membrane stability in the presence of specific impurities such as acetaldehyde. Thus, chapter two is based on the development of new materials to tune the separation performances and the formation of innovative cross-linking methods resistant in particular to acetaldehyde. For this purpose, the commercial copolymer, PNVP-*co*-DMAEMA and an alternative, P(NVP-*co*-PNVIm) are synthesized by varying the composition of each monomer. In order to enhance the stability of the membrane, a method to induce crystallinity is investigated. The presence of crystalline phases in PVA is crucial to improve its robustness. The crystallinity of PVA directly influences many of its mechanical and physicochemical properties, essential for membrane lifetime and efficiency. The crystalline regions within PVA act as reinforcement points within the polymer matrix, thereby increasing the mechanical strength and thermal stability of the polymer. Furthermore, the degree of crystallinity affects the permeability and selectivity of the membrane. A more ordered structure can reduce the swelling phenomenon and inhibit the permeation of undesired molecules, while promoting the selective transport of other substances. Our objective is to develop a membrane that not only meets the separation requirements but also withstands the challenges posed by impurities in bioethanol. This research, therefore, aims to explore how variations in copolymer composition can influence critical membrane properties such as flux and selectivity, with the ultimate goal of achieving a formulation that maximizes separation efficiency, while withstanding exposure to impurities.

Innovation in membrane design is essential to overcome the limitations of existing systems. In the third chapter, we tackle this challenge by focusing on the synthesis of block copolymers with properties and structures specifically designed to produce membranes without the need for crosslinking agents or catalysts. This approach is based on exploiting the individual features of each segment of these copolymers, which are carefully designed to perform specific functions: on the one hand, to ensure the separation properties necessary for the desired application, and on the other, to ensure membrane stability and integrity. This research therefore aims to overcome the limitations of traditional materials used in pervaporation membranes by

developing copolymers that, through their unique molecular design, offer significant advantages. The potential benefits of these innovative copolymers include the ability to achieve more selective and stable separation, while avoiding the complexities and costs associated with the use of external chemical additives in membrane manufacturing processes.

The development of advanced membranes for pervaporation offers promising prospects for the bioethanol industry. By enhancing the chemical stability of membranes against impurities, it is possible to extend their lifetime, increase separation efficiency, and contribute to the production of high-purity bioethanol, thereby reinforcing its role in the future of sustainable energy. These developments are of critical importance for the industrial scale-up of these technologies and for the full exploitation of the cost-reduction potential associated with these membrane technologies for the latest generation bioethanol production processes.

3. pH-triggered membrane in pervaporation process

This chapter contains parts of a published work: Alessandro Angelini, Csaba Fodor, Wilfredo Yave, Luigi Leva, Anja Car and Wolfgang Meier. *ACS Omega* **2018,** *3* (12), 18950-18957.

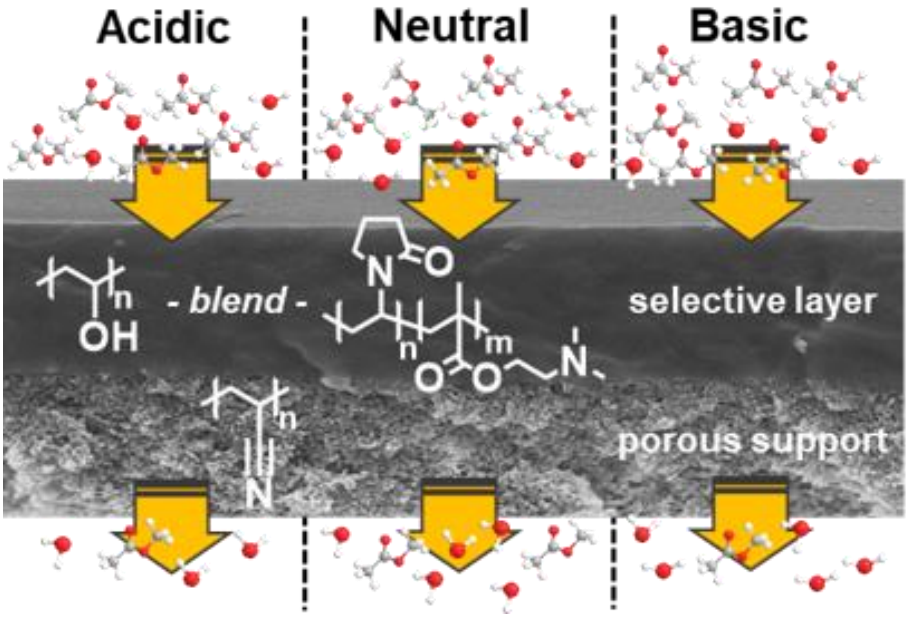

3.1. Introduction

In the last decades, great attention has been dedicated to developing and scaling up novel and advanced membrane materials.[183-184] However, only few polymers are used to produce membranes at large scale.[185-186] Lack of understanding of material properties and its correlation with membrane behavior under real operating conditions are usually the reasons for failing.

One of those novel materials are the so-called stimuli-responsive polymers. Such polymers as membranes are also known as intelligent or smart membranes[184, 187] as they allow intelligent control of separation when the environment changes. Because they exhibit trigger behavior predictably to pH,[188] temperature,[189] different fields,[190] or ionic strength,[191] new applications can be developed based on these polymeric membranes. In fact, by introducing pH-responsive groups and controlling ionic strength, the membranes were able to release drugs,[192] improve the separation performance in water treatment[193] and perform as chemical sensor and flow regulator.[194]

The commonly available pH-responsive functional polymers are weak polyelectrolytes with carboxyl, pyridine, or amino groups.[195-197] The presence of acidic groups in polymers (e.g. carboxyl groups, pyridine) at low pH induces the intermolecular hydrogen bonding formation, thus leading to shrinkage of the polymer chains. While at high pH, carboxyl groups dissociate into carboxylate ions, resulting in a high charge density, which trigger the swelling of the polymer. Polymers containing basic groups (e.g. amino groups) show opposite behavior compared to polyacids. At low pH, the amino group is protonated, and the material exhibits hydrophilic character and at high pH, hydrophobic properties are pronounced. As a result of protonation/deprotonation, swelling properties of these polymeric materials are changed.[184]

A typical polymer containing amino groups used to prepare stimuli-responsive membranes is PDMAEMA. The interesting feature of this polymer and derivatives (copolymers) is their pH- and temperature-responsive nature.[198] These polymers were used as graft material in the membrane and as a blend with other polymers to obtain dual stimuli-responsive properties.[199-200] PDMAEMA was also used as membrane material for gas separation,[201-204] nanofiltration,[205] and microfiltration.[200, 206] In addition, PDMAEMA copolymers were synthesized and investigated as micelles for drug delivery.[195, 207-208] Despite the overall high number of references discussing pervaporation membranes,[68] up to date there are only few works about pH-triggered membranes for pervaporation and their behavior under variable and industrial separation conditions.[209-211]

In the present work, pervaporation membranes based on P(NVP-*co*-DMAEMA) with pH-trigger behavior are investigated. These membranes are the commercial PERVAP™ 4155-XX membranes for alcohol removal from other solvents. Although these membranes are already applied for dehydration of various solvents and methanol removal from neutral mixtures,[212-213] the feature as pH-responsive pervaporation membrane in acidic and basic mixtures has not been reported yet. In the industry, during the dehydration processes and methanol removal from other solvents, many mixtures have acidic and/or basic nature, depending on impurities present in the streams. Thus, understanding the membrane behavior under triggered conditions is extremely important for the membrane process and scale up. In particular, these membranes are stable in the presence of acetaldehyde, *i.e.*, their separation performance remains unchanged over a long period of exposure, indicating their compatibility with bioethanol feedstocks containing significant impurities, particularly acetaldehyde. Although these membranes show remarkable stability, their selectivity in the separation of ethanol-water mixtures remains insufficient for industrial-scale applications (bioethanol). This limitation highlights the need to improve selectivity without compromising flux. In this context, the pH-responsive character of the

incorporated copolymer offers a promising way to fine-tune the separation properties by adjusting the pH of the medium. A binary mixture of methyl acetate/water is commonly employed to assess the quality and performance of production lots of commercial membranes PERVAP™ 4155-XX. The use of this specific mixture enables a more thorough examination of the membrane's behavior, particularly the observation of how its separation performance may vary with the pH of the environment. In order to better understand this phenomenon, experiments are performed under acidic, basic and neutral conditions. The purpose of these tests is to evaluate variations in membrane performance and to identify potentially favorable conditions for maximizing selectivity. The objective is to gain insight into the behavior of the membrane in different pH environments. In particular, it is of interest to study the structural changes that occur in order to develop strategies for improving the membrane's selectivity. A significant increase in selectivity could make the membrane efficient enough to justify its use on an industrial scale, offering a viable solution for bioethanol processes.

3.2. Results and discussion

It is first necessary to describe the methodological procedures adopted to characterize the materials and assess their functional properties before turning to the detailed analysis of separation performance. Initially, an extensive study of the physicochemical properties of the copolymer utilized in the membrane was performed. The objective of this preliminary characterization was to identify the composition of the copolymer and the properties that could influence membrane performance variation during pervaporation. Subsequently, in order to provide an accurate representation of the behavior of commercial membranes, dense films with the same PVA/copolymer composition were prepared. These films served as models for further characterization and allowed rigorous evaluation of properties in various chemical environments. Finally, pervaporation tests were carried out under different media conditions (acidic, basic, and neutral) to observe variations in membrane behavior. These tests provided essential data on separation efficiency and membrane stability.

According to DeltaMem AG, the two tested membranes are fabricated from PVA and P(NVP-*co*-DMAEMA).[214] The copolymer content in PERVAP™ 4155-30 and PERVAP™ 4155-70 is 70 and 30 wt.%, respectively. NMR and ATR–FTIR were performed to verify the molecular structure of used P(NVP-*co*-DMAEMA). Homopolymers of PNVP and PDMAEMA were also analyzed to correlate with the copolymer.

Figure 3-1 displays the ^{1}H NMR spectra, where the observed peaks fit to the expected chemical structure of the copolymers. The peaks also agree with those reported in the literature for similar copolymers.[215] The characteristic peaks of the copolymer backbone related to the VP units appeared between 1.3 and 1.78 ppm, and between 3.00 and 3.40 ppm. Peaks from 1.80 to 2.50 ppm and between 3.00 and 3.40 ppm are assigned with the protons of the heterocyclic ring in the VP units. The signals of the DMAEMA units in the copolymer structure appear in the region of 1.05 to 1.23 ppm and 1.80 to 2.10 ppm, corresponding to the methyl and methylene protons in the backbone. The methyl protons of the DMAEMA units appear at around 2.30 ppm, and the characteristic peaks around 2.56 and 4.08 ppm are assigned with the methylene groups in the DMAEMA units.

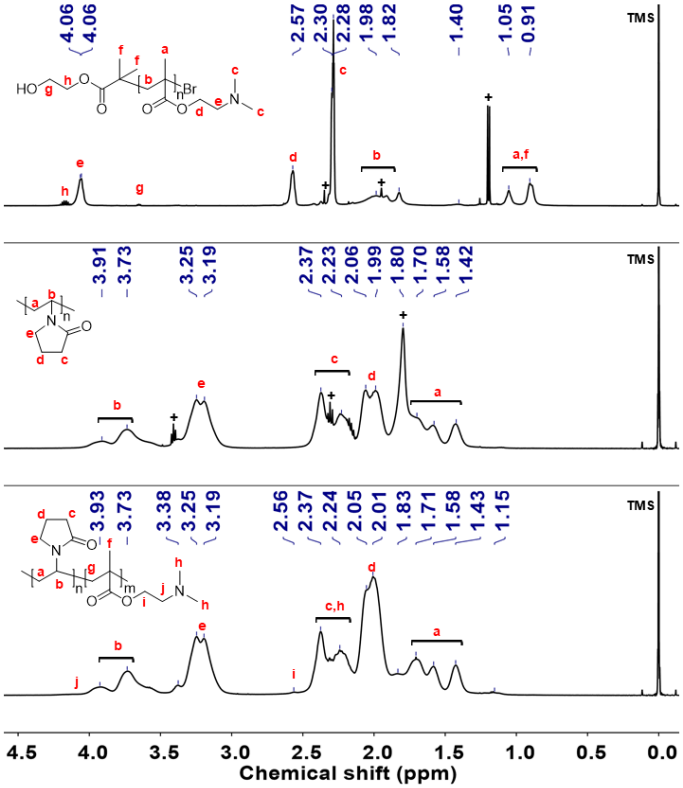

Figure 3-1. Phase and baseline-corrected ^{1}H NMR spectra of the neat polymers (PDMAEMA and PNVP) and the P(NVP-*co*-DMAEMA) copolymer (solvent: $CDCl_3$, temperature: RT, number of transients (n_t): 256 and relaxation time (d_1): 1.5).

The ATR–FTIR spectra of both homopolymers and P(NVP-*co*-DMAEMA) copolymer, depicted in Figure 3-2, were found to be consistent with the corresponding macromolecular structures.[215-216] The absorption bands at 1465 and 1425 cm^{-1} are characteristic absorptions of the pyrrolidinyl group, and the bands at 1654 and 1024 cm^{-1} are attributed to the carbonyl group

as well as the C–N stretching vibrations in PNVP. The characteristic absorption bands of PDMAEMA homopolymer can be assigned to the C═O stretching vibration at 1730 cm^{-1}, (C–H(−N(CH_3)$_2$)) stretching vibrations between 2770–2940 cm^{-1} as well as the N(CH_3)$_2$ deformational stretching vibrations around 1459 cm^{-1}. The characteristic bands of the copolymer can be noted to stretching vibration of the carbonyl group at 1732 cm^{-1}, the deformational stretching vibrations of the secondary amine functional group at 2773–2790 cm^{-1}, and the stretching vibration of C–N bond at 1120–1170 cm^{-1}, related to the DMAEMA content in the structure. The band around 1640 cm^{-1} arising from the C═O stretching vibration mode, the C–N stretching vibrations appear around 1410 cm^{-1} due to the VP units in the copolymer.

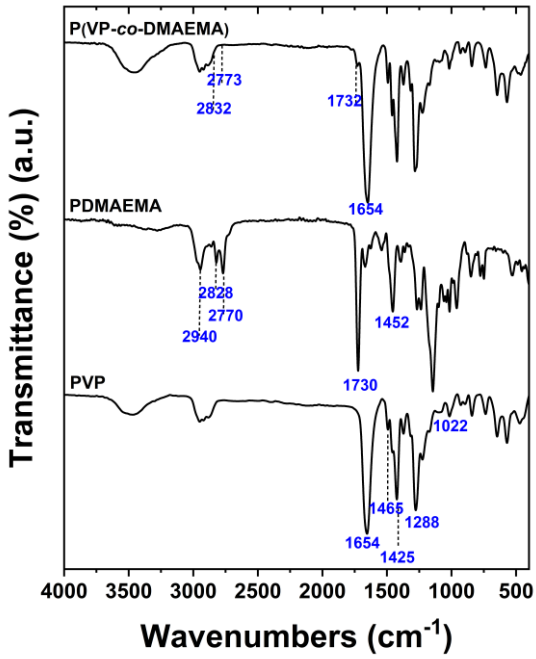

Figure 3-2. ATR–FTIR spectra of the neat polymers (PDMAEMA and PNVP) and the P(NVP-*co*-DMAEMA) copolymer (scan number: 128, nominal resolution: 4 cm^{-1}).

The membrane structure of PERVAP™ 4155-30 and PERVAP™ 4155-70 was analyzed by SEM, and the cross-section of the membranes is shown in Figure 3-3. The PVA and copolymer-based selective layer is at the upper part of membrane tightly adhered to the polyacrylonitrile (PAN) porous support (bottom), and neither of the PERVAP™ 4155-30 and 4155-70 samples have voids, indicating a good compatibility between the porous support and the selective layer. In both cases, the membrane thickness is around 2 μm. These representative SEM images are

tilted, and thus, in addition to the membrane cross-section, the surfaces of the composite membranes are also visible, which are uniform.

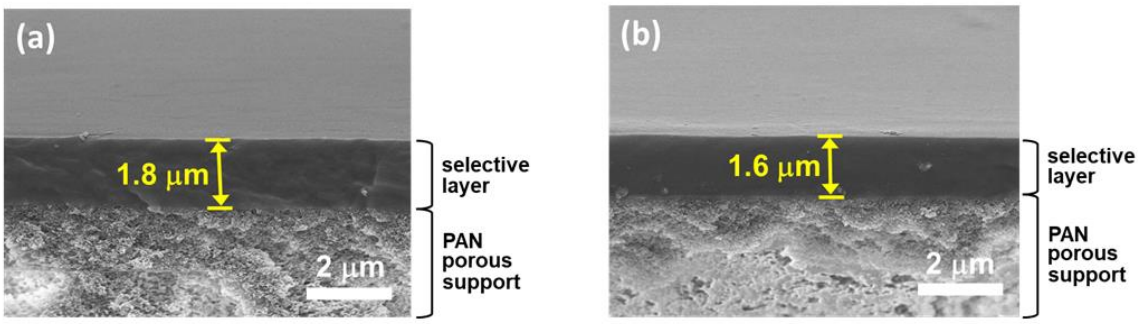

Figure 3-3. Representative SEM images of membrane cross-section and surface (a) PERVAP™ 4155-30 and (b) PERVAP™ 4155-70.

Unlike other reports on membranes with pH-responsive nature, where the membranes are first treated with acidic and basic aqueous solutions before testing, here the membranes are not pretreated and are continuously contacted by different mixtures. The pervaporation tests are performed by using MeAc/water mixtures containing HCl and NaOH, and in both cases, the concentration is controlled (2 mmol/L). We have controlled the HCl and NaOH concentration because the pH measurement in organic mixtures is not reliable due to the unstable readings, long response time, measurement errors, and because pH is a measure of H^+ concentration in aqueous solutions.

The pervaporation operating conditions were identical for all tests, that is neutral, acidic, and basic condition. Therefore, the comparison of flux and permeate concentration as separation performance data is possible. Two sets of pervaporation tests were performed. On one hand, for each mixture and for each test, a new membrane sample was used. On the other hand, the same membrane was tested in all conditions to see the reversibility of separation performance. The order of tests was as follows: neutral, acidic, neutral, basic, and neutral.

The water flux and permeate concentration as a function of feed water concentration for both membranes are shown in Figure 3-4. The permeate concentration values (red circle data) for PERVAP™ 4155-30 (Figure 3-4a) are slightly lower than those for PERVAP™ 4155-70 (Figure 3-4b). These results are expected due to the cross-linking degree of the membranes. PERVAP™ 4155-30 has 70 wt.% of copolymer and 30 wt.% of PVA, and because of PVA content in the membrane, this membrane is less cross-linked than PERVAP™ 4155-70. The content of PVA in the polymer matrix is directly correlated with the degree of cross-linking,

that is, the higher the PVA content in the membrane, the higher the cross-linking degree (information received from DeltaMem AG). Because PERVAP™ 4155-30 is less cross-linked than PERVAP™ 4155-70, it swells more (see Figure 3-5) and presents slightly lower values of water permeate concentration.

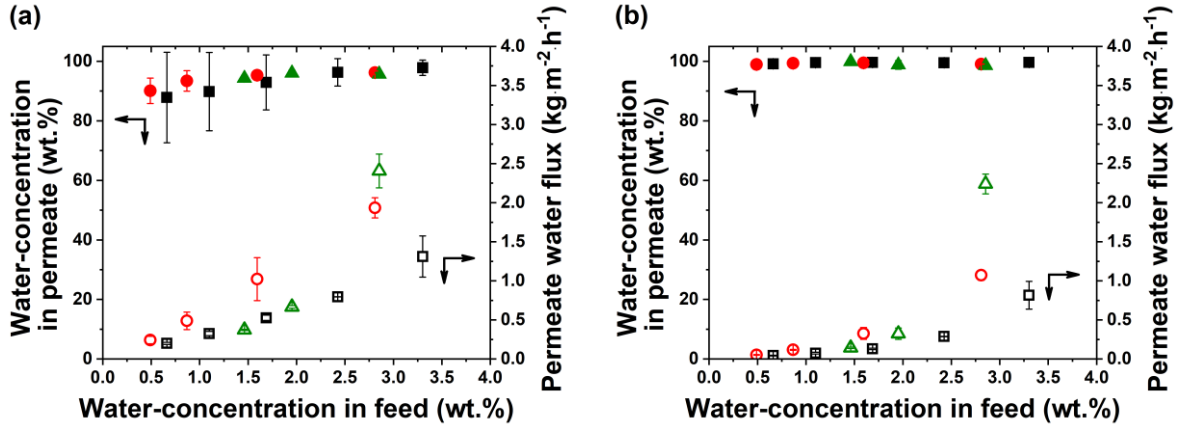

Figure 3-4. Separation performance of membranes (a) PERVAP™ 4155-30 and (b) PERVAP™ 4155-70 for dehydration of binary MeAc/water mixtures at 85 °C and 10 mbar under different conditions (black square: acidic, red circle: neutral, green triangle: basic).

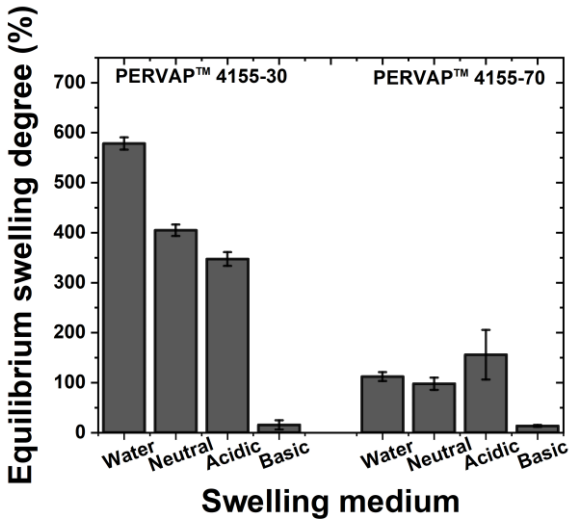

Figure 3-5. Equilibrium swelling ratio (ESR) (%) of the free-standing dense films with different P(NVP-*co*-DMAEMA) and PVA ratios in water and various binary (MeAc/water) mixtures.

The permeate concentration values in PERVAP™ 4155-70 are not dependent on feed nature (acidic, neutral or basic). While for PERVAP™ 4155-30 in acidic condition, they are shifted to higher values (Figure 3-4a). The water permeate concentration increase in this membrane is due to the presence of the pH-responsive copolymer and its high content; hence, under acidic

condition, this membrane swells less and is more hydrophilic (discussed later), and thus, the selectivity of the membrane is improved.

Pervaporation tests performed with neutral mixture show that PERVAP™ 4155-30 exhibits higher water flux than PERVAP™ 4155-70 (compare open red circle in Figure 3-4a,b). This difference is also explained by the content of PVA in the membrane (cross-linking degree and swelling of membrane, described above). As PERVAP™ 4155-30 has 70 wt.% of copolymer, the shifting of water flux to lower values is more pronounced than that in PERVAP™ 4155-70, when the pervaporation tests are performed in acidic conditions (compare the red and black experimental points). The decrease of water flux and the increase of permeate concentration are interesting results, and they are attributed to the DMAEMA units in the copolymer. As described above, the PDMAEMA is a pH-responsive polymer, and thus, this segment of copolymer is protonated in acidic mixture. Because of amine protonation and the presence of PVA (containing $^{-}$OH) and Cl^{-} ions (from HCl), the free movement of copolymer segment containing the protonated amine is slowed down, and the material as such does not swell or slightly shrinks (PERVAP™ 4155-30, Figure 3-5). This makes the material less flexible and decreases the fractional free volume of polymer that results in a water flux decrease through the membrane and selectivity improvement.

Under basic conditions, the pervaporation tests gave even more interesting results. At the beginning, at higher water concentration in the mixture, the water flux is higher than in the neutral condition (see the open green triangle at > 2.5 wt.% of water in feed, Figure 3-4). After the mixture is dehydrated, the water flux drops to lower values like in acidic conditions. These results can be partially explained by the decreased swelling of the membrane (Figure 3-5) and by the hydrophilic nature of the material under basic conditions (Figure 3-6). High water content in the mixture under basic conditions and the hydrophilic nature of material seem to increase the swelling of the membrane. However, it happens only at the beginning of tests. Later, once the MeAc is dehydrated, a pronounced decrease of flux is observed. This behavior can be explained by the gradual deprotonation of amine groups and simultaneous hydrogen bonding between deprotonated amine and OH- groups present in PVA. At the end, the material (membrane) becomes less swollen because of the lower water content in the mixture, the membrane shrinks, and consequently the water flux drops. Because of a complex mechanism of deprotonation and formation of hydrogen bonds, the PNVP segment present in the copolymer may also play a certain role on water flux decrease.

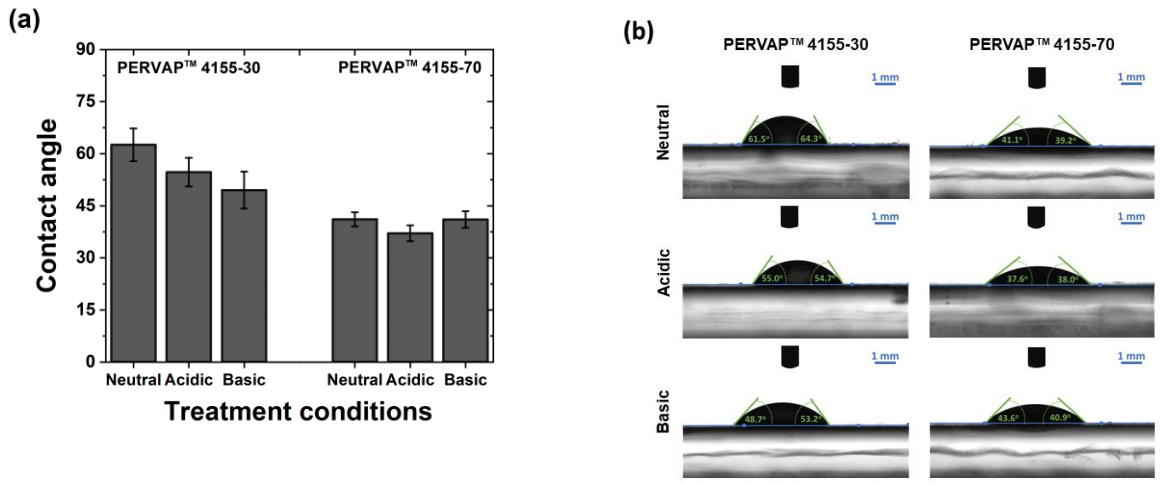

Figure 3-6. PERVAP™ 4155-30 and PERVAP™ 4155-70 composite membranes (a) CAs after different treatments and (b) their representative shapes of water drops.

As discussed above, the swelling and hydrophilicity of the selective layer play important roles in the pervaporation process. The degree of swelling of the membranes depends on the composition and the structure of the polymer matrix. Thus, PERVAP™ 4155-30 and 4155-70 should exhibit different behavior in terms of swelling. This investigation is carried out by using dense films in pure water and mixtures used for pervaporation tests, that is, binary mixtures of MeAc and water in neutral, acidic, and basic conditions.

The swelling degree of these films is presented in Figure 3-5. In general, it is observed that the degree of swelling of PERVAP™ 4155-30 is higher than PERVAP™ 4155-70. This is due to the cross-linking degree of the membrane (less content of PVA means less degree of cross-linking) and hydrophilic nature of the copolymer. The swelling of films in binary (MeAc/water) mixtures is less than that in water, and this can be explained by the wettability properties of polymer system itself. In mixtures containing acid, the swelling of membrane PERVAP™ 4155-30 decreases compared to neutral mixtures. Thus, this result agrees with the water flux decrease. However, PERVAP™ 4155-70 does not show remarkable changes in swelling degree between tests in water, neutral and acidic mixture. This result may be due to the high content of PVA in the membrane (high degree of cross-linking).

In basic conditions, both types of membranes do not swell at all (Figure 3-5). This observation supports the pervaporation results well (Figure 3-4), where a decrease of water flux is observed once the MeAc is dehydrated.

The hydrophilicity of the PERVAP™ 4155 membrane surface with different PVA content was studied by static contact angle (CA) with water as a probe liquid. As shown in Figure 3-6, the

CA of the liquid decreased with increasing PVA content in the membrane. This means that the PERVAP™ 4155-70 is more hydrophilic than PERVAP™ 4155-30 because of more hydroxyl group in the membrane (higher PVA content) as well as because of the slightly different roughness of membrane surface, derived from the different composition. In other words, higher PVA content in the membrane produces a smoother, continuous hydrophilic surface.

PERVAP™ 4155-30 samples exhibit slightly different CA when they are treated with different liquid mixtures. In basic conditions, this membrane becomes more hydrophilic, while PERVAP™ 4155-70 does not show notable changes.

It should be noted that during the pervaporation tests at different conditions (basic and acidic) random ring-opening of the pyrrolidone ring in the copolymer may occur, which can facilitate the polymer chain reconfiguration and constructs hydrogen bonding with the DMAEMA units in the polymer system.[217-221] The presence of opened ring NVP units were analyzed by ATR–FTIR and confirmed by the appearance of the characteristic band at around 1732 cm^{-1}, corresponding to the carboxyl acid group in the ring-opened NVP.[222] To prove the structural rearrangement and the ring-opening, the cross-linked free-standing dense films made from P(NVP-*co*-DMAEMA) and PVA were exposed to the acidic and basic mixtures under the same conditions used in pervaporation tests. A slight color change was observed in the case of acidic treatment.

Figure 3-7a shows the ATR–FTIR spectra of the neutral and the acid and base treated samples at 85 °C. A characteristic peak at around 1650 cm^{-1} represents the carbonyl moiety present in the NVP unit, and after treatment, a new characteristic peak of carboxylic acid group appeared at around 1720 cm^{-1}, revealing that ring opening occurred during the treatment of the samples in acidic and basic conditions. The treated samples were also used for swelling measurements in pure water and in binary MeAc/water mixtures (Figure 3-7b); this was done to investigate the possible self cross-linking of the polymeric material. After the samples are treated in both acidic and basic conditions, the PERVAP™ 4155-30 sample exhibited lower equilibrium swelling ratio, especially in MeAc/water mixtures, and thus, because of high amount of the P(NVP-*co*-DMAEMA) in this sample, the additional self cross-linking due to the ring-opening can be confirmed by these tests. The PERVAP™ 4155-70 sample also showed an evidence of the ring-opening NVP (Figure 3-7a), but according to the swelling measurements, the additional self cross-linking could not be noticed (Figure 3-7b). Contrary to PERVAP™ 4155-30, this result can be explained by the PVA content in this sample, which might suppress this effect and act as a stabilizing matrix.

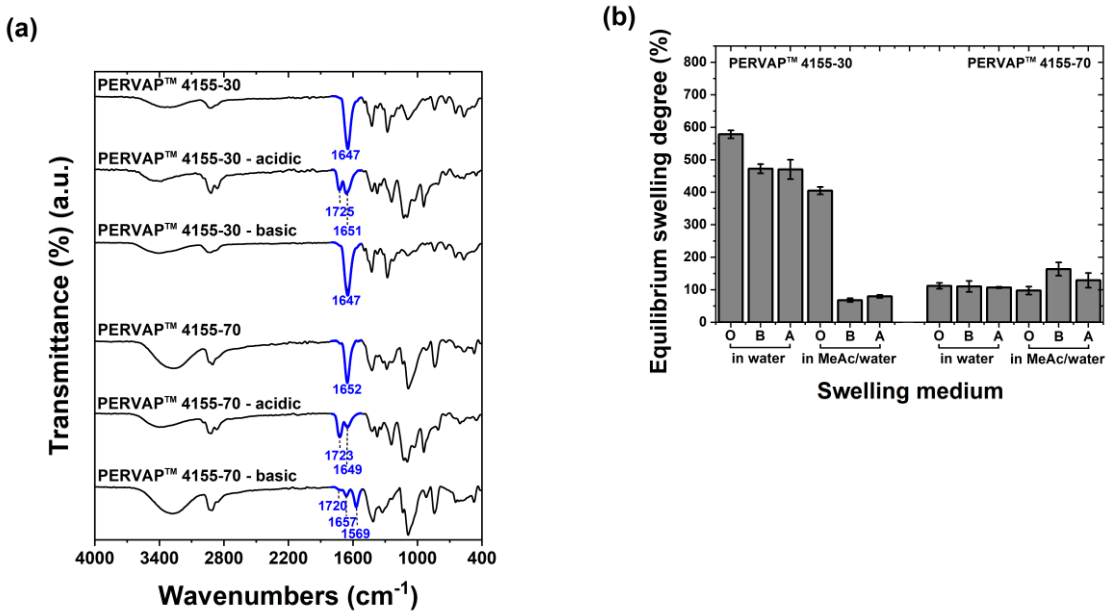

Figure 3-7. (a) ATR–FTIR spectra of the treated free-standing dense films (scan number: 128, nominal resolution: 4 cm^{-1}) and (b) equilibrium swelling ratio (%) of the original (O), basic (B), and acidic (A) treated free-standing dense films (in water and neutral binary MeAc/water mixture).

The appearance of the new characteristic band of the carboxyl acid group in the treated samples and the swelling tests corroborate the separation performance change during the pervaporation tests under different conditions, that is, it contributed to water flux decrease, which can be due to the self cross-linking and hydrogen bonding between the carboxylic acid group and amine from PDMAEMA segment and PVA.

By last, to confirm the responsive nature of these membranes and their reversibility, additional pervaporation tests were performed with the same membrane sample by using different mixtures, as follows: neutral−acid−neutral−basic−neutral.

Figure 3-8 shows the results for this set of experiments. The trend and range of water flux and permeate concentration are like previous experiments, this means the measurements are highly reproducible and the membranes show a responsive behavior. However, the water flux with neutral mixture after the experiments with acidic and basic mixture, does not recover as the initial values. This phenomenon could be explained as follows: (i) the cleaning of membrane may require multiple steps (long-term washing) to remove the remaining H^+ from the membrane after the tests with acidic mixture, and (ii) the separation property of membrane is not entirely reversible, suggested because of the chemical changes. As ring-opening might occur during the pervaporation test in acidic and basic conditions, the amine and carboxylic

acid moieties can further react to lead to an amide moiety, inducing self cross-linking of the material.[221] Therefore, although the membranes have pH-responsive nature, the separation performance in terms of water flux could not be recovered once the membrane is exposed to acidic and basic mixtures. So, the results show that chemical changes and self cross-linking could have happened in the polymer system, that is, the polymer matrix is more cross-linked and is responsible for the water flux decrease.

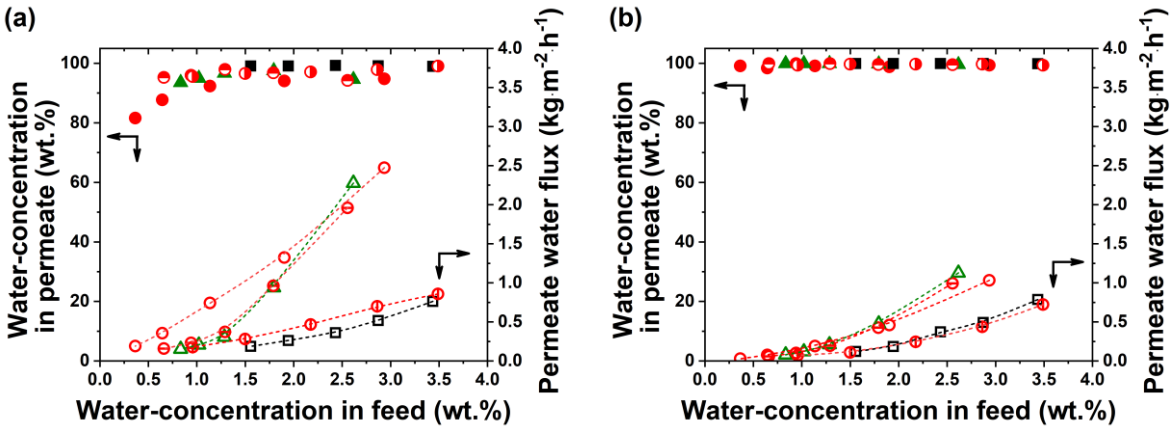

Figure 3-8. Separation performance of membranes (a) PERVAP™ 4155-30 and (b) PERVAP™ 4155-70 for dehydration of binary MeAc/water mixtures from neutral to acidic and from neutral to basic condition at 85 °C and 10 mbar (black square: acidic, red circles: neutral (various stages), green triangle: basic).

The change of separation performance in pervaporation processes (in this case the water flux and permeate concentration) is very important during the process design and industrial plant sizing. Thus, the information derived from this work is profitable for membrane developers and end users. In addition, the observed membrane behavior can be used in a useful way, especially in mixtures where acidic and basic compounds are present, for example, for obtaining higher water flux at higher water concentration in basic mixtures, for enhancing the selectivity or for preventing the separation performance change, that is, by neutralizing the acidic and basic mixtures before the streams go to the membrane modules.

Commercially available membranes, such as PERVAP™ 4155 (DeltaMem AG) are typically employed for simultaneous removal of methanol and water from various solvent mixtures containing impurities as organic acids and aldehydes. These membranes are blends based on cross-linked PVA and a commercial hydrophilic copolymer;[214] they are compatible with industrial streams containing aldehydes and are available in different grades.[223] The results indicate that those membranes are pH-sensitive and can be also applied in solvent dehydration processes by varying the pH of the mixture.[224] However, due to the low degree of cross-linking

and presence of the copolymer, those membranes show poor performance for ethanol/water separation, *i.e.*, the selectivity is too low. These findings highlight the need to synthesize tailored copolymers with precisely tuned compositions and structures to optimize specific interactions with water and ethanol molecules. The synthesis of such copolymers would not only enhance selectivity and separation efficiency, but also facilitate the design of membranes that align with the specifications of industrial processes in a more precise manner. It is therefore essential to further investigate the synthesis of innovative copolymers and their integration into the manufacture of pervaporation membranes, with a focus on achieving optimal separation performance for bioethanol dehydration.

3.3. Conclusion

Two commercial pervaporation membranes containing P(NVP-*co*-DMAEMA) were investigated as pH-responsive membranes. The copolymer itself, the composite membrane, and dense films were characterized in detail to understand the pH-responsive nature of these membranes.

By changing the MeAc/water mixture nature from neutral to acidic and from neutral to basic mixture, the water flux through the membrane dropped during the dehydration of MeAc by pervaporation. In PERVAP™ 4155-30, the water permeate concentration was enhanced. This membrane behavior was attributed to swelling and shrinking of the polymer matrix because of the presence of DMAEMA units in the copolymer.

Pervaporation tests carried out with the same membrane sample under neutral, acidic, and basic conditions showed that the membrane performance (water flux) change is irreversible once the conditions changed. As proposed, the chemical structure changes occurred in the polymer system. Ring opening of NVP units and self cross-linking has been hypothesized and later confirmed by the sample analyses.

Because these membranes are commercial and they are industrially applied for neutral mixtures, stability tests under acidic and basic conditions are needed to confirm if subsequent changes occur for a longer period. Thus, depending on the application and impurities present in the mixture, the pH-responsive nature of these membranes can be advantageous.

Due to the low degree of cross-linking and presence of the copolymer, those membranes have poor performance for ethanol/water separation, *i.e.*, the selectivity is too low. The main reason is that the copolymer used in this formulation is commercial and originally designed for other

types of application. Therefore, there is a need to tailor the copolymer properties to develop new membrane formulations that are more adapted for ethanol dehydration.

4. Synthesis and characterization of tailor-made *N*-vinylpyrrolidone copolymers and their blend membranes with poly(vinyl alcohol) for bioethanol dehydration by pervaporation

This chapter contains parts of a published work: Alessandro Angelini, Csaba Fodor, Luigi Leva, Anja Car, Ionel Adrian Dinu, Wilfredo Yave and Wolfgang Meier. *Journal of Applied Polymer Science* **2022**, 139 (4), 51562.

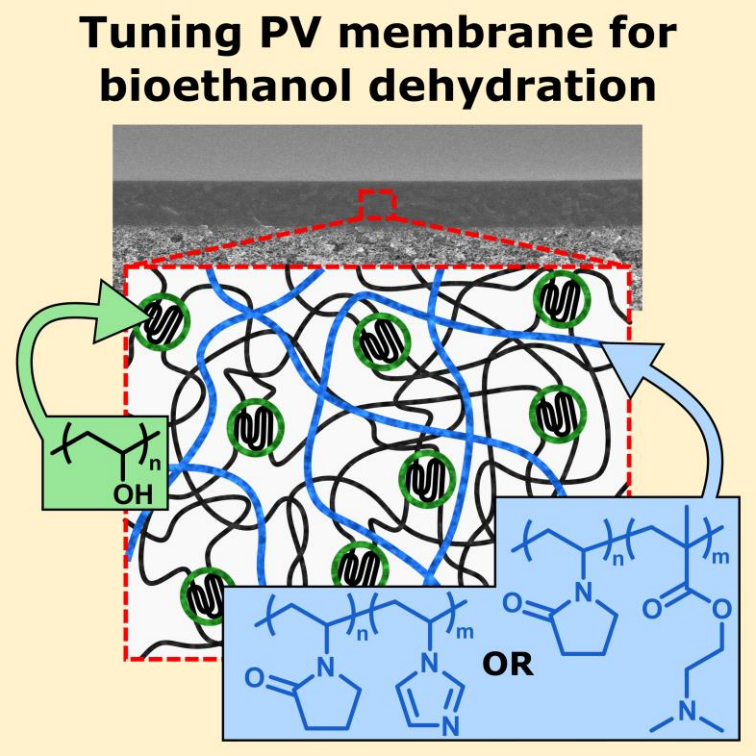

4.1. Introduction

Pervaporation is a membrane-based technology, where the separation is not limited by the vapor-liquid equilibrium, and thus, azeotropes can be easily separated by this technique. In addition, pervaporation is cheaper than molecular sieves and the total energy consumption for drying ethanol can be reduced for more than 30%, which reduces the total costs of bioethanol production.[57] Although pervaporation presents many advantages compared to distillation and

molecular sieves, existing commercial membranes for pervaporation both polymeric and ceramic membranes need to be more efficient and competitive for large-scale bioethanol production. Therefore, the synthesis of new membrane materials or the modification of existing ones are very important for developing robust membranes with higher permeability and selectivity.

Currently, two different types of membranes are mainly employed in pervaporation for bioethanol dehydration, which are from zeolites and polymers.[225] These membranes are hydrophilic and can also be used for dehydration of other alcohols, ethers, esters, etc. They selectively separate water from the other components due to the specific affinity between the water molecules and the membrane material, *i.e.*, water is preferentially absorbed by the membrane material. If there is a driving force between the feed and permeate side of the membrane, the water molecules are transported through the membrane by a diffusion process.[140] The driving force in all membrane processes is a gradient in the chemical potential between the feed and permeate side. In pervaporation, this gradient is best described by a difference in partial vapor pressure.

Among all hydrophilic polymeric membranes, the PVA membrane remains the most investigated and the most used in industrial applications. This is because PVA offers several advantages like good film-forming properties, high hydrophilicity, chemical/thermal stability, biodegradability and non-toxicity.[226-227] Various methods have been reported on membrane fabrication since PVA membranes became commercial. Those methods allow to tailor the membrane performance like flux, selectivity and lifetime according to the needs. In fact, for the dehydration of different organic solvents, chemical cross-linking methods were developed to avoid or control the swelling of PVA due to the presence of water.[228] The cross-linked PVA membrane is also used for bioethanol dehydration, but depending on its provenance (*e.g.*, grain or wood fermentation), the impurities present in the bioethanol streams harm PVA membranes. Organic acids and aldehydes are the most harmful contaminants that damage polymeric and ceramic membranes, especially at high concentrations.[18]

Commercially available membranes, such as PERVAP™ 4155 (DeltaMem AG) are typically employed for simultaneous removal of methanol and water from various solvent mixtures containing impurities as organic acids and aldehydes. These membranes are blends based on cross-linked PVA and a commercial hydrophilic copolymer;[214] they are compatible with industrial streams containing aldehydes and are available in different grades.[223] In a previous work, we have investigated some of those membranes as pH-responsive, and we have

demonstrated that they can be also applied in solvent dehydration processes by varying the pH of the mixture.[224] However, due to the low degree of cross-linking and presence of the copolymer, those membranes show poor performance for ethanol/water separation, *i.e.*, the selectivity is too low. Thus, being encouraged by the results of our previous study, we hypothesized that the synthesis and use of tailor-made copolymers (rather than commercial copolymers produced for other applications) based on NVP, DMAEMA and NVIm with a controlled molar ratio of monomers in the copolymer, can improve the water/ethanol selectivity of this type of membranes.

PNVP is known as a hydrophilic polymer with a high tendency to form hydrogen bonds with PVA,[229] which would lead to blends with enhanced separation properties.[230] Poly(2-(dimethylamino)ethyl methacrylate) (PDMAEMA) has been previously reported as a membrane material for gas separation.[201] This polymer can be quaternized[231] and, as a polyelectrolyte is well-known to form both highly permeable and highly selective membranes.[232] Similarly, poly(*N*-vinylimidazole) (PNVIm) is a possible candidate to be associated with PVA in the fabrication of pervaporation membranes. It has been previously investigated as membrane material[233-235] and its hydrophilicity and thermal properties[236] reveal the high potential for improving the properties of PVA membrane.

The previous work has demonstrated how important it is to use polymers whose properties and architectures are specifically adapted to the targeted applications. In this context, we have synthesized tailor-made P(NVP-*co*-DMAEMA) and P(NVP-*co*-NVIm) copolymers *via* free radical polymerization, starting from various and controlled monomer ratio. After chemical and thermal characterization, membrane blends with different PVA/copolymer ratio (80:20 and 95:5, mass ratio in percent) were prepared and characterized. Composite membranes fabricated by solution casting on a porous (PAN) support have been further investigated for dehydration of ethanol/water mixtures by pervaporation, in order to identify the most promising copolymer and the optimal formulation. These tests assessed the impact of various copolymer compositions on membrane performance, in terms of flux and selectivity. The objective was to identify the optimal combination (copolymer and blend ratio) that maximized separation efficiency. Thus, we demonstrated that the new membrane formulation based on tailor-made copolymers allows obtaining better membranes for bioethanol dehydration. In addition, to validate the industrial potential of the optimized membrane prototype, stability test results with ethanol containing up to 600 ppm of acetaldehyde are reported in this work. These tests are essential for ensuring that the membrane can maintain its performance under real conditions, particularly to confirm that the membrane developed is viable in industrial applications. To our

knowledge, no prior studies report the stability of polymeric and ceramic membranes with bioethanol containing acetaldehyde within this range of concentration.

4.2. Results and discussion

4.2.1. Synthesis and characterizations of NVP-based copolymers

Controlling the molar ratio of monomers, a series of tailor-made homopolymers and copolymers were synthesized by free radical polymerization. The effect of monomer ratio and type of moieties (linear side group of DMAEMA and cyclic side group of NVIm) on the structure-property relationship was systematically investigated. The schematic representation of the copolymer synthesis is illustrated in Figure 4-1.

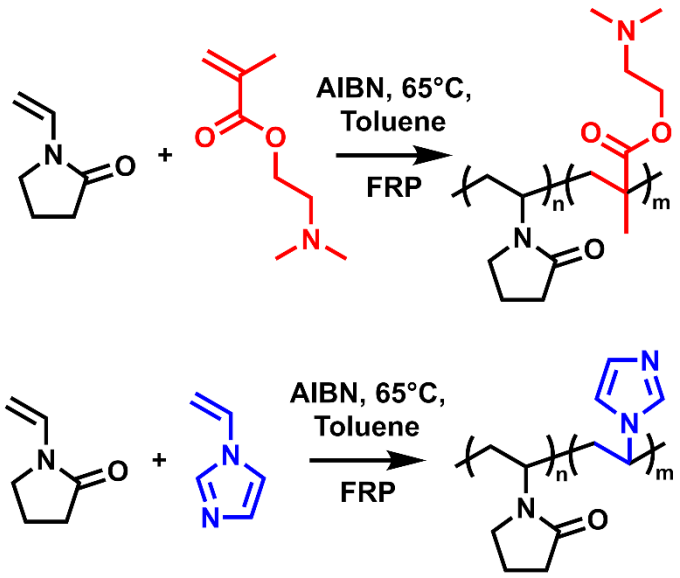

Figure 4-1. Schematic of P(NVP-*co*-DMAEMA) and P(NVP-*co*-NVIm) synthesis by free radical polymerization (FRP).

The synthesized P(NVP-*co*-DMAEMA) copolymers were characterized first by ^{1}H NMR (Figure 4-2), and their spectra were compared with those of corresponding homopolymers (the number in the sample name indicates the content of the DMAEMA units in the copolymer, in mol percent). The observed peaks are in agreement with those reported in the literature for similar copolymers.[215] The two aliphatic protons of the backbone from the NVP units have their characteristic peaks between 1.30 and 1.78 ppm (Figure 4-2, peak a). From 1.80 to 2.50 ppm (Figure 4-2, peak d) appear the signals corresponding to the protons of the heterocyclic ring and from 3.00 to 3.40 ppm (Figure 4-2, peak c) to the methylene protons of the heterocyclic ring, that are adjacent to the nitrogen atom. The CH protons from the backbone, adjacent to the

heteroatom from the NVP units, are associated to the resonance from 3.50 to 4.00 ppm (Figure 4-2, peak b). For the DMAEMA units, the signal of the protons from the methyl group on the backbone arise at 0.90 ppm (Figure 4-2, peak g). Between 1.70 and 2.10 ppm (Figure 4-2, peak f) appear the methylene protons from the corresponding backbone. The signal at 2.28 ppm (Figure 4-2, peak j) is characteristic to the two methyl groups of the pendant moieties and the peaks at 2.57 and 4.06 ppm (Figure 4-2, peaks h, i) belongs to the methylene groups in the DMAEMA units.

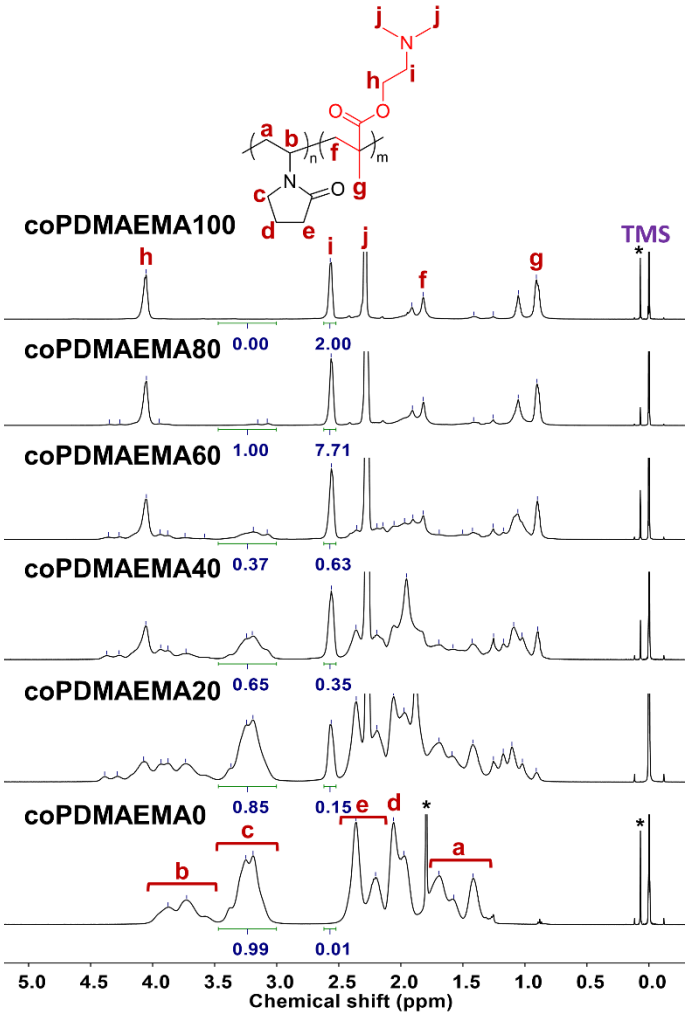

Figure 4-2. ^{1}H NMR spectra of the P(NVP-*co*-DMAEMA) copolymers in $CDCl_3$ at RT (number of transients (nt): 256, residual solvent is marked with an asterisk).

The composition of the copolymers was determined by integration of the specific signals at 2.57 ppm (Figure 4-2, peak i) for the DMAEMA and from 3.00 to 3.40 ppm (Figure 4-2, peak c) for the NVP units (Appendix, Table 9-1). Due to free radical polymerization without specific initiator, no end group signals could be used as an internal reference.

Figure 4-3 shows the ^{1}H NMR spectra of the synthesized P(NVP-*co*-NVIm) copolymers (like in DMAEMA copolymers, the number in the sample name indicates the content of the NVIm units in the copolymer, in mol percent). A characteristic signal arising from NVP units appear at 1.30 ppm (Figure 4-3, peak a), corresponding to the methylene protons from the backbone. The peaks from 2.90 to 3.82 ppm (Figure 4-3, peaks b, c) are related to the proton from the backbone adjacent to the heterocyclic ring and two protons of the ring adjacent to the nitrogen atom. Six protons are featured from 1.43 to 2.36 ppm (Figure 4-3, peaks a, d, e) corresponding to the methylene protons from the backbone and from the lactam moiety. For the NVIm units, the peaks from 1.54 to 2.23 ppm (Figure 4-3, peak f) correspond to the methylene groups CH2 and the signals from 2.77 to 3.20 ppm (Figure 4-3, peak g) are associated to the CH from the backbone. The signals of the protons of the imidazole ring appear between 6.61 and 7.56 ppm (Figure 4-3, peaks h, i, j).

The composition of the P(NVP-*co*-NVIm) copolymers was determined (Appendix, Table 9-1) by integrating the signals from 6.61 to 7.56 ppm for the NVIm units (3 protons H) and the signals from 1.30 to 2.36 ppm, where both NVIm (2 protons H) and NVP (6 protons H) units have the characteristic resonances appearing. To obtain the integration of the NVP units in the copolymers (peaks a, d and e), the integration of the protons from the imidazole ring was set to 3, so that the methylene protons (peak f) could be subtracted (I_(a.d.e)=I_(a,d,e,f) – 2), with the resulting integration value corresponding to the protons of the NVP units.

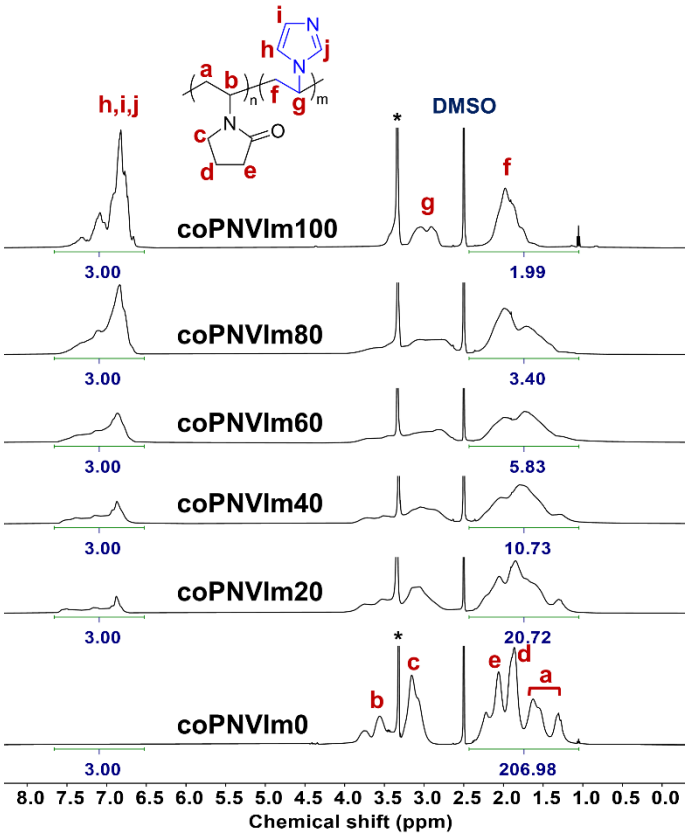

Figure 4-3. ^{1}H NMR spectra of the P(NVP-*co*-NVIm) copolymers in DMSO-d_6 at RT (number of transients (nt): 256, residual solvent is marked with an asterisk).

The results obtained from ATR-FTIR spectroscopy further support the successful synthesis of the various homopolymers and copolymers (Figure 4-4). The intense band at 3440 cm−1 corresponds to the vibrations of OH group from the adsorbed water molecules. For the NVP units, the peaks from 3000 to 2800 cm^{-1} and the peak at 1410 cm^{-1} are attributed to the C-H stretching vibration of aliphatic and to the C-H bending vibration of methylene groups, respectively. The absorption band at 1659 cm^{-1} is attributed to the carbonyl group, C=O, and the band at 1274 cm^{-1} is representative of the C–N stretching vibrations of the lactam ring.[237] The characteristic absorption bands of DMAEMA units are referred to the (C-H(-N(CH3)2) stretching vibrations between 2990-2770 cm^{-1}, the carbonyl group, C=O, stretching vibration at 1720 cm^{-1}, the CH2 bending and the N(CH3)2 deformational stretching vibrations around 1455 cm^{-1} and the C–O–C stretching vibration at 1150 cm^{-1} (the last three absorption bands increase according to the content of DMAEMA units).[238]

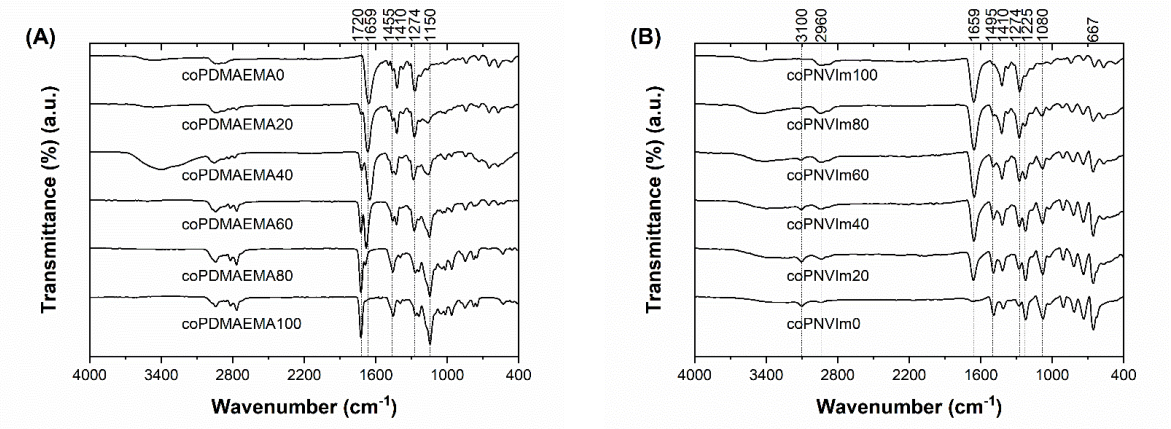

Figure 4-4. ATR-FTIR spectra of (A) P(NVP-*co*-DMAEMA) and (B) P(NVP-*co*-NVIm) copolymers (scan number: 128, nominal resolution: 4 cm^{-1}).

At 3100 cm^{-1} arises the characteristic C-H stretching of the imidazole ring. From 2960 to 2873 cm^{-1}, the absorption band corresponds to C-H and CH2 stretching from the polymeric backbone adjacent to NVIm units. The strong band at 1495 cm^{-1}, represents the C-C ring stretching, while the absorption at 1225 cm^{-1} is characteristic for the C-N (ring) stretching. The peak at 1080 cm^{-1} characterizes the C-H (ring) in-plane bending vibration. The aforementioned bands of homopolymers are also present in various extents in the spectra of copolymers, confirming the presence of the specific units in the final materials.[239] Thermal characterization has been performed to study the possible microphase separation and glass transition temperature (T_g) changes as a function of the copolymer composition. All DSC results show that the homopolymers and copolymers are amorphous and do not present any crystallinity (the thermograms are displayed in Figure 4-5), which are also in agreement with the literature.[240] Briefly, the PDMAEMA and PNVP homopolymers have their T_g values at 37 °C and 175 °C, respectively, whereas the thermograms of the copolymers show a specific trend of the two distinct T_g values, and those values are plotted in Figure 4-6.

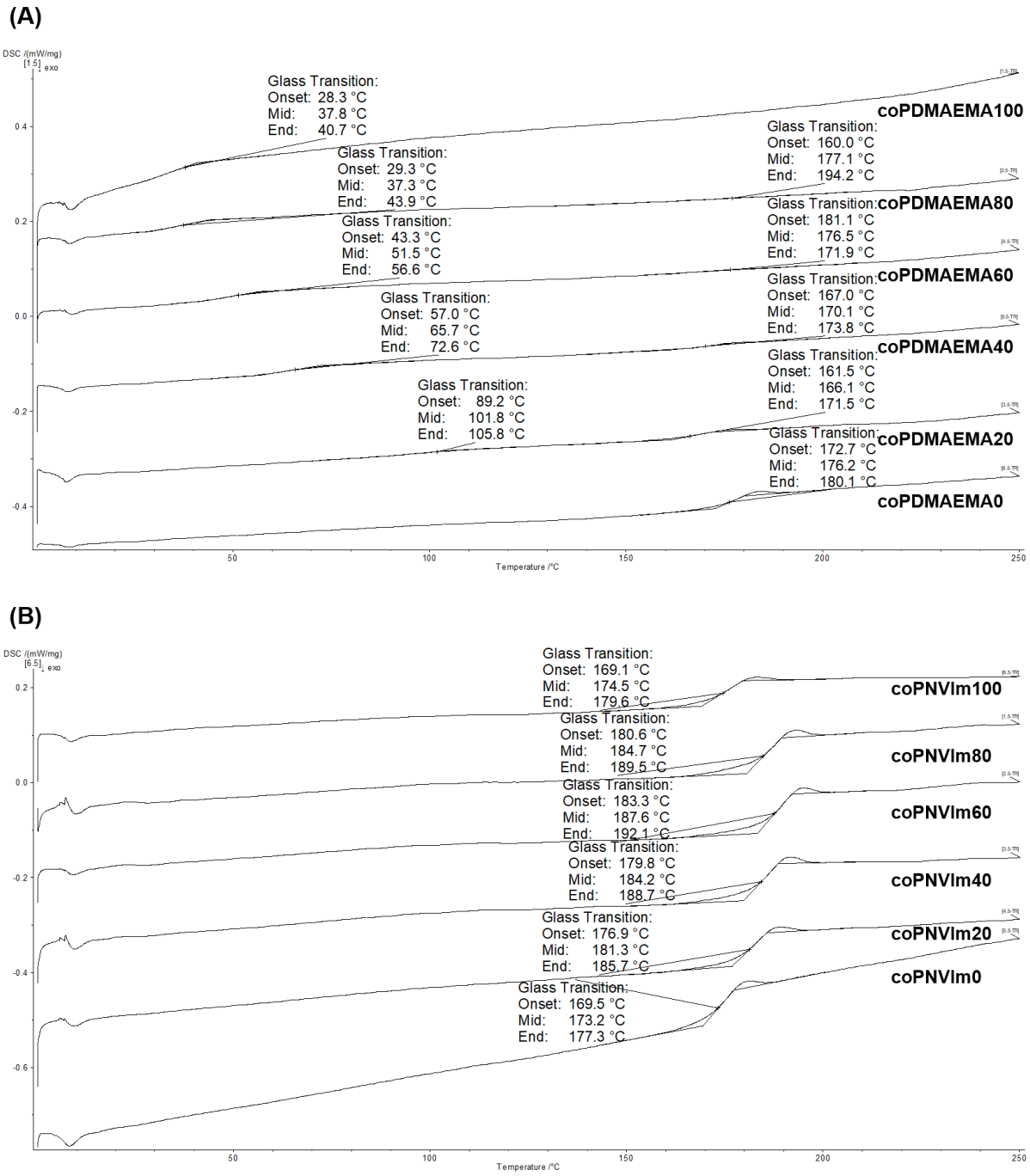

Figure 4-5. DSC thermograms (second heating scans, heating rate = 10 K.min^{-1}) of (A) P(NVP-*co*-DMAEMA) and (B) P(NVP-*co*-NVIm) copolymers.

The first T_g is attributed to the PDMAEMA block and the second to the PNVP block. These results indicate that in P(NVP-*co*-DMAEMA) copolymers there is a clear microphase separation. This phenomenon is generally observed for copolymers with a large molecular weight, composed by monomers having reactivity ratios significantly different, and thus, during copolymerization, the units tend to form sequences of almost pure PNVP and PDMAEMA segments.[241-242] In our case, the synthesized homopolymers and copolymers were obtained with

high molecular weights as a requisite (> 105 g.mol-1, see Appendix, Table 9-1). In addition, the T_g value of the PDMAEMA blocks increases at a higher content of NVP units, suggesting an incorporation of DMAEMA units within PNVP pseudo-blocks. The T_g changes are further supported by the good agreement with the predicted T_g values from the Fox equation (dashed lines in Figure 4-6A), which indicates a good miscibility of both units in this microphase. Even though there is an incorporation of the DMAEMA units to NVP pseudo-blocks, the copolymer has still a random structure and do not evidence alternated monomer units through the polymer chain.

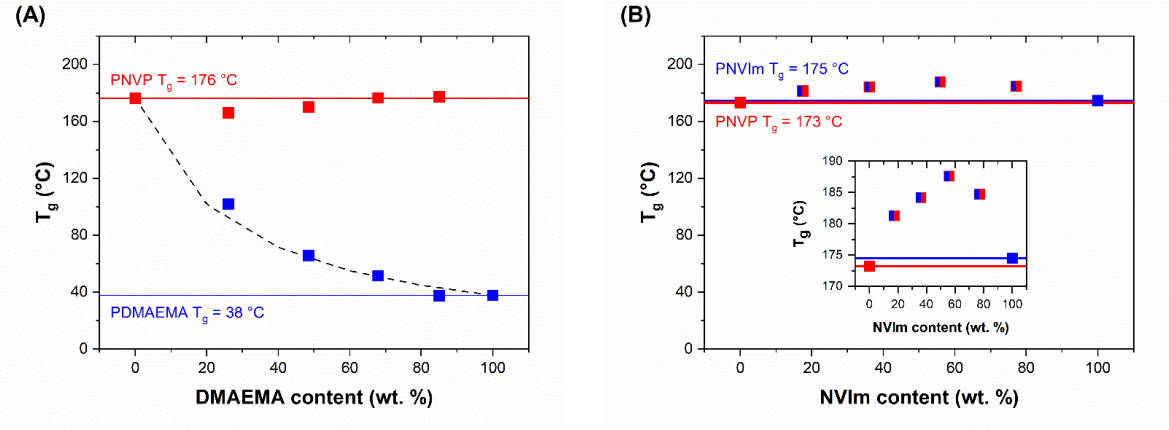

Figure 4-6. Glass transition temperature (T_g) values for P(NVP-*co*-DMAEMA) (A) and P(NVP-*co*-NVIm) (B) copolymers as a function of DMAEMA or NVIm content. The red line indicates the T_g of the PNVP homopolymer, whereas the blue line indicates the T_g of the PDMAEMA and PNVIm homopolymers, accordingly. The dashed black line shows the estimated T_g by the Fox equation.

Figure 4-6B shows the T_g values for the P(NVP-*co*-NVIm) copolymers. Although both homopolymers have similar T_g values,[243] the presence of a single T_g confirms the good miscibility between the NVP and NVIm units. Moreover, the T_g values of the copolymers are slightly higher than those of the homopolymers, indicating a favorable intermolecular interaction between both monomer units in the copolymer.[244] In this case, the T_g values of the copolymers are higher than the ones of the homopolymers. The Fox equation cannot be applied to these copolymers due to the strong intermolecular interaction.

The results presented above confirm the successful synthesis of random P(NVP-*co*-DMAEMA) and P(NVP-*co*-NVIm) copolymers containing different microstructures with controlled monomer ratio. These synthesized tailor-made copolymers are expected to have a good compatibility with PVA, and they should exhibit good separation and thermal properties for improving the pervaporation membranes.

4.2.2. PVA/copolymer blends preparation and characterization

The homopolymers and copolymers synthesized here are combined with PVA in two different mass ratios, 80:20 and 95:5, respectively. These formulations are expected to display better separation properties than that of commercial membrane PERVAP™ 4155-80. Other blend ratios are not considered here because they swell to a great extent, and thus, the separation performance of those membranes would not be suitable for ethanol dehydration. Compared to the commercial PERVAP™ 4155-80 (membrane based on PVA and a commercial copolymer), the blends formulated here are based on tailor-made copolymers with controlled monomer molar ratio.

Freestanding dense films were investigated to determine the film properties in bulk. Table 4-1 shows the PVA/copolymer ratio and the degree of crystallinity of all prepared blends. As described above, the numbers in the sample name correspond to the mol fraction in percent of the indicated monomer in the final copolymer based on the initial monomer mixture.

Table 4-1: List of the prepared PVA/copolymer blends and their crystallinity.

Sample	**PVA/copolymer [mass ratio in percent]**	**Crystallinity [%]**
PVA	100:0	28.6 ± 0.5
PVA/coPDMAEMA100	80:20	23.1 ± 1.8
PVA/coPDMAEMA80	80:20	23.6 ± 1.6
PVA/coPDMAEMA60	80:20	24.2 ± 0.4
PVA/coPDMAEMA40	80:20	24.3 ± 0.7
PVA/coPDMAEMA20	80:20	26.4 ± 1.9
PVA/coPDMAEMA0	80:20	19.9 ± 1.9
PVA/coPNVIm100	80:20	18.3 ± 2.4
PVA/coPNVIm80	80:20	19.1 ± 1.3
PVA/coPNVIm60	80:20	19.0 ± 1.4
PVA/coPNVIm40	80:20	15.4 ± 1.1
PVA/coPNVIm20	80:20	17.7 ± 1.3
PVA/coPNVIm0	80:20	21.2 ± 0.9
PVA/coPDMAEMA100	95:5	25.9 ± 1.8
PVA/coPDMAEMA80	95:5	25.4 ± 0.8
PVA/coPDMAEMA60	95:5	25.4 ± 2.4
PVA/coPDMAEMA40	95:5	28.4 ± 1.1

PVA/coPDMAEMA20	95:5	31.2 ± 1.3
PVA/coPDMAEMA0	95:5	27.8 ± 1.3
PVA/coPNVIm100	95:5	23.1 ± 1.4
PVA/coPNVIm80	95:5	24.7 ± 2.4
PVA/coPNVIm60	95:5	23.6 ± 1.1
PVA/coPNVIm40	95:5	20.1 ± 3.5
PVA/coPNVIm20	95:5	25.7 ± 0.3
PVA/coPNVIm0	95:5	28.3 ± 0.7

In the DSC thermograms (Appendix, Figure 9-2 to Figure 9-4), two endothermic peaks are visible for PVA and blend samples. The first broad transition results from moisture evaporation from the sample, whereas the second transition represents the endothermic melting transition of the PVA crystalline domains.[236, 245] As discussed above, the homopolymers and copolymers of P(NVP-*co*-DMAEMA) and P(NVP-*co*-NVIm) are amorphous, and thus, in blends with PVA, the endothermic transition corresponds only to PVA. The T_g of copolymers in the blends is not observed in the thermograms due to the small content of copolymer (< 20 wt.%) in the sample.

From the obtained enthalpy of fusion, the crystallinity of PVA is estimated by using the melting enthalpy of 100% crystalline PVA (138.6 J.g^{-1}),[244] as follows:

$$X_c = \frac{\Delta H_f}{\Delta H_f^0} \times 100 \qquad (8)$$

where X_c is the degree of crystallinity (%), ΔH_f is the enthalpy of fusion from the endothermic melting peak (J.g^{-1}) and ΔH_f^0 is the enthalpy of fusion of the totally crystalline polymer (J.g^{-1}).

When blends of the same mass ratio (PVA/copolymer) are compared, the crystallinity of blends composed of P(NVP-*co*-DMAEMA) is slightly higher than those containing P(NVP-*co*-NVIm). This result is attributed 1) to the lower T_g of the DMAEMA segments compared to the NVIm segments, and 2) to the crystallization inhibitor effect of NVIm segment. On the one hand, due to the low T_g, the DMAEMA segments in the copolymer leads to a less rigid system, hence PVA chains can crystallize. On the other hand, PNVIm is known to have a crystallization inhibitor effect,[246] and thus, the NVIm segments in the copolymer lead to blends with less crystallinity. The crystallization inhibition is clearly seen when we compare the two set of

PVA/P(NVP-*co*-NVIm) blends, 80:20 and 95:5, i.e., the blends with ratio 95:5 present a higher degree of crystallinity (21-26%) than those of 80:20 (15-21%). Therefore, a higher content of P(NVP-*co*-NVIm) inhibited the PVA crystallization in the blend.

The crystallinity in blends containing P(NVP-*co*-PDMAEMA) does not change too much compared to PVA sample and it is random, albeit those with ratio 80:20 present slightly lower values.

Examining only the blends containing the homopolymers, the degree of crystallinity increases in the following order: PNVIm (coPNVIm100) < PNVP (coPDMAEMA0 or coPNVIm0) < PDMAEMA (coPDMAEMA100).

The water uptake experiments with these blend samples (dense films) are not possible to perform with accuracy because the samples are too hydrophilic, they swell up fast and a lot, and they are sticky. Thus, to overcome this problem, the uptake experiments were performed with binary ethanol/water mixture, as described in the experimental part (Table 4-2). However, to determine the uptake, the films were gently wiped to remove the excess of liquid. Unfortunately, this part of the experiment turned out to be tedious due to the irregularity of the force applied in removing the excess liquid. Therefore, because of the size and the mass of the dense films, small variation in this process led to big deviations in the results. A clear trend of the equilibrium-swelling ratio is not observed for each set of blends. However, the values for all blends are higher than that for PVA sample. Those results indicate that the blends will show higher values of flux and permeance. Considering that the swelling is mostly due to the water content in the mixture, these PVA/copolymer blends should be promising because they are highly hydrophilic.

Table 4-2: List of the prepared PVA/copolymer blends and their EtOH/water mixture uptake.

Sample	**PVA/copolymer (mass ratio in percent)**	**ESR (%)**
PVA	100:0	63.2 ± 6.1
PVA/coPDMAEMA100	80:20	69.1 ± 4.1
PVA/coPDMAEMA80	80:20	79.7 ± 2.9
PVA/coPDMAEMA60	80:20	77.1 ± 3.6
PVA/coPDMAEMA40	80:20	106.9 ± 2.7
PVA/coPDMAEMA20	80:20	82.5 ± 5.9
PVA/coPDMAEMA0	80:20	62.9 ± 2.9
PVA/coPNVIm100	80:20	74.2 ± 2.4

PVA/coPNVIm80	80:20	58.4 ± 2.5
PVA/coPNVIm60	80:20	72.6 ± 9.6
PVA/coPNVIm40	80:20	78.4 ± 9.2
PVA/coPNVIm20	80:20	73.8 ± 1.3
PVA/coPNVIm0	80:20	67.3 ± 6.6
PVA/coPDMAEMA100	95:5	73.4 ± 5.0
PVA/coPDMAEMA80	95:5	64.5 ± 3.9
PVA/coPDMAEMA60	95:5	91.0 ± 9.7
PVA/coPDMAEMA40	95:5	75.0 ± 6.4
PVA/coPDMAEMA20	95:5	86.7 ± 9.5
PVA/coPDMAEMA0	95:5	96.1 ± 5.3
PVA/coPNVIm100	95:5	73.6 ± 9.0
PVA/coPNVIm80	95:5	83.1 ± 6.3
PVA/coPNVIm60	95:5	81.8 ± 8.6
PVA/coPNVIm40	95:5	53.5 ± 8.8
PVA/coPNVIm20	95:5	62.9 ± 5.5
PVA/coPNVIm0	95:5	59.5 ± 4.6

The films (blends) were also analyzed by ATR-FTIR to investigate the possible interactions between PVA and the functional groups of the copolymers. The results for all samples are presented in Appendix (Figure 9-5 and Figure 9-6), whereas Figure 4-7 shows only the most representative samples. The ATR-FTIR results display the characteristic bands of each copolymer indicating their presence in the blend as well as the PVA bands. The broad bands at around 3400 cm^{-1} results from the stretching vibrations of the OH moieties as side chains of PVA, because of intermolecular and intramolecular hydrogen bonds. The medium band at 2924 cm^{-1} arises from the stretching of CH groups from the backbone. The band at 1420 cm^{-1} corresponds to the bending vibrations of the CH2. The medium band at 1322 cm^{-1} from the OH bending and the strong peak at 1083 cm^{-1} from the stretching C-O are the characteristic bands of alcohol groups. The crystalline structures observed in the DSC thermograms are further confirmed and supported by the band at 1140 cm^{-1} which is known to be related to the carboxyl stretching band, CO, and frequently employed to confirm the crystallinity of PVA.[247-249]

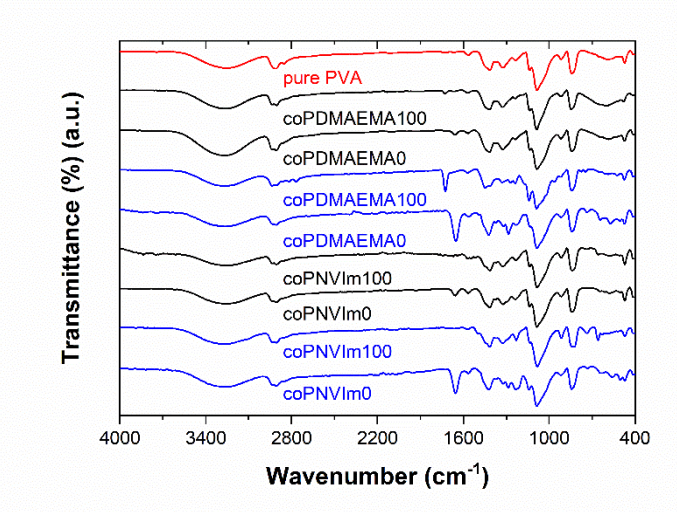

Figure 4-7. ATR-FTIR spectra obtained for the films made from PVA/P(NVP-*co*-DMAEMA) and PVA/P(NVP-*co*-NVIm) blends. Pure PVA (red), 95:5 blends (black), and 80:20 blends (blue) (scan number: 128, nominal resolution: 4 cm^{-1}).

All synthesized copolymers have a hydrophilic nature and a good miscibility with PVA (the obtained films were homogeneous and transparent) due to their mutual interactions, especially due to the hydrogen bonds.[250-252] From the performed characterizations on various freestanding dense films, the most representative samples are chosen to further prepare the composite membranes.

4.2.3. Composite membranes and pervaporation results

The blends with ratio 80:20 and 95:5 containing the homopolymers (PVA/coPDMAEMA100, PVA/coPDMAEMA0, PVA/coPNVIm100 and PVA/coPNVIm0) and four copolymers (PVA/coPDMAEMA60, PVA/coPDMAEMA20, PVA/coPNVIm60 and PVA/coPNVIm20) are chosen for composite membrane preparation. These membranes represent the blends with homopolymers and copolymers with middle and low DMAEMA and NVIm content. In total, 17 samples were prepared, and the list is presented in Table 9-2 (Appendix). In addition, the gas flow values are also reported in that table to evaluate the presence of surface defects, like pinholes.

The analysis by SEM confirmed the formation of a dense top layer on the PAN support with a homogeneous thickness of ~2 µm (Figure 4-8).

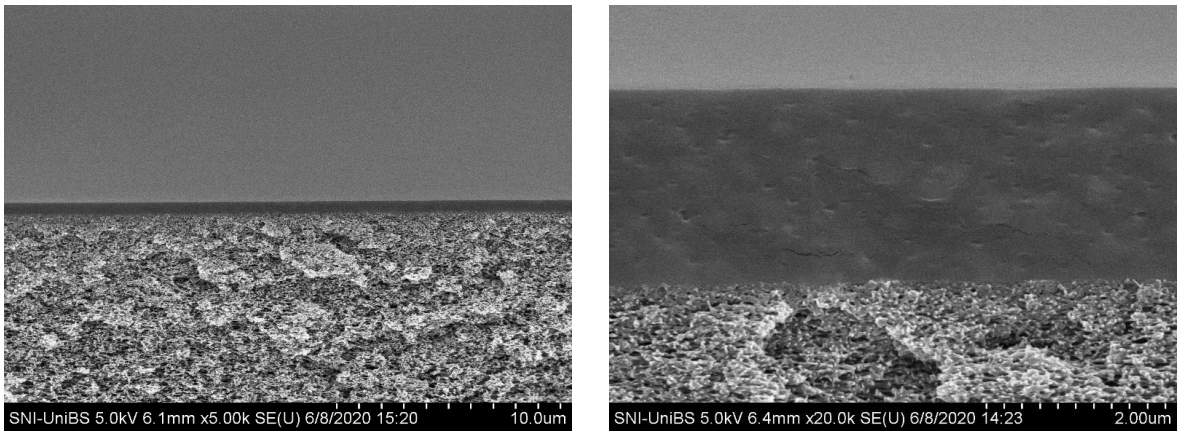

Figure 4-8. SEM pictures of the membrane cross-section showing the selective layer made of the blend PVA/coPDMAEMA100 on PAN asymmetric porous structure.

The separation performances of all these membranes are compared with pristine PVA membrane (prepared under the same conditions as the blend membranes) and a commercial membrane, PERVAP™ 4155-80 (Figure 4-9 and Figure 4-12). Although several commercial and non-commercial membranes exist for water separation from ethanol by pervaporation, there are no reports on membranes compatible with ethanol containing acetaldehyde and acids; hence a comparison with other membranes that are not tested with mixtures containing those contaminants would be misleading. As highlighted in introduction part, the series PERVAP™ 4155-XX are compatible with acids and aldehydes. However, the water/ethanol selectivity is extremely poor for application in bioethanol dehydration.

The dehydration of ethanol by pervaporation is performed at 95 °C, 2 bar in the feed side and 10 mbar in the permeate side. The water concentration in the feed, for which the data are collected, covers the typical industrial stream in the last step of bioethanol dehydration.

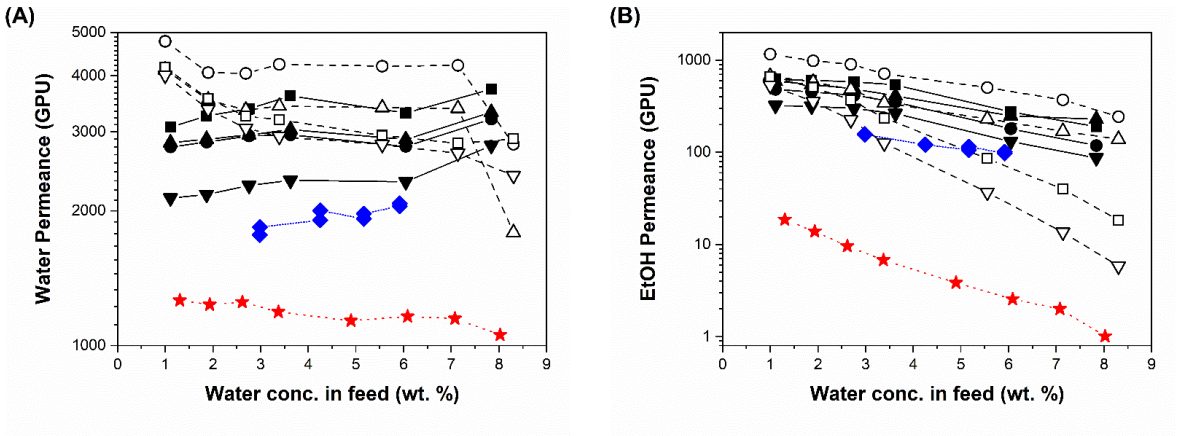

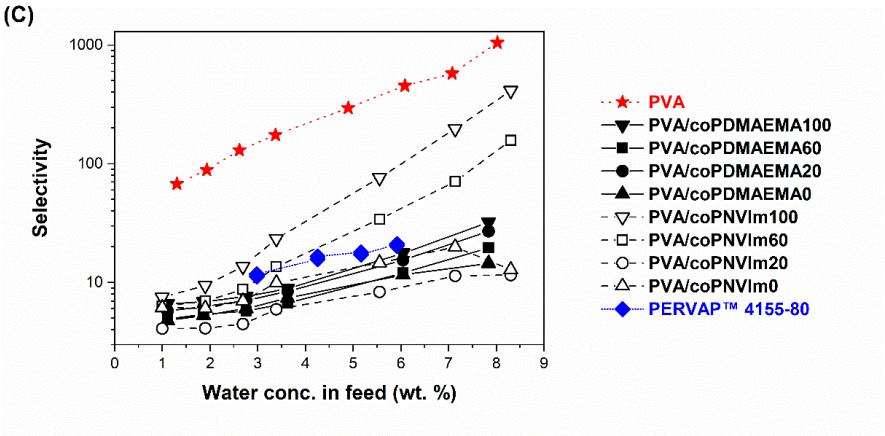

Figure 4-9. Separation performance of the composite membranes from blend 80:20 (PVA/copolymer) for the dehydration of binary EtOH/water mixtures. (A) water permeance, (B) ethanol permeance and (C) selectivity at 95 °C, 2 bar in the feed side and 10 mbar in the permeate side.

The composite membranes from PVA/copolymer blends with ratio 80:20 exhibit extremely high water permeance (Figure 4-9A). However, the selectivity is low (Figure 4-9C). The blend with the coPNVIm20 exhibited the highest water permeance (four times higher than PVA) but at the same time, the lowest selectivity. These results are mainly attributed to the presence of copolymer, which represents the 20 wt.% of the membrane material. The copolymer present in the PVA matrix disrupts the crystallization of PVA chains, and thus, the crystallinity is decreased in the blends 80:20 (Table 4-1). In addition to the crystallinity decrease (compared to pristine PVA), the hydrophilicity nature of copolymers also contributed to the increase of water permeance.

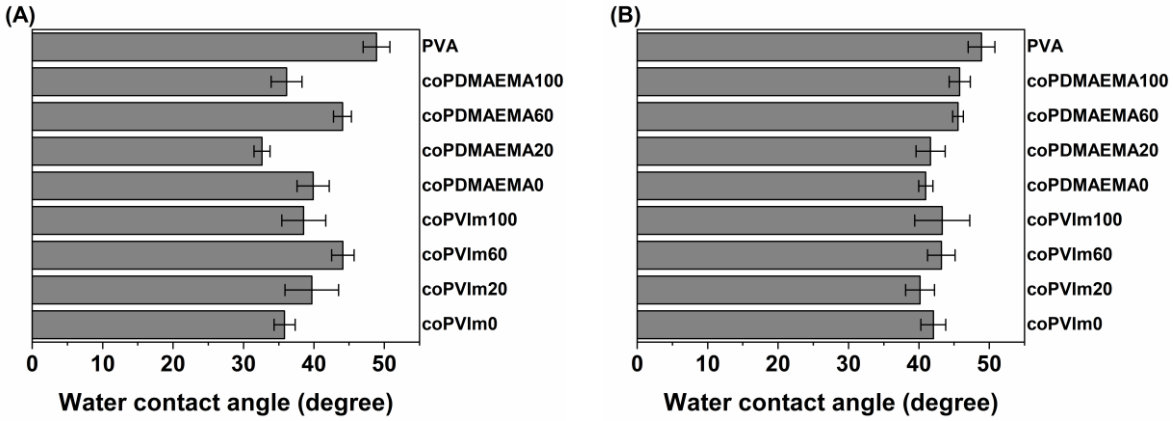

Figure 4-10. Contact angle measurements on composite membranes, PVA/copolymer ratio (A) 95:5 and (B) 80:20.

The CA measurements (Figure 4-10) confirm the high hydrophilicity of membranes containing the copolymers. They are even more hydrophilic than the pristine PVA membrane (CA of blend

membranes < 50°). These results indicate the preferential adsorption of water molecules on the selective layer, which enhances the water permeance.

Compared to the commercial membrane PERVAP™ 4155-80, all blend membranes exhibit higher water permeances. Because the ethanol permeance is slightly high through these membranes, the overall water/ethanol selectivity is lower than the commercial one, except for the membranes containing the PNVIm homopolymer (coPNVIM100) and the copolymer coPNVIm60.

In terms of water/ethanol selectivity, these membranes (from blends with ratio 80:20) are not suitable for ethanol dehydration. Nevertheless, they are potential candidates for dehydration of higher alcohols like isopropanol (Figure 4-11), butanol, pentanol, etc.

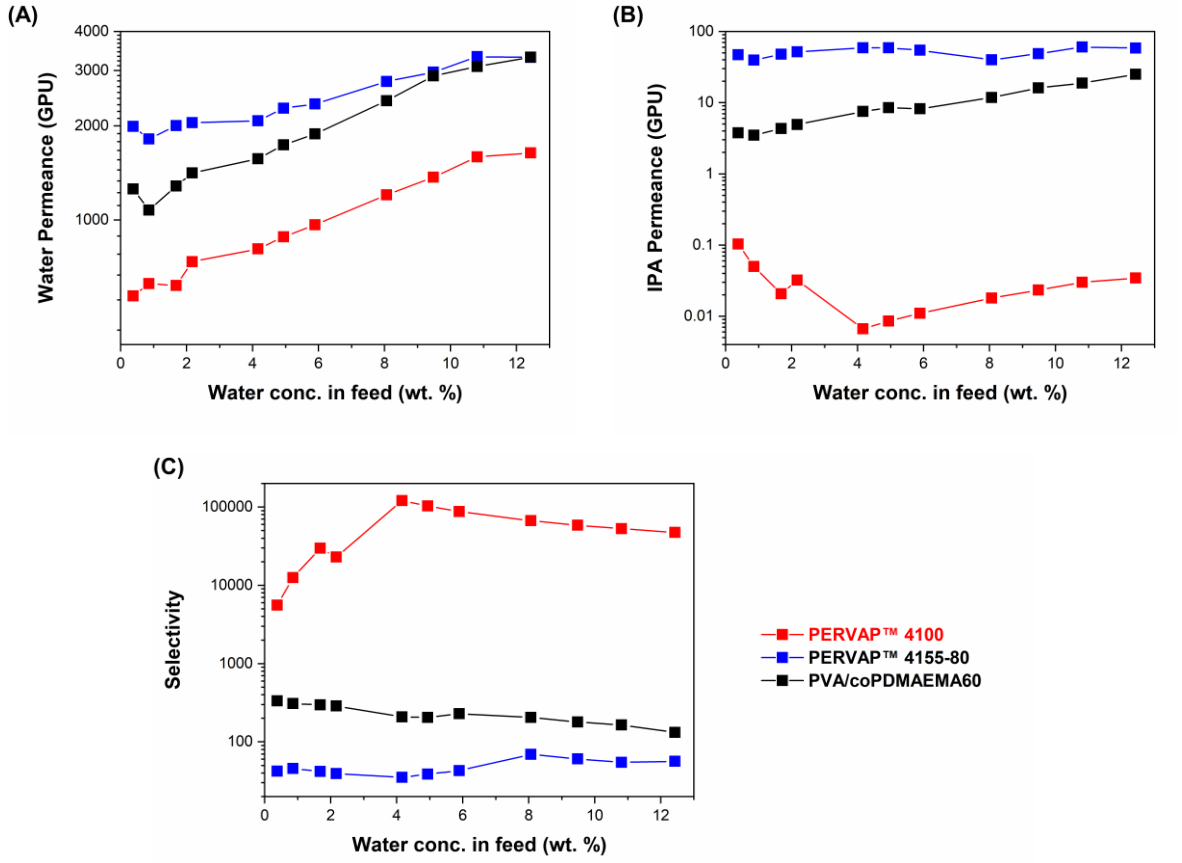

Figure 4-11. Separation performances of the composite membrane from PVA/coPDMAEMA60 (95:5) blend (black square), standard commercial membrane PERVAP™ 4100 (red square) and membrane PERVAP™ 4155-80 (blue square) for the dehydration of binary IPA/water mixture. (A) water permeance, (B) isopropanol permeance and (C) selectivity at 95 °C, 2 bar on the feed side and 10 mbar at the permeate side.

Figure 4-12 shows the separation performance of membranes prepared from blends with ratio 95:5. The water permeance of these membranes are also higher than PVA membrane (Figure 4-12A). Although the water permeance values of these membranes are slightly lower than those previously discussed (blend membranes with ratio 80:20), the water/ethanol selectivity values are higher. Thus, with a lower content of copolymer in the blend, the water permeance is kept higher than PVA and PERVAP™ 4155-80 (compared to PERVAP™ 4155-80, the samples containing the homopolymers, coPDMAEMA100, coPDMAEMA0 and coPNVIm0 show lower permeance values).

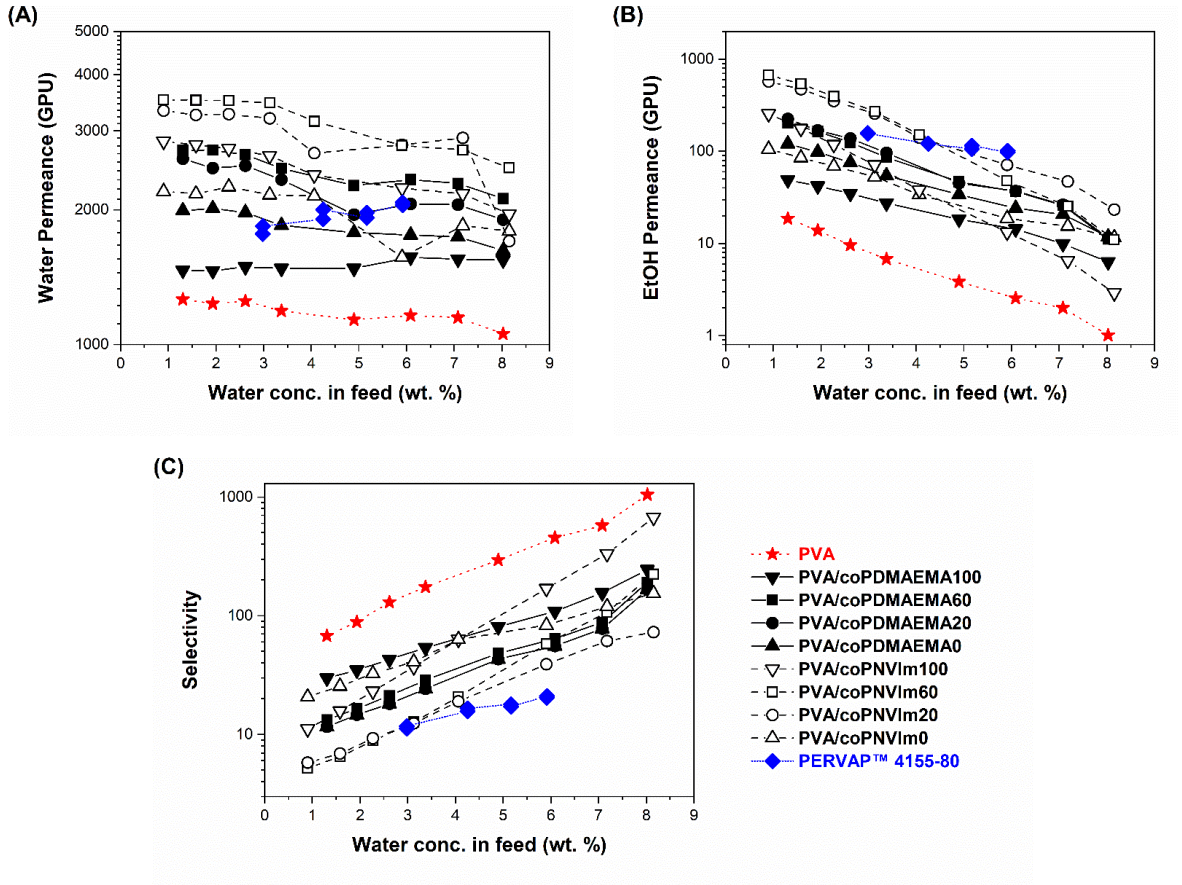

Figure 4-12. Separation performances of the composite membranes from blend 95:5 (PVA/copolymer), for the dehydration of binary EtOH/water mixtures. (A) water permeance, (B) ethanol permeance and (C) selectivity at 95 °C, 2 bar in the feed side and 10 mbar in the permeate side.

Because the ethanol permeance values are low in these blend membranes (Figure 4-12B), the water/ethanol selectivity is high. The improvement of selectivity is supported by the crystallinity (Table 4-1) which fit very well to pervaporation results, i.e., the blend membranes with ratio 95:5 exhibit higher degree of crystallinity than blend membranes with ratio 80:20, and thus, the permeation of ethanol through the membranes containing 5 wt.% of copolymers

is less due to the less plasticization effect (by the water). Because of less amorphous phase in the membrane material, the membranes swell less, which results in lower ethanol permeance and higher water selectivity.

As maximize the water/ethanol selectivity by controlling the copolymer type and content (tailor-made copolymers) is the aim of this work, the membranes containing the copolymers with a ratio of 95:5 are promising for ethanol dehydration, since they show higher selectivity and permeance than the commercial PERVAP™ 4155-80.

The membranes containing the copolymers coPDMAEMA60 and coPDMAEMA20 present slightly lower selectivity values than those containing the homopolymer (coPDMAEMA100), but they are still higher than PERVAP™ 4155-80. The water permeance is also high (more than 50%) compared to the blend with its homopolymer. This trend is also observed for the copolymer containing PNVIm, albeit to a lesser extent.

The highest water permeance values are obtained for the blend membranes containing the copolymer of PNVIm (coPNVIm60 and coPNVIm20). However, the selectivity values are lower than those for copolymers of PDMAEMA. These results can be mainly attributed to the degree of crystallinity in the blend (Table 4-1), i.e., the blends (95:5) with PNVIm copolymer contain less crystallinity than the blend with PDMAEMA copolymers, which results in a higher water permeance but lower selectivity. Another factor could also be the chemical composition of the copolymer and the structure of NVIm unit, which has a cyclic side group and contains an aromatic nitrogen atom that improves the wettability of the blend.

On the one hand, the membrane from blend PVA/coPDMAEMA100 (ratio 95:5) exhibits the highest water/ethanol selectivity, especially at lower feed water concentration. On the other hand, the membranes from blends PVA/coPDMAEMA60 and PVA/coPDMAEMA20 with the ratio 95:5 provide the optimal trade-off between water permeance and water/ethanol selectivity. The material formulation with these copolymers produces membranes with higher water permeance than the pristine PVA membrane. Compared to PERVAP™ 4155-80, the membranes prepared with the tailor-made copolymer show higher water permeance and higher selectivity.

From an industrial point of view, the stability of a membrane under industrial operating conditions is crucial; hence it needs to be evaluated and confirmed before its production and its application at industrial scale. In this regard, the thermal stability and the chemical resistance against acetaldehyde were continuously monitored (long term tests) in this work.

As first step, the membrane with the highest selectivity (from blend PVA/coPDMAEMA100) is investigated at 95 °C with a mixture of ethanol/water (5 wt.% of water) containing acetaldehyde up to 600 ppm (this mixture simulates a typical bioethanol stream containing acetaldehyde). The water flux and water concentration in the permeate monitored continuously during 270 h are presented in Figure 4-13 (full raw data of stability test to see the deviation/error are presented in Appendix, Figure 9-7). Throughout the test period, the membrane did not show any change, i.e., the separation performance (both water flux and permeate concentration) is stable over time for the operating conditions described above. The successful long term stability test proves the potential of this new membrane formulation for bioethanol dehydration containing acetaldehyde. As described in the introduction part, the presence of acetaldehyde in bioethanol streams harms the cross-linked PVA membrane.

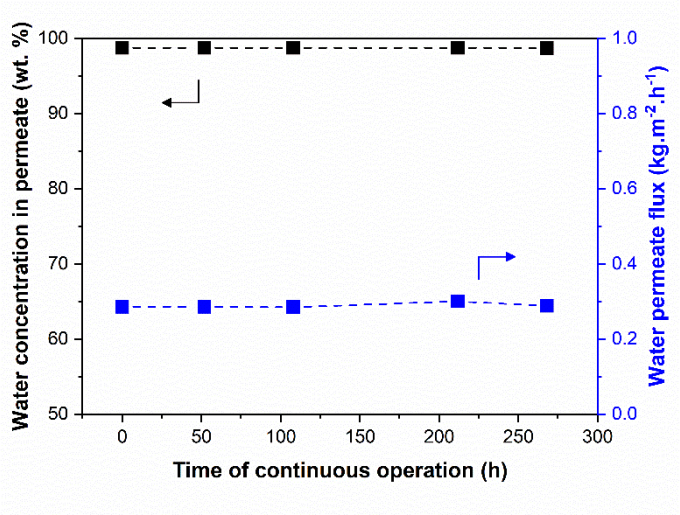

Figure 4-13. Long-term stability test of the composite membrane from blend PVA/ coPDMAEMA100 (ratio 95:5) for the dehydration of a simulated bioethanol stream (EtOH/water) at 95 °C, 2 bar in the feed side and 10 mbar in the permeate side. The water permeate fluxes and concentrations in the permeate are the results obtained for a water concentration in feed of 5 wt.%.

The other two promising formulations (PVA/coPDMAEMA60 and PVA/coPDMAEMA20) with ratio 95:5 are also being investigated at DeltaMem in long term to confirm their stability with different bioethanol streams.

4.3. Conclusion

A series of tailor-made P(NVP-*co*-DMAEMA) and P(NVP-*co*-NVIm) copolymers with defined monomer ratio were synthesized and characterized in terms of chemical composition and thermal properties. Thereafter, PVA/copolymer blends with mass ratio of 80:20 and 95:5 were successfully prepared and used to prepare freestanding dense films for characterization as membrane materials ahead of the fabrication of composite membranes.

The copolymer synthesis by free radical polymerization allowed obtaining tailor-made random copolymers with controlled composition and molecular weight. These copolymers blended with PVA resulted to be better than the commercial copolymer employed for the fabrication of PERVAP™ 4155-80, *i.e.*, membranes with better separation performance for bioethanol dehydration were obtained.

As a general trend, all membranes containing copolymers showed a higher water permeance. The membranes composed of blends with a mass ratio of 80:20 present poor selectivity for ethanol dehydration, albeit show the highest water permeance values. Hence, these membranes are less suitable for ethanol dehydration, but show interesting performance for dehydration of solvents with higher molecular weight than ethanol. The membranes made from blends with a ratio of 95:5 exhibit higher selectivity values than those prepared from 80:20 blends.

The membrane containing the homopolymer coPDMAEMA100 (blend, 95:5) exhibited the highest water/ethanol selectivity, while the P(NVP-*co*-DMAEMA) copolymers containing DMAEMA units (20 and 60 mol.%) allow obtaining composite membranes (blend 95:5) with an optimal trade-off between water permeance and water/ethanol selectivity. These last membranes perform better than the commercial membrane PERVAP™ 4155-80.

The tailored copolymers significantly influenced the crystallinity of the resulting PVA/copolymer blends. Specifically, imidazole moieties were confirmed to inhibit the formation of crystalline domains. Comparatively, the aliphatic side group of PDMAEMA, in contrast to the aromatic imidazole moiety of PNVP, likely resulted in reduced steric hindrance. Consequently, a lower degree of crystallinity was achieved, leading to composite membranes with diminished selectivity. These crystalline regions, being impermeable, act as robust crosslinking points, unaffected by the presence of acetaldehyde. By fine-tuning the copolymer properties through synthesis and adjusting the blend composition with PVA, the enhanced crystallinity contributed to the development of membranes that not only surpassed commercial

membranes in separation performance but also exhibited exceptional chemical stability, as demonstrated in long-term stability tests.

This work demonstrated that by synthesizing tailor-made copolymers (rather using the commercial ones) and blending with PVA, the formulation of membrane material has been tuned for producing membranes with improved separation properties.

The results also confirm that a well-structured work on polymer synthesis and characterization, blend preparation, dense film characterization and composite membrane preparation is very important for understanding the final membrane properties and developing better and robust membranes.

5. Amphiphilic poly(vinyl alcohol) membranes leaving out chemical cross-linkers: Design, synthesis and function of tailor-made poly(vinyl alcohol)-*b*-poly(styrene) copolymers

This chapter contains parts of a published work: Alessandro Angelini, Anja Car, Ionel Adrian Dinu, Luigi Leva, Wilfredo Yave. *Macromolecular Rapid Communications* **2023**, 44, 2200875.

This work is dedicated to our beloved mentor, friend, scientist, collaborator, and great person Prof. Wolfgang Meier. We will remember him for his energy, tenacity, and his positive thoughts. He was a brilliant and visionary scientist who gained worldwide scientific recognition for his work. Despite the hard illness, he stayed passionate about science until the last breath. "He will stay in our hearts."

5.1. Introduction

Design, synthesis, and use of new nanostructured materials are very important in today's world. According to the Sustainable Development Goals (SDG) from the United Nations (Goal 7), "energy is central to nearly every major challenge and opportunity the world faces today".[253] Therefore, innovation in material synthesis and material processing is a key and a driving force to achieve goals related to clean/sustainable energy and to energy efficient processes.

In the last twenty years, scientists focused on design and synthesis of new amphiphilic block copolymers with fascinating properties for nanolithography, photonics, photovoltaics, membranes, and drug delivery.[254-260] These copolymers are a family of polymers having two or more polymer chains (blocks) chemically bonded to each other, and they can self-assemble into ordered nanodomains due to their peculiar chemical and physical properties.[261-263] The control and manipulation of those nanostructured patterns by different methods has been intensively studied too.[262, 264-270] In fact, block copolymer thin films coated on a flat substrate have attracted attention because they are precursor materials for nanodevices and for synthetic membranes that are used in separation technologies. As membranes, they have been studied as

nanostructured dense and porous membranes, they displayed stimuli-responsive properties and superior separation performance than those obtained from conventional polymers used in the membrane fabrication.[271-276] However, very often, the right block-copolymer as membrane material (with specific molecular weight and block ratio) does not exist or its synthesis is very difficult, and thus, the design and synthesis of tailor-made block-copolymers for separation membranes are still challenging within the scientific community.

Due to the polymer solution properties and as solid films, amphiphilic block copolymers based on PVA and poly(styrene) (PVA-*b*-PS) could become important and attractive in the field of coatings, thin films, drug delivery and emulsion systems.[248, 277-279] Both PVA and PS blocks as homopolymers are widely used in a range of industrial products, from packing, membranes, electronics and automotive to food, medical and pharmaceutical applications.[280-282] Although PVA-*b*-PS copolymers were already synthesized in the past following different methods of synthesis,[283-286] they have not attracted much attention compared to other block copolymers. This could have happened because high molecular weight copolymers with narrow molecular weight distribution and controlled PVA/PS block ratio are difficult to obtain.[171, 285-292] The reported copolymers exhibit low molecular weights, and the ratio of PVA/PS are not suitable for applications where they could have a great potential, *e.g.*, for membrane fabrication. So, obtaining block copolymers with high molecular weights and controlled PVA block is a great challenge. Briefly, PVA-*b*-PS with molecular weights within the range of 2 kDa to 60 kDa has been reported. Although the PVA/PS ratio can be well controlled, the combination of PVA/PS ratio with the molecular weight of copolymer are not the appropriate as membrane material. To produce synthetic membranes, the copolymer must have good film-forming property. Thus, PVA-*b*-PS copolymers with the combination of molecular weight higher than 60 kDa and PVA/PS ratio between 4 and 20 (wt.%/wt.%) are needed.

In the field of membranes, PVA homopolymer is industrially used to produce different types of membranes because it is one of the most hydrophilic polymers, as well as simple to process.[248, 282, 293-294] In addition, PVA is a semicrystalline polymer with good mechanical and thermal properties.[294-296] Because of this feature (semicrystalline and highly hydrophilic), the amorphous phase of PVA absorbs water, and thus, this leads to the polymer swelling, and in boiling water, the PVA crystallites can be easily dissolved.[248, 294-297] To limit the swelling and dissolution of PVA, membranes are chemically cross-linked, most commonly using aldehydes and dicarboxylic acids, which under acid catalysis react with PVA to form cross-links.[293-294, 298] Methods of PVA cross-linking are of great interest since PVA has been industrially used. Today, PVA membranes are still being produced by using chemical cross-linkers and acid

catalyst.[214, 282] Physical or thermal cross-linking methods were also proposed to make PVA resistant to water, the key in these methods is the crystallinity.[244, 248, 295, 299-300] By heat treatment (HT) or thermal annealing (above glass transition temperature), the PVA chain motion in the amorphous phase (apparent molten state) increases, and because of attraction forces due to the hydrogen bonding, they can form new crystallites and induce the growth of existing crystallites, consequently the crystallinity increases. By freezing-thawing cycles, the crystallinity, and the size of crystallites in PVA can be also controlled, this method has been widely used in the production of hydrogels[248, 301-303] and films for drug-release.[303-305] Thus, new routes of either chemical or physical PVA cross-linking are still of great importance.

In this work, we focus on the design, synthesis and self-assembly of tailor-made PVA-*b*-PS as membrane material. To our knowledge, this is the first report on synthesis of PVA-*b*-PS copolymers with high molecular weight and good film-forming properties. Combining the benchmark hydrophilic block (PVA) with a small hydrophobic domain (PS) within the membrane matrix, we demonstrate that PS nanodomains act as cross-linking points, so chemical cross-linkers and acid catalysts would no longer be needed. Pervaporation tests were carried out using a standard mixture of ethanol and water to evaluate block copolymer membranes' separation performance. We also show that by an additional thermal annealing, the crystallinity of the block copolymer can be enhanced, making the material more resistant to water and solvents. Therefore, the use of this type of block copolymers in the membrane field would become a breakthrough since the use of regulated chemical compounds (acids and cross-linkers) can be eliminated, and the manufacturing cost of end products could be reduced.

5.2. Results and discussion

5.2.1. Synthesis and structural characterization of block copolymers

The synthesis of PVA-*b*-PS or PS-*b*-PVA copolymers with low Mn and narrow dispersity is straightforward, as reported by Altintas et al[171] [38] and other authors (Table 9-3, Appendix). However, when we attempted to synthesize copolymers with high Mn and high content of PVA block, we ran into some limiting factors that hindered the polymerization reaction, i.e., the growth of polymer chain was limited.

To overcome this problem, we first synthesized PS-Br homopolymers according to Altintas et al, the kinetic of polymerization was investigated, and the results showed that high concentration of initiator and catalyst, and low concentration of reducing agent ($Sn(EH)_2$)

produce well controlled ($Đ$ < 1.10) polymers, but with low Mn. The rate of polymerization was quite linear until the conversion reached 20-30%, and the values of $Ln[M]_0/[M]_t$ increased linearly with time at this stage. However, for longer time of polymerization, both the conversion and the values of $Ln[M]_0/[M]_t$ did not show linearity anymore, they showed a plateau (Figure 9-8, Appendix), and thus, polymers with lower Mn than 32 kDa were obtained (Figure 9-8, Appendix). As a second step, lower concentration of initiator and catalyst were used to reduce the number of polymer chains and to minimize the β-hydrogen elimination,[306-308] respectively. After several polymerization experiments, the reducing agent ($Sn(EH)_2$) was increased with the aim of regenerating the active catalyst (Cu^I/Ligand), since during the termination process, Cu^{II}/Ligand is formed.[309] Thus, these changes in the formulation allowed obtaining PS-Br homopolymers with higher M_n and high conversion.

The chain extension of PS-CTA by vinyl acetate (VAc) in presence of 2,2'-azobis(2-methylpropionitrile) (AIBN) was more straightforward, here we only increased the concentration of VAc monomer with respect to PS-CTA macroinitiator, and both the conversion and the M_n could be controlled (see Figure 9-8 in Appendix).

Figure 5-1 shows the results of the analysis performed during the PS-*b*-PVA synthesis (*e.g.*, PS_{100}-*b*-PVA_{1639}): the synthesis of PS-Br by ARGET-ATRP (Activators ReGenerated by Electron Transfer atom transfer radical polymerization; ^{1}H NMR and GPC), the bromine substitution by the azide group (GPC), the CTA attachment (GPC), the chain extension by RAFT polymerization of VAc (GPC) and the obtention of PS-*b*-PVA by hydrolysis (^{1}H NMR and ATR-FTIR). The ^{1}H NMR spectra corresponding to PS-Br, PS-N_3, PS-CTA, PS-*b*-PVAc and PS-*b*-PVA are presented in Appendix (Figure 9-9). Here, we show only the spectra for PS-Br and PS-*b*-PVA (Figure 5-1, a and b), the observed peaks are consistent with literature,[171, 290-291, 310-311] the characteristic signals corresponding to aromatic protons of the PS block are clearly identified in both spectra, these are associated to the resonance from 7.24 to 6.30 ppm (peaks c, d and e). The signals from 1.62 to 1.33 ppm arise from the aliphatic protons from the block copolymer backbone (peaks a, b, and f) except for the protons adjacent to the hydroxyl groups which appear at 3.84 ppm (peak g). The signals at 4.68, 4.52 and 4.28 ppm are related to the different tacticity of the hydroxyl proton from the PVA block (peak h = isotactic, i = atactic and j = syndiotactic).

The change of molecular structure from PS-Br to PS-N_3 to PS-CTA and to PS-*b*-PVAc is nicely monitored by the GPC elugrams (Figure 5-1c). GPC elugrams at different stages during the synthesis show that the synthesized PS-Br homopolymer exhibits narrow molecular weight

distributions ($Đ$ = 1.08), this dispersity value is kept when the bromine group is substituted by the azide group. Later, the PS-CTA shows a slight increase of dispersity to 1.10. These results confirm a good control of the PS-CTA macroinitiator synthesis. However, in this last step, a small bump appeared at the lower elution volume (21 mL) which would correspond to the formation of small amount of higher molecular weight species. After chain extension of PS-CTA with VAc, the GPC curve corresponding to PS-*b*-PVAc shows a significant shift to lower elution volume, what confirms the increase of molecular weight of polymer, the dispersity value in this case increased to 1.74. Two small shoulders are also observed, the first one matching to the PS-Br precursor (23.5 mL) and the second one (21 mL) to the PS-CTA. Both small shoulders would correspond to inactive chain ends that did not lead to chain extension, and thus, they contributed to the increase of PD. These small fractions of both PS-Br and PS-CTA can be tolerated in this step, since in the next step (hydrolysis) they should not precipitate. Even though a broader molecular weight distribution is observed, in practice they should be lower when PS-*b*-PVAc is hydrolyzed to PS-*b*-PVA. Compared to other PS-*b*-PVAc reported in the literature (Table 9-3, Appendix), the dispersity that we have obtained are similar or lower.

The full conversion of PVAc block to PVA block is confirmed by ^{1}H NMR (Figure 9-9, Appendix) and ATR-FTIR (Figure 5-1d) analyses. The complete disappearance of C=O stretch at 1735 cm^{-1} and appearance of the broad O-H signal around 3287 cm^{-1} confirm that PVAc was completely hydrolyzed.[171, 311-312] The peaks corresponding to PS (C-H stretching of the benzene ring at 3026 cm^{-1}, carbon ring vibration at 1601 and 1493 cm^{-1}, and the out-of-plane ring vibration at 755, 698 and 540 cm^{-1})[171, 313] remained unaffected. Besides the confirmation of the successful hydrolysis, few other characteristic peaks were identified, like the medium band at 2924 cm^{-1} which is attributed to the stretching of CH groups from the backbone, the increase of the band at 1420 cm^{-1} that is characteristic for the bending vibrations of the CH_2, the medium band at 1323 cm^{-1} and the strong peak at 1088 cm^{-1} associated to the OH bending and the C-O stretching of the alcohol group, respectively. The semicrystalline feature of PVA that is represented by the C-O stretching vibration at 1141 cm^{-1} [314-315] is also observed.

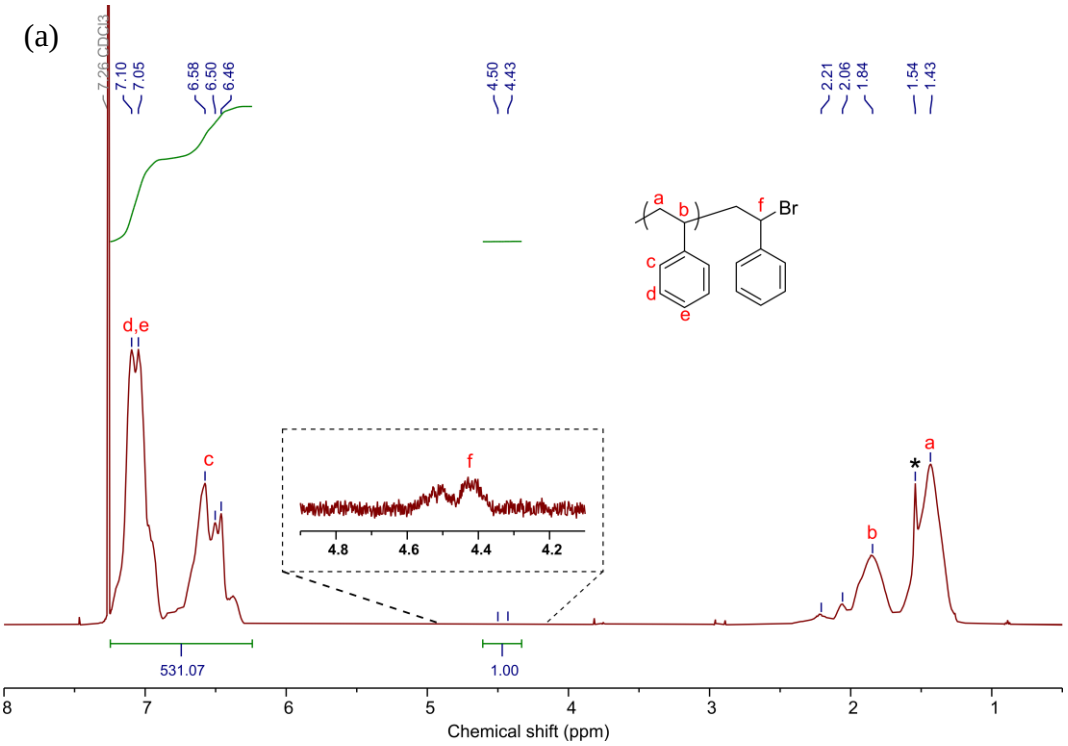
(a)
7.26 CDCl3
7.10
7.05
6.58
6.50
6.46
4.50
4.43
2.21
2.06
1.84
1.54
1.43
a
b
f
Br
c
d
e
d,e
c
f
4.8
4.6
4.4
4.2
b
a
*
531.07
1.00
8
7
6
5
4
3
2
1
Chemical shift (ppm)

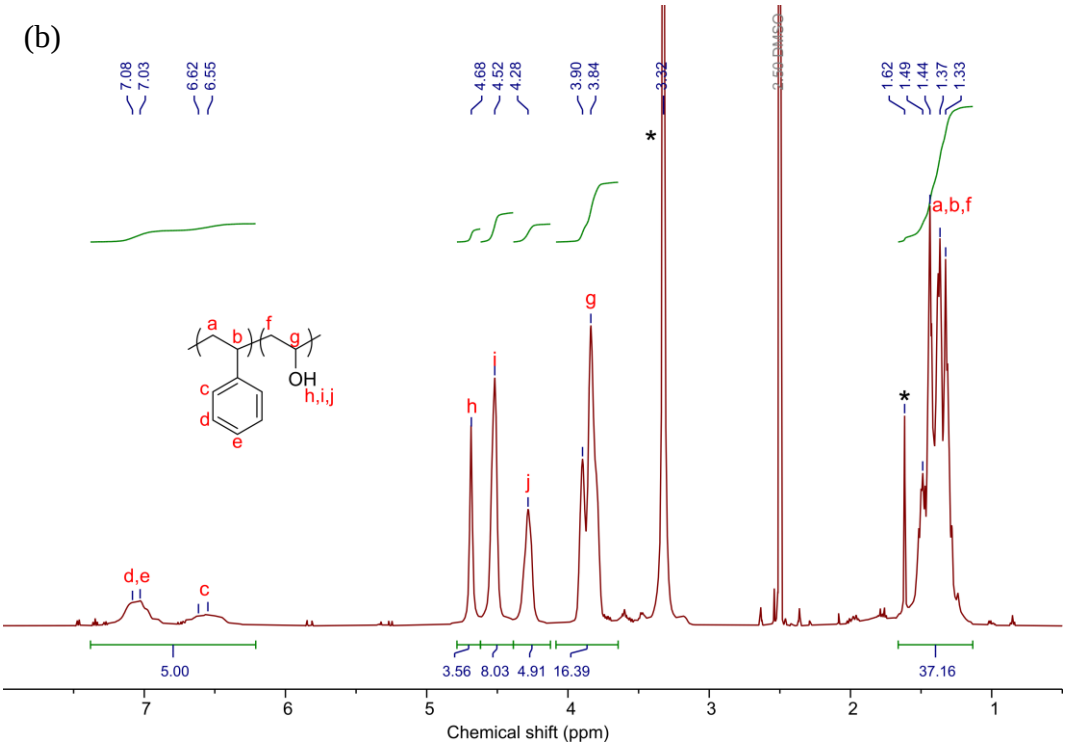
(b)
7.08
7.03
6.62
6.55
4.68
4.52
4.28
3.90
3.84
3.32
3.50 DMSO
1.62
1.49
1.44
1.37
1.33
a
b
f
g
OH
h,i,j
c
d
e
h
i
j
g
*
a,b,f
d,e
c
5.00
3.56
8.03
4.91
16.39
37.16
7
6
5
4
3
2
1
Chemical shift (ppm)

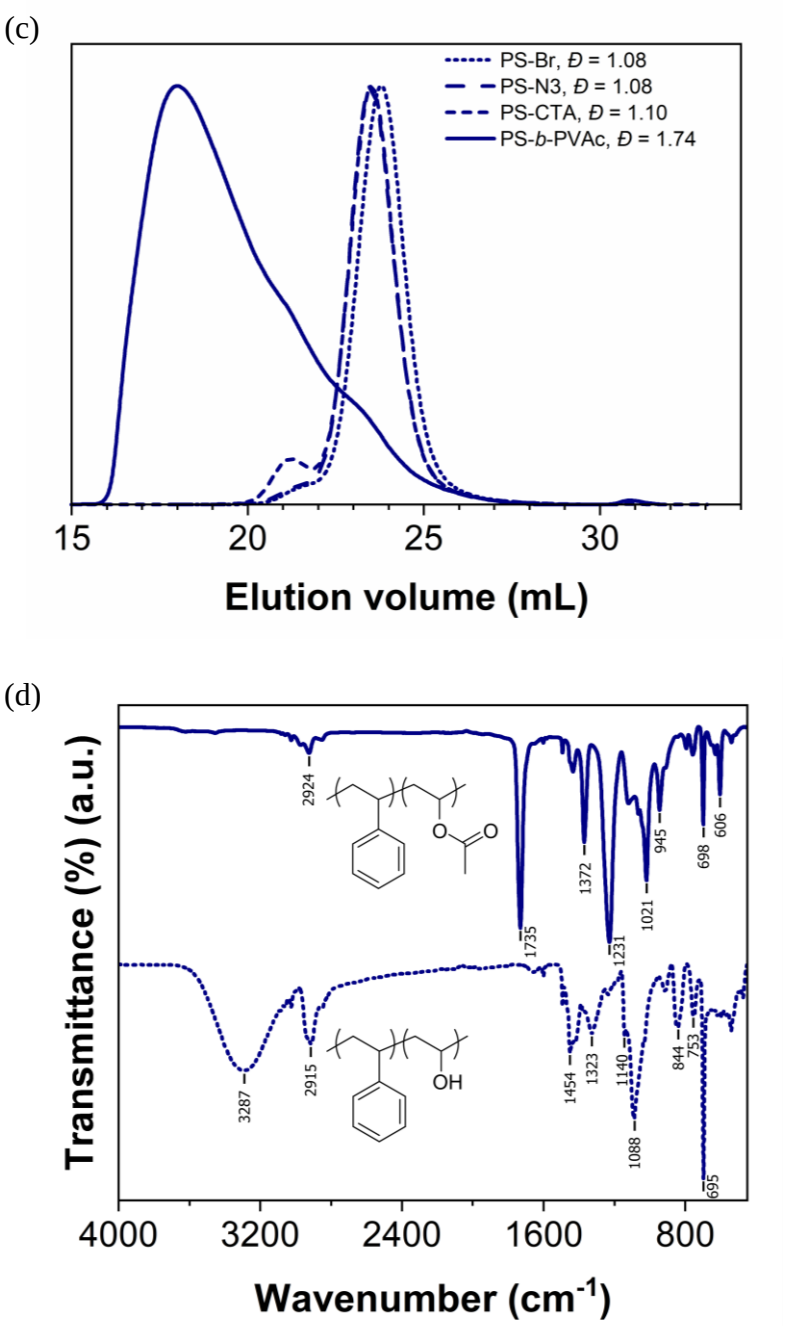

Figure 5-1. Chemical structural characterization of synthesized homopolymers and diblock copolymers: a) ^{1}H NMR spectrum corresponding to PS-Br homopolymer, and b) ^{1}H NMR spectrum of PS-*b*-PVA block copolymer. The peaks marked with an asterisk (*) correspond to the trace of solvents used during synthesis and purification steps (water and THF in CDCl3 and DMSO-d6, respectively. c) GPC elugrams of PS-Br, PS-N_3, PS-CTA and PS-*b*-PVAc polymers, and d) ATR-FTIR spectra of PS-*b*-PVAc and PS-*b*-PVA diblock copolymers.

A list of copolymers synthesized for this work are presented in Table 5-1. In addition to the hydrophilic block-copolymers, a block copolymer containing high PS block was synthesized for comparison. The names of block copolymers are referred to PVA content (weight fraction)

obtained by ^{1}H NMR spectroscopy. The M_n values are also obtained from the ^{1}H NMR analysis. As seen, we were able to obtain copolymers with Mn higher than 60 kDa and PVA block content higher than 80 wt.%. Because the PS-*b*-PVA copolymers are not soluble in almost all typical solvents used in GPC analyses (Table 9-5, Appendix), the reported dispersity corresponds to PS-*b*-PVAc, so we assume that the dispersity values do not change during the hydrolysis step, or even they decrease due to the presence of inactive PS-Br and PS-CTA that did not precipitate together with PS-*b*-PVA, described above.

Table 5-1: Composition, conversion, M_n, $Đ$ and f_{PVA} of synthesized PS-*b*-PVA copolymers.

Sample	Composition [a]	Conversion [%]	M_n [a] [g/mol]	$Đ$ [b]	f_{PVA} [a]
PVA-31	PS_{298}-*b*-PVA_{318}	5	45000	1.29	0.31
PVA-68	PS_{192}-*b*-PVA_{948}	25	61700	1.53	0.68
PVA-79	PS_{139}-*b*-PVA_{1220}	61	68200	1.45	0.79
PVA-87	PS_{100}-*b*-PVA_{1639}	55	82500	1.74	0.87
PVA-92	PS_{56}-*b*-PVA_{1500}	66	71800	2.11	0.92

[a)] obtained by ^{1}H NMR; [b)] corresponds to PS-*b*-PVAc (obtained by GPC)

The copolymers that have high M_n (> 60 kDa) and high content of PVA block (> 80 wt.%) are tailor-made for applications in the membrane field (discussed later). The other copolymers with low M_n and low content of PVA do not show good film-forming property (Figure 9-13, Appendix), and are less hydrophilic, and thus, they cannot be used as membrane material. However, they can have potential applications in others field.

5.2.2. Thermal characterization of block copolymers

DSC and TGA measurements were performed to determine the glass transition temperature (T_g), melting temperature (T_m), crystallinity and decomposition temperature (T_d) of homopolymers (PS and PVA) and block copolymers (Figure 5-2), respectively. The DSC thermograms (Figure 5-2a) confirm that the copolymers are constituted by two blocks that tend to microphase separation (presence of two glass transitions). The first transition observed between 74 and 81 °C corresponds to the glass transition of PVA,[316] while those between 101 and 106 °C to the glass transition of PS.[317] The T_g of the short block either PS or PVA in the block copolymers (PVA-92 and PVA-31) cannot be distinguished, this can be because when a polymer segment of the block copolymer decreases in length, its T_g can be suppressed relative

to the other segment.[318] At 180 °C, an endothermic peak corresponding to the melting transition of the PVA crystalline domains appears,[244-245, 316] from this endothermic peak we obtained the T_m (> 220°C) and the crystallinity of PVA block. The fraction of crystallinity is calculated from the ratio between the enthalpy of fusion from the endothermic melting peak (ΔH_f) of sample and the enthalpy of fusion of the totally crystalline polymer PVA (ΔH_f^0) by using ΔH_f^0 = 138.6 J g^{-1}.[244]

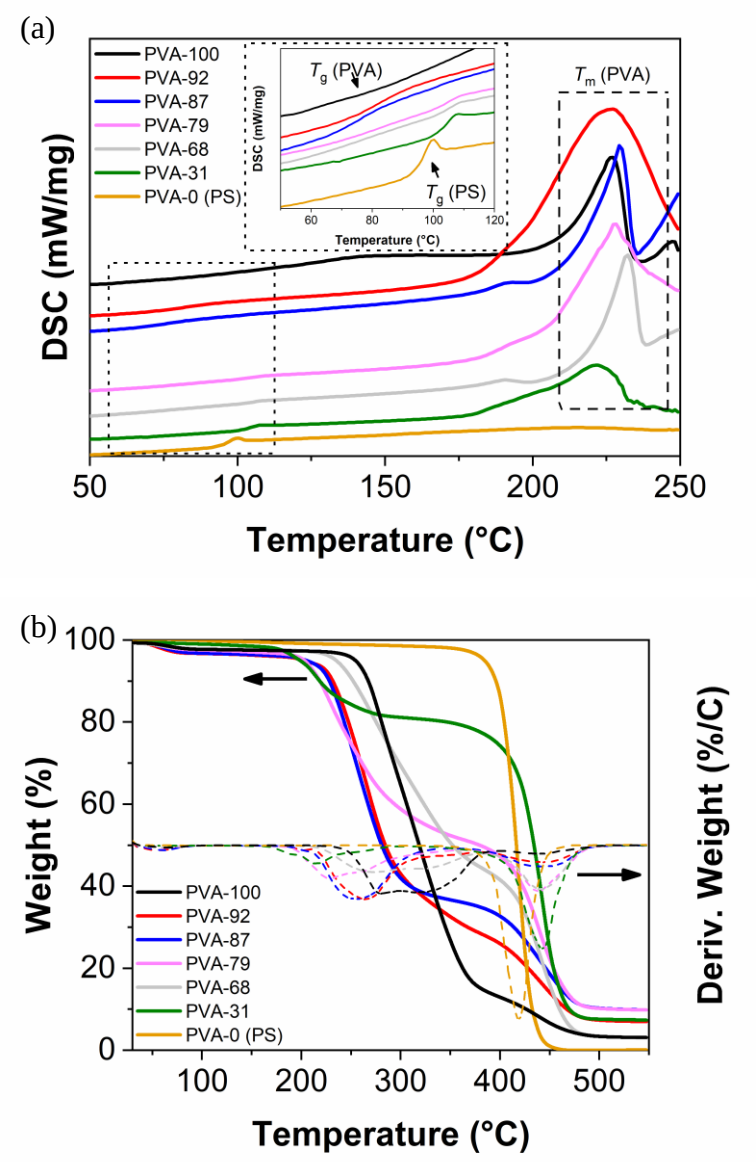

Figure 5-2. DSC (a) and TGA (b) thermograms for PVA and PS homopolymers and for PS-*b*-PVA copolymers.

The TGA shows three distinct degradation regions (Figure 5-2b), the first weight loss (≈100°C) is attributed to the evaporation of water, which is absorbed by the hydrophilic samples (except the PS homopolymer). From ≈200°C to 240°C, the decomposition of PVA starts, and the lowest

value corresponds to the copolymer with low M_n and low content of PVA, while the other copolymers exhibit higher values of T_d, which are expected because the M_n and PVA content in the copolymers increase. The second weight loss is observed in the range of 400-450 °C, this T_d corresponds to PS. All thermal properties corresponding to the copolymers of interest and homopolymers are summarized in Table 5-2.

Table 5-2: Thermal properties of PS, PVA and PS-*b*-PVA copolymers with high M_n.

Sample	T_g^{PVA} [°C]	T_g^{PS} [°C]	T_m^{PVA} [°C]	Crystallinity [%]	T_d^{PVA} [°C]	T_d^{PS} [°C]
PVA-0 (PS)	n.a.	95.2 ± 0.3	n.a.	n.a.	n.a.	401
PVA-31	-	103.4 ± 0.1	223.1 ± 1.1	27.4 ± 1.6	192.0	418.0
PVA-68	72.1 ± 0.2	105.4 ± 0.4	231.8 ± 0.4	32.4 ± 1.7	237.0	419.0
PVA-79	74.8 ± 1.5	104.4 ± 0.6	226.4 ± 1.4	35.6 ± 2.8	207.0	416.0
PVA-87	75.2 ± 0.9	103.2 ± 1.8	229.1 ± 0.6	39.6 ± 1.2	225.0	405.0
PVA-92	77.4 ± 1.3	-	231.5 ± 0.2	52.6 ± 0.6	231.0	411.0
PVA-100	76.4 ± 0.2	n.a.	229.0 ± 1.4	55.2 ± 1.7	250.0	n.a.

The full conversion of PVAc to PVA by hydrolysis was also confirmed by DSC (Figure 9-11, Appendix). For the PS-*b*-PVAc, the thermogram shows that the block copolymers are amorphous, *i.e.*, only glass transitions of each block are observed (*e.g.*, T_g^{PVAc} = 39.7 °C and T_g^{PS} = 101.8 °C). However, after the hydrolysis of PVAc block to PVA, the T_g corresponding to PVAc disappears completely, and the endothermic peak corresponding to the PVA melting transition appears. According to the DCS analysis, the copolymers are composed by two separated microphases, one that corresponds to PS amorphous phase, and the other one where PVA amorphous and crystalline phase coexist. The interesting of these copolymers is that PS is completely amorphous, glassy, and acts as barrier, while PVA is semicrystalline, its amorphous phase can swell in presence of water, and the swollen state of this phase allows permeating water and other molecules depending on molecular size and affinity. Thus, these features give the possibility of tunning the final transport property of material.

5.2.3. Thick dense film preparation and characterization

As this block copolymers are not soluble in common solvents (Table 9-5, Appendix), the Hansen Solubility Parameters (HSPs) of each block were plotted together with those of

common solvents (Figure 5-3). This 3D plot helps to identify possible formulations (mixtures of solvents) which may allow obtaining a homogeneous solution. The dashed line (gray) between the PS and PVA core represents the calculated parameters according to the hydrophilic block content, *e.g.*, for a balanced ratio (50/50 wt.%/wt.%), N,N-Dimethylacetamide (DMAc) should be an ideal candidate because the HSP values are in the middle of the line. The choice of this solvent is in good agreement with the literature, since PS-*b*-PVA block copolymers with low M_n and low PVA content were dissolved in DMAc.[171] In our case, the dissolution of PVA-*b*-PS with high M_n and high PVA content turned out to be impossible. Other solvents and mixtures of thereof did not provide satisfying results, and after several attempts, the only solvent that dissolved to the block copolymers was hot DMSO, except to PVA-31 block copolymer that has high content of PS block.

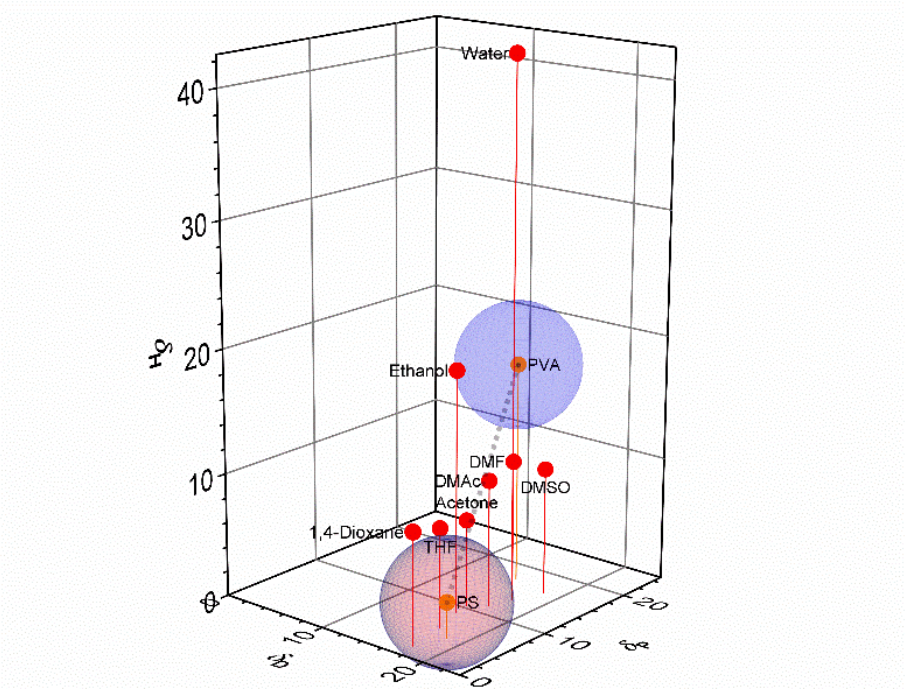

Figure 5-3. Representation of the Hansen Solubility Parameters in 3D space for PVA, PS, PVA-*b*-PS and typical solvents used for membrane preparation.

Self-standing dense films with thicknesses ranging between 15-20 µm were prepared by casting from solutions of block copolymer in DMSO. For comparison purposes, commercial PVA and PS homopolymers (referred to as PVA-100 and PVA-0) films were also prepared.

CA measurements performed on the self-standing films (Figure 5-4a) show that the block copolymer samples are less hydrophilic than the sample prepared from PVA homopolymer, which is correlated with the PVA content. The PVA film shows the lowest CA value (57°), while the PS film has the highest one (95°). Interestingly, the CA values of the block copolymer

films increase in a very cute way as the PS content increases. Compared to the chemically cross-linked PVA (55°),[319] the block copolymer films exhibit high values of CA. Although the CA values of copolymer films slightly increase (from 74.9° to 83.5°) as the PS content increases, the degree of swelling of samples (Figure 5-4b) in ethanol/water mixture is almost the same (≈ 20%), which means that the content of PS block (< 32 wt.%) in these copolymers did not affect the swelling of block copolymer films. These results could be attributed to three factors: 1) a balance between PVA content in the copolymer and PVA amorphous fraction, *i.e.*, high PVA content balances the low amorphous fraction of PVA (see Table 5-1 and Table 5-2), 2) the slight variation of M_n (Table 5-1), and 3) the water content in the mixture (7 wt.% water in ethanol) used for the swelling tests. The fact of using ethanol/water mixture instead of water for the swelling test is to obtain realistic results that represent the medium where the membranes will be used, since the swelling tests are important for the membrane material, because the separation performance and stability of polymeric membranes depend strongly on swelling degree of material. Last, the PS film did not swell at all, and the chemically cross-linked PVA swelled up only 5%.

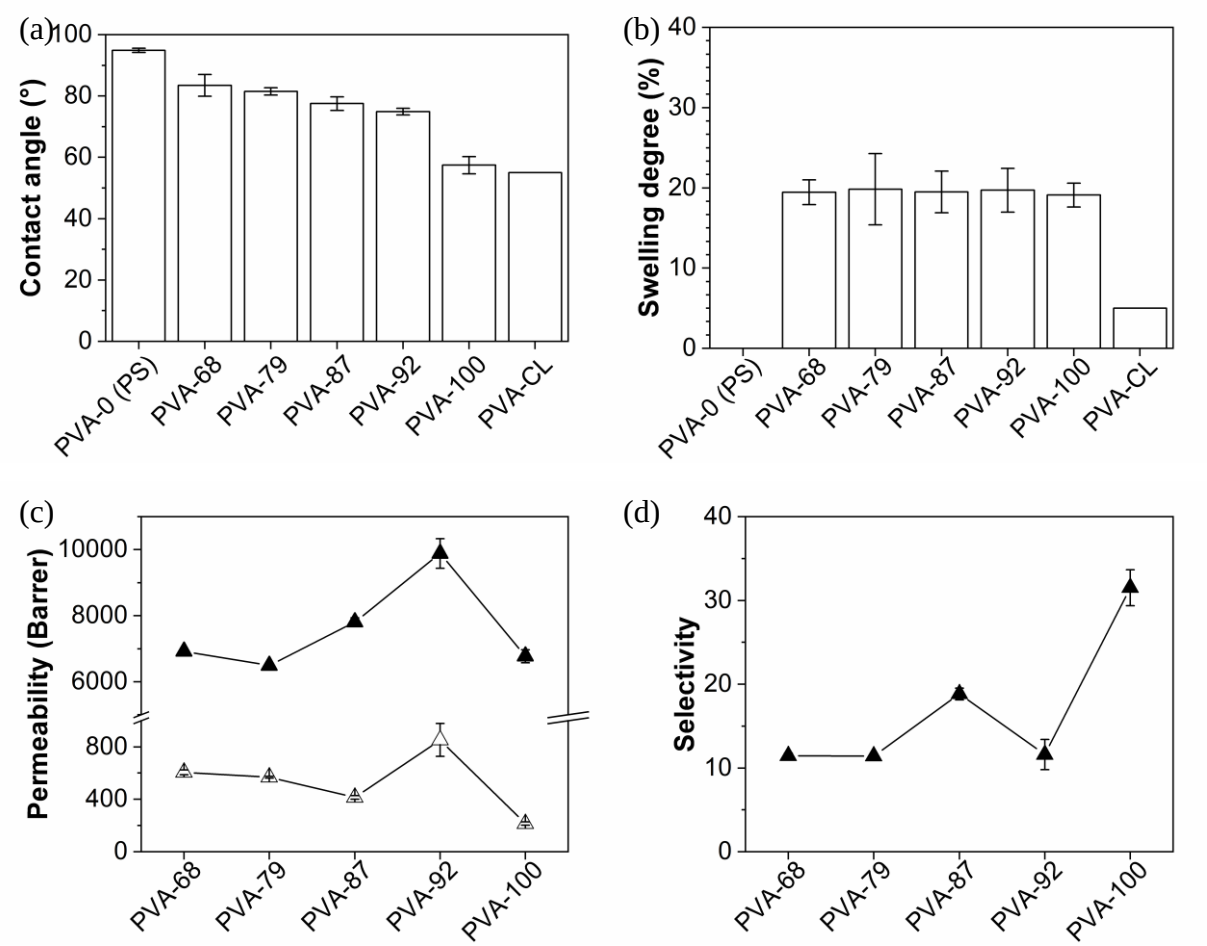

Figure 5-4. Properties of self-standing dense films: a) Contact angle, b) swelling degree, c) water (filled experimental points) and ethanol (unfilled experimental points) permeability, and d) water/ethanol selectivity.

Figure 5-4c shows the water and ethanol permeability through the dense films. Those were obtained by carrying out pervaporation tests (feed: ethanol/water mixture with 4.5 wt.% water, operating temperature: 95 °C, and permeate pressure: 10mbar). The water permeability values for copolymer membranes with less than 80% of PVA block are lower than those with 87% and 92%. This result is attributed to the PVA hydrophilicity (Figure 5-4), *i.e.*, the higher the hydrophilicity of membrane, the higher the water permeability.[43, 73] However, the PVA homopolymer sample showed even lower water permeability, which was not expected and is contrary to the previous statement. Therefore here, the PS domain played an important role. In films from PVA homopolymer, the polymeric chains of PVA crystallized to a major extent, which resulted in higher crystallinity and less PVA permeable amorphous phase, hence it led to lower water permeability. In films from PVA-*b*-PS copolymers, the presence of PS nanodomains hindered the PVA crystallization and thus, it led to less crystallinity (Table 9-6,

Appendix). Therefore, a controlled quantity of PS domain allowed to obtain potential membrane materials like PVA-87 and PVA-92.

As seen, the water permeability increases slowly as the PS content decreases within PVA matrix until reaching a maximum (PVA-92), these results agree with the hydrophilicity nature of the copolymers. This means the affinity of water molecules is favored as the PVA content in the block copolymer increases.

On the other hand, the water/ethanol selectivity values for the block copolymer films are lower than the sample prepared from PVA homopolymer. The PVA film shows the highest value of selectivity (≈ 30), because the crystallinity is high and the homopolymer is the most hydrophilic, where the water affinity is high. This behavior fits well with the tradeoff of polymeric membranes, the higher the selectivity, the lower the permeability (see Figure 5-4c,d).

In block copolymer films, the water/ethanol selectivity shows a maximum that could be between 80 and 95 wt.% of PVA content. As the water permeability also shows a maximum around 92 wt.% of PVA, we believe this to be due to the nanostructure of block copolymer. At the beginning of this work, we targeted to synthesize tailor-made block copolymers with PVA content higher than 80 wt.% and high M_n, and we hypothesized that small quantity of PS domains within the PVA matrix will act as cross-linking points without affecting much the separation performance of PVA membranes. Surprisingly, here we confirm our hypothesis, according to Bates and Frederickson,[261, 320] and Groot and Madden,[321] the self-assembly of di-block copolymers and its nanostructure domains can be predicted knowing χN and f (where χ is the Flory-Huggins parameter, N is the polymer length, and f the ratio of block size). So, the copolymer PVA-92 falls within the disorder region and the resulting nanostructure may be disorder cubic arrays, and the PVA-87 enters in the cubic symmetry phase with ordered nanodomains as body centered cubic structure. Thus, the characteristic of these nanostructures supports the water permeability results, since a cylindrical and/or lamellar nanostructure would lead to lower water permeability due to the PS continuous nanodomains that would act as impermeable phases.

The nanostructure in melt, the properties, and the self-assembly of these block copolymers (for the entire range of composition) will be investigated and discussed in a separate work. Here, we only focus on block copolymers with > 80 wt.% of PVA block and high M_n.

5.2.4. Self-assembly of block copolymers in solution

Obtaining ordered nanostructures with block copolymers is complicated because different factors such as substrate, polymer solution concentration, thickness of the thin film, method of preparation, ambient conditions, method of post-treatment among others affect the self-assembly. Thus, the control of nanostructure formation by different methods is considered crucial for obtaining large areas (m^2) of thin films or membranes.[265, 271, 322-324]

To induce and control the self-assembly of block copolymers, we used the method of "solvent switch" by dialysis (Figure 5-5), this method is very versatile because allows controlling the solvent exchange rate and the final solute concentration. First, the PVA-*b*-PS copolymer is dissolved in DMSO (3 wt.%), as described in section 7.4. Second, water is added dropwise to the solution; while water is being added, the block copolymer chains start to self-assemble to form micelles with PS block as core, surrounded by PVA as shell, this happens because the medium is aqueous and the PVA block is hydrophilic. Third, when DMSO is completely removed by dialysis, the self-assembled micelles coexist in water and are stable (Figure 9-12, Appendix). Last, the self-assembled micelles can be cast onto a substrate to obtain nanostructured thin films.

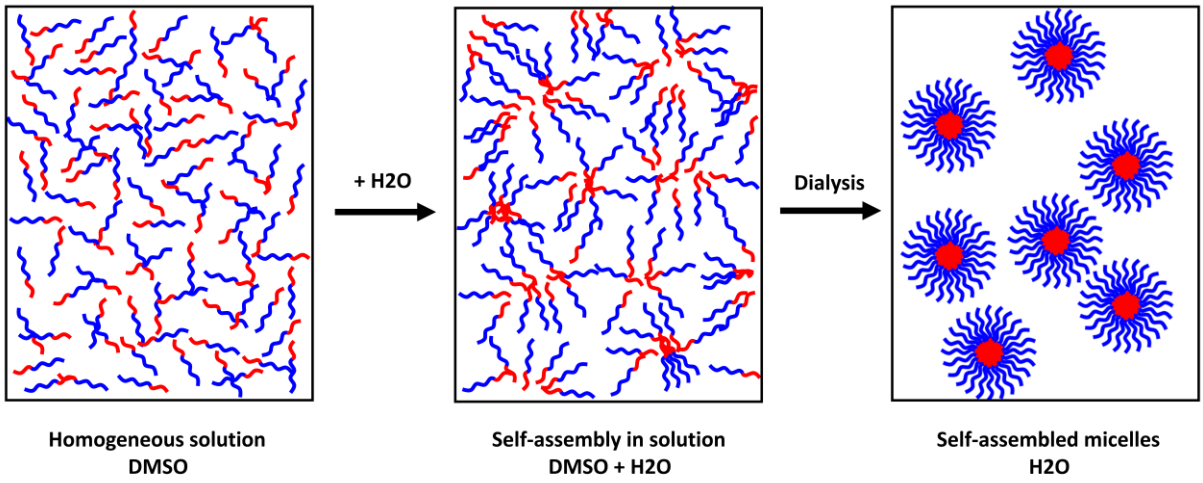

Figure 5-5. Self-assembly of PVA-b-PS copolymer in solution by "solvent switch" method.

The prepared PVA-*b*-PS micelle solutions were characterized by dynamic light scattering (DLS) and TEM (Figure 5-6). The DLS results show the presence of a trimodal distribution, the first peaks correspond to the single micelles, whereas the second and the third one would correspond to aggregates that resulted due to the aggregation of single micelles because of strong hydrogen bonding between PVA shells. The highest intensity peak corresponds to single micelles with (D_h) ≈ 70, 90 and 100 nm, for PVA-92, PVA-87, and PVA-79 copolymers,

respectively. Compared to literature,[286, 291, 325-326] the measured sizes are in good agreement, considering the high molecular weight obtained in this work. The aggregates have larger diameters, 400 nm, 700 nm and 5 μm, respectively. Because the samples were not filtered, the formation of aggregates was expected, since typical protocols for DLS analysis include sample filtration. In our case, the samples were not filtered because the solution is used for the thin film preparation as it is obtained. TEM images confirmed the self-assembly (Figure 5-6b-d) of block copolymers in solution. The images reveal the presence of a plethora of micellar nanostructures, the presence of worm-like structures also confirm that the micelles tend to aggregate, as observed in DLS analysis. Although many micelles are partially aggregated, it is possible to measure the diameters of the dried single micelle nanostructure, which are 19 ± 2 nm. Compared to DLS analysis, the D_h values obtained by TEM are lower, however they are expected due to the differences in the methods used and sample nature. In DLS, the single micelles are highly swollen and due to the PVA content and concentration of solutions (15 mg mL^{-1}), the single micelles are big and tend to aggregate in a greater extent, while for the TEM analysis the solution is diluted (0.1 mg mL^{-1}), the nanostructures are frozen trapped and dried, and thus, the single micelles and aggregates shrink.

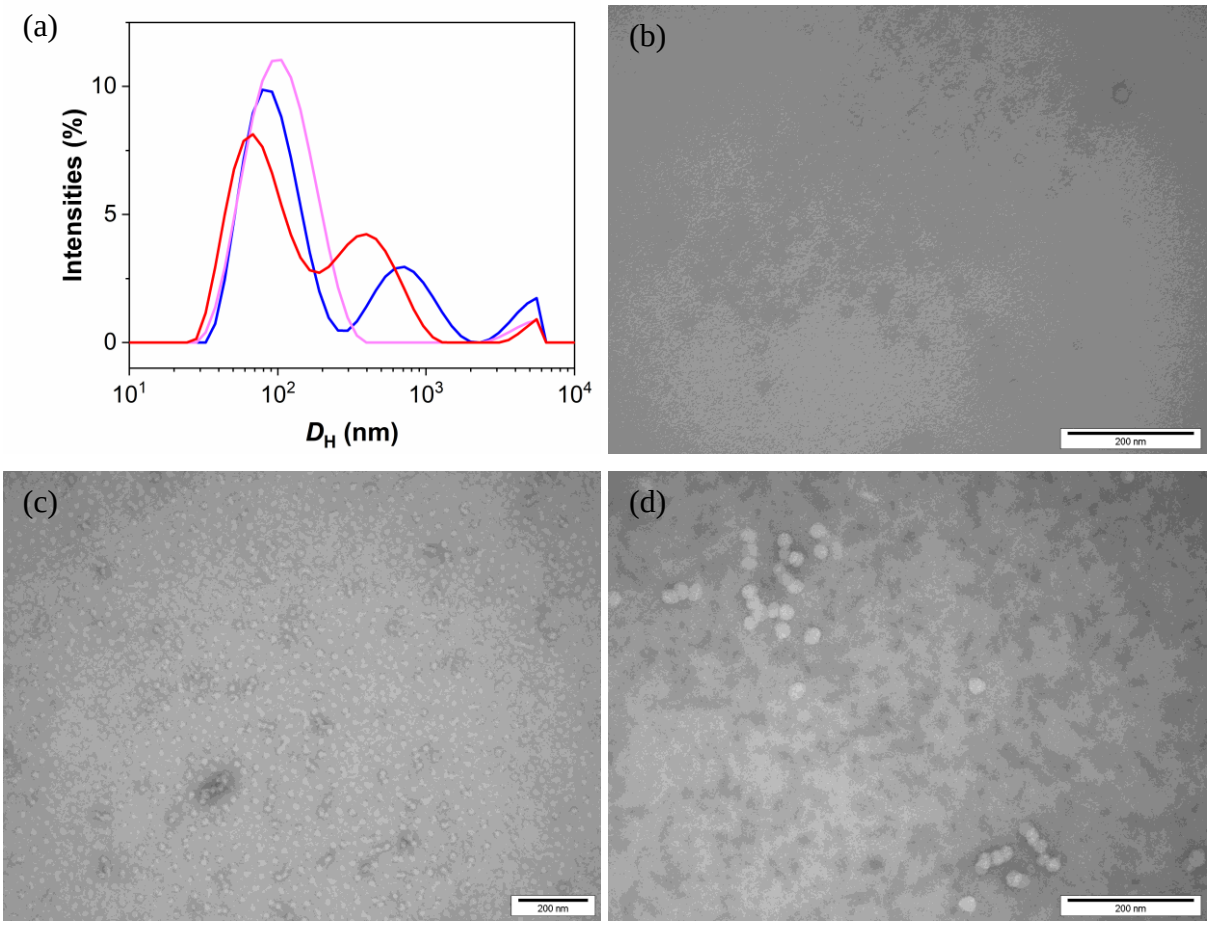

Figure 5-6. DLS results corresponding to PVA-92 (red line), PVA-87 (blue line) and PVA-79 (pink line) aqueous solution (a), TEM micrographs of PVA-92 (b), PVA-87 (c), and PVA-79 (d).

5.2.5. Thin films from self-assembled micelles

Although self-standing thin films are possible to obtain as small samples (Figure 9-13, Appendix), for practical purposes, thin films onto poly(acrylonitrile) (PAN) porous substrate were prepared from the self-assembled micelles in solution. Because the micelles are dispersed in water and do not contain any chemical cross-linkers or acid catalysts, we think our process is a very clean and innovative green process. Our approach of using these tailor-made copolymers is to leave out the chemical cross-linkers during the PVA membrane preparation (state-of-the-art of PVA membranes includes the use of chemical cross-linkers). The thin film membranes prepared from these block copolymers would show interesting separation performance due to the nanostructure within the membrane matrix. The micelles in solution after the casting aggregate as the water evaporates, and when they are dried, the PVA blocks make up the matrix of membrane and the dispersed PS nanodomains act as cross-linking points. Thus, this membrane would no longer need chemical cross-linkers.

We selected the PVA-87 sample to prepare thin film membranes, according to the copolymer composition and micelle formation in the aqueous solution, the resulting membrane would be composed of a PVA matrix with PS nanodomains uniformly distributed as body centered cubic structure. For comparison, thin film from PVA homopolymer was also prepared under same conditions.

Figure 5-7 shows the separation performance of thin films (permeance and selectivity) as a function of temperature of thermal annealing or HT. As expected, the water permeance in block copolymer thin films is higher (≈ 100%) than that in PVA homopolymer (Figure 5-7a), and a thermal annealing (145 and 160 °C) of the thin films led to lower water permeances, but still higher than PVA homopolymer film. Thermal annealing of block copolymers is applied to induce molecular organization and to improve the micro-phase separation.[327-328] In addition, thermal annealing induce crystallization of PVA chains,[244, 295] and thus, the permeability or permeance decreases. In samples annealed or heat treated at 160°C, the water permeance decreased more than 50% compared to the no-heat treated sample. In the case of ethanol permeance, the decrease is more pronounced, *i.e.*, after HT at 145 or 160°C, the ethanol permeance in block copolymer films decreased by a factor of 15 and 45, respectively. These results confirm that within the membrane matrix, the micro-phase separation between blocks and the PVA crystallinity are enhanced because of thermal annealing (Figure 9-14, Appendix). In PVA homopolymer film, the permeance decrease is attributed only to the increase of crystallinity.

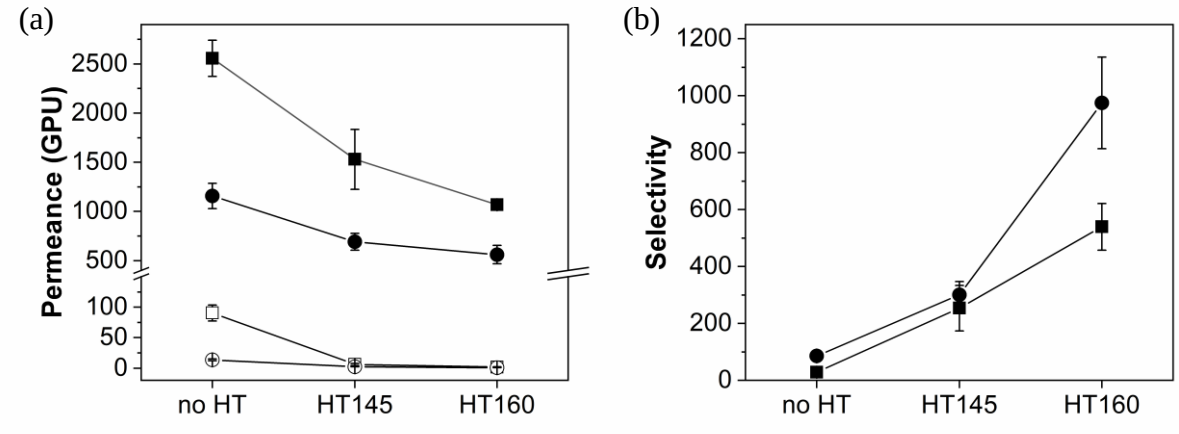

Figure 5-7. Separation performance of thin film membranes for PVA-87 block copolymer (square experimental points) and PVA homopolymer (circle experimental points); (a) water (filled points) and ethanol (unfilled points) permeance, and (b) water/ethanol selectivity.

Due to the enhanced microphase separation and increased PVA crystallinity, the water/ethanol selectivity in the block copolymer thin films increased by a factor of 9 after a heat treatment at 145 °C. A subsequent heat treatment at 160 °C, the selectivity enhancement is almost by a factor of 20. These changes in the membrane performance are impressive and are explained by the nature of block-copolymer, *i.e.*, the fraction of free volume decreased within the PVA amorphous region due to the presence of cross-linking points because of both, the PS nanodomains and the PVA crystallites (enhanced by thermal annealing). Therefore, ethanol transport is hindered in greater extent than the water transport, what results in higher water/ethanol selectivity values.

The thickness of thin films is ≈ 1000 nm. SEM micrographs of thin-film membranes are presented in the Supporting Information (Figure 9-15, Appendix).

5.3. Conclusion

Tailor-made PVA-*b*-PS copolymers with high molecular weight (> 70 kDa), and high content of PVA (> 80 wt.%) were successfully synthesized by ARGET-ATRP and RAFT techniques. To reach our target, we optimized the synthesis of block copolymer by decreasing the concentration of initiator and catalyst during the polymerization, and by increasing the reducing agent ($Sn(EH)_2$) and VAc monomer with respect to PS-CTA macroinitiator. These changes led to reduce the birth of new polymer chains, to minimize the β-hydrogen elimination, to regenerate the active catalyst, and to extend the length of final polymeric chain, respectively.

The chemical structure of synthesized block copolymers and their thermal properties were confirmed by different analysis techniques. The most important features of these copolymers are the good film-forming property and their solubility in solvents. They are not soluble in any solvent, except hot DMSO. Thus, these copolymers can be considered as solvent resistant materials. Nevertheless, by switching the solvent by dialysis, self-assembled micelles in water can be obtained.

Self-standing films are prepared by using DMSO and characterized in terms of permeability and selectivity as membrane material for pervaporation applications. Although the block copolymer films are less hydrophilic than PVA homopolymer, the water permeability is high when ≈ 10 wt.% of PS is present in the copolymer chain. Those results were attributed to the nanostructure of block copolymer because of microphase separation, *i.e.*, the membranes with disordered nanodomains (disorder cubic arrays) and ordered nanodomains as body centered

cubic structure exhibit higher water permeability than that in PVA homopolymer. At the same time, we confirmed that PS nanodomains would be acting as cross-linking points.

Because the block copolymers are not soluble in any solvent, we investigated the switch of solvent from DMSO to water by dialysis. By using this method, we demonstrated the control of self-assembly of these block copolymers in solution (aqueous media), *i.e.*, by adding water to DMSO solution in a controlled way, the block copolymers form micelle nanostructures, and then, when DMSO is completely removed, the micelles (70–100 nm) coexist and are stable in the aqueous solution. The formation of micelles was confirmed by DLS and TEM.

The self-assembled micelle solution later can be cast onto a porous substrate to form thin-film membranes. The thin-film membranes obtained in this form confirmed the higher water permeance than that in PVA homopolymer. By a subsequent thermal annealing of thin films, the water permeance decreased (more than 50%), but it was still higher than that in PVA homopolymer. However, the selectivity of the membrane was extremely enhanced (up to a factor of 20). These results were attributed to the improved microphase separation of block copolymers and to the crystallinity increase of PVA block due to the thermal annealing. Due to the PS domains present in the PVA matrix, we also demonstrated that chemical cross-linkers are not needed anymore to make PVA membranes.

Although these block copolymers are still in laboratory stage (complex synthesis, therefore expensive), we believe that in the near future, simpler synthetic methods will be developed. Thus, this kind of tailor-made block copolymers might have a great impact in the membrane field.

6. Conclusions and perspectives

With the major concerns about fossil fuels, the next generations of bioethanol (second and third) become more and more attractive. Due to low energy consumption and its positive environmental impact, pervaporation is a suitable and sustainable technology to produce energy from renewable resources. As bioethanol progress leads to more complex situations, the membrane materials used in pervaporation should follow up the trend in order to continue to thrive.

In this thesis work, we focused on strategies to develop membrane materials compatible with such bioethanol feedstocks. In the first part, we concentrated our efforts on two commercial PVA membranes containing a copolymer. The ability of commercial membranes to adjust their performance according to the pH of the environment represents a significant advance in the design and application of membrane separation technologies. This pH-responsive characteristic opens promising opportunities for adapting membranes to specific applications, enabling targeted optimization according to the requirements of different industrial processes. Furthermore, the well-known stability of these membranes in the presence of acetaldehyde broadens the potential for use in demanding environments, enabling performance to be fine-tuned. However, the pH-responsiveness expected from the DMAEMA moieties did not behave according to our expectations. Surprisingly, when the pervaporation tests were performed with the same membrane under different conditions, the membrane performance was irreversible. From the performed samples analyses, crosslinking was observed because of the NVP moieties. Hence the pH-responsiveness of such commercial membranes is compromised even though some separation performance variation can be beneficial depending on the application. Nevertheless, this adaptation of selectivity has clearly defined the potential of these membranes and provided a path for the future synthesis of copolymers specifically designed to improve membrane selectivity.

Considering the composition of the commercial copolymer investigated in the first part (only 5% of DMAEMA units), in the second part we decided to synthesize tailor-made P(NVP-*co*-DMAEMA) together with an alternative copolymer P(NVP-*co*-NVIm) with defined monomer ratio by FRP. PVA/copolymer blends were successively prepared with two compositions (80:20 and 95:5). The comprehensive characterization of these copolymers and the analysis of their

behavior in membranes have enabled the correlation between polymer physicochemical properties and separation performance. This has provided a solid basis for membrane optimization in terms of selectivity and stability. The synthesized copolymers showed better separation performances for bioethanol dehydration than the PERVAP™ 4155-80 containing the commercial copolymer. The blends 80:20 displayed lower selectivity than the 95:5 blends for ethanol dehydration while having the highest water permeance values at the same time. Such membranes are not suitable for ethanol dehydration but they can be used for higher molecular weight alcohols. It was found that the 95:5 blends displayed the best performances with an optimal trade-off between water permeance and selectivity. An increase in the crystallinity of membranes as their PVA composition increases has a significant impact on membrane performance. The degree of crystallinity is correlated with enhanced membrane selectivity. This property is derived from the ordered structure of the polymer chains, which enables the membrane to separate molecules passing through it with greater precision. Furthermore, these highly crystalline membranes are more stable, as they do not rely on traditional cross-linking points that can be susceptible to degradation when exposed to harsh chemicals such as acetaldehyde. The capacity to regulate crystallinity by varying the type of copolymer incorporated into the membrane structure represents a valuable tool for controlling the final structure and properties of the membrane. The incorporation of specific copolymers can inhibit the formation of crystalline domains, resulting in a more amorphous membrane that may be more permeable or suitable for applications requiring greater flexibility. This structural control enables the design of customized membranes that meet the specific requirements of various industrial applications by fine-tuning the balance between selectivity, permeability, and mechanical and chemical stability. Hence, this part confirmed that through an appropriate structured work on polymer synthesis and the corresponding characterizations, it is possible to develop better and robust membranes. The major achievement has been the development of membranes with improved selectivity, which have demonstrated remarkable stability in the presence of acetaldehyde in long-term pervaporation tests. These membranes have been specifically designed for use in second- and third generation bioethanol processes. The successful fabrication of these prototypes under feasible production conditions represents a crucial step towards the commercialization of these membranes. The research perspectives opened by these results are promising. On the one hand, the possibility of fine-tuning the composition and properties of copolymers encourages further investigation into the wide variety of polymers and their effects on membrane performance. This approach could lead to the development of optimal formulations for specific applications, increasing the efficiency and

cost-effectiveness of separation processes. On the other hand, the demonstrated stability of these membranes under real industrial conditions encourages the need for larger-scale (pilot) tests.

In the last part, the successful synthesis of PVA-*b*-PS block copolymers, with specific adaptation of the synthesis method to achieve high molecular weights, represents an important step in membrane technologies. These copolymers demonstrate the potential of targeted synthetic adjustments to optimize material properties for specific applications. In addition, the ability to precisely control molecular weight opens possibilities for the manufacture of innovative membranes in the field of separation and purification. This highlights the necessity of continued research and development in this field. A particularly interesting feature of these block copolymers is their insolubility in almost all common solvents, apart from hot DMSO. This property endows the copolymers with remarkable solvent resistance, making them ideal for applications where chemical resistance is crucial. Furthermore, the use of the solvent switch technique has enabled the formation of micelles in water that are not only more affordable but also more environmentally friendly compared to other organic solvents commonly used in membrane fabrication processes. The formation of micelles from PVA-*b*-PS block copolymers has facilitated not only the preparation of films for characterization but also the development of nanostructured composite membranes. The presence of PS at the core of these micelles plays an important role as cross-linking points, providing the membranes with an organized nanostructure. The use of heat treatment was particularly effective, leading to an increase in the crystalline phases in the membrane structure. This increase in crystallinity considerably improved selectivity, an essential factor for more efficient separation processes. Remarkably, this improvement in selectivity was achieved without compromising membrane flux, which remained high. These results demonstrate that membranes can be effectively prepared using exclusively block copolymer formulations, without the need for cross-linking agents or catalysts. This approach marks a significant step forward towards the production of more robust membranes, free from additives, through precise control of nanostructures formation. In summary, these developments represent a considerable advancement in membrane technology, offering promising prospects for industrial applications where material durability, efficiency, and autonomy are paramount. Although these copolymers are still at the laboratory stage, with complex and expensive synthesis methods, the perspectives for simplifying these methods and reducing costs are promising. The future development of simpler synthesis methods could enable a broader application of these copolymers in the field of membranes, where they could

lead to a breakthrough in separation technologies thanks to their ability to combine high performance, chemical stability and ease of manufacture.

Here are few points to be considered regarding further optimizations of membranes based on amphiphilic block copolymers for bioethanol dehydration:

- Two blocks completely opposite, with totally different types of interactions available, should be taken with caution. The high incompatibility of the two blocks is a great advantage for the microphase separation that triggers self-assembly. In the case of oligomers, or lower molecular weight diblock copolymers, the margin of operation is still acceptable to dissolve the polymer. However, for membrane fabrication, higher molecular weight is required in order to ensure appropriate film forming properties. This brings major solubility issues, where the margin of operation mentioned before is now drastically reduced. Hopefully, in our specific case DMSO was still able to dissolve the polymer and self-assembly could be realized afterwards.
- The synthesis of PS-*b*-PVA involves two different CRP with end-group modification steps in between. High end-group fidelity throughout the different steps is very important to ensure optimal chain extension with the second block.
- In the literature, the synthesis of this BCP is not well established yet. In particular for higher molecular weights. Some early studies suggested synthesizing separately PS and PVAc. The two blocks can be combined at later stages and hydrolysis can be realized to produce the PVA block.
- Recently, dithiocarbamate RAFT agents were proposed as compatible with both MAM and LAM. Hence, it has potential interest for the synthesis of PS-*b*-PVA in fewer steps with an easier procedure.
- The integration of hydrophobic segments with varying thermal and mechanical properties, while maintaining PVA hydrophilic block could facilitate the customization of membrane characteristics. The influence of different hydrophobic segments on the overall membrane behavior can be crucial, affecting parameters such as permeability, chemical resistance, and membrane stability under harsh conditions.
- The crystallinity of PVA, in combination with the hydrophobic and insoluble segments of block copolymers, represents a fundamental aspect that should be used as a foundational starting point for further innovations. It represents a promising alternative to produce PVA-based membranes without the use of crosslinkers and catalysts in the

formulation. Consequently, the membranes produced exhibit a simpler formulation that no longer exhibits weak points towards impurities present in bioethanol streams.

7. Experimental

7.1. Materials

Chapter 3: For the pervaporation tests, commercial pervaporation membranes PERVAP™ 4155-30 and PERVAP™ 4155-70 from DeltaMem AG, Switzerland were used.[291] For the dense film preparation, the P(VP-*co*-DMAEMA) and poly(vinyl alcohol) (PVA) were supplied by DeltaMem AG. Polyvinylpyrrolidone (PVP) with average molecular weight of around 55 kDa, methyl acetate (MeAc, 99%) and sodium hydroxide (NaOH, 90%, flakes) were purchased from Sigma-Aldrich. PDMAEMA with a molecular weight of 98 kDa and hydrochloric acid (HCl, 37%) were obtained from Polymer Source Inc. and VWR, respectively. Deuterated chloroform ($CDCl_3$, D 99.8%) with 0.05 v/v % TMS was obtained from Cambridge Isotope Laboratories. Distilled water was used for the experiments, unless stated otherwise.

Chapter 4: *N*-Vinylpyrrolidone (NVP, ≥ 99%, Aldrich) and *N*-Vinylimidazole (NVIm, ≥ 99%, Aldrich) were distilled under reduced pressure at 92 °C and 72 °C, respectively, and stored under nitrogen until used. 2-(dimethylamino)ethyl methacrylate (DMAEMA, 98%, Aldrich) was purified by passing through a column of activated basic alumina (Aldrich) to remove the inhibitor and kept under nitrogen. 2,2′-Azobis(2-methylpropionitrile) (AIBN, ≥ 98%, Aldrich) was recrystallized from methanol before use. Toluene (Acros Organics, extra dry) and petroleum ether (technical grade, Biosolve) were used without further purification. Deuterated chloroform ($CDCl_3$, D 99.8%) with 0.05 v/v % TMS and deuterated dimethyl sulfoxide (DMSO-d_6) were obtained from Cambridge Isotope Laboratories.

For the preparation of membranes and pervaporation experiments, distilled water was used. PVA solution ready for casting, PAN porous support, ethanol, isopropanol (technical grade) and commercial pervaporation membranes (PERVAP™ 4155–80) were supplied by DeltaMem AG.

Chapter 5: Styrene (Sty, ≥ 99%, Aldrich) and vinyl acetate (VAc, ≥ 99%, Aldrich) were purified by passing through columns of basic aluminium oxide (Aldrich) and neutral aluminium oxide (Aldrich), respectively, to remove inhibitors prior to use. 2,2'-Azobis(2-methylpropionitrile) (AIBN, ≥ 98%, Aldrich) was recrystallized from methanol before use. Anisole (99%, Aldrich), benzyl bromide (98%, Aldrich), copper(II) bromide ($CuBr_2$, 99.99%, Aldrich), tin(II) 2-ethylhexanoate ($Sn(EH)_2$, 92.5-100.0%, Aldrich), tris[2-(dimethylamino)ethyl]amine

(Me_6TREN, 97%, Aldrich), sodium azide (NaN_3, 99.5%, Aldrich), *N*,*N*-dimethylformamide (DMF, extra dry, Acros Organics), potassium ethyl xanthogenate (96%, Aldrich), propargyl bromide solution (80 wt.% in toluene, Aldrich), copper(I) bromide (CuBr, 99.99%, Aldrich), tetrahydrofuran (THF, extra dry, Acros Organics), *N,N,N',N'',N''*-pentamethyldiethylenetriamine (PMDETA, 99%, Aldrich), potassium hydroxide (90%, Aldrich), pentane (technical grade, Biosolve), methanol (technical grade, Biosolve), and diethyl ether (technical grade, Biosolve) were used as received. Deuterated chloroform ($CDCl_3$, D 99.8%) with 0.05 v/v % TMS and deuterated dimethyl sulfoxide (DMSO-d_6) were obtained from Cambridge Isotope Laboratories.

For the preparation of membranes and pervaporation experiments, distilled water and dimethyl sulfoxide (≥ 99.9%, Aldrich) were used. Poly(acrylonitrile) (PAN) porous support, ethanol (technical grade) and commercial pervaporation membranes (PERVAP™ 4100) were supplied by DeltaMem AG.

7.2. Characterization techniques

7.2.1. Nuclear magnetic resonance (NMR) spectroscopy

The chemical structure of the synthesized copolymers was evaluated by proton nuclear magnetic resonance (^{1}H NMR) spectroscopy. All spectra were recorded at RT using a Bruker Ascend 500 spectrometer operated at 500 MHz for ^{1}H nucleus. Deuterated chloroform ($CDCl_3$) was used for P(NVP-*co*-DMAEMA) copolymers, PS macro precursors and PS-*b*-PVAc. Deuterated dimethyl sulfoxide (DMSO-d_6) was used for P(NVP-*co*-NVIm) copolymers and PS-*b*-PVA. All the (block) copolymers were dissolved at RT. Chemical shifts (δ) are reported in ppm and quoted in respect to tetramethylsilane (TMS, δ 0.00 ppm) used as internal reference for ^{1}H NMR. The collected spectra were analyzed by MestReNova (v12.0) (Mestrelab Research S.L).

7.2.2. GPC

Gel permeation chromatography (GPC) traces were analyzed and recorded in WinGPC Unichrom software (v 8.33 build 9050, PSS polymer, Germany). Traces of the copolymers were recorded using an Agilent based system composed of a 1100 series pump and an autosampler. The GPC system was equipped with a series of linear-S SDV columns (precolumn (5 cm), three analytical columns (30 cm) all with 5 μm particles sizes. All the columns have a diameter of

0.8 cm, PSS polymer, Germany) and a refractive index detector (RI) (1260 Infinity II). When *N*,*N*-Dimethylformamide (DMF) was used as the eluent (flow rate of 1 ml.min$^{-1)}$, the RI detector was kept at 45 °C and the columns were kept at 60°C and when $CHCl_3$, stabilized with EtOH, was used as the eluent (flow rate of 1 mL.min^{-1}) the RI detector and the columns were kept at 35 °C. The system was calibrated with narrowly distributed polystyrene standards.

7.2.3. Attenuated total reflection–Fourier transform infrared (ATR-FTIR)

Background corrected ATR–FTIR were also used for chemical structure analysis of the (block) copolymers. The spectra were recorded on a Bruker spectrophotometer or on a PerkinElmer UATR Two spectrophotometer in the range of 4000–400 cm^{-1}.

7.2.4. Thermogravimetric analysis (TGA)

TGA was performed on a TGA5500 (TA Instruments) instrument under constant nitrogen flow and coupled to a MKII mass spectrometer, . After weight stabilization, the temperature was equilibrated at 30 °C before heating at a rate of 10 °C/min to 550 °C and cooled down to ambient temperature.

7.2.5. Differential scanning calorimetry (DSC)

DSC measurements were carried out on a DSC 214 Polyma (Netzsch). The data analysis was performed by Netzsch Proteus Software. During the second heating, the inflection points of the specific heat increase in the transition region were reported as the glass transition temperature (T_g).

Chapter 4: All samples were first annealed at 250 °C under nitrogen to remove the effect of thermal history. Subsequently, the samples were cooled to 0°C, and then a heating/cooling cycle with a rate of 10 K.min^{-1} was applied for all the scans. The Fox equation was used to predict the glass transition temperature as follows,

$$\frac{1}{T_{g,mix}} = \frac{\omega_i}{T_{g,i}} + \frac{\omega_j}{T_{g,j}} \tag{9}$$

where $T_{g,mix}$, $T_{g,i}$ and $T_{g,j}$ correspond to the glass transition temperatures of the copolymer and the respective homopolymers, whereas ω_i and ω_j are the weight fractions.

Chapter 5: For the block copolymer thermal properties analysis, all samples were first annealed at 180 °C under nitrogen to remove the effect of thermal history. Subsequently, the samples

were cooled to 0 °C, and then a heating/cooling cycle with a rate of 10 K.min^{-1} was applied for all the scans. For the freestanding dense films prepared for the pervaporation tests, one single heating/cooling cycle with a rate of 10 K.min^{-1} was applied.

7.2.6. Swelling measurements

The membrane swelling measurements were performed on free-standing dense films prepared in the laboratory. The solvent uptake ratios of the dense film were determined gravimetrically in the corresponding mixture. Dried films were used and placed in the selected solvent mixture at room temperature and then left to swell until constant weight. The samples were removed from the mixture between times, wiped with a filter paper and weighed, and placed back into the mixture until the equilibrium swelling ratios is obtained. Three parallel measurements were carried out for each sample and average values as well as standard deviation were calculated.

$$ESR(\%) = \frac{(W_s - W_d)}{W_d} \times 100 \qquad (10)$$

where W_s and W_d are the masses of the swollen and dried films, respectively.

7.2.7. Static contact angle (CA)

The static CA was measured for the dense films and the composite membranes with a CA goniometer, CAM 100 (LOT quantum design), based on a CDD camera with 50 mm optics. Droplets of ultrapure water were placed on the sample surface with a micro syringe, and the CA was automatically recorded and analyzed by the instrument software by fitting the experimental curve with the Young–Laplace equation. The drop volume (2 μL) was kept constant for all measurements. The average values as well as standard deviation were reported based on at least four measurements taken at different location of the surface.

7.2.8. Scanning electron microscopy (SEM)

The thickness of the selective layer in composite membranes was confirmed by SEM images, which were acquired using a Hitachi S-4800 SEM (Hitachi High-Technologies Corporation, Japan) with a cold field-emission electron source. Electrically conducting surfaces were achieved by sputtering the surface with a gold layer of 5 nm thickness.

7.2.9. Dynamic light scattering (DLS)

The hydrodynamic diameter (D_h) of the self-assembled micelle nanostructures (15 mg mL^{-1}) was measured with a Zetasizer Nano ZSP (Malvern Instruments). Each measurement was taken at 20 °C, after an equilibration time of 300 s with a backscattering angle of 173°.

7.2.10. Transmission electron microscopy (TEM)

The PS-*b*-PVA self-assembled micelles were imaged by TEM. The nanostructures micelles in water (0.1 mg mL^{-1}) were adsorbed a on glow-discharged carbon copper grid and negatively stained with 2% aqueous uranyl acetate. Micrographs were recorded with a Philips CM100 microscope at an accelerating voltage of 80 kV.

7.2.11. Karl-Fischer titration

During pervaporation tests, the water concentration in the feed/retentate samples was determined by coulometer Karl Fischer titration (737 KF Coulometer, Metrohm or 917 Coulometer, Metrohm).

7.2.12. Gas chromatography (GC)

The compositions of permeates were measured by using an Agilent 6890 gas chromatography equipped with a thermal conductivity detector and HP-PLOT Q column.

7.3. Synthetic procedures

7.3.1. Synthesis of P(NVP-*co*-DMAEMA) and P(NVP-*co*-NVIm)

The copolymerization of NVP with DMAEMA or NVIm were carried out in a flask with toluene as reaction medium and AIBN as initiator.[71] Typically, the initial monomer mixture ($[M]_{mixture}$ = 1.7 $mol.L^{-1}$) and AIBN (M:I = 100:1) were first dissolved in toluene. Then, the reaction mixture was purged with nitrogen, and then immediately sealed. The polymerization was promoted by placing the flask in a preheated oil bath (65 °C) and kept under constant magnetic stirring. After 22 h, the polymerization process was stopped by cooling down the flask to room temperature (RT) in an ice-cold water bath and opening to the atmosphere. The purified copolymer was obtained by three successive precipitations into cold petroleum ether and subsequent drying in a vacuum oven at 40°C until constant weight.

7.3.2. Synthesis of PS-*b*-PVA

The block copolymers were synthesized according to a previously described procedure with modifications in order to obtain the desired properties.[215]

A representative synthetic protocol is described below with optimized conditions for the preparation of PS-*b*-PVA with 87% hydrophilic ratio (PVA-87).

Synthesis of polystyrene macro precursor

Benzyl bromide solution in anisole (0.043 mol.L^{-1}, 40.21 mL, 1.72 mmol, 1 eq.) and tin^{II} 2-ethylhexanoate solution in anisole ($Sn(EH)_2$, 0.086 mol.L^{-1}, 41.16 mL, 3.44 mmol, 2 eq.) were separately purged with argon for 90 min. In a Schlenk flask, equipped with a stirring bar, styrene (100 mL, 859 mmol, 500 eq.), copper(II) bromide ($CuBr_2$, 38 mg, 0.172 mmol, 0.1 eq.), and tris[2-(dimethylamino)ethyl]amine (Me_6TREN, 40 µL, 0.172 mmol, 0.1 eq.) were dissolved in anisole (20 mL) and purged with argon for 90 min. The initiator and reducing agent solutions were transferred to the Schlenk flask via a cannula. The polymerization was carried out in thermostated oil-bath at 90 °C for 2.5 h. Then, the flask was cooled to room temperature in an ice-cold water bath and the reaction was stopped by exposure to the air. The copper catalyst was removed by passing the solution over a column of neutral alumina oxide. The polymer was precipitated into cold methanol. The polymer was filtered and dried under vacuum at room temperature (white powder). ^{1}H NMR (500 MHz, $CDCl_3$, 295 K, δ, ppm): 7.24–6.30 (m, 5H, –CH_2–CH(*C_6H_5*)–), 4.59–4.35 (m, 1H, –CH_2–*CH*(C_6H_5)–Br), 2.13–1.68 (m, 1H, –CH_2–*CH*(C_6H_5)–), 1.65–1.24 (m, 2H, –*CH_2*–CH(C_6H_5)–).

Synthesis of PS-N3

PS-Br, 11 g, 1.1 mmol, 1 eq.) was dissolved in 50 mL of DMF in a round-bottom flask. Sodium azide (NaN_3, 3.97 g, 60 mmol, 50 eq.) was added to the solution. The reaction was stirred overnight at room temperature. The reaction was poured into 500 mL of water and the polymer was filtered and dried under vacuum (white powder). ^{1}H NMR (500 MHz, $CDCl_3$, 295 K, δ, ppm): 7.24–6.30 (m, 5H, –CH_2–CH(*C_6H_5*)–), 4.04–3.83 (m, 1H, –CH_2–*CH*(C_6H_5)–N_3), 2.13–1.68 (m, 1H, –CH_2–*CH*(C_6H_5)–), 1.65–1.24 (m, 2H, –*CH_2*–CH(C_6H_5)–).

Synthesis of PS-CTA

O-Ethyl *S*-(prop-2-yn-1-yl) carbonodithioate was synthesized according to literature procedures.[171] PS-N_3 (10 g, 1 mmol, 1 eq.), *O*-Ethyl *S*-(prop-2-yn-1-yl) carbonodithioate (0.33 mL, 2 mmol, 2 eq.), PMDETA (0.383 mL, 2 mmol, 2 eq.) were dissolved in THF (104 mL).

The mixture was purged with argon for 90 min and subsequently copper(I) bromide (CuBr, 0.26 g, 2 mmol, 2 eq.) was added to the mixture under argon atmosphere. The reaction was stirred overnight at RT. The copper catalyst was removed by passing the solution over a column of neutral alumina oxide. The purified polymer was obtained by successive precipitations into methanol. The polymer was filtered and dried under vacuum (yellowish powder). ^{1}H NMR (500 MHz, $CDCl_3$, 295 K, δ, ppm): 7.24–6.30 (m, 5H, –CH_2–CH(*C_6H_5*)–), 5.10–4.90 (m, 1H, –CH_2–*CH*(C_6H_5)–triazole ring), 4.72–4.59 (2H, –C*H_2*−S–), 4.54–4.32 (2H, –O−C*H_2*), 1.65–1.24 (m, 2H, –*CH_2*–CH(C_6H_5)–).

Synthesis of PS-b-PVAc

In a dried and nitrogen purged polymerization Schlenk-flask, vinyl acetate (VAc, 65 mL, 0.682 mmol, 3000 eq.), PS-CTA (2.5 g, 0.23 mmol, 1 eq.), azobisisobutyronitrile solution in THF (AIBN, 0.05 mol.L^{-1}, 0.57 mL, 0.028 mmol, 0.125 eq.) and THF (16.9 mL) were added. After purging with nitrogen by cooling the flask in an ice bath, the tube was backfilled with argon, sealed, placed in an oil bath at 70 °C and removed after 17 h. The tube was subsequently cooled with liquid nitrogen to cease the reaction. The reaction mixture was diluted with THF and subsequently precipitated into 500 mL of methanol/water (1 : 1, v/v). The polymer was filtrated and dried overnight under vacuum (white powder). ^{1}H NMR (500 MHz, $CDCl_3$, 295 K, δ, ppm): 7.24–6.30 (m, 5H, –CH_2–CH(*C_6H_5*)–)), 5.10–4.90 (1H, –CH_2–C*H*(O–C(CH3)=O)–), 2.10–2.00 (3H, aliphatic protons of PVAc), 1.65–1.24 (m, 2H, –*CH_2*–CH(C_6H_5)–).

Synthesis of PS-b-PVA

The block polymer (PS-*b*-PVAc, 136 kDa, 29 g, 2 mmol, 1 eq.) was dissolved in 215 mL of THF. Potassium hydroxide solution in methanol (1.78 mol.L^{-1}, 18 mmol) was prepared and 144 mL were added to the polymer solution (THF/MeOH, 1.5:1, v/v). The obtained mixture was stirred at room temperature for 4 h. The precipitated product was filtrated, washed with methanol and dried under vacuum a white powder. ^{1}H NMR (500 MHz, DMSO-d_6, 295 K, δ, ppm): 7.24–6.30 (m, 5H, –CH_2–CH(*C_6H_5*)–), 4.68–4.24(3H, –CH_2–CH(O*H*), 3.84 (1H, –CH_2–C*H*(OH)–), 1.65–1.24 (aliphatic protons of PVA and PS).

7.4. Dense film and composite membranes preparation

Chapter 3: For copolymer characterization, freestanding dense films from P(VP-*co*-DMAEMA) were prepared in Teflon molds by solution casting (5.0 wt.% aqueous solutions). The drying of the films was performed in two steps: first the solvent was slowly evaporated

(two days) under atmospheric pressure at room temperature, and then, the drying is completed at 40 °C under vacuum (400 mbar) for one day. For the membrane characterization, free-standing dense films from PVA and P(VP-*co*-DMAEMA) were obtained by casting on Teflon sheets. Polymer solutions with the same composition as the commercial composite membranes (PERVAP™ 4155-30 and 4155-70) were used. The wet film thickness was adjusted with a knife blade to 500 µm. The procedure of drying and crosslinking is described elsewhere.[329]

Chapter 4: The solutions (5 wt.%) containing the copolymers were prepared in water. Then, the respective solutions of copolymer and PVA solution provided by DeltaMem AG were mixed to obtain the desired PVA/copolymer blend ratio. All solutions were stirred overnight at RT to ensure homogeneity. Two sets of PVA/copolymer blends were prepared, with the mass ratio of 80:20 and 95:5, respectively.

Several dense films from each blend (different PVA/copolymer ratios) were prepared by solution casting on Teflon plates, dried and cross-linked at 145 °C in an oven,[26, 27] and then detached from the support as freestanding films. The obtained films were transparent and had thicknesses between 20 and 60 µm.

Composite membranes were also prepared by solution casting, but this time on a PAN porous support, using a micrometer-adjustable film applicator (film casting doctor blade 180 mm width) with a casting thickness adjusted to 150 µm. After the casting, the membrane was dried and cross-linked in an oven at 145 °C.[13] After the complete drying, membrane samples were cut as disc shapes with an area of 3.8×10^{-5} m^2. Each membrane was controlled with a nitrogen flow meter to spot the presence of defects before and after the pervaporation experiments.

Chapter 5: Casting solutions (3 wt.% copolymer) were prepared by stirring the copolymers (powder) in DMSO overnight (flask immersed in an oil bath at 70 °C). The thick dense films were prepared by casting the homogeneous solution on poly(ether-ether-ketone) (PEEK) plates by using a micrometer-adjustable film applicator (doctor blade 100 mm width, EQ-Se-KTQ-100, MTI Corporation, USA). The gap of doctor blade was adjusted to 200 µm, and the solvent was evaporated at 70 °C for 90 min in a convection oven. Then, the freestanding dense films were peeled off from PEEK plates and their thicknesses were measured using a micrometer thickness gauge.

Thin film membranes were prepared from aqueous polymer solutions (dispersed micelles). Water was added dropwise to the block copolymer solution obtained above; this process is carried out to obtain a mixture of water/DMSO (80/20 wt.%/wt.%) to trigger the formation of

self-assembled micelles. After complete addition of water, DMSO was removed by dialysis through a regenerated cellulose membrane (MWCO 8 kDa, RC6, Spectra Por, USA). The resulting aqueous solution was then cast onto the microporous PAN substrate followed by drying in the convection oven (145 °C and 6 min). Both thick dense films and thin film membranes were cut (area = 3.8×10^{-5} m^2) for the characterization.

7.5. Pervaporation

Chapter 3: The pervaporation tests are performed with binary MeAc/water mixtures, neutral and containing 2 mmol/L of HCl and 2 mmol/L of NaOH, respectively. The setup includes two pervaporation cells, which allows testing simultaneously two different types of membranes. The effective membrane area in each cell is 3.8×10^{-3} m^2. The mixture (V = 0.5 L) is filled into a feed tank and recirculated by a pump with a feed flow parallel to the membrane surface. The feed goes to the membrane cells, and then, the product from the cells is returned to the feed tank as retentate. A heating system maintains constant the feed/retentate temperature at 85 °C. In the permeate side, a vacuum of 10 mbar is maintained by a vacuum pump. Permeate samples are collected in a cold trap with dry ice and ethanol mixture. For each measurement point, the amount of permeate, time, as well as the feed/retentate samples are collected. As the water concentration in the feed decreases over time, the water flux is smaller. Therefore, longer collecting times were applied. Typically, the initial collecting time is 30 minutes, and the final is two hours.

Chapter 4: The pervaporation tests were performed in a bench-top unit including six membrane cells (each cell with an effective area of 3.8×10^{-3} m^2), which allowed us the simultaneous testing of different types of membranes. Binary ethanol/water mixtures (V = 2.5-3 L, with an initial water concentration of 10 wt.%) were filled into the tank and recirculated by a pump with a feed flow parallel to the membrane surface. The feed goes to the membrane cells and then, the product from the cells is returned to the feed tank as retentate. A heating system maintains the feed/retentate temperature of each cell at 95 °C. The pervaporation unit is kept at a pressure of 2 bar for the given temperature, which ensures keeping the binary mixture in liquid phase according to the vapor–liquid equilibrium diagram (Figure 9-1). In the permeate side, a constant vacuum of 10 mbar was maintained by a vacuum pump. The permeate samples were collected in a trap cooled down with dry ice/ethanol mixture. For each measurement point, the time was recorded while feed/retentate and permeate samples were collected. As the water concentration in the feed decreases over time, the water flux is smaller. Therefore, longer collecting times

were applied. Typically, the initial collecting time is 30 minutes, and the final is two hours. Pervaporation long-term stability tests were continuously performed for more than 300 hours under the same operating conditions. Pervaporation plant operations are simulated by carrying out processes of shutdown and startup. The dehydrated solvent (batch) is replaced by a new mixture (new batch). After several batches, the separation performance must remain unchanged to confirm the stability of the membrane.

Chapter 5: The pervaporation tests were performed in a bench-top unit including two membrane cells (each cell with an effective area of 3.8×10^{-3} m^2), which allowed us the simultaneous testing of different types of membranes. Binary ethanol/water mixtures (V = 0.5 L, 93/7, in weight ratio) were filled into the tank and recirculated by a pump with a feed flow parallel to the membrane surface. The feed goes to the membrane cells and then, the product from the cells is returned to the feed tank as retentate. A heating system maintains the feed/retentate temperature of each cell at 95 °C. The pervaporation unit is kept at a pressure of 2 bar for the given temperature, which ensures keeping the binary mixture in liquid phase according to the vapor-liquid equilibrium [214]. In the permeate side, a constant vacuum of 10 mbar was maintained by a vacuum pump. The permeate samples were collected in a trap cooled down with dry ice/ethanol mixture. For each measurement point, the time was recorded while feed/retentate and permeate samples were collected. As the water concentration in the feed decreases over time, the water flux is smaller. Therefore, longer collecting times were applied. Typically, the initial collecting time is 30 minutes, and the final is two hours.

The separation performance of all membranes was evaluated based on the permeate concentration (wt.%) and water permeate flux J_i ($kg.m^{-2}.h^{-1}$),

$$J_i = \frac{m_i}{A \times t} \tag{11}$$

where m_i is the amount of water in the permeate (kg), A is the effective membrane area (m^2), and t is the operating time (h) between sample collection.

When the produced membranes are composites, the thickness of the active layer is unknown. Hence, permeability values cannot be reported, so partial fluxes are employed to determine permeance values. Permeance allows describing the separation performance based on the intrinsic properties of the fabricated membranes as follows,[330]

$$\left(\frac{P_i}{l}\right) = \frac{J_i}{x_i \gamma_i p_i^{sat} - y_i p^p} \tag{12}$$

where (P_i/l), the ratio between membrane permeability P_i of component i and the membrane thickness l, is called permeance, x_i and y_i are the mole fractions of component i in the feed and in the permeate, respectively. γ_i is the activity coefficient of component i in the feed liquid calculated by the UNIQUAC and NRTL theories for ethanol/water mixtures, respectively,[126] p_i^{sat} is the saturated vapor pressure of the component i in the feed (calculated using Antoine equation) and p^p is the permeate pressure. The permeance is expressed in GPU (1 GPU = 1×10^{-6} cm^3 (STP)/(cm^{-2}·s·cmHg)).

For dense films with known thicknesses, the permeability is used to evaluate the separation performances.

The membrane selectivity α_{ij} is defined as the ratio of the permeances of components i and j:

$$\alpha_{ij} = \frac{(P_i/l)}{(P_j/l)} \tag{13}$$

8. References

1. Ritchie, H.; Roser, M.; Mispy, J.; Ortiz-Ospina, E. Measuring progress towards the Sustainable Development Goals. SDG-Tracker.org.
2. Ritchie, H.; Roser, M.; Rosado, P., CO_2 and greenhouse gas emissions. *Our world in data* **2020**.
3. Pata, U. K., Renewable and non-renewable energy consumption, economic complexity, CO2 emissions, and ecological footprint in the USA: testing the EKC hypothesis with a structural break. *Environmental Science and Pollution Research* **2021,** *28* (1), 846-861.
4. Kumar, B.; Verma, P., Biomass-based biorefineries: An important architype towards a circular economy. *Fuel* **2021,** *288*, 119622.
5. Chia, S. R.; Nomanbhay, S.; Ong, M. Y.; Shamsuddin, A. H. B.; Chew, K. W.; Show, P. L., Renewable diesel as fossil fuel substitution in Malaysia: A review. *Fuel* **2022,** *314*, 123137.
6. Holechek, J. L.; Geli, H. M. E.; Sawalhah, M. N.; Valdez, R., A Global Assessment: Can Renewable Energy Replace Fossil Fuels by 2050? *Sustainability* **2022,** *14* (8), 4792.
7. Martinez-Burgos, W. J.; de Souza Candeo, E.; Pedroni Medeiros, A. B.; Cesar de Carvalho, J.; Oliveira de Andrade Tanobe, V.; Soccol, C. R.; Sydney, E. B., Hydrogen: Current advances and patented technologies of its renewable production. *Journal of Cleaner Production* **2021,** *286*, 124970.
8. Wicker, R. J.; Kumar, G.; Khan, E.; Bhatnagar, A., Emergent green technologies for cost-effective valorization of microalgal biomass to renewable fuel products under a biorefinery scheme. *Chemical Engineering Journal* **2021,** *415*, 128932.
9. Bundschuh, J.; Kaczmarczyk, M.; Ghaffour, N.; Tomaszewska, B., State-of-the-art of renewable energy sources used in water desalination: Present and future prospects. *Desalination* **2021,** *508*, 115035.
10. Quynh, N. V.; Ali, Z. M.; Alhaider, M. M.; Rezvani, A.; Suzuki, K., Optimal energy management strategy for a renewable-based microgrid considering sizing of battery energy storage with control policies. *International Journal of Energy Research* **2021,** *45* (4), 5766-5780.
11. Olabi, A. G.; Abdelkareem, M. A., Renewable energy and climate change. *Renewable and Sustainable Energy Reviews* **2022,** *158*, 112111.
12. Chen, J.; Zhang, B.; Luo, L.; Zhang, F.; Yi, Y.; Shan, Y.; Liu, B.; Zhou, Y.; Wang, X.; Lü, X., A review on recycling techniques for bioethanol production from lignocellulosic biomass. *Renewable and Sustainable Energy Reviews* **2021,** *149*, 111370.
13. Kumakiri, I.; Yokota, M.; Tanaka, R.; Shimada, Y.; Kiatkittipong, W.; Lim, J. W.; Murata, M.; Yamada, M., Process Intensification in Bio-Ethanol Production–Recent Developments in Membrane Separation. *Processes* **2021,** *9* (6), 1028.
14. Segovia-Hernández, J. G.; Sánchez-Ramírez, E., Current status and future trends of computer-aided process design, applied to purification of liquid biofuels, using process intensification: A short review. *Chemical Engineering and Processing - Process Intensification* **2022,** *172*, 108804.
15. Huang, H.-J.; Ramaswamy, S.; Tschirner, U. W.; Ramarao, B. V., A review of separation technologies in current and future biorefineries. *Separation and Purification Technology* **2008,** *62* (1), 1-21.
16. Lipnizki, F., Membrane process opportunities and challenges in the bioethanol industry. *Desalination* **2010,** *250* (3), 1067-1069.

17. Frolkova, A. K.; Raeva, V. M., Bioethanol dehydration: State of the art. *Theoretical Foundations of Chemical Engineering* **2010,** *44* (4), 545-556.
18. Vane, L. M., Review: membrane materials for the removal of water from industrial solvents by pervaporation and vapor permeation. *Journal of Chemical Technology & Biotechnology* **2019,** *94* (2), 343-365.
19. Tgarguifa, A.; Abderafi, S.; Bounahmidi, T., Energy efficiency improvement of a bioethanol distillery, by replacing a rectifying column with a pervaporation unit. *Renewable Energy* **2018,** *122*, 239-250.
20. Hajilary, N.; Rezakazemi, M.; Shirazian, S., Biofuel types and membrane separation. *Environmental Chemistry Letters* **2019,** *17* (1), 1-18.
21. Liu, C.-G.; Xiao, Y.; Xia, X.-X.; Zhao, X.-Q.; Peng, L.; Srinophakun, P.; Bai, F.-W., Cellulosic ethanol production: Progress, challenges and strategies for solutions. *Biotechnology Advances* **2019,** *37* (3), 491-504.
22. Tgarguifa, A.; Abderafi, S. In *A comparative study of separation processes for bioethanol production*, 2016 International Renewable and Sustainable Energy Conference (IRSEC), 14-17 Nov. 2016; 2016; pp 890-895.
23. Gnansounou, E.; Dauriat, A., Chapter 6 - Technoeconomic Analysis of Lignocellulosic Ethanol. In *Biofuels*, Pandey, A.; Larroche, C.; Ricke, S. C.; Dussap, C.-G.; Gnansounou, E., Eds. Academic Press: Amsterdam, 2011; pp 123-148.
24. Bertrand, E.; Vandenberghe, L. P. S.; Soccol, C. R.; Sigoillot, J.-C.; Faulds, C., First Generation Bioethanol. In *Green Fuels Technology: Biofuels*, Soccol, C. R.; Brar, S. K.; Faulds, C.; Ramos, L. P., Eds. Springer International Publishing: Cham, 2016; pp 175-212.
25. Cavalett, O.; Junqueira, T. L.; Dias, M. O. S.; Jesus, C. D. F.; Mantelatto, P. E.; Cunha, M. P.; Franco, H. C. J.; Cardoso, T. F.; Maciel Filho, R.; Rossell, C. E. V.; Bonomi, A., Environmental and economic assessment of sugarcane first generation biorefineries in Brazil. *Clean Technologies and Environmental Policy* **2012,** *14* (3), 399-410.
26. Mohanty, S. K.; Swain, M. R., Chapter 3 - Bioethanol Production From Corn and Wheat: Food, Fuel, and Future. In *Bioethanol Production from Food Crops*, Ray, R. C.; Ramachandran, S., Eds. Academic Press: 2019; pp 45-59.
27. Panella, L., Sugar Beet as an Energy Crop. *Sugar Tech* **2010,** *12* (3), 288-293.
28. Amorim, H. V.; Lopes, M. L.; de Castro Oliveira, J. V.; Buckeridge, M. S.; Goldman, G. H., Scientific challenges of bioethanol production in Brazil. *Applied Microbiology and Biotechnology* **2011,** *91* (5), 1267-1275.
29. Kang, Q.; Appels, L.; Tan, T.; Dewil, R., Bioethanol from Lignocellulosic Biomass: Current Findings Determine Research Priorities. *The Scientific World Journal* **2014,** *2014* (1), 298153.
30. Hemansi; Gupta, R.; Yadav, G.; Kumar, G.; Yadav, A.; Saini, J. K.; Kuhad, R. C., Second Generation Bioethanol Production: The State of Art. In *Sustainable Approaches for Biofuels Production Technologies: From Current Status to Practical Implementation*, Srivastava, N.; Srivastava, M.; Mishra, P. K.; Upadhyay, S. N.; Ramteke, P. W.; Gupta, V. K., Eds. Springer International Publishing: Cham, 2019; pp 121-146.
31. Rocha-Meneses, L.; Raud, M.; Orupõld, K.; Kikas, T., Second-generation bioethanol production: a review of strategies for waste valorisation. *Agronomy research* **2017,** *15*, 830-847.
32. Jambo, S. A.; Abdulla, R.; Mohd Azhar, S. H.; Marbawi, H.; Gansau, J. A.; Ravindra, P., A review on third generation bioethanol feedstock. *Renewable and Sustainable Energy Reviews* **2016,** *65*, 756-769.
33. Tan, I. S.; Lam, M. K.; Foo, H. C. Y.; Lim, S.; Lee, K. T., Advances of macroalgae biomass for the third generation of bioethanol production. *Chinese Journal of Chemical Engineering* **2020,** *28* (2), 502-517.

34. Teixeira, A. C. R.; Sodré, J. R.; Guarieiro, L. L. N.; Vieira, E. D.; de Medeiros, F. F.; Alves, C. T., A Review on Second and Third Generation Bioethanol Production. SAE International: 2016.
35. Alam, F.; Mobin, S.; Chowdhury, H., Third Generation Biofuel from Algae. *Procedia Engineering* **2015,** *105*, 763-768.
36. Botshekan, M.; Moheb, A.; Vatankhah, F.; Karimi, K.; Shafiei, M., Energy saving alternatives for renewable ethanol production with the focus on separation/purification units: A techno-economic analysis. *Energy* **2022,** *239*, 122363.
37. Lei, Z.; Li, C.; Chen, B., Extractive Distillation: A Review. *Separation & Purification Reviews* **2003,** *32* (2), 121-213.
38. Widagdo, S.; Seider, W. D., Journal review. Azeotropic distillation. *AIChE Journal* **1996,** *42* (1), 96-130.
39. Karimi, S.; Karri, R. R.; Tavakkoli Yaraki, M.; Koduru, J. R., Processes and separation technologies for the production of fuel-grade bioethanol: a review. *Environmental Chemistry Letters* **2021,** *19* (4), 2873-2890.
40. Beluhan, S.; Mihajlovski, K.; Šantek, B.; Ivančić Šantek, M., The Production of Bioethanol from Lignocellulosic Biomass: Pretreatment Methods, Fermentation, and Downstream Processing. *Energies* **2023,** *16* (19), 7003.
41. Lee, Y. H.; Chen, C. H.; Umi Fazara, M. A.; Irfan Hatim, M. D. M., Production of fuel grade anhydrous ethanol: a review. *IOP Conference Series: Earth and Environmental Science* **2021,** *765* (1), 012016.
42. Rumbo Morales, J. Y.; Ortiz-Torres, G.; García, R. O. D.; Cantero, C. A. T.; Rodriguez, M. C.; Sarmiento-Bustos, E.; Oceguera-Contreras, E.; Hernández, A. A. F.; Cerda, J. C. R.; Molina, Y. A.; García, M. M.; Sanz, E. S., Review of the Pressure Swing Adsorption Process for the Production of Biofuels and Medical Oxygen: Separation and Purification Technology. *Adsorption Science & Technology* **2022,** *2022*, 3030519.
43. Van der Bruggen, B.; Luis, P., Pervaporation as a tool in chemical engineering: a new era? *Current Opinion in Chemical Engineering* **2014,** *4*, 47-53.
44. Redfield Energy, on a journey towards Net Zero with Whitefox ICE® Plus membrane solution. Whitefox Technologies: 2023.
45. Lane, J. The Digest's 2024 Multi-Slide Guide to membrane technology and Whitefox. https://www.biofuelsdigest.com/bdigest/2024/05/14/the-digests-2024-multi-slide-guide-to-membrane-technology-and-whitefox/.
46. US ethanol producer to install Whitefox ICE membrane dehydration system. https://www.filtsep.com/content/news/us-ethanol-producer-to-install-whitefox-ice-membrane-dehydration-system/.
47. BGW integrates Whitefox ICE- XL membrane dehydration system at Polish plant. https://www.filtsep.com/content/news/bgw-integrates-whitefox-ice-xl-membrane-dehydration-system-at-polish-plant/.
48. Western Plains to install Whitefox ICE-XL system. https://ethanolproducer.com/articles/western-plains-to-install-whitefox-ice-xl-system-19750.
49. Strategic Partnerships for Marketing of Zeolite Membranes for Bioethanol Production. https://www.mcgc.com/english/news_mcc/2018/1203875_7663.html.
50. Mitsubishi ZEBREX(TM) Technology to be Implemented by Aemetis to Reduce Energy Use and Lower Carbon Intensity of Biofuel. https://www.globenewswire.com/news-release/2018/08/30/1563353/0/en/Mitsubishi-ZEBREX-TM-Technology-to-be-Implemented-by-Aemetis-to-Reduce-Energy-Use-and-Lower-Carbon-Intensity-of-Biofuel.html.
51. Albrecht, T. The Way Forward. https://ethanolproducer.com/articles/the-way-forward-15425.

52. Niemistö, J.; Pasanen, A.; Hirvelä, K.; Myllykoski, L.; Muurinen, E.; Keiski, R. L., Pilot study of bioethanol dehydration with polyvinyl alcohol membranes. *Journal of Membrane Science* **2013,** *447*, 119-127.
53. Vane, L. M., Review of pervaporation and vapor permeation process factors affecting the removal of water from industrial solvents. *Journal of Chemical Technology & Biotechnology* **2020,** *95* (3), 495-512.
54. Pulyalina, A.; Tataurov, M.; Faykov, I.; Rostovtseva, V.; Polotskaya, G., Polyimide Asymmetric Membrane vs. Dense Film for Purification of MTBE Oxygenate by Pervaporation. *Symmetry* **2020,** *12* (3), 436.
55. Baker, R. W., Pervaporation. In *Membrane Technology and Applications*, 2012; pp 379-416.
56. Liu, G.; Jin, W., Pervaporation membrane materials: Recent trends and perspectives. *Journal of Membrane Science* **2021,** *636*, 119557.
57. Wei, P.; Cheng, L. H.; Zhang, L.; Xu, X. H.; Chen, H. L.; Gao, C. J., A review of membrane technology for bioethanol production. *Renewable & Sustainable Energy Reviews* **2014,** *30*, 388-400.
58. Peng, P.; Lan, Y.; Liang, L.; Jia, K., Membranes for bioethanol production by pervaporation. *Biotechnol Biofuels* **2021,** *14* (1), 10.
59. Bukusoglu, E.; Kalıpçılar, H.; Yılmaz, L., Dehydration of Industrial Byproduct Solutions for Recycling via Pervaporation–Adsorption Hybrid Process. *Industrial & Engineering Chemistry Research* **2018,** *57* (6), 2277-2286.
60. Huang, R.; Yeom, C., Pervaporation separation of aqueous mixtures using crosslinked poly (vinyl alcohol)(PVA). II. Permeation of ethanol-water mixtures. *Journal of membrane science* **1990,** *51* (3), 273-292.
61. Marín Cardona, E. S.; Rojas Camargo, J.; Ciro Monsalve, Y. A., A review of polyvinyl alcohol derivatives: promising materials for pharmaceutical & biomedical applications. **2014**.
62. Sapalidis, A. A., Porous Polyvinyl alcohol membranes: Preparation methods and applications. *Symmetry* **2020,** *12* (6), 960.
63. Heydari, M.; Moheb, A.; Ghiaci, M.; Masoomi, M., Effect of cross-linking time on the thermal and mechanical properties and pervaporation performance of poly (vinyl alcohol) membrane cross-linked with fumaric acid used for dehydration of isopropanol. *Journal of applied polymer science* **2013,** *128* (3), 1640-1651.
64. Sonker, A. K.; Rathore, K.; Nagarale, R. K.; Verma, V., Crosslinking of Polyvinyl Alcohol (PVA) and Effect of Crosslinker Shape (Aliphatic and Aromatic) Thereof. *Journal of Polymers and the Environment* **2018,** *26* (5), 1782-1794.
65. Bolto, B.; Tran, T.; Hoang, M.; Xie, Z., Crosslinked poly(vinyl alcohol) membranes. *Progress in Polymer Science* **2009,** *34* (9), 969-981.
66. Gohil, J.; Bhattacharya, A.; Ray, P., Studies on the crosslinking of poly (vinyl alcohol). *Journal of polymer research* **2006,** *13* (2), 161-169.
67. Cordes, E.; Bull, H., Mechanism and catalysis for hydrolysis of acetals, ketals, and ortho esters. *Chemical Reviews* **1974,** *74* (5), 581-603.
68. Ong, Y. K.; Shi, G. M.; Le, N. L.; Tang, Y. P.; Zuo, J.; Nunes, S. P.; Chung, T.-S., Recent membrane development for pervaporation processes. *Progress in Polymer Science* **2016,** *57*, 1-31.
69. Gautam, L.; Warkar, S. G.; Ahmad, S. I.; Kant, R.; Jain, M., A review on carboxylic acid cross-linked polyvinyl alcohol: Properties and applications. *Polymer Engineering & Science* **2022,** *62* (2), 225-246.
70. Dmitrenko, M.; Penkova, A.; Kuzminova, A.; Missyul, A.; Ermakov, S.; Roizard, D., Development and Characterization of New Pervaporation PVA Membranes for the Dehydration Using Bulk and Surface Modifications. *Polymers (Basel)* **2018,** *10* (6), 571.

71. Yave, W., The improved pervaporation PERVAP membranes. *Filtration + Separation* **2017,** *54* (3), 14-15.
72. Kurkuri, M. D.; Toti, U. S.; Aminabhavi, T. M., Syntheses and characterization of blend membranes of sodium alginate and poly (vinyl alcohol) for the pervaporation separation of water+ isopropanol mixtures. *Journal of Applied Polymer Science* **2002,** *86* (14), 3642-3651.
73. Dong, Y. Q.; Zhang, L.; Shen, J. N.; Song, M. Y.; Chen, H. L., Preparation of poly(vinyl alcohol)-sodium alginate hollow-fiber composite membranes and pervaporation dehydration characterization of aqueous alcohol mixtures. *Desalination* **2006,** *193* (1-3), 202-210.
74. Kalyani, S.; Smitha, B.; Sridhar, S.; Krishnaiah, A., Separation of ethanol− water mixtures by pervaporation using sodium alginate/poly (vinyl pyrrolidone) blend membrane crosslinked with phosphoric acid. *Industrial & engineering chemistry research* **2006,** *45* (26), 9088-9095.
75. Zhao, Q.; An, Q. F.; Ji, Y.; Qian, J.; Gao, C., Polyelectrolyte complex membranes for pervaporation, nanofiltration and fuel cell applications. *Journal of membrane science* **2011,** *379* (1-2), 19-45.
76. Wang, X.-S.; Ji, Y.-L.; Zheng, P.-Y.; An, Q.-F.; Zhao, Q.; Lee, K.-R.; Qian, J.-W.; Gao, C.-J., Engineering novel polyelectrolyte complex membranes with improved mechanical properties and separation performance. *Journal of Materials Chemistry A* **2015,** *3* (14), 7296-7303.
77. Ohya, H.; Kudryavsev, V.; Semenova, S. I., *Polyimide membranes: applications, fabrications and properties*. CRC Press: 1997.
78. Vane, L. M., Review: Membrane Materials for the Removal of Water from Industrial Solvents by Pervaporation and Vapor Permeation. *J Chem Technol Biotechnol* **2019,** *94* (2), 343-365.
79. Caro, J.; Noack, M., Zeolite membranes – Recent developments and progress. *Microporous and Mesoporous Materials* **2008,** *115* (3), 215-233.
80. Kondo, M.; Kita, H., Permeation mechanism through zeolite NaA and T-type membranes for practical dehydration of organic solvents. *Journal of Membrane Science* **2010,** *361* (1-2), 223-231.
81. Liu, D. Z.; Zhang, Y. T.; Jiang, J.; Wang, X. R.; Zhang, C.; Gu, X. H., High-performance NaA zeolite membranes supported on four-channel ceramic hollow fibers for ethanol dehydration. *Rsc Advances* **2015,** *5* (116), 95866-95871.
82. Jiang, J.; Wang, L.; Peng, L.; Cai, C.; Zhang, C.; Wang, X.; Gu, X., Preparation and characterization of high performance CHA zeolite membranes from clear solution. *Journal of Membrane Science* **2017,** *527*, 51-59.
83. Sorenson, S. G.; Payzant, E. A.; Gibbons, W. T.; Soydas, B.; Kita, H.; Noble, R. D.; Falconer, J. L., Influence of zeolite crystal expansion/contraction on NaA zeolite membrane separations. *Journal of membrane science* **2011,** *366* (1-2), 413-420.
84. Castricum, H. L.; Sah, A.; Kreiter, R.; Blank, D. H.; Vente, J. F.; ten Elshof, J. E., Hybrid ceramic nanosieves: stabilizing nanopores with organic links. *Chem Commun (Camb)* **2008,** (9), 1103-5.
85. Asaeda, M.; Sakou, Y.; Yang, J.; Shimasaki, K., Stability and performance of porous silica–zirconia composite membranes for pervaporation of aqueous organic solutions. *Journal of Membrane Science* **2002,** *209* (1), 163-175.
86. van Veen, H., Dewatering of organics by pervaporation with silica membranes. *Separation and Purification Technology* **2001,** *22-23* (1-2), 361-366.
87. Klinov, A. V.; Akberov, R. R.; Fazlyev, A. R.; Farakhov, M. I., Experimental investigation and modeling through using the solution-diffusion concept of pervaporation dehydration of ethanol and isopropanol by ceramic membranes HybSi. *Journal of membrane science* **2017,** *524*, 321-333.

88. Park, H. B.; Kamcev, J.; Robeson, L. M.; Elimelech, M.; Freeman, B. D., Maximizing the right stuff: The trade-off between membrane permeability and selectivity. *Science* **2017,** *356* (6343), eaab0530.
89. Huang, Z.; Guan, H.-m.; lee Tan, W.; Qiao, X.-Y.; Kulprathipanja, S., Pervaporation study of aqueous ethanol solution through zeolite-incorporated multilayer poly (vinyl alcohol) membranes: Effect of zeolites. *Journal of Membrane Science* **2006,** *276* (1-2), 260-271.
90. Dmitrenko, M. E.; Penkova, A. V.; Kuzminova, A. I.; Morshed, M.; Larionov, M. I.; Alem, H.; Zolotarev, A. A.; Ermakov, S. S.; Roizard, D., Investigation of new modification strategies for PVA membranes to improve their dehydration properties by pervaporation. *Applied Surface Science* **2018,** *450*, 527-537.
91. Zhu, Y.; Xia, S.; Liu, G.; Jin, W., Preparation of ceramic-supported poly(vinyl alcohol)–chitosan composite membranes and their applications in pervaporation dehydration of organic/water mixtures. *Journal of Membrane Science* **2010,** *349* (1), 341-348.
92. Dmitrenko, M.; Kuzminova, A.; Zolotarev, A.; Ermakov, S.; Roizard, D.; Penkova, A., Enhanced Pervaporation Properties of PVA-Based Membranes Modified with Polyelectrolytes. Application to IPA Dehydration. *Polymers* **2020,** *12* (1), 14.
93. Dmitrenko, M.; Atta, R.; Zolotarev, A.; Kuzminova, A.; Ermakov, S.; Penkova, A., Development of Novel Membranes Based on Polyvinyl Alcohol Modified by Pluronic F127 for Pervaporation Dehydration of Isopropanol. *Sustainability* **2022,** *14* (6), 3561.
94. Yang, G.; Xie, Z.; Cran, M.; Ng, D.; Gray, S., Enhanced desalination performance of poly (vinyl alcohol)/carbon nanotube composite pervaporation membranes via interfacial engineering. *Journal of Membrane Science* **2019,** *579*, 40-51.
95. Selim, A.; Toth, A. J.; Fozer, D.; Süvegh, K.; Mizsey, P., Facile Preparation of a Laponite/PVA Mixed Matrix Membrane for Efficient and Sustainable Pervaporative Dehydration of C1–C3 Alcohols. *ACS Omega* **2020,** *5* (50), 32373-32385.
96. Li, M.; Wang, J.; Zhou, S.; Xue, A.; Wu, F.; Zhao, Y., Polyacrylonitrile-supported self-aggregation crosslinked poly (vinyl alcohol) pervaporation membranes for ethanol dehydration. *European Polymer Journal* **2020,** *122*, 109359.
97. Chen, X.; Hung, W.-S.; Liu, G.; Lee, K.-R.; Jin, W., PDMS mixed-matrix membranes with molecular fillers via reactive incorporation and their application for bio-butanol recovery from aqueous solution. *Journal of Polymer Science* **2020,** *58* (18), 2634-2643.
98. Knozowska, K.; Kujawa, J.; Lagzdins, R.; Figoli, A.; Kujawski, W., A New Type of Composite Membrane PVA-NaY/PA-6 for Separation of Industrially Valuable Mixture Ethanol/Ethyl Tert-Butyl Ether by Pervaporation. *Materials* **2020,** *13* (17), 3676.
99. Li, X.; Liu, C.; Yin, W.; Chong, T. H.; Wang, R., Design and development of layer-by-layer based low-pressure antifouling nanofiltration membrane used for water reclamation. *Journal of Membrane Science* **2019,** *584*, 309-323.
100. Schick, C., Differential scanning calorimetry (DSC) of semicrystalline polymers. *Analytical and Bioanalytical Chemistry* **2009,** *395* (6), 1589-1611.
101. Hyder, M. N.; Huang, R. Y. M.; Chen, P., Correlation of physicochemical characteristics with pervaporation performance of poly(vinyl alcohol) membranes. *Journal of Membrane Science* **2006,** *283* (1), 281-290.
102. Zhao, Q.; Qian, J.; An, Q.; Zhu, M.; Yin, M.; Sun, Z., Poly(vinyl alcohol)/polyelectrolyte complex blend membrane for pervaporation dehydration of isopropanol. *Journal of Membrane Science* **2009,** *343* (1), 53-61.
103. Xiao, S.; Feng, X.; Huang, R. Y. M., Investigation of sorption properties and pervaporation behaviors under different operating conditions for trimesoyl chloride-crosslinked PVA membranes. *Journal of Membrane Science* **2007,** *302* (1), 36-44.
104. Yang, G.; Xie, Z.; Thornton, A. W.; Doherty, C. M.; Ding, M.; Xu, H.; Cran, M.; Ng, D.; Gray, S., Ultrathin poly (vinyl alcohol)/MXene nanofilm composite membrane with facile

intrusion-free construction for pervaporative separations. *Journal of Membrane Science* **2020,** *614*, 118490.
105. Saadatkhah, N.; Carillo Garcia, A.; Ackermann, S.; Leclerc, P.; Latifi, M.; Samih, S.; Patience, G. S.; Chaouki, J., Experimental methods in chemical engineering: Thermogravimetric analysis—TGA. *The Canadian Journal of Chemical Engineering* **2020,** *98* (1), 34-43.
106. Liu, C.; Xue, T.; Yang, Y.; Ouyang, J.; Chen, H.; Yang, S.; Li, G.; Cai, D.; Si, Z.; Li, S.; Qin, P., Effect of crosslinker 3-methacryloxypropylmethyldimethoxysilane on UV-crosslinked PDMS-PTFPMS block copolymer membranes for ethanol pervaporation. *Chemical Engineering Research and Design* **2021,** *168*, 13-24.
107. Serrano, J. M.; Liu, T.; Khan, A. U.; Botset, B.; Stovall, B. J.; Xu, Z.; Guo, D.; Cao, K.; Hao, X.; Cheng, S.; Liu, G., Composition Design of Block Copolymers for Porous Carbon Fibers. *Chemistry of Materials* **2019,** *31* (21), 8898-8907.
108. Devi, D. A.; Smitha, B.; Sridhar, S.; Aminabhavi, T. M., Pervaporation separation of dimethylformamide/water mixtures through poly(vinyl alcohol)/poly(acrylic acid) blend membranes. *Separation and Purification Technology* **2006,** *51* (1), 104-111.
109. Bhargava, R.; Wang, S.-Q.; Koenig, J. L., FTIR Microspectroscopy of PolymericSystems. In *Liquid Chromatography / FTIR Microspectroscopy / MicrowaveAssisted Synthesis*, Springer Berlin Heidelberg: Berlin, Heidelberg, 2003; pp 137-191.
110. do Nascimento, F. C.; de Aguiar, L. C. V.; Costa, L. A. T.; Fernandes, M. T.; Marassi, R. J.; Gomes, A. d. S.; de Castro, J. A., Formulation and characterization of crosslinked polyvinyl alcohol (PVA) membranes: effects of the crosslinking agents. *Polym Bull* **2021,** *78* (2), 917-929.
111. Castro-Muñoz, R.; Buera-González, J.; Iglesia, Ó. d. l.; Galiano, F.; Fíla, V.; Malankowska, M.; Rubio, C.; Figoli, A.; Téllez, C.; Coronas, J., Towards the dehydration of ethanol using pervaporation cross-linked poly(vinyl alcohol)/graphene oxide membranes. *Journal of Membrane Science* **2019,** *582*, 423-434.
112. Orlando, A.; Franceschini, F.; Muscas, C.; Pidkova, S.; Bartoli, M.; Rovere, M.; Tagliaferro, A., A Comprehensive Review on Raman Spectroscopy Applications. *Chemosensors* **2021,** *9* (9), 262.
113. Hu, S. Y.; Zhang, Y.; Lawless, D.; Feng, X., Composite membranes comprising of polyvinylamine-poly(vinyl alcohol) incorporated with carbon nanotubes for dehydration of ethylene glycol by pervaporation. *Journal of Membrane Science* **2012,** *417-418*, 34-44.
114. Liang, B.; Zhan, W.; Qi, G.; Lin, S.; Nan, Q.; Liu, Y.; Cao, B.; Pan, K., High performance graphene oxide/polyacrylonitrile composite pervaporation membranes for desalination applications. *Journal of Materials Chemistry A* **2015,** *3* (9), 5140-5147.
115. Stevie, F. A.; Donley, C. L., Introduction to x-ray photoelectron spectroscopy. *Journal of Vacuum Science & Technology A* **2020,** *38* (6).
116. Greczynski, G.; Haasch, R. T.; Hellgren, N.; Lewin, E.; Hultman, L., X-ray photoelectron spectroscopy of thin films. *Nature Reviews Methods Primers* **2023,** *3* (1), 40.
117. Yang, Y.; Liu, Q.; Wang, H.; Ding, F.; Jin, G.; Li, C.; Meng, H., Superhydrophobic modification of ceramic membranes for vacuum membrane distillation. *Chinese Journal of Chemical Engineering* **2017,** *25* (10), 1395-1401.
118. Zhang, W.; Li, G.; Fang, Y.; Wang, X., Maleic anhydride surface-modification of crosslinked chitosan membrane and its pervaporation performance. *Journal of Membrane Science* **2007,** *295* (1), 130-138.
119. Mlynárik, V., Introduction to nuclear magnetic resonance. *Analytical Biochemistry* **2017,** *529*, 4-9.
120. Spiess, H. W., Nuclear Magnetic Resonance Spectroscopy in Macromolecular Science. *Macromolecular Chemistry and Physics* **2003,** *204* (2), 340-346.

121. Zhao, Q.; Qian, J.; An, Q.; Zhu, Z.; Zhang, P.; Bai, Y., Studies on pervaporation characteristics of polyacrylonitrile–b-poly(ethylene glycol)–b-polyacrylonitrile block copolymer membrane for dehydration of aqueous acetone solutions. *Journal of Membrane Science* **2008,** *311* (1), 284-293.
122. Li, C.; Li, J.; Cao, T.; Cai, P.; Wang, N.; An, Q.-F., Impact of crosslinking on organic solvent nanofiltration performance in polydimethylsiloxane composite membrane: Probed by in-situ low-field nuclear magnetic resonance spectroscopy. *Journal of Membrane Science* **2021,** *633*, 119382.
123. Parrondo, J.; Arges, C. G.; Niedzwiecki, M.; Anderson, E. B.; Ayers, K. E.; Ramani, V., Degradation of anion exchange membranes used for hydrogen production by ultrapure water electrolysis. *RSC Advances* **2014,** *4* (19), 9875-9879.
124. Kober, P. A., Pervaporation, Perstillation and Percrystallization.1. *Journal of the American Chemical Society* **1917,** *39* (5), 944-948.
125. Lakshmy, K. S.; Lal, D.; Nair, A.; Babu, A.; Das, H.; Govind, N.; Dmitrenko, M.; Kuzminova, A.; Korniak, A.; Penkova, A.; Tharayil, A.; Thomas, S., Pervaporation as a Successful Tool in the Treatment of Industrial Liquid Mixtures. *Polymers* **2022,** *14* (8), 1604.
126. Baker, R. W.; Wijmans, J. G.; Huang, Y., Permeability, permeance and selectivity: A preferred way of reporting pervaporation performance data. *Journal of Membrane Science* **2010,** *348* (1-2), 346-352.
127. Lipnizki, F.; Trägårdh, G., MODELLING OF PERVAPORATION: MODELS TO ANALYZE AND PREDICT THE MASS TRANSPORT IN PERVAPORATION. *Separation and Purification Methods* **2001,** *30* (1), 49-125.
128. Wijmans, J. G., Process performance = membrane properties + operating conditions. *Journal of Membrane Science* **2003,** *220* (1-2), 1-3.
129. Castro-Muñoz, R., Pervaporation: The emerging technique for extracting aroma compounds from food systems. *Journal of Food Engineering* **2019,** *253*, 27-39.
130. Wee, S.-L.; Tye, C.-T.; Bhatia, S., Membrane separation process—Pervaporation through zeolite membrane. *Separation and Purification Technology* **2008,** *63* (3), 500-516.
131. Lonsdale, H. K., The growth of membrane technology. *Journal of Membrane Science* **1982,** *10* (2), 81-181.
132. Koros, W. J.; Zhang, C., Materials for next-generation molecularly selective synthetic membranes. *Nature materials* **2017,** *16* (3), 289-297.
133. Crespo, J. G.; Böddeker, K. W., *Membrane processes in separation and purification*. Springer Science & Business Media: 2013; Vol. 272.
134. Ferrarini, R.; Ciman, G. M.; Camin, F.; Bandini, S.; Gostoli, C., Variation of oxygen isotopic ratio during wine dealcoholization by membrane contactors: Experiments and modelling. *Journal of Membrane Science* **2016,** *498*, 385-394.
135. Zhang, Q. G.; Liu, Q. L.; Zhu, A. M.; Xiong, Y.; Ren, L., Pervaporation performance of quaternized poly (vinyl alcohol) and its crosslinked membranes for the dehydration of ethanol. *Journal of Membrane Science* **2009,** *335* (1-2), 68-75.
136. Liu, L.; Kentish, S. E., Pervaporation performance of crosslinked PVA membranes in the vicinity of the glass transition temperature. *Journal of Membrane Science* **2018,** *553*, 63-69.
137. Oh, B.-K.; Lee, Y. M., Effects of functional group and operating temperature on the separation of pyridine-water mixture by pervaporation. *Journal of Membrane Science* **1996,** *113* (2), 183-189.
138. Yong, S. K.; Sang, W. L.; Un, Y. K.; Jyong, S. S., Pervaporation of water-ethanol mixtures through crosslinked and surface-modified poly(vinyl alcohol) membrane. *Journal of Membrane Science* **1990,** *51* (1), 215-226.
139. Wang, Y.; Widjojo, N.; Sukitpaneenit, P.; Chung, T.-S., Membrane Pervaporation. In *Separation and Purification Technologies in Biorefineries*, 2013; pp 259-299.

140. Shao, P.; Huang, R. Y. M., Polymeric membrane pervaporation. *Journal of Membrane Science* **2007,** *287* (2), 162-179.
141. Wang, L.; Wang, Y.; Wu, L.; Wei, G., Fabrication, Properties, Performances, and Separation Application of Polymeric Pervaporation Membranes: A Review. *Polymers* **2020,** *12* (7), 1466.
142. Chapman, P. D.; Oliveira, T.; Livingston, A. G.; Li, K., Membranes for the dehydration of solvents by pervaporation. *Journal of Membrane Science* **2008,** *318* (1), 5-37.
143. Hunger, K.; Schmeling, N.; Jeazet, H. B. T.; Janiak, C.; Staudt, C.; Kleinermanns, K., Investigation of Cross-Linked and Additive Containing Polymer Materials for Membranes with Improved Performance in Pervaporation and Gas Separation. *Membranes* **2012,** *2* (4), 727-763.
144. Lu, J.; Nguyen, Q.; Zhou, L.; Xu, B.; Ping, Z., Study of the role of water in the transport of water and THF through hydrophilic membranes by pervaporation. *Journal of Membrane Science* **2003,** *226* (1), 135-143.
145. Hyder, M. N.; Huang, R. Y. M.; Chen, P., Effect of selective layer thickness on pervaporation of composite poly(vinyl alcohol)–poly(sulfone) membranes. *Journal of Membrane Science* **2008,** *318* (1), 387-396.
146. Ribelli, T. G.; Lorandi, F.; Fantin, M.; Matyjaszewski, K., Atom Transfer Radical Polymerization: Billion Times More Active Catalysts and New Initiation Systems. *Macromolecular Rapid Communications* **2019,** *40* (1), 1800616.
147. Perrier, S., 50th Anniversary Perspective: RAFT Polymerization—A User Guide. *Macromolecules* **2017,** *50* (19), 7433-7447.
148. Keddie, D. J., A guide to the synthesis of block copolymers using reversible-addition fragmentation chain transfer (RAFT) polymerization. *Chemical Society Reviews* **2014,** *43* (2), 496-505.
149. Feng, H.; Lu, X.; Wang, W.; Kang, N.-G.; Mays, J. W., Block Copolymers: Synthesis, Self-Assembly, and Applications. *Polymers* **2017,** *9* (10), 494.
150. Hadjichristidis, N.; Pitsikalis, M.; Iatrou, H., Synthesis of block copolymers. In *Block Copolymers I*, Springer: 2005; pp 1-124.
151. Szwarc, M., 'Living' Polymers. *Nature* **1956,** *178* (4543), 1168-1169.
152. Szwarc, M.; Levy, M.; Milkovich, R., POLYMERIZATION INITIATED BY ELECTRON TRANSFER TO MONOMER. A NEW METHOD OF FORMATION OF BLOCK POLYMERS1. *Journal of the American Chemical Society* **1956,** *78* (11), 2656-2657.
153. Hadjichristidis, N.; Iatrou, H.; Pispas, S.; Pitsikalis, M., Anionic polymerization: High vacuum techniques. *J Polym Sci Pol Chem* **2000,** *38* (18), 3211-3234.
154. Miyamoto, M.; Sawamoto, M.; Higashimura, T., Living polymerization of isobutyl vinyl ether with hydrogen iodide/iodine initiating system. *Macromolecules* **1984,** *17* (3), 265-268.
155. Higashimura, T.; Mitsuhashi, M.; Sawamoto, M., Synthesis of p-Methoxystyrene-Isobutyl Vinyl Ether Block Copolymers by Living Cationic Polymerization with Iodine. *Macromolecules* **1979,** *12* (2), 178-182.
156. Aoshima, S.; Kanaoka, S., A Renaissance in Living Cationic Polymerization. *Chemical Reviews* **2009,** *109* (11), 5245-5287.
157. Herzberger, J.; Niederer, K.; Pohlit, H.; Seiwert, J.; Worm, M.; Wurm, F. R.; Frey, H., Polymerization of Ethylene Oxide, Propylene Oxide, and Other Alkylene Oxides: Synthesis, Novel Polymer Architectures, and Bioconjugation. *Chemical Reviews* **2016,** *116* (4), 2170-2243.
158. Hillmyer, M. A.; Bates, F. S., Synthesis and Characterization of Model Polyalkane−Poly(ethylene oxide) Block Copolymers. *Macromolecules* **1996,** *29* (22), 6994-7002.

159. Christian, D. A.; Tian, A.; Ellenbroek, W. G.; Levental, I.; Rajagopal, K.; Janmey, P. A.; Liu, A. J.; Baumgart, T.; Discher, D. E., Spotted vesicles, striped micelles and Janus assemblies induced by ligand binding. *Nature Materials* **2009,** *8* (10), 843-849.
160. Wu, D. L.; Spulber, M.; Itel, F.; Chami, M.; Pfohl, T.; Palivan, C. G.; Meier, W., Effect of Molecular Parameters on the Architecture and Membrane Properties of 3D Assemblies of Amphiphilic Copolymers. *Macromolecules* **2014,** *47* (15), 5060-5069.
161. Matyjaszewski, K.; Xia, J., Atom Transfer Radical Polymerization. *Chemical Reviews* **2001,** *101* (9), 2921-2990.
162. Matyjaszewski, K., Atom Transfer Radical Polymerization (ATRP): Current Status and Future Perspectives. *Macromolecules* **2012,** *45* (10), 4015-4039.
163. Matyjaszewski, K.; Tsarevsky, N. V., Macromolecular Engineering by Atom Transfer Radical Polymerization. *Journal of the American Chemical Society* **2014,** *136* (18), 6513-6533.
164. Pintauer, T.; Matyjaszewski, K., Structural aspects of copper catalyzed atom transfer radical polymerization. *Coordination Chemistry Reviews* **2005,** *249* (11), 1155-1184.
165. Matyjaszewski, K., Current status and outlook for ATRP. *European Polymer Journal* **2024,** *211*, 113001.
166. Chiefari, J.; Chong, Y. K.; Ercole, F.; Krstina, J.; Jeffery, J.; Le, T. P. T.; Mayadunne, R. T. A.; Meijs, G. F.; Moad, C. L.; Moad, G.; Rizzardo, E.; Thang, S. H., Living Free-Radical Polymerization by Reversible Addition−Fragmentation Chain Transfer: The RAFT Process. *Macromolecules* **1998,** *31* (16), 5559-5562.
167. Moad, G.; Rizzardo, E.; Thang, S. H., Living Radical Polymerization by the RAFT Process. *Australian Journal of Chemistry* **2005,** *58* (6), 379-410.
168. Moad, G.; Rizzardo, E.; Thang, S. H., Radical addition–fragmentation chemistry in polymer synthesis. *Polymer* **2008,** *49* (5), 1079-1131.
169. Moad, C. L.; Moad, G., Fundamentals of reversible addition–fragmentation chain transfer (RAFT). *Chemistry Teacher International* **2021,** *3* (2), 3-17.
170. Nicolaÿ, R.; Kwak, Y.; Matyjaszewski, K., Synthesis of poly(vinyl acetate) block copolymers by successive RAFT and ATRP with a bromoxanthate iniferter. *Chemical Communications* **2008,** (42), 5336-5338.
171. Altintas, O.; Speros, J. C.; Bates, F. S.; Hillmyer, M. A., Straightforward synthesis of model polystyrene-block-poly(vinyl alcohol) diblock polymers. *Polymer Chemistry* **2018,** *9* (31), 4243-4250.
172. Meeuwissen, S. A.; Bruekers, S. M. C.; Chen, Y.; Pochan, D. J.; van Hest, J. C. M., Spontaneous shape changes in polymersomes via polymer/polymer segregation. *Polymer Chemistry* **2014,** *5* (2), 489-501.
173. Fauquignon, M.; Ibarboure, E.; Carlotti, S.; Brûlet, A.; Schmutz, M.; Le Meins, J.-F., Large and Giant Unilamellar Vesicle(s) Obtained by Self-Assembly of Poly(dimethylsiloxane)-b-poly(ethylene oxide) Diblock Copolymers, Membrane Properties and Preliminary Investigation of Their Ability to Form Hybrid Polymer/Lipid Vesicles. *Polymers* **2019,** *11* (12), 2013.
174. Discher, D. E.; Ahmed, F., POLYMERSOMES. *Annual Review of Biomedical Engineering* **2006,** *8* (1), 323-341.
175. Garni, M.; Wehr, R.; Avsar, S. Y.; John, C.; Palivan, C.; Meier, W., Polymer membranes as templates for bio-applications ranging from artificial cells to active surfaces. *European Polymer Journal* **2019,** *112*, 346-364.
176. Mai, Y.; Eisenberg, A., Self-assembly of block copolymers. *Chemical Society Reviews* **2012,** *41* (18), 5969-5985.
177. Nunes, S. P., Chapter 11 - Block Copolymer Membranes. In *Sustainable Nanoscale Engineering*, Szekely, G.; Livingston, A., Eds. Elsevier: 2020; pp 297-316.
178. Gröschel, A. H.; Müller, A. H. E., Self-assembly concepts for multicompartment nanostructures. *Nanoscale* **2015,** *7* (28), 11841-11876.

179. Fetsch, C.; Gaitzsch, J.; Messager, L.; Battaglia, G.; Luxenhofer, R., Self-Assembly of Amphiphilic Block Copolypeptoids – Micelles, Worms and Polymersomes. *Scientific Reports* **2016,** *6* (1), 33491.
180. Daubian, D.; Gaitzsch, J.; Meier, W., Synthesis and complex self-assembly of amphiphilic block copolymers with a branched hydrophobic poly(2-oxazoline) into multicompartment micelles, pseudo-vesicles and yolk/shell nanoparticles. *Polymer Chemistry* **2020,** *11* (6), 1237-1248.
181. Dionzou, M.; Morere, A.; Roux, C.; Lonetti, B.; Marty, J. D.; Mingotaud, C.; Joseph, P.; Goudouneche, D.; Payre, B.; Leonetti, M.; Mingotaud, A. F., Comparison of methods for the fabrication and the characterization of polymer self-assemblies: what are the important parameters? *Soft Matter* **2016,** *12* (7), 2166-76.
182. Habe, H.; Shinbo, T.; Yamamoto, T.; Sato, S.; Shimada, H.; Sakaki, K., Chemical Analysis of Impurities in Diverse Bioethanol Samples. *Journal of the Japan Petroleum Institute* **2013,** *56* (6), 414-422.
183. Ulbricht, M., Advanced functional polymer membranes. *Polymer* **2006,** *47* (7), 2217-2262.
184. Zhao, C.; Nie, S.; Tang, M.; Sun, S., Polymeric pH-sensitive membranes—A review. *Progress in Polymer Science* **2011,** *36* (11), 1499-1520.
185. Fane, A. G.; Wang, R.; Hu, M. X., Synthetic Membranes for Water Purification: Status and Future. *Angewandte Chemie International Edition* **2015,** *54* (11), 3368-3386.
186. Hennessy, J., Membranes from academia to industry. *Nature Materials* **2017,** *16* (3), 280-282.
187. Wandera, D.; Wickramasinghe, S. R.; Husson, S. M., Stimuli-responsive membranes. *Journal of Membrane Science* **2010,** *357* (1), 6-35.
188. Turner, J. S.; Cheng, Y. L., pH dependence of PDMS–PMAA IPN morphology and transport properties. *Journal of Membrane Science* **2004,** *240* (1), 19-24.
189. Li, P.-F.; Xie, R.; Jiang, J.-C.; Meng, T.; Yang, M.; Ju, X.-J.; Yang, L.; Chu, L.-Y., Thermo-responsive gating membranes with controllable length and density of poly(N-isopropylacrylamide) chains grafted by ATRP method. *Journal of Membrane Science* **2009,** *337* (1), 310-317.
190. Manouras, T.; Vamvakaki, M., Field responsive materials: photo-, electro-, magnetic- and ultrasound-sensitive polymers. *Polymer Chemistry* **2017,** *8* (1), 74-96.
191. Singh, N.; Wang, J.; Ulbricht, M.; Wickramasinghe, S. R.; Husson, S. M., Surface-initiated atom transfer radical polymerization: A new method for preparation of polymeric membrane adsorbers. *Journal of Membrane Science* **2008,** *309* (1), 64-72.
192. Einfalt, T.; Goers, R.; Dinu, I. A.; Najer, A.; Spulber, M.; Onaca-Fischer, O.; Palivan, C. G., Stimuli-Triggered Activity of Nanoreactors by Biomimetic Engineering Polymer Membranes. *Nano Letters* **2015,** *15* (11), 7596-7603.
193. Nunes, S. P.; Behzad, A. R.; Hooghan, B.; Sougrat, R.; Karunakaran, M.; Pradeep, N.; Vainio, U.; Peinemann, K.-V., Switchable pH-Responsive Polymeric Membranes Prepared via Block Copolymer Micelle Assembly. *ACS Nano* **2011,** *5* (5), 3516-3522.
194. Abu-Thabit, N.; Umar, Y.; Ratemi, E.; Ahmad, A.; Ahmad Abuilaiwi, F., A Flexible Optical pH Sensor Based on Polysulfone Membranes Coated with pH-Responsive Polyaniline Nanofibers. *Sensors* **2016,** *16* (7), 986.
195. Car, A.; Baumann, P.; Duskey, J. T.; Chami, M.; Bruns, N.; Meier, W., pH-Responsive PDMS-b-PDMAEMA Micelles for Intracellular Anticancer Drug Delivery. *Biomacromolecules* **2014,** *15* (9), 3235-3245.
196. Franck-Lacaze, L.; Sistat, P.; Huguet, P., Determination of the pKa of poly (4-vinylpyridine)-based weak anion exchange membranes for the investigation of the side proton leakage. *Journal of Membrane Science* **2009,** *326* (2), 650-658.

197. Osada, Y.; Honda, K.; Ohta, M., Control of water permeability by mechanochemical contraction of poly(methacrylic acid)-grafted membranes. *Journal of Membrane Science* **1986,** *27* (3), 327-338.
198. Han, X.; Zhang, X.; Zhu, H.; Yin, Q.; Liu, H.; Hu, Y., Effect of Composition of PDMAEMA-b-PAA Block Copolymers on Their pH- and Temperature-Responsive Behaviors. *Langmuir* **2013,** *29* (4), 1024-1034.
199. Fan, X. X.; Xie, R.; Zhao, Q.; Li, X. Y.; Ju, X. J.; Wang, W.; Liu, Z.; Chu, L. Y., Dual pH-responsive smart gating membranes. *Journal of Membrane Science* **2018,** *555*, 20-29.
200. Xue, J.; Chen, L.; Wang, H. L.; Zhang, Z. B.; Zhu, X. L.; Kang, E. T.; Neoh, K. G., Stimuli-Responsive Multifunctional Membranes of Controllable Morphology from Poly(vinylidene fluoride)-graft-Poly[2-(N,N-dimethylamino)ethyl methacrylate] Prepared via Atom Transfer Radical Polymerization. *Langmuir* **2008,** *24* (24), 14151-14158.
201. Du, R.; Feng, X.; Chakma, A., Poly(N,N-dimethylaminoethyl methacrylate)/polysulfone composite membranes for gas separations. *Journal of Membrane Science* **2006,** *279* (1), 76-85.
202. Du, R.; Chakma, A.; Feng, X., Interfacially formed poly(N,N-dimethylaminoethyl methacrylate)/polysulfone composite membranes for CO2/N2 separation. *Journal of Membrane Science* **2007,** *290* (1), 19-28.
203. Masakazu, Y.; Kiyoshi, F.; Hirokazu, K.; Toshio, K.; Naoya, O., Selective Permeation of Carbon Dioxide through Synthetic Polymeric Membranes Having Amine Moiety. *Chemistry Letters* **1994,** *23* (2), 243-246.
204. Matsuyama, H.; Teramoto, M.; Sakakura, H., Selective permeation of CO2 through poly 2-(N,N-dimethyl)aminoethyl methacrylate membrane prepared by plasma-graft polymerization technique. *Journal of Membrane Science* **1996,** *114* (2), 193-200.
205. Du, R.; Zhao, J., Properties of poly (N,N-dimethylaminoethyl methacrylate)/polysulfone positively charged composite nanofiltration membrane. *Journal of Membrane Science* **2004,** *239* (2), 183-188.
206. Mika, A. M.; Childs, R. F.; Dickson, J. M., Salt separation and hydrodynamic permeability of a porous membrane filled with pH-sensitive gel. *Journal of Membrane Science* **2002,** *206* (1), 19-30.
207. Agarwal, S.; Zhang, Y.; Maji, S.; Greiner, A., PDMAEMA based gene delivery materials. *Materials Today* **2012,** *15* (9), 388-393.
208. Hu, J.; Zhang, G.; Ge, Z.; Liu, S., Stimuli-responsive tertiary amine methacrylate-based block copolymers: Synthesis, supramolecular self-assembly and functional applications. *Progress in Polymer Science* **2014,** *39* (6), 1096-1143.
209. Li, J.; Si, X.; Li, X.; Wang, N.; An, Q.; Ji, S., Preparation of acid-resistant PEI/SA composite membranes for the pervaporation dehydration of ethanol at low pH. *Separation and Purification Technology* **2018,** *192*, 205-212.
210. Nam, S. Y.; Lee, Y. M., Pervaporation and properties of chitosan-poly(acrylic acid) complex membranes. *Journal of Membrane Science* **1997,** *135* (2), 161-171.
211. Wang, N.; Zhang, G.; Ji, S.; Qin, Z.; Liu, Z., The salt-, pH- and oxidant-responsive pervaporation behaviors of weak polyelectrolyte multilayer membranes. *Journal of Membrane Science* **2010,** *354* (1), 14-22.
212. Li, W.; Luis, P., Understanding coupling effects in pervaporation of multi-component mixtures. *Separation and Purification Technology* **2018,** *197*, 95-106.
213. Li, W.; Sreerangappa, R.; Estager, J.; Monbaliu, J.-C. M.; Debecker, D. P.; Luis, P., Application of pervaporation in the bio-production of glycerol carbonate. *Chemical Engineering and Processing - Process Intensification* **2018,** *132*, 127-136.
214. Frania, M.; Huebner, A.; Maus, E. Membrane having a pore-free separating layer and use and method of manufacturing a membrane. 2018.

215. Deboudt, K.; Delporte, M.; Loucheux, C., Copolymers of N-vinyl-2-pyrrolidone and 2-(dimethylamino)ethyl methacrylate, 1. Synthesis, characterization, quaternization. *Macromolecular Chemistry and Physics* **1995,** *196* (1), 279-290.
216. Roy-Chowdhury, P.; Kirtiwar, M. S., Adiabatic compressibility of polyelectrolytes: Effect of solvents on copolymers of vinyl pyrrolidone with acrylic acid and N-dimethylaminoethyl methacrylate. *Journal of Applied Polymer Science* **1982,** *27* (6), 1883-1895.
217. Abashzadeh, S.; Hajimiri, M. H.; Atyabi, F.; Amini, M.; Dinarvand, R., Novel Physical Hydrogels Composed of Opened-Ring Poly(vinyl pyrrolidone) and Chitosan Derivatives: Preparation and Characterization. *Journal of Applied Polymer Science* **2011,** *121* (5), 2761-2771.
218. Conix, A.; Smets, G., Ring Opening in Lactam Polymers. *Journal of Polymer Science* **1955,** *15* (79), 221-229.
219. Perrino, M. P.; Navarro, R.; Tardajos, M. G.; Gallardo, A.; Reinecke, H., A novel route to substituted poly(vinyl pyrrolidone)s via simple functionalization of 1-vinyl-2-pyrrolidone in the 3-position by ring-opening reactions. *European Polymer Journal* **2010,** *46* (7), 1557-1562.
220. Piirma, I., Polymeric surfactants in emulsion polymerization. *Makromolekulare Chemie. Macromolecular Symposia* **1990,** *35-36* (1), 467-475.
221. Yin, M.; Ye, Y.; Sun, M.; Kang, N.; Yang, W., Facile one-pot synthesis of a polyvinylpyrrolidone-based self-crosslinked fluorescent film. *Macromol Rapid Commun* **2013,** *34* (7), 616-20.
222. Wienk, I. M.; Meuleman, E. E. B.; Borneman, Z.; van den Boomgaard, T.; Smolders, C. A., Chemical treatment of membranes of a polymer blend: Mechanism of the reaction of hypochlorite with poly(vinyl pyrrolidone). *Journal of Polymer Science Part A: Polymer Chemistry* **1995,** *33* (1), 49-54.
223. Brueckner, T. M.; Pickup, P. G.; Hawboldt, K. A., Improvement of bark pyrolysis oil and value added chemical recovery by pervaporation. *Fuel Processing Technology* **2020,** *199*, 106292.
224. Angelini, A.; Fodor, C.; Yave, W.; Leva, L.; Car, A.; Meier, W., pH-Triggered Membrane in Pervaporation Process. *ACS Omega* **2018,** *3* (12), 18950-18957.
225. Peng, P.; Lan, Y.; Liang, L.; Jia, K., Membranes for bioethanol production by pervaporation. *Biotechnology for Biofuels* **2021,** *14* (1), 10.
226. Vane, L.; Namboodiri, V.; Lin, G.; Abar, M.; Alvarez, F., Preparation of Water-Selective Polybutadiene Membranes and Their Use in Drying Alcohols by Pervaporation and Vapor Permeation Technologies. *Acs Sustainable Chemistry & Engineering* **2016,** *4* (8), 4442-4450.
227. Selim, A.; Toth, A. J.; Haaz, E.; Fozer, D.; Szanyi, A.; Hegyesi, N.; Mizsey, P., Preparation and characterization of PVA/GA/Laponite membranes to enhance pervaporation desalination performance. *Separation and Purification Technology* **2019,** *221*, 201-210.
228. Membrane Technology and Applications - R. W. BAKER.
229. Sunitha, K.; Kumar, Y. V. L. R.; Sridhar, S., Effect of PVP loading on pervaporation performance of poly(vinyl alcohol) membranes for THF/water mixtures. *Journal of Materials Science* **2009,** *44* (23), 6280-6285.
230. Zhu, T.; Luo, Y.; Lin, Y.; Li, Q.; Yu, P.; Zeng, M., Study of pervaporation for dehydration of caprolactam through blend NaAlg–poly(vinyl pyrrolidone) membranes on PAN supports. *Separation and Purification Technology* **2010,** *74* (2), 242-252.
231. Dinu, I. A.; Duskey, J. T.; Car, A.; Palivan, C. G.; Meier, W., Engineered non-toxic cationic nanocarriers with photo-triggered slow-release properties. *Polymer Chemistry* **2016,** *7* (20), 3451-3464.

232. Bolto, B.; Hoang, M.; Xie, Z. L., A review of membrane selection for the dehydration of aqueous ethanol by pervaporation. *Chemical Engineering and Processing-Process Intensification* **2011,** *50* (3), 227-235.
233. Semenova, S. I.; Ohya, H.; Soontarapa, K., Hydrophilic membranes for pervaporation: An analytical review. *Desalination* **1997,** *110* (3), 251-286.
234. Chen, Z.; Yang, J. H.; Yin, D. H.; Li, Y. H.; Wu, S. F.; Lu, J. M.; Wang, J. Q., Fabrication of poly(1-vinylimidazole)/mordenite grafting membrane with high pervaporation performance for the dehydration of acetic acid. *Journal of Membrane Science* **2010,** *349* (1-2), 175-182.
235. Cheng, L.; Zhang, P. B.; Zhao, Y. F.; Zhu, L. P.; Zhu, B. K.; Xu, Y. Y., Preparation and characterization of poly (N-vinyl imidazole) gel-filled nanofiltration membranes. *Journal of Membrane Science* **2015,** *492*, 380-391.
236. Fodor, C.; Bozi, J.; Bazso, M.; Ivan, B., Thermal Behavior, Stability, and Decomposition Mechanism of Poly(N-vinylimidazole). *Macromolecules* **2012,** *45* (22), 8953-8960.
237. El Achaby, M.; Essamlali, Y.; El Miri, N.; Snik, A.; Abdelouahdi, K.; Fihri, A.; Zahouily, M.; Solhy, A., Graphene oxide reinforced chitosan/polyvinylpyrrolidone polymer bio-nanocomposites. *Journal of Applied Polymer Science* **2014,** *131* (22), n/a-n/a.
238. Roy, D.; Knapp, J. S.; Guthrie, J. T.; Perrier, S., Antibacterial cellulose fiber via RAFT surface graft polymerization. *Biomacromolecules* **2008,** *9* (1), 91-9.
239. Lippert, J. L.; Robertson, J. A.; Havens, J. R.; Tan, J. S., Structural Studies of Poly(N-Vinylimidazole) Complexes by Infrared and Raman-Spectroscopy. *Macromolecules* **1985,** *18* (1), 63-67.
240. Teoh, R. L.; Guice, K. B.; Loo, Y. L., Atom transfer radical copolymerization of hydroxyethyl methacrylate and dimethylaminoethyl methacrylate in polar solvents. *Macromolecules* **2006,** *39* (25), 8609-8615.
241. Gray, M. K.; Zhou, H. Y.; Nguyen, S. T.; Torkelson, J. M., Synthesis and glass transition behavior of high molecular weight styrene/4-acetoxystyene and styrene/4-hydroxystyrene gradient copolymers made via nitroxide-mediated controlled radical polymerization. *Macromolecules* **2004,** *37* (15), 5586-5595.
242. Roka, N.; Kokkorogianni, O.; Pitsikalis, M., Statistical copolymers of N-vinylpyrrolidone and 2-(dimethylamino)ethyl methacrylate via RAFT: Monomer reactivity ratios, thermal properties, and kinetics of thermal decomposition. *J Polym Sci Pol Chem* **2017,** *55* (22), 3776-3787.
243. Fodor, C.; Kali, G.; Iván, B., Poly(N-vinylimidazole)-l-Poly(tetrahydrofuran) Amphiphilic Conetworks and Gels: Synthesis, Characterization, Thermal and Swelling Behavior. *Macromolecules* **2011,** *44* (11), 4496-4502.
244. Peppas, N. A.; Merrill, E. W., Differential scanning calorimetry of crystallized PVA hydrogels. *Journal of Applied Polymer Science* **1976,** *20* (6), 1457-1465.
245. Hasimi, A.; Stavropoulou, A.; Papadokostaki, K. G.; Sanopoulou, M., Transport of water in polyvinyl alcohol films: Effect of thermal treatment and chemical crosslinking. *European Polymer Journal* **2008,** *44* (12), 4098-4107.
246. Fodor, C.; Domjan, A.; Ivan, B., Unprecedented scissor effect of macromolecular cross-linkers on the glass transition temperature of poly(N-vinylimidazole), crystallinity suppression of poly(tetrahydrofuran) and molecular mobility by solid state NMR in poly(N-vinylimidazole)-l-poly(tetrahydrofuran) conetworks. *Polymer Chemistry* **2013,** *4* (13), 3714-3724.
247. Peppas, N. A.; Wright, S. L., Solute diffusion in poly(vinyl alcohol) poly(acrylic acid) interpenetrating networks. *Macromolecules* **1996,** *29* (27), 8798-8804.
248. Hassan, C. M.; Peppas, N. A., Structure and Applications of Poly(vinyl alcohol) Hydrogels Produced by Conventional Crosslinking or by Freezing/Thawing Methods. In

Biopolymers · PVA Hydrogels, Anionic Polymerisation Nanocomposites, Springer Berlin Heidelberg: Berlin, Heidelberg, 2000; pp 37-65.
249. Mansur, H. S.; Orefice, R. L.; Mansur, A. A. P., Characterization of poly(vinyl alcohol)/poly(ethylene glycol) hydrogels and PVA-derived hybrids by small-angle X-ray scattering and FTIR spectroscopy. *Polymer* **2004,** *45* (21), 7193-7202.
250. Ping, Z. H.; Nguyen, Q. T.; Neel, J., Investigations of Poly(Vinyl Alcohol) Poly(N-Vinyl-2-Pyrrolidone) Blends .2. Influence of the Molecular-Weights of the Polymer Components on Crystallization. *Makromol Chem* **1990,** *191* (1), 185-198.
251. Guo, D.; Zhuo, Y. Z.; Lai, A. N.; Zhang, Q. G.; Zhu, A. M.; Liu, Q. L., Interpenetrating anion exchange membranes using poly(1-vinylimidazole) as bifunctional crosslinker for fuel cells. *Journal of Membrane Science* **2016,** *518*, 295-304.
252. Jayadevan, J.; Alex, R.; Gopalakrishnapanicker, U., Deproteinised natural rubber latex grafted poly(dimethylaminoethyl methacrylate) - poly(vinyl alcohol) blend membranes: Synthesis, properties and application. *Int J Biol Macromol* **2018,** *107* (Pt B), 1821-1834.
253. https://www.un.org/sustainabledevelopment/energy/ (accessed 10).
254. Mansky, P.; Harrison, C. K.; Chaikin, P. M.; Register, R. A.; Yao, N., Nanolithographic templates from diblock copolymer thin films. *Applied Physics Letters* **1996,** *68* (18), 2586-2588.
255. Urbas, A.; Sharp, R.; Fink, Y.; Thomas, E. L.; Xenidou, M.; Fetters, L. J., Tunable Block Copolymer/Homopolymer Photonic Crystals. *Advanced Materials* **2000,** *12* (11), 812-814.
256. Darling, S. B., Block copolymers for photovoltaics. *Energy & Environmental Science* **2009,** *2* (12), 1266-1273.
257. Pyun, J.; Kowalewski, T.; Matyjaszewski, K., Synthesis of Polymer Brushes Using Atom Transfer Radical Polymerization. *Macromolecular Rapid Communications* **2003,** *24* (18), 1043-1059.
258. Car, A.; Stropnik, C.; Yave, W.; Peinemann, K.-V., Tailor-made Polymeric Membranes based on Segmented Block Copolymers for CO2 Separation. *Advanced Functional Materials* **2008,** *18* (18), 2815-2823.
259. Jeong, B.; Bae, Y. H.; Lee, D. S.; Kim, S. W., Biodegradable block copolymers as injectable drug-delivery systems. *Nature* **1997,** *388* (6645), 860-862.
260. Meier, M. A. R.; Aerts, S. N. H.; Staal, B. B. P.; Rasa, M.; Schubert, U. S., PEO-b-PCL Block Copolymers: Synthesis, Detailed Characterization, and Selected Micellar Drug Encapsulation Behavior. *Macromolecular Rapid Communications* **2005,** *26* (24), 1918-1924.
261. Bates, F. S., Polymer-Polymer Phase Behavior. *Science* **1991,** *251* (4996), 898-905.
262. Thurn-Albrecht, T.; Schotter, J.; Kästle, G. A.; Emley, N.; Shibauchi, T.; Krusin-Elbaum, L.; Guarini, K.; Black, C. T.; Tuominen, M. T.; Russell, T. P., Ultrahigh-Density Nanowire Arrays Grown in Self-Assembled Diblock Copolymer Templates. *Science* **2000,** *290* (5499), 2126-2129.
263. Hamley, I. W., Introduction to Block Copolymers. In *Developments in Block Copolymer Science and Technology*, 2004; pp 1-29.
264. Jeong, U.; Ryu, D. Y.; Kho, D. H.; Kim, J. K.; Goldbach, J. T.; Kim, D. H.; Russell, T. P., Enhancement in the Orientation of the Microdomain in Block Copolymer Thin Films upon the Addition of Homopolymer. *Advanced Materials* **2004,** *16* (6), 533-536.
265. Peinemann, K. V.; Abetz, V.; Simon, P. F., Asymmetric superstructure formed in a block copolymer via phase separation. *Nat Mater* **2007,** *6* (12), 992-6.
266. Ruokolainen, J.; Mäkinen, R.; Torkkeli, M.; Mäkelä, T.; Serimaa, R.; Brinke, G. t.; Ikkala, O., Switching Supramolecular Polymeric Materials with Multiple Length Scales. *Science* **1998,** *280* (5363), 557-560.
267. Wu, M.-L.; Wang, D.; Wan, L.-J., Directed block copolymer self-assembly implemented via surface-embedded electrets. *Nature Communications* **2016,** *7* (1), 10752.

268. Gopinadhan, M.; Deshmukh, P.; Choo, Y.; Majewski, P. W.; Bakajin, O.; Elimelech, M.; Kasi, R. M.; Osuji, C. O., Thermally Switchable Aligned Nanopores by Magnetic-Field Directed Self-Assembly of Block Copolymers. *Advanced Materials* **2014,** *26* (30), 5148-5154.
269. Yu, H.; Qiu, X.; Nunes, S. P.; Peinemann, K.-V., Self-Assembled Isoporous Block Copolymer Membranes with Tuned Pore Sizes. *Angewandte Chemie International Edition* **2014,** *53* (38), 10072-10076.
270. Sutisna, B.; Polymeropoulos, G.; Musteata, V.; Peinemann, K.-V.; Avgeropoulos, A.; Smilgies, D.-M.; Hadjichristidis, N.; Nunes, S. P., Design of block copolymer membranes using segregation strength trend lines. *Mol Syst Des Eng* **2016,** *1* (3), 278-289.
271. Fasolka, M. J.; Mayes, A. M., Block Copolymer Thin Films: Physics and Applications. *Annual Review of Materials Research* **2001,** *31* (1), 323-355.
272. Yang, S. Y.; Ryu, I.; Kim, H. Y.; Kim, J. K.; Jang, S. K.; Russell, T. P., Nanoporous Membranes with Ultrahigh Selectivity and Flux for the Filtration of Viruses. *Advanced Materials* **2006,** *18* (6), 709-712.
273. Yave, W.; Huth, H.; Car, A.; Schick, C., Peculiarity of a CO2-philic block copolymer confined in thin films with constrained thickness: "a super membrane for CO2-capture". *Energy & Environmental Science* **2011,** *4* (11), 4656-4661.
274. Yan, N.; Wang, Z. G.; Wang, Y., Highly permeable membranes enabled by film formation of block copolymers on water surface. *Journal of Membrane Science* **2018,** *568*, 40-46.
275. Chiang, Y.-W.; Chang, J.-J.; Chou, C.-Y.; Wu, C.-S.; Lin, E.-L.; Thomas, E. L., Stimulus-Responsive Thin-Film Photonic Crystals from Rapid Self-Assembly of Block Copolymers for Photopatterning. *Advanced Optical Materials* **2015,** *3* (11), 1517-1523.
276. Jung, A.; Filiz, V.; Rangou, S.; Buhr, K.; Merten, P.; Hahn, J.; Clodt, J.; Abetz, C.; Abetz, V., Formation of Integral Asymmetric Membranes of AB Diblock and ABC Triblock Copolymers by Phase Inversion. *Macromolecular Rapid Communications* **2013,** *34* (7), 610-615.
277. Chiellini, E.; Corti, A.; D'Antone, S.; Solaro, R., Biodegradation of poly (vinyl alcohol) based materials. *Progress in Polymer Science* **2003,** *28* (6), 963-1014.
278. Tousignant, M. N.; Rice, N. A.; Peltekoff, A.; Sundaresan, C.; Miao, C.; Hamad, W. Y.; Lessard, B. H., Improving Thin-Film Properties of Poly(vinyl alcohol) by the Addition of Low-Weight Percentages of Cellulose Nanocrystals. *Langmuir* **2020,** *36* (13), 3550-3557.
279. Gref, R.; Minamitake, Y.; Peracchia, M. T.; Trubetskoy, V.; Torchilin, V.; Langer, R., Biodegradable Long-Circulating Polymeric Nanospheres. *Science* **1994,** *263* (5153), 1600-1603.
280. INEOS. https://www.ineos-styrolution.com/index.html (accessed October 2022).
281. Kuraray. https://www.kuraray-poval.com/ (accessed October 2022).
282. DeltaMem AG. https://www.deltamem.ch/ (accessed October 2022).
283. Imoto, M.; Otsu, T.; Yonezawa, J., Preparation and properties of styrene-vinyl alcohol block copolymers. Vinyl polymerization XLII. *Die Makromolekulare Chemie* **1960,** *36* (1), 93-101.
284. Bataille, P.; Charifi-Sandjani, N., Copolymerization of styrene with vinyl acetate in presence of tributyl amine (TBA). *Journal of Polymer Science: Polymer Chemistry Edition* **1978,** *16* (10), 2527-2538.
285. Lu, Z.; Huang, X.; Huang, J., Synthesis and characterization of amphiphilic diblock copolymer of polystyrene and polyvinyl alcohol using ethanolamine–benzophenone as photochemical binary initiation system. *Journal of Polymer Science Part A: Polymer Chemistry* **1998,** *36* (1), 109-115.
286. Jeon, H. J.; Youk, J. H., Synthesis of Poly(vinyl acetate)-b-polystyrene and Poly(vinyl alcohol)-b-polystyrene Copolymers by a Combination of Cobalt-Mediated Radical Polymerization and RAFT Polymerization. *Macromolecules* **2010,** *43* (5), 2184-2189.

287. Muller, J.; Marchandeau, F.; Prelot, B.; Zajac, J.; Robin, J.-J.; Monge, S., Self-organization in water of well-defined amphiphilic poly(vinyl acetate)-b-poly(vinyl alcohol) diblock copolymers. *Polymer Chemistry* **2015,** *6* (16), 3063-3073.
288. Quemener, D.; Davis, T. P.; Barner-Kowollik, C.; Stenzel, M. H., RAFT and click chemistry: a versatile approach to well-defined block copolymers. *Chem Commun (Camb)* **2006,** (48), 5051-3.
289. Rajput, F.; Colantuoni, A.; Bayahya, S.; Dhane, R.; Servio, P.; Maric, M., Poly(styrene/pentafluorostyrene)-block-poly(vinyl alcohol/vinylpyrrolidone) amphiphilic block copolymers for kinetic gas hydrate inhibitors: Synthesis, micellization behavior, and methane hydrate kinetic inhibition. *Journal of Polymer Science Part A: Polymer Chemistry* **2018,** *56* (21), 2445-2457.
290. Wang, M. Q.; Jiang, X. W.; Luo, Y. J.; Zhang, L. F.; Cheng, Z. P.; Zhu, X. L., Facile synthesis of poly(vinyl acetate)-b-polystyrene copolymers mediated by an iniferter agent using a single methodology. *Polymer Chemistry* **2017,** *8* (38), 5918-5923.
291. Mishra, A. K.; Choi, C.; Maiti, S.; Seo, Y.; Lee, K. S.; Kim, E.; Kim, J. K., Sequential synthesis of well-defined poly(vinyl acetate)-block-polystyrene and poly(vinyl alcohol)-block-polystyrene copolymers using difunctional chloroamide-xanthate iniferter. *Polymer* **2018,** *139*, 68-75.
292. Chen, Y.-J.; Wu, B.-J.; Wang, F.-S.; Chi, M.-H.; Chen, J.-T.; Peng, C.-H., Hybridization of CMRP and ATRP: A Direct Living Chain Extension from Poly(vinyl acetate) to Poly(methyl methacrylate) and Polystyrene. *Macromolecules* **2015,** *48* (19), 6832-6838.
293. Farhan, N. M.; Ibrahim, S. S.; Leva, L.; Yave, W.; Alsalhy, Q. F., The combination of a new PERVAPTM membrane and molecular sieves enhances the ethanol drying process. *Chemical Engineering and Processing - Process Intensification* **2022,** *174*, 108863.
294. Bolto, B.; Tran, T.; Hoang, M.; Xie, Z. L., Crosslinked poly(vinyl alcohol) membranes. *Progress in Polymer Science* **2009,** *34* (9), 969-981.
295. Hiroyuki, T.; Syûzô, S.; Isamu, N., The Crystallinity of Solid High Polymers. I. The Crystallinity of Polyvinyl Alcohol Film. *Bulletin of the Chemical Society of Japan* **1955,** *28* (8), 559-564.
296. Krumova, M.; Lopez, D.; Benavente, R.; Mijangos, C.; Perena, J. M., Effect of crosslinking on the mechanical and thermal properties of poly(vinyl alcohol). *Polymer* **2000,** *41* (26), 9265-9272.
297. Jeck, S.; Scharfer, P.; Schabel, W.; Kind, M., Water sorption in semicrystalline poly(vinyl alcohol) membranes: In situ characterisation of solvent-induced structural rearrangements. *Journal of Membrane Science* **2012,** *389*, 162-172.
298. NASA. https://ntrs.nasa.gov/citations/19790012957/ (accessed October 2022).
299. Hyon, S. H.; Chu, H. D.; Kitamaru, R., Structure and Physico-Chemical Properties of Polyvinyl Alcohol, Stretched at the Amorphous State and Annealed (Special Issue on Polymer Chemistry XI). *Bulletin of the Institute for Chemical Research, Kyoto University* **1975,** *53* (4), 367-380.
300. Ueda, Y.; Tanaka, T.; Iizuka, A.; Sakai, Y.; Kojima, T.; Satokawa, S.; Yamasaki, A., Membrane Separation of Ethanol from Mixtures of Gasoline and Bioethanol with Heat-Treated PVA membranes. *Industrial & Engineering Chemistry Research* **2011,** *50* (2), 1023-1027.
301. Stauffer, S. R.; Peppast, N. A., Poly(vinyl alcohol) hydrogels prepared by freezing-thawing cyclic processing. *Polymer* **1992,** *33* (18), 3932-3936.
302. Peppas, N. A.; Stauffer, S. R., Reinforced uncrosslinked poly (vinyl alcohol) gels produced by cyclic freezing-thawing processes: a short review. *Journal of Controlled Release* **1991,** *16* (3), 305-310.
303. Peppas, N. A.; Scott, J. E., Controlled release from poly (vinyl alcohol) gels prepared by freezing-thawing processes. *Journal of Controlled Release* **1992,** *18* (2), 95-100.

304. Takamura, A.; Ishii, F.; Hidaka, H., Drug release from poly(vinyl alcohol) gel prepared by freeze-thaw procedure. *Journal of Controlled Release* **1992,** *20* (1), 21-27.
305. Flores-Arriaga, J. C.; Chavarría-Bolaños, D.; Pozos-Guillén, A. d. J.; Escobar-Barrios, V. A.; Cerda-Cristerna, B. I., Synthesis of a PVA drug delivery system for controlled release of a Tramadol–Dexketoprofen combination. *Journal of Materials Science: Materials in Medicine* **2021,** *32* (5), 56.
306. Matyjaszewski, K.; Jakubowski, W.; Min, K.; Tang, W.; Huang, J.; Braunecker, W. A.; Tsarevsky, N. V., Diminishing catalyst concentration in atom transfer radical polymerization with reducing agents. *Proceedings of the National Academy of Sciences* **2006,** *103* (42), 15309-15314.
307. Jakubowski, W.; Kirci-Denizli, B.; Gil, R. R.; Matyjaszewski, K., Polystyrene with Improved Chain-End Functionality and Higher Molecular Weight by ARGET ATRP. *Macromolecular Chemistry and Physics* **2008,** *209* (1), 32-39.
308. Mueller, L.; Jakubowski, W.; Matyjaszewski, K.; Pietrasik, J.; Kwiatkowski, P.; Chaladaj, W.; Jurczak, J., Synthesis of high molecular weight polystyrene using AGET ATRP under high pressure. *European Polymer Journal* **2011,** *47* (4), 730-734.
309. Jakubowski, W.; Min, K.; Matyjaszewski, K., Activators Regenerated by Electron Transfer for Atom Transfer Radical Polymerization of Styrene. *Macromolecules* **2006,** *39* (1), 39-45.
310. Li, H.; Zhang, Y. M.; Xue, M. Z.; Liu, Y. G., Amphiphilic Block Copolymers of Polyvinyl Alcohol and Polystyrene and Their Surface Properties. *Polymer Journal* **2005,** *37* (11), 841-846.
311. Huang, X.; Huang, Z.; Huang, J., Copolymerization of styrene and vinyl acetate by successive photoinduced charge-transfer polymerization. *Journal of Polymer Science Part A: Polymer Chemistry* **2000,** *38* (5), 914-920.
312. Costa, L.; Avataneo, M.; Bracco, P.; Brunella, V., Char formation in polyvinyl polymers I. Polyvinyl acetate. *Polymer Degradation and Stability* **2002,** *77* (3), 503-510.
313. Liang, C. Y.; Krimm, S., Infrared spectra of high polymers. VI. Polystyrene. *Journal of Polymer Science* **1958,** *27* (115), 241-254.
314. Isasi, J. R.; Cesteros, L. C.; Katime, I., Hydrogen Bonding and Sequence Distribution in Poly(vinyl acetate-co-vinyl alcohol) Copolymers. *Macromolecules* **1994,** *27* (8), 2200-2205.
315. Otsuka, E.; Kudo, S.; Sugiyama, M.; Suzuki, A., Effects of microcrystallites on swelling behavior in chemically crosslinked poly(vinyl alcohol) gels. *Journal of Polymer Science Part B: Polymer Physics* **2011,** *49* (2), 96-102.
316. Strawhecker, K. E.; Manias, E., Structure and Properties of Poly(vinyl alcohol)/Na+ Montmorillonite Nanocomposites. *Chemistry of Materials* **2000,** *12* (10), 2943-2949.
317. Schawe, J. E. K., Measurement of the thermal glass transition of polystyrene in a cooling rate range of more than six decades. *Thermochimica Acta* **2015,** *603*, 128-134.
318. Christie, D.; Register, R. A.; Priestley, R. D., Direct Measurement of the Local Glass Transition in Self-Assembled Copolymers with Nanometer Resolution. *ACS Central Science* **2018,** *4* (4), 504-511.
319. Data from DeltaMem AG. Contact directly DeltaMem AG.
320. Bates, F. S.; Fredrickson, G. H., Block copolymer thermodynamics: theory and experiment. *Annual review of physical chemistry* **1990,** *41* (1), 525-557.
321. Groot, R. D.; Madden, T. J., Dynamic simulation of diblock copolymer microphase separation. *The Journal of Chemical Physics* **1998,** *108* (20), 8713-8724.
322. Nunes, S. P.; Sougrat, R.; Hooghan, B.; Anjum, D. H.; Behzad, A. R.; Zhao, L.; Pradeep, N.; Pinnau, I.; Vainio, U.; Peinemann, K.-V., Ultraporous Films with Uniform Nanochannels by Block Copolymer Micelles Assembly. *Macromolecules* **2010,** *43* (19), 8079-8085.

323. Ahn, H.; Park, S.; Kim, S.-W.; Yoo, P. J.; Ryu, D. Y.; Russell, T. P., Nanoporous Block Copolymer Membranes for Ultrafiltration: A Simple Approach to Size Tunability. *ACS Nano* **2014,** *8* (11), 11745-11752.
324. Bucher, T.; Filiz, V.; Abetz, C.; Abetz, V., Formation of Thin, Isoporous Block Copolymer Membranes by an Upscalable Profile Roller Coating Process—A Promising Way to Save Block Copolymer. *Membranes* **2018,** *8* (3), 57.
325. Debuigne, A.; Caille, J.-R.; Willet, N.; Jérôme, R., Synthesis of Poly(vinyl acetate) and Poly(vinyl alcohol) Containing Block Copolymers by Combination of Cobalt-Mediated Radical Polymerization and ATRP. *Macromolecules* **2005,** *38* (23), 9488-9496.
326. Li, G.-H.; Cho, C.-G., Synthesis and micellar behavior of poly(vinyl alcohol-b-styrene) copolymers containing PVA blocks with different syndiotacticity. *Colloid and Polymer Science* **2005,** *283* (9), 946-953.
327. Majewski, P. W.; Yager, K. G., Latent Alignment in Pathway-Dependent Ordering of Block Copolymer Thin Films. *Nano Letters* **2015,** *15* (8), 5221-5228.
328. Majewski, P. W.; Yager, K. G., Rapid ordering of block copolymer thin films. *Journal of Physics: Condensed Matter* **2016,** *28* (40), 403002.
329. Akeroyd, N.; Pfukwa, R.; Klumperman, B., Triazole-Based Leaving Group for RAFT-Mediated Polymerization Synthesized via the Cu-Mediated Huisgen 1,3-Dipolar Cycloaddition Reaction. *Macromolecules* **2009,** *42* (8), 3014-3018.
330. Gmehling, J.; Onken, U., *Vapor-liquid equilibrium data collection. Aqueous-organic systems*. Deutsche Gesellschaft fuer Chemisches Apparatewesen,Frankfurt, Germany;: 1977; p Medium: X; Size: Pages: 700.

9. Appendix

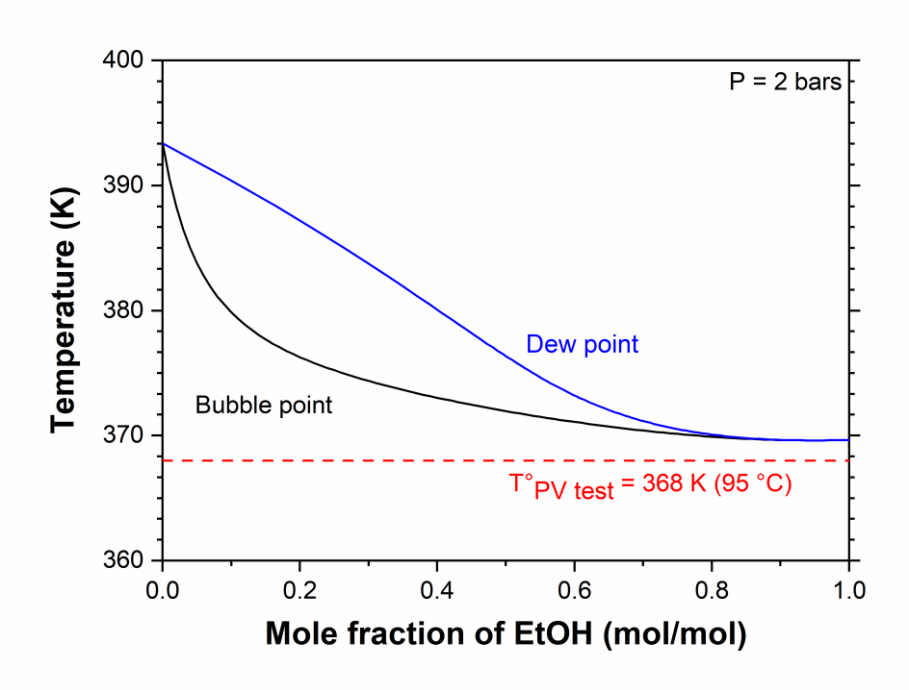

Figure 9-1. *Tx-y* diagram describing the vapor liquid equilibrium (VLE) of a binary ethanol/water mixture at 2 bar. The black curve represents the liquid-phase boundary (bubble point) and the blue curve represents the vapor-phase boundary (dew point). The dashed red line indicates the operating temperature applied during the pervaporation tests.

Table 9-1: Mole fractions of NVP monomer in feed mixture (f1), mole fractions of NVP in final copolymer (obtained by ^{1}H NMR) (F1) and molecular weight of synthesized copolymers P(NVP-*co*-DMAEMA) and P(NVP-*co*-NVIm)

Sample	**f1**	**F1**	**Mw (g.mol^{-1})**
coPDMAEMA100	0	0	2514400
coPDMAEMA80	0.20	0.11	412390
coPDMAEMA60	0.40	0.35	458390
coPDMAEMA40	0.60	0.58	393410
coPDMAEMA20	0.80	0.80	157910
coPDMAEMA0	1	1	277780
coPNVIm100	0	0	287550
coPNVIm80	0.20	0.19	748110
coPNVIm60	0.40	0.39	468880
coPNVIm40	0.60	0.59	299400
coPNVIm20	0.80	0.76	235290
coPNVIm0	1	1	143820

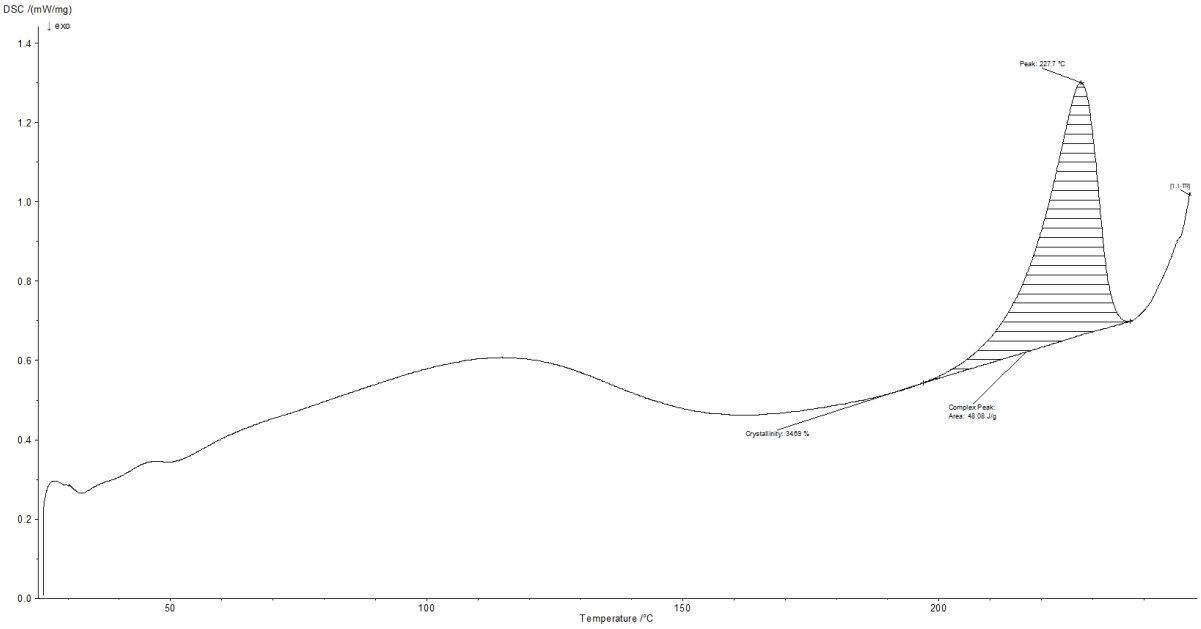

Figure 9-2. DSC thermogram (first heating scan, heating rate = 10 $K.min^{-1}$) of the film made of pure PVA.

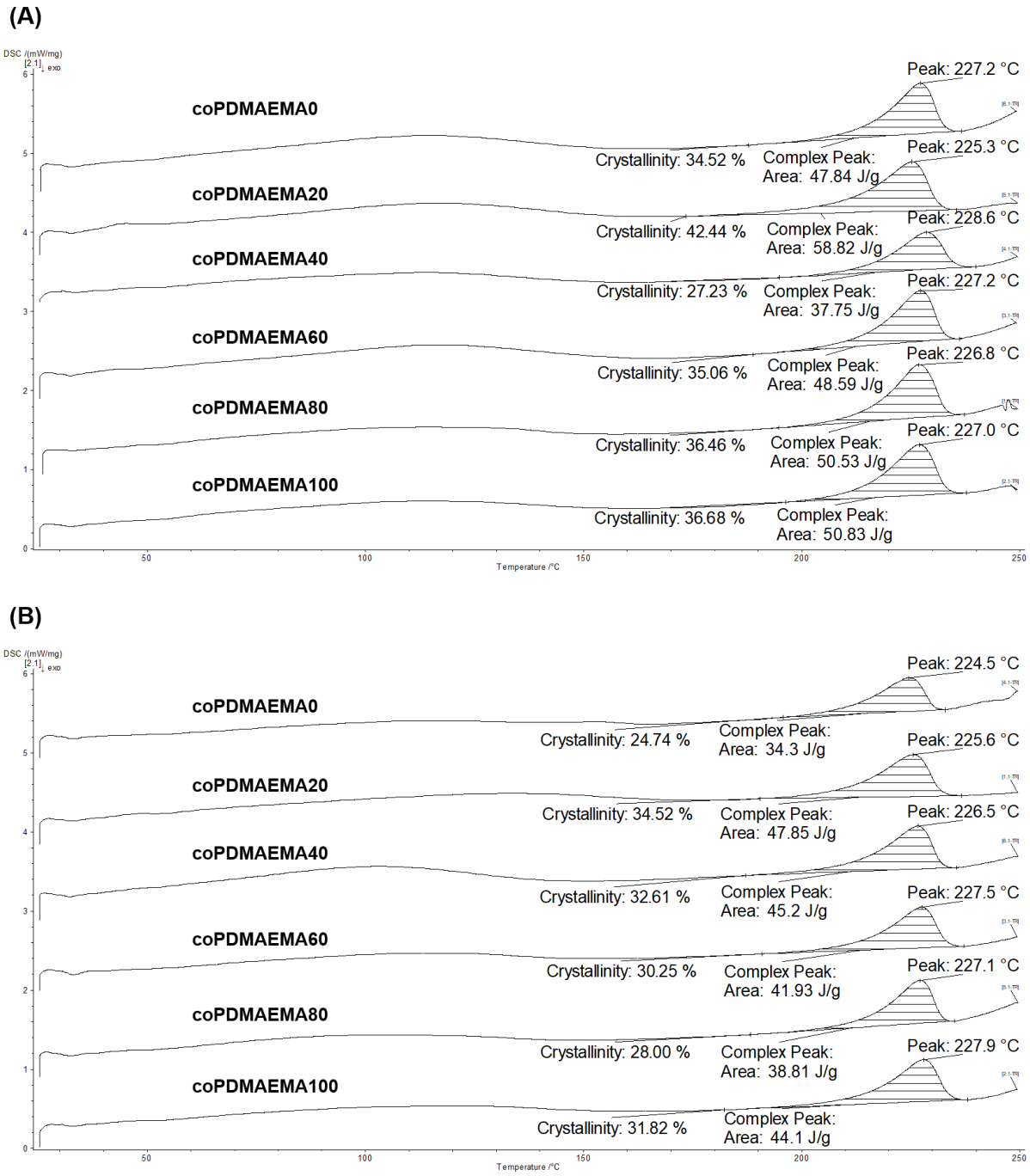

Figure 9-3. DSC thermograms (first heating scan, heating rate = 10 K.min^{-1}) of the films made of PVA/P(NVP-*co*-DMAEMA) blends (A) 95:5 and (B) 80:20.

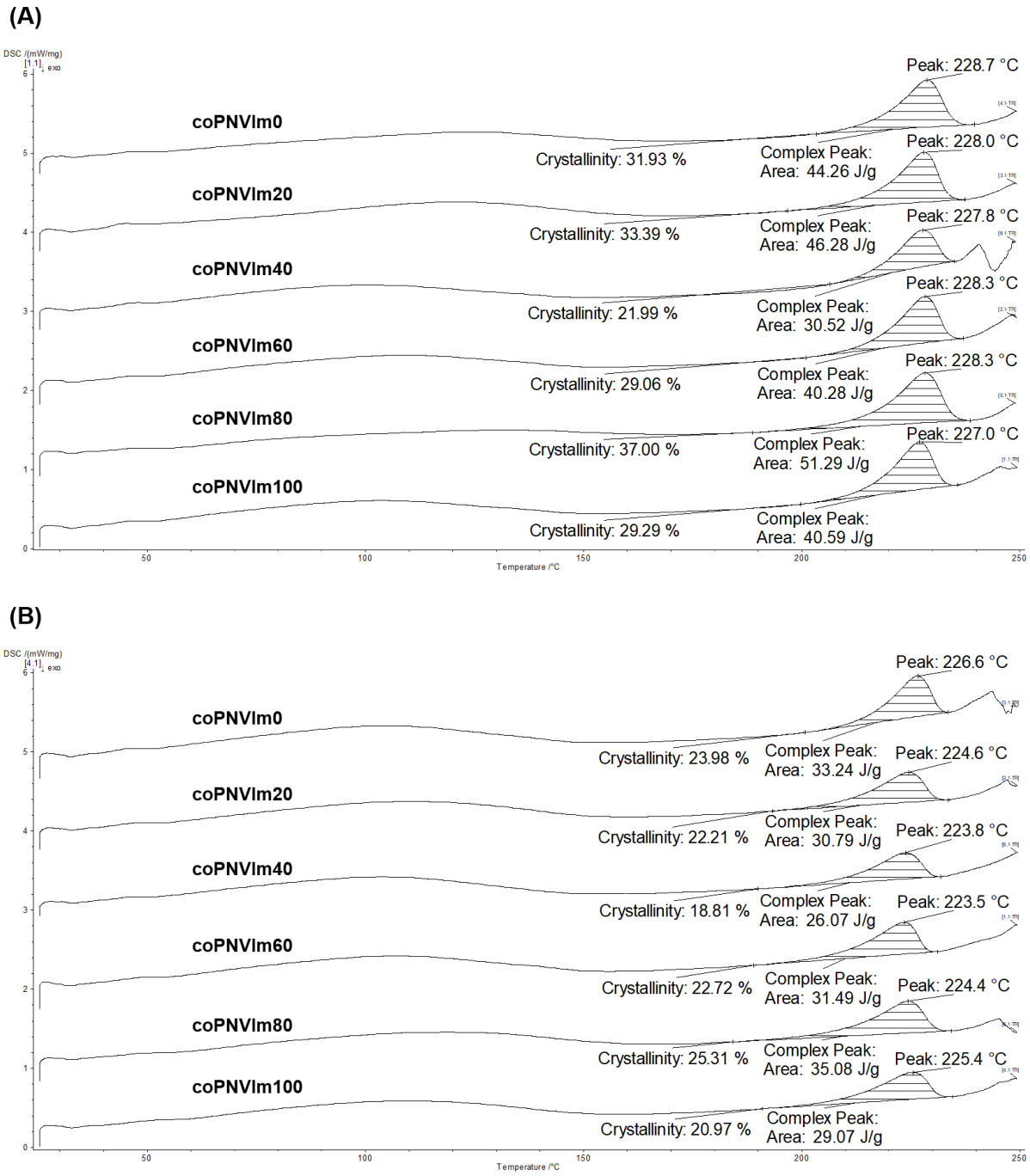

Figure 9-4. DSC thermograms (first heating scan, heating rate = 10 K.min^{-1}) of the films made of PVA/P(NVP-*co*-NVIm) blends (A) 95:5 and (B) 80:20.

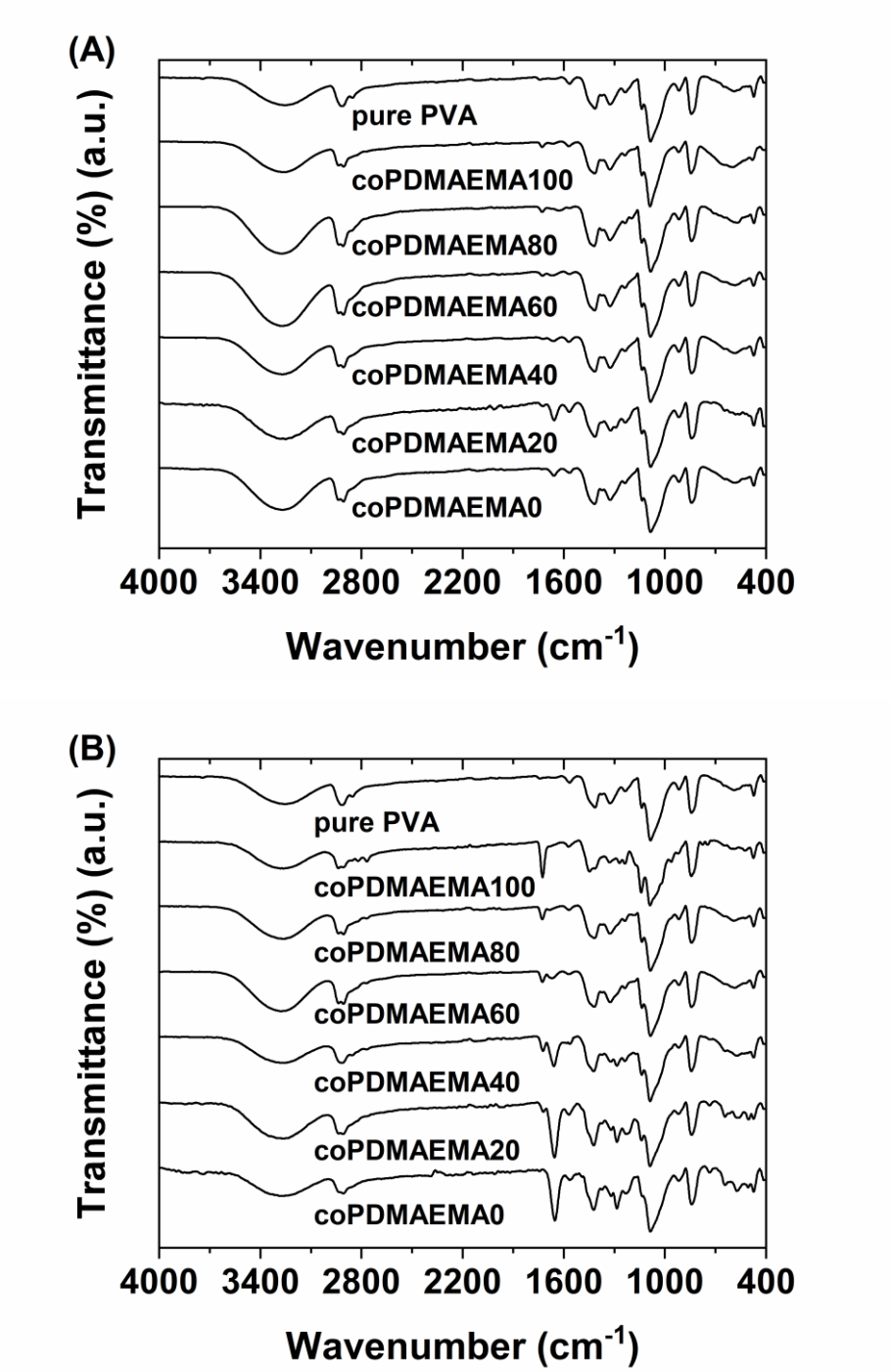

Figure 9-5. ATR-FTIR spectra obtained for the films made of PVA/P(NVP-*co*-DMAEMA) blends (A) 95:5 and (B) 80:20 (scan number: 128, nominal resolution: 4 cm^{-1}).

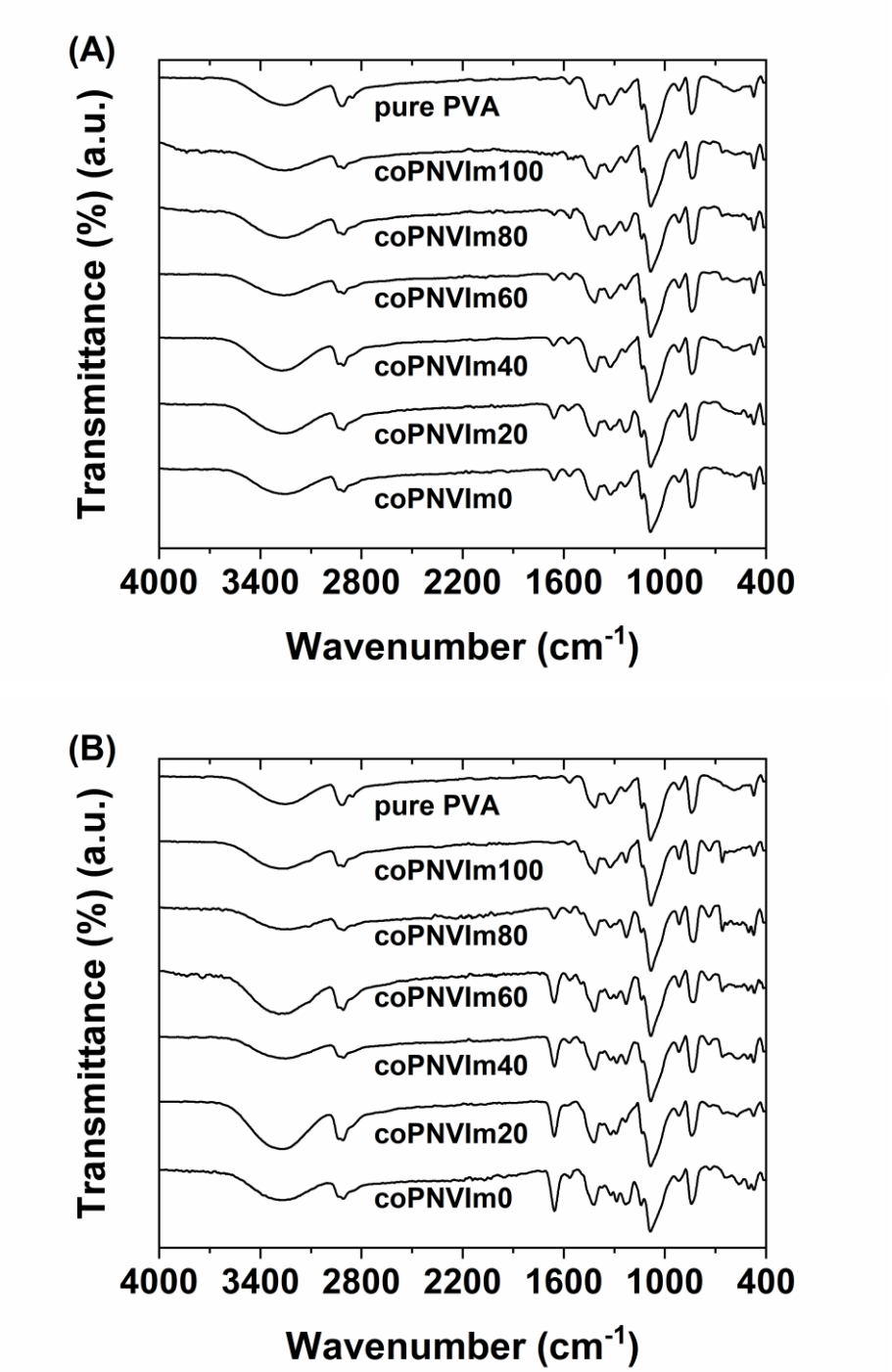

Figure 9-6. ATR-FTIR spectra obtained for the films made of PVA/P(NVP-*co*-NVIm) blends (A) 95:5 and (B) 80:20 (scan number: 128, nominal resolution: 4 cm^{-1}).

Table 9-2: List of the composite membranes prepared from blends of PVA and P(NVP-*co*-DMAEMA) or P(NVP-*co*-NVIm) with two different ratios and the nitrogen flow measurements before and after pervaporation tests (nitrogen flow ≤0.05 indicates samples free of defects).

Copolymer ID	**Membrane**	**PVA/copolymer (mass ratio in percent)**	**N2 flow ($L.h^{-1}$)**	
			Before test	**After test**
-	PVA	100:0	0.05	0.05
AA26	PVA/coPDMAEMA100	80:20	0.05	0.07
AA21	PVA/coPDMAEMA60		0.05	0.05
AA23	PVA/coPDMAEMA20		0.05	0.05
AA25	PVA/coPDMAEMA0		0.05	0.05
CF66	PVA/coPNVIm100		0.05	0.35
CF61	PVA/coPNVIm60		0.05	0.05
CF63	PVA/coPNVIm20		0.05	0.05
CF65	PVA/coPNVIm0		0.05	0.15
AA26	PVA/coPDMAEMA100	95:5	0.05	0.05
AA21	PVA/coPDMAEMA60		0.05	0.05
AA23	PVA/coPDMAEMA20		0.05	0.05
AA25	PVA/coPDMAEMA0		0.05	0.05
CF66	PVA/coPNVIm100		0.05	0.05
CF61	PVA/coPNVIm60		0.05	0.05
CF63	PVA/coPNVIm20		0.05	0.05
CF65	PVA/coPNVIm0		0.05	0.05

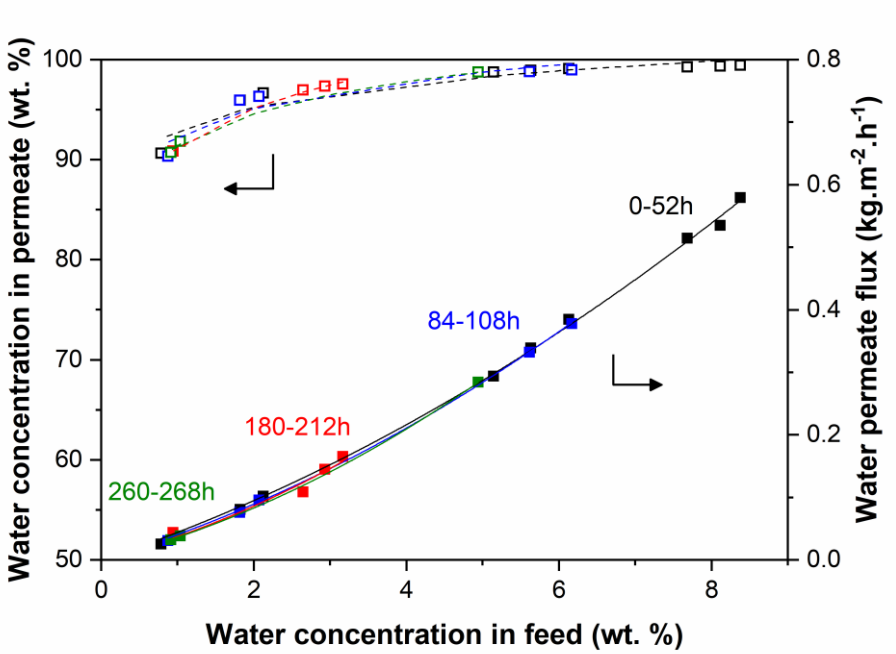

Figure 9-7. Long-term stability test of the composite membrane from blend PVA/ coPDMAEMA100 (ratio 95:5) for the dehydration of a simulated bioethanol stream containing acetaldehyde up to 600ppm, at 95 °C, 2 bar in the feed side and 10 mbar in the permeate side. The water flux and permeate concentration data are obtained at different time intervals while operating continuously: 0-52 hours (black), 84-108 hours (blue), 180-212 hours (red) and 260-268 hours (green). The trendlines for each set of data show negligible deviations.

Table 9-3: Summary of articles reporting copolymers of PVA and PS (including those as PVAc instead of PVA because they can be hydrolyzed to obtain PVA).

Year	Copolymer	Mn (NMR or GPC)	PD	PVA/PS ratio	Reference
1960	PS-*b*-PVA	17-44 kDa PS (η)	n.a.	0.3-1.2	Die Macromolekulare Chemie 36 (1960) 93
1966	PVA-*alt*-PS	n.a.	n.a.	0.9-1.1	J Polym Scie B: Polym Letters 4 (1966) 187
1978	PVAc-PS	8-50 kDa	1.3-5.1	0.2-0.3	J Polym Scie: Polym Chem Edition 16 (1978) 2527
1993	PS-*b*-PVAc	PS: 9-16 kDa	n.a.	0.3-1.2	J Appl Polym Scie 48 (1993) 425
1995	PS-*g*-PVA	22 kDa (PS)	xx	0.9-10	Polymer 36 (1995) 4515
1997	PVA-*b*-PS-*b*-PVA	5-15 kDa	PS: 1.5	0.05-0.3	J Appl Polym Scie 63 (1997) 849
1998	PS-*b*-PVA	26-34 kDa	> 2	1.3-4.0	J Polym Sci A: PolymChem 36 (1998) 109
1999	PVA-*g*-PS	8-23 kDa	xx	1.4-23	Langmuir 15 (1999) 3197
1999	PVAc-*b*-PS	8-99 kDa	1.4-2.2	0.2-1.2	Macromolecules 32 (1999) 7023
2000	PVAc-*b*-PS		1.2-1.4		Macromol: Chem Phys 201 (2000) 1189
2002	PVA-*b*-PS	5-15 kDa	1.3-1.4	0.4-0.5	Macromol Res 10 (2002) 339
2003	PVA-PmAS	1,5-1,9 kDa	1.8-2.2	0.1-1.0	J Membr Scie 216 (2003) 107
2005	PVA-*b*-PS	5-7 kDa	1.2-1.5	3.0-1.0	Colloid Polym Scie 283 (2005) 946
2005	PVA-*b*-PS	20 kDa	1.3-1.3	0.2-0.2	Macromolecules 38 (2005) 9488
2005	PVA-*b*-PS	5-30 kDa	1.3-1.5	1.6-1.6	Polym J. 37 (2005) 841
2006	PVA-*b*-PS	12-45 kDa	1.1-1.2	0.5-4.0	Chemm Comm (2006) 5051
2006	PVA-*b*-PS	9-15 kDa	xx	0.4-0.8	Macromol Res 14 (2006) 504
2007	PVA-*b*-PS	30-45 kDa	1.5-1.7	0.3-0.5	J Polym Sci A: PolymChem 45 (2007) 81
2008	PVAc-*b*-PS		1.25		Chemm Comm 42 (2008) 5336
2008	PVA-*b*-PS	2-5 kDa	xx	0.7-2.5	Korean J Chem Eng 25 (2008) 1444
2008	PVAc-*b*-PS	12-72 kDa	1.4-1.5		Macromolecules 41 (2008) 7339
2010	PVA-*b*-PS	15-25 kDa	1.3-1.5	0.5-1.5	Macromolecules 43 (2010) 2184
2010	PVA-*b*-PS				Polymer 51 (2010) 3083
2015	PVAc-*b*-PS				Macromolecules 48 (2015) 6832
2017	PVAc-*b*-PS	31-64 kDa	1.3-1,5		Polym Chem 8 (2017) 5918
2018	PS-*b*-PVA	9-15 kDa	1.3-1,4	0.5-1.3	Polym Chem 9 (2018) 4243
2018	PS-*b*-PVA	43 kDa	1.4	10.0-10.1	J Polym Sci A: PolymChem 56 (2018) 2445
2018	PVA-*b*-PS	5-42 kDa	1.2	0.3-2.7	Polymer 139 (2018) 68
2022	PVA-*g*-PS	125 kDa PVA		65-330	Ind Eng Chem Res 61 (2022) 5797
2022	PVA-*b*-PS	5-15 kDa	2.0-2.6	0.2-0.6	Polymer source
2022	PVA-*b*-PS	5-94 kDa	1.5-2.0	0.1-0.6	Polymer source

Table 9-4: PS-Br homopolymers obtained with different formulations and PS-*b*-PVAc.

Sample	Mn [g/mol]	Conversion [%]	PD
PS_{57}	5900	11	1.11
PS_{100}	10400	20	1.08

PS_{57}-*b*-$PVAc_{225}$	25000	56	1.52
PS_{57}-*b*-$PVAc_{587}$	32000	59	1.55

Table 9-5: Solubility test of copolymers in different solvents.

Sample	**Solvent**	**Result**
PVA-63, PVA-81	acetone	insoluble
	acetonitrile	insoluble
	(MeOH, EtOH and IPA)	insoluble
	CHCl3	insoluble
	DMAc	soluble (with heat)
	dioxane	insoluble
	DMF	insoluble
	DMSO	soluble
	ethyl acetate	insoluble
	THF	insoluble
	toluene	insoluble
	water	insoluble
PVA-68, PVA-79, PVA-87, PVA-92	acetone	insoluble
	acetonitrile	insoluble
	(MeOH, EtOH and IPA)	insoluble

CHCl3	insoluble
DMAc	poorly soluble (with heat)
dioxane	insoluble
DMF	insoluble
DMSO	soluble
ethyl acetate	insoluble
THF	insoluble
toluene	insoluble
water	insoluble

Table 9-6: Crystallinity and melting point of PVA block in dense films.

Sample	**Crystallinity [%]**	T_m^{PVA} **[°C]**
PVA-68	39.3	230.3
PVA-79	10.5	217.7
PVA-87	20.3	222.0
PVA-92	24.6	223.8
PVA-100	50.6	231.0

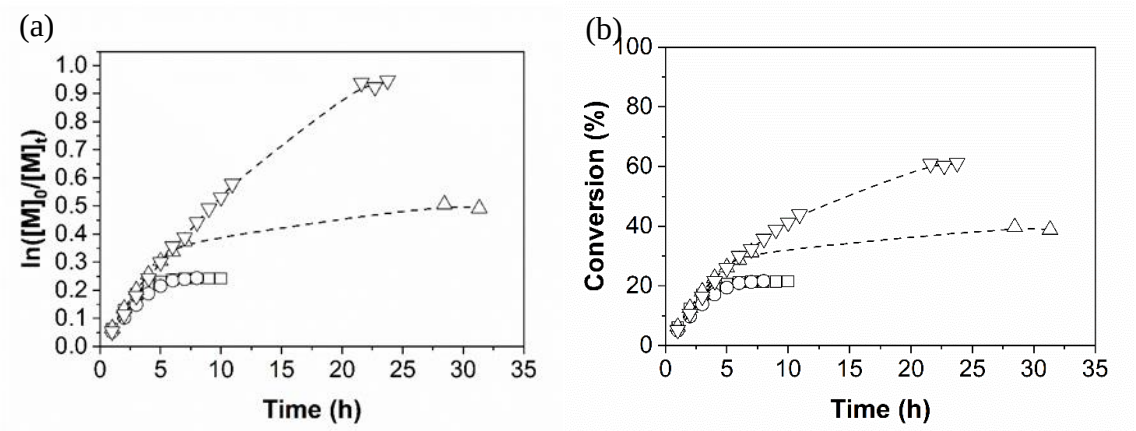

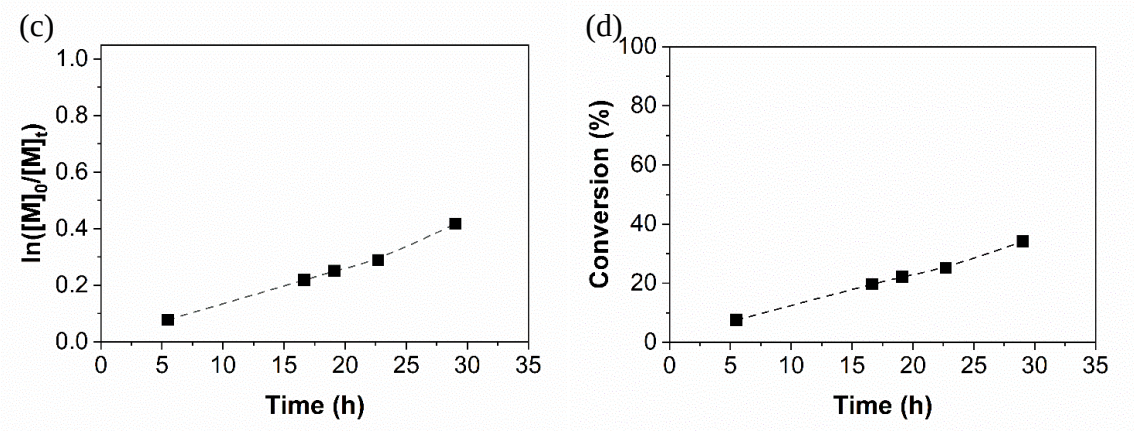

Figure 9-8. (a) and (b), kinetic study of PS synthesis by ARGET-ATRP (square data: according to Altintas et al, circle data: reduced initiator and catalyst, triangle up data: increased reducing agent x2, and triangle down data: increased reducing agent x4), and (c) and (d), polymer chain extension by VAc polymerization via RAFT.

(a)

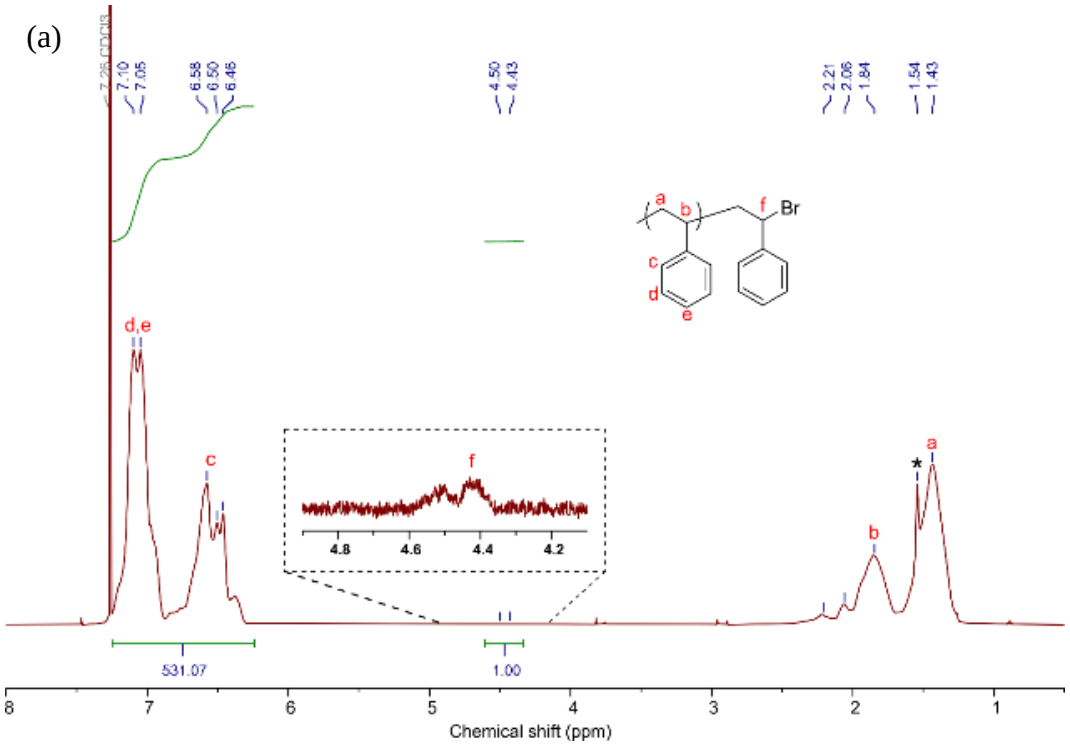
7.26 CDCl3
7.10
7.05
6.58
6.50
6.46
4.50
4.43
2.21
2.06
1.84
1.54
1.43
a
b
c
d
e
f
Br
d,e
c
f
4.8
4.6
4.4
4.2
a
*
b
531.07
1.00
8
7
6
5
4
3
2
1
Chemical shift (ppm)

(b)

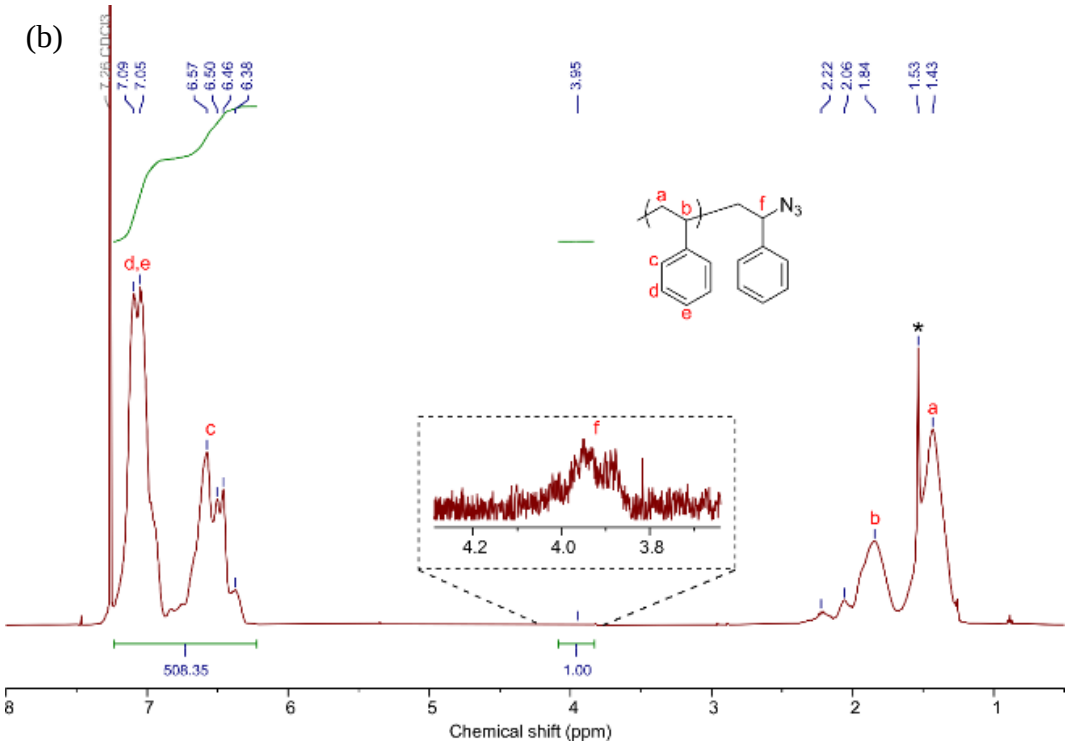
7.26 CDCl3
7.09
7.05
6.57
6.50
6.46
6.38
3.95
2.22
2.06
1.84
1.53
1.43
a
b
c
d
e
f
N3
d,e
c
f
4.2
4.0
3.8
*
a
b
508.35
1.00
8
7
6
5
4
3
2
1
Chemical shift (ppm)

(c)

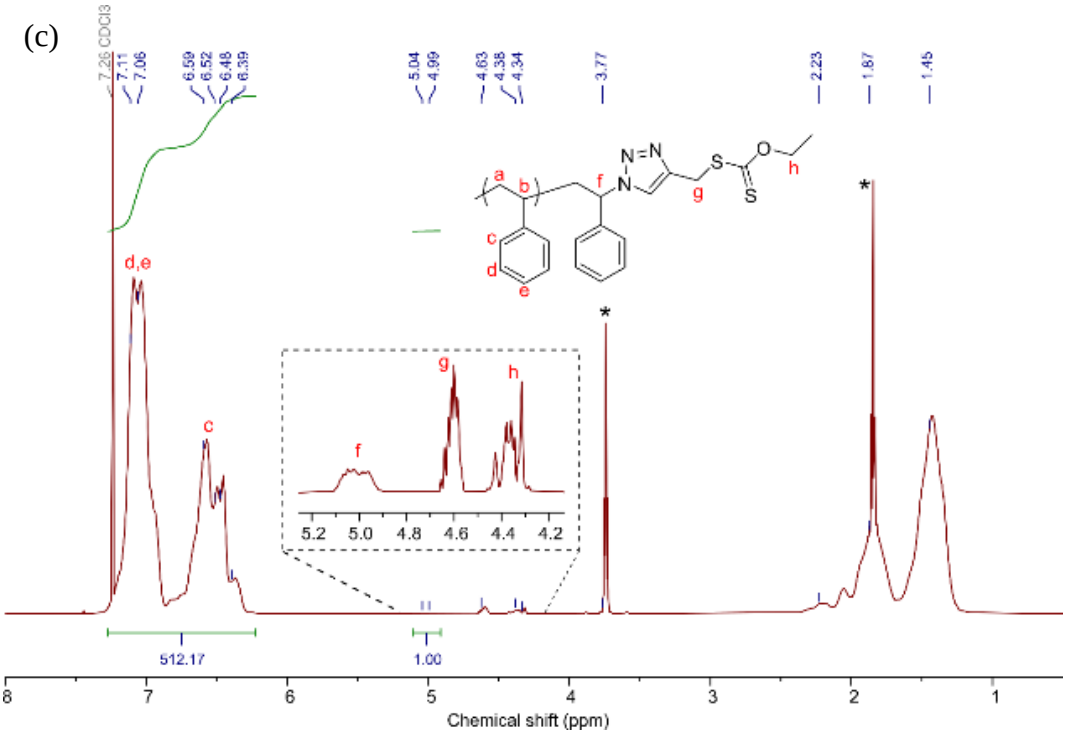
7.26 CDCl3
7.11
7.06
6.59
6.52
6.48
6.39
5.04
4.99
4.63
4.38
4.34
3.77
2.23
1.87
1.45
d,e
c
f
g
h
*
5.2
5.0
4.8
4.6
4.4
4.2
512.17
1.00
Chemical shift (ppm)

(d)

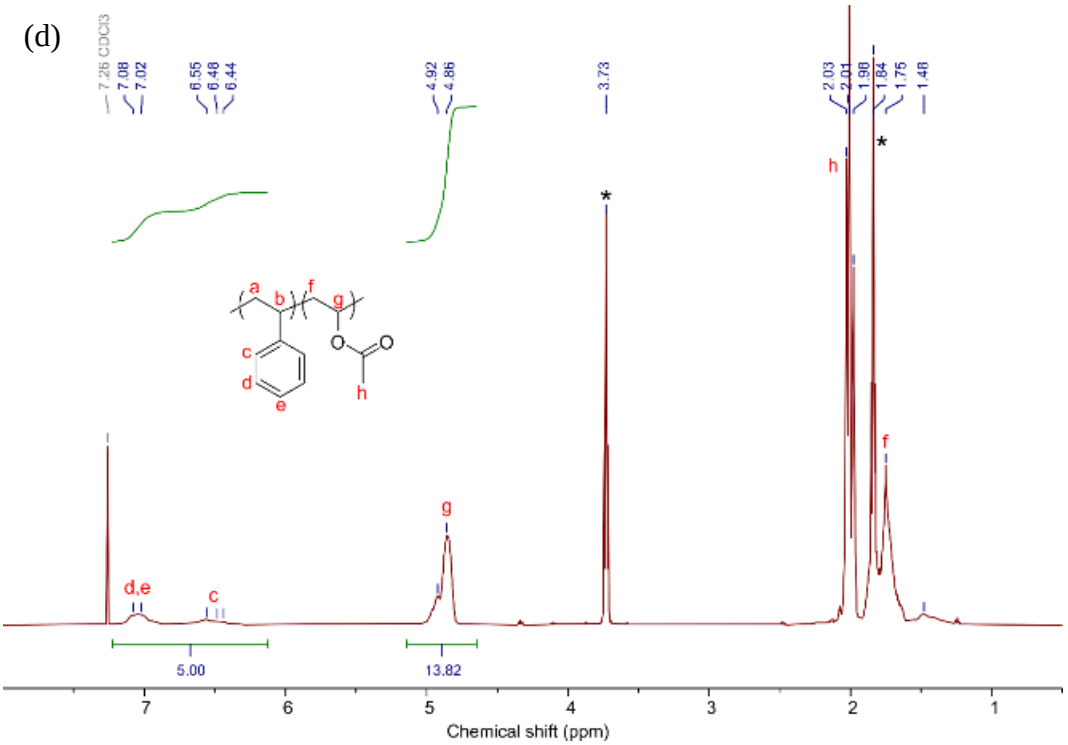
7.26 CDCl3
7.08
7.02
6.55
6.48
6.44
4.92
4.86
3.73
2.03
2.01
1.98
1.84
1.75
1.46
h
*
f
g
d,e
c
5.00
13.82
Chemical shift (ppm)

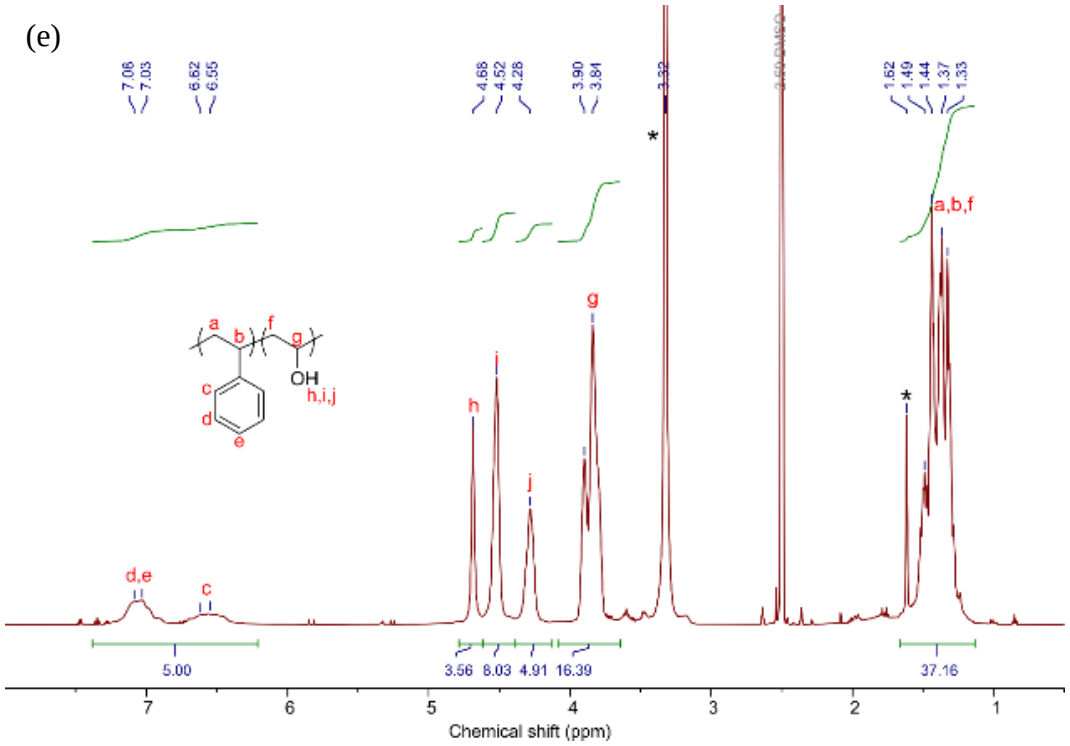

Figure 9-9. ^{1}H NMR spectra corresponding to PS-Br (a), PS-N3 (b), PS-CTA (c), PS-*b*-PVAc (d) in CDCl3, and PS-*b*-PVA (e) copolymer in DMSO-d6 at room temperature (residual solvent is marked with an asterisk.

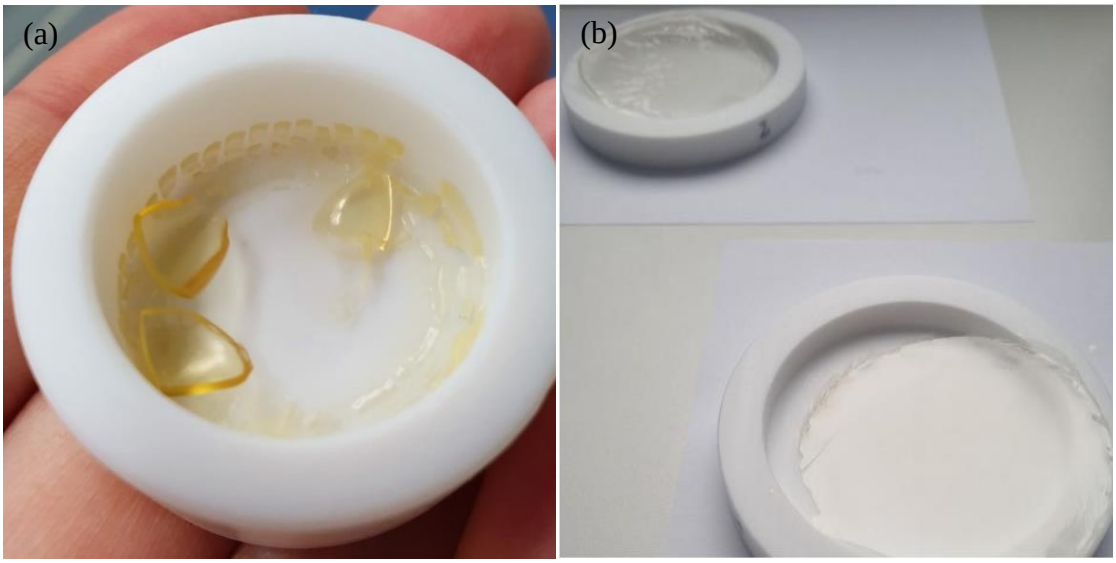

Figure 9-10. Pictures of self-standing dense films prepared from (a) copolymers with low Mn and (b) copolymers with high Mn.

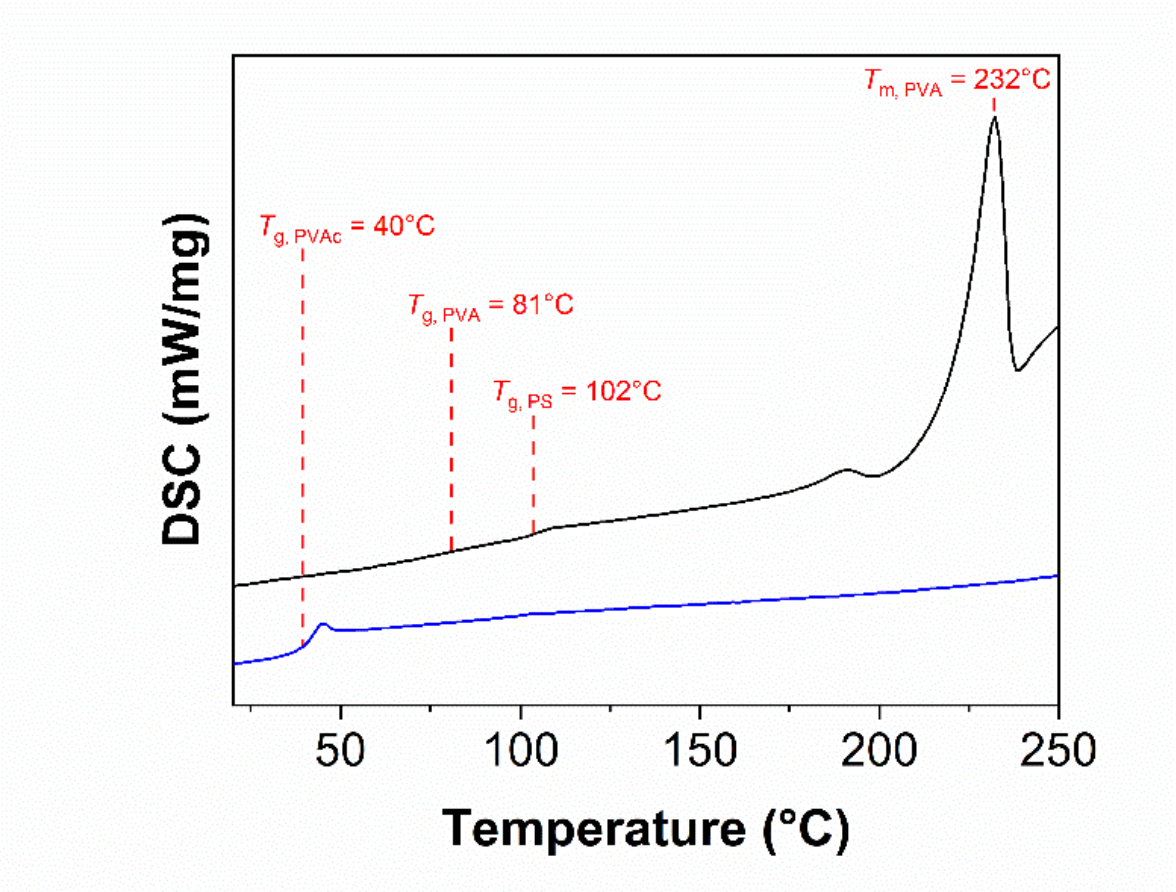

Figure 9-11. DSC thermograms (second heating scans, heating rate = 10 K min^{-1}) corresponding to PS-*b*-PVAc (blue), and after hydrolysis to obtain PS-*b*-PVA (black).

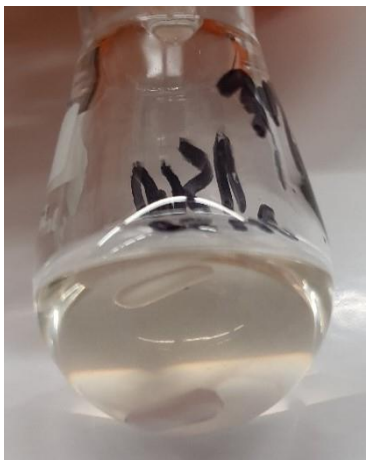

Figure 9-12. Picture of self-assembled micelle solution obtained by switching the solvent (from DMSO to water) by dialysis.

Figure 9-13. Picture of the self-standing thin film obtained from the self-assembled micelle solution (difficult to handle).

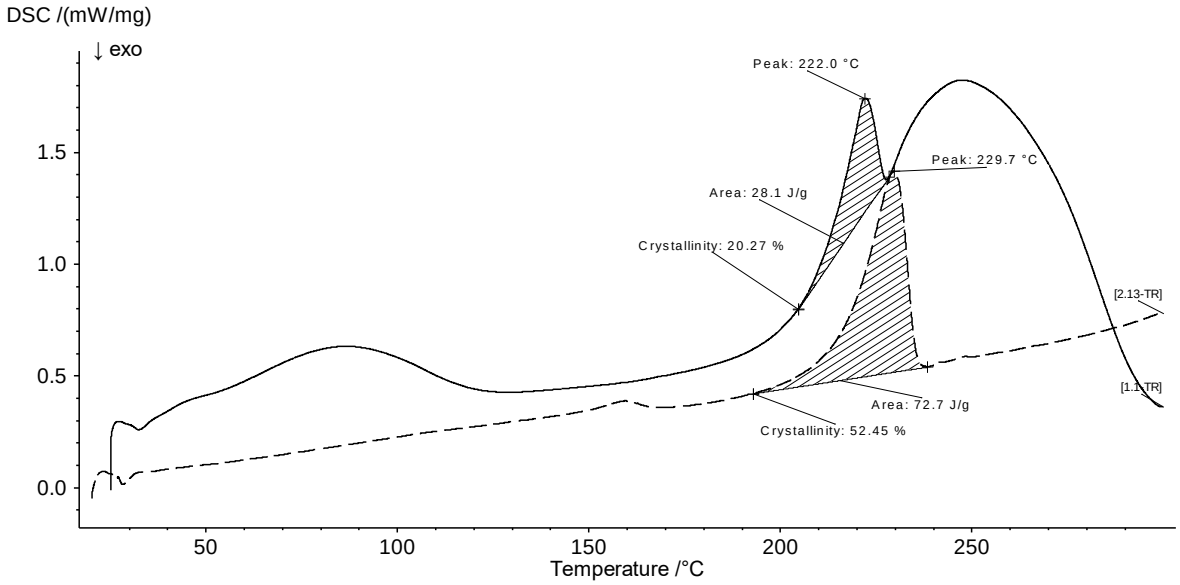

Figure 9-14. DSC thermograms corresponding to PVA-87 film before and after thermal annealing at 145 °C. As seen, the crystallinity of PVA block increases from 20.27% to 52.45% (the bump after the melting of PVA in the sample before the annealing is due to the polymer degradation, since the heating cycle reaches 250°C).

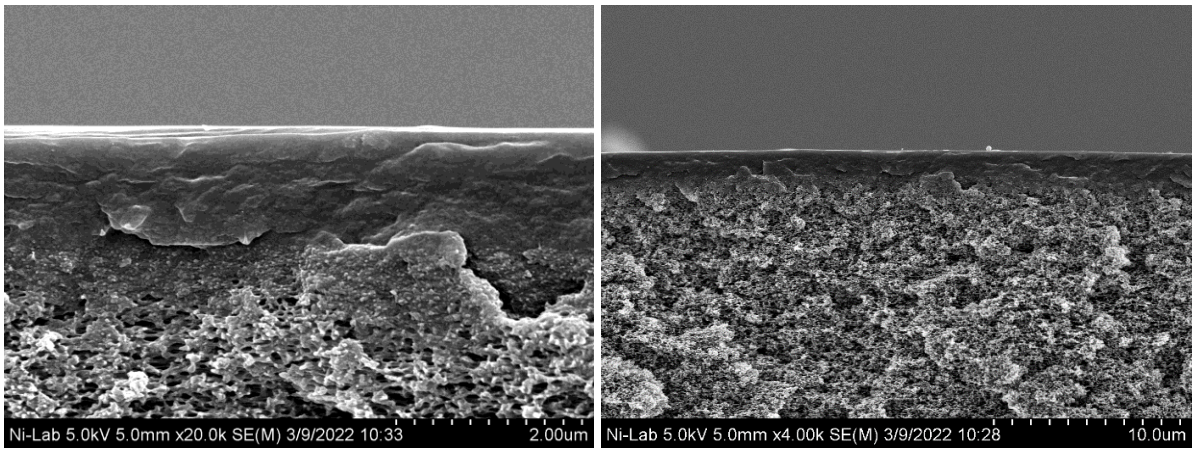

Figure 9-15. SEM micrographs of thin film membrane on porous substrate, sample PVA-87.